

Copyright is owned by the Author of the thesis. Permission is given for a copy to be downloaded by an individual for the purpose of research and private study only. The thesis may not be reproduced elsewhere without the permission of the Author.

PREDICTION OF CHILLING TIMES OF FOODS

SUBJECT TO

BOTH CONVECTIVE AND EVAPORATIVE COOLING

AT THE PRODUCT SURFACE

A thesis presented in partial fulfilment of the requirements for the degree of Doctor of Philosophy in Biotechnology and Bioprocess Engineering at Massey University.

Sawitri (Rojanasaroj) Chuntranuluck

1995

ABSTRACT

No published chilling time prediction method which covers a wide range of practical conditions, and which can be applied using only simple algebraic calculations for chilling with evaporation at the product surface has been proven accurate. The objective of the present work was to develop and test a simple chilling time prediction method with wide application for situations where significant evaporation as well as convective cooling occurs from the product surface.

A numerical method (finite differences) was used to simulate convection and evaporation at the product surface in cooling of solid products of simple shape (infinite slab, infinite cylinder, and sphere) with constant surface water activity. Semi-log plots relating temperature change to be accomplished to time were linearised by appropriate scale transformations based on the Lewis relationship. The effect of evaporation on cooling rate was measured by considering the slope and intercept of such plots, and comparing these to the slope and intercept that would arise in convection-only cooling. The enhancement of cooling rate due to the evaporative effect depended on six parameters; initial product temperature, cooling medium temperature, Biot number, relative humidity, product shape factor, and surface water activity.

Four simple algebraic equations were curved-fitted to the numerically simulated data for predicting temperature-time profiles at centre and mass average positions in the product. The numerically generated results and the simple algebraic equations agreed well with a mean difference close to 0 % for all three shapes, and 95% confidence bounds of about ± 3 % for the infinite cylinder, and ± 5 % for the infinite slab and the sphere geometries.

To test the simple models, chilling experiments were conducted in a controlled air flow tunnel across a range of conditions likely to occur in industrial practice. Trials were conducted using infinite cylinders of a food analogue as an idealised product (with saturated salt solutions percolating over a wet cloth on the product surface to maintain constant surface water activity), and carrots (both peeled and unpeeled) as examples of real food products.

Measured centre temperatures for both the idealised products and peeled carrots were predicted by the proposed method, assuming a constant surface water activity, within a range of differences which was almost totally explainable by experimental uncertainty. For unpeeled carrots, predictions made using three different surface water activities in the model (one to represent the initial condition, one to represent the active chilling phase, and one to represent the quasi-equilibrium state at the end of chilling) agreed sufficiently well with experimental centre temperature data for the lack of fit to be largely attributable to experimental uncertainty. No experimental verification for prediction of mass-average temperatures was attempted.

The proposed method is recommended for predicting chilling times of food products of infinite slab, infinite cylinder or sphere shapes, across a wide range of commonly occurring chilling conditions provided the product has constant surface water activity. The establishment of bounds on a theoretical basis for limiting the ranges in which surface water activity values are selected for making predictions for products with non-constant surface water activity is proposed, and some guidance on application of these bounds established. Further work to refine the use of these bounds for a range of food products, to consider a wider range of shapes, to test the ability of the proposed method to predict mass-average temperatures is recommended.

ACKNOWLEDGEMENTS

I would like to thank :

Professor Andrew C Cleland, Department of Food Technology and **Dr. Colin Wells**, Department of Agricultural Engineering, Massey University, for their advice, assistance, and patient during the course of this project;

Professor Donald Cleland, Department of Process Environmental Technology, Massey University, for his advice in solving some problems with the refrigeration plant plus his comments on this thesis; and

Mr. Bruce Collins, Electronics Technician, **Mr. Don McLean**, Technician, and **Mr. John Alger**, Technical Officer, for their technical assistance during the experimental phase of the project.

I would like to thank **the Royal Thai Government** and **Kasetsart University, Thailand**, for the scholarship & funding.

Finally, thank to **my family** across the ocean for their continual moral and financial support.

TABLE OF CONTENTS

ABSTRACT	ii
ACKNOWLEDGEMENTS	iv
TABLE OF CONTENTS	v
APPENDICES	x
LIST OF FIGURES	xi
LIST OF TABLES	xix

CHAPTER	PAGE
1 INTRODUCTION	1
2 LITERATURE SURVEY	3
2.1 INTRODUCTION	3
2.2 CHILLING WITHOUT INTERNAL HEAT GENERATION OR EVAPORATION	3
2.2.1 Analytical Solutions	3
2.2.1.1 Low Biot Number (typically $Bi < 0.2$)	3
2.2.1.2 Higher Biot Number (typically $Bi > 0.2$)	5
2.2.2 Empirical Solutions	9
2.2.3 Numerical Solutions	13
2.3 CHILLING WITH INTERNAL HEAT GENERATION BUT NO EVAPORATION	14
2.3.1 Description of Internal Heat Generation by Respiration	14
2.3.2 Analysis of Cooling with Internal Heat Generation	15
2.4 COOLING INCLUDING RADIATION	16
2.5 COOLING INCLUDING EVAPORATION	16
2.5.1 Moisture Transport Phenomena	16
2.5.2 Modelling of Evaporative Heat Transfer at the Product Surface	17
2.5.3 Evaporation of Mass Transfer Coefficients	20

2.5.4	Influence of Product Shape	21
2.5.5	Contribution of Evaporation to Chilling Rate	21
2.5.6	Effect of Internal Heat Generation	22
2.5.7	Steady State Models for Moisture Loss with and without Internal Heat Generation	22
2.5.8	Analytical and Empirical Models for Moisture Loss during Chilling	24
2.5.9	Analytical and Empirical Chilling Time Prediction Methods	24
2.5.10	Numerical Chilling Time Prediction Methods	26
2.5.11	Incorporation of Internal Heat Generation in Numerical Prediction Methods	28
3	PRELIMINARY CONSIDERATIONS	29
4	THEORETICAL MODELLING OF IDEALISED SYSTEMS	31
4.1	INTRODUCTION	31
4.2	THEORETICAL DEVELOPMENT	31
4.2.1	Nonlinear Partial Differential Equations	31
4.2.1.1	Energy Balance	32
4.2.1.2	Mass Balance	34
4.2.2	Finite Difference Schemes	35
4.2.2.1	Energy Transfer Equations	36
4.2.2.2	Mass Transfer Equations	39
4.2.3	Vapour Pressure Equations	41
4.2.4	Use of the Lewis Relationship	42
4.3	Computer Program Development and Testing	43
4.4	Simulation Performed	43
4.5	Discussion of Simulation Behaviour	44
4.5.1	Steady State (Equilibrium) Condition	44
4.5.2	Active Chilling Period (Unsteady State Condition)	45

5	MODEL DEVELOPMENT & RESULT	49
5.1	INTRODUCTION	49
5.2	DESCRIPTION OF CONVECTION-ONLY COOLING	49
5.3	COMPLICATIONS INTRODUCED BY EVAPORATIVE COOLING	51
5.4	DEVELOPMENT OF AN EQUILIBRIUM REFERENCE TEMPERATURE	52
5.5	DEVELOPMENT OF A MODIFIED Y VALUE	55
5.6	ISOLATION OF THE EVAPORATIVE EFFECT ON COOLING RATE	56
5.7	MODEL DEVELOPMENT OF EMPIRICAL EQUATIONS FOR f_{Evap}/f_{Conv} AND j_{Evap}/j_{Conv}	57
5.7.1	The Effects of Product Properties on f_{Evap} and j_{Evap} Values	58
5.7.2	The Reference Shape	58
5.7.3	Models for Centre Temperature Position	58
5.7.3.1	Model Development for f_{cEvap}/f_{cConv}	59
5.7.3.2	Model Development for j_{cEvap}/j_{cConv}	60
5.7.4	Models for Mass-Average Temperature Position	62
5.7.4.1	Model Development for f_{avEvap}/f_{avConv}	62
5.7.4.2	Model Development for j_{avEvap}/j_{avConv}	63
5.7.5	Time and Temperature Prediction Equations	64
5.7.6	Quality of Prediction from The Simple Models Relative to The Numerical Simulations Results and Conclusions	64
5.8	SUMMARY	66
6	EXPERIMENTAL DESIGN AND METHODS - IDEALISED PRODUCTS	86
6.1	INTRODUCTION	86
6.2	EXPERIMENTAL DESIGN	86
6.3	EXPERIMENTS	87
6.3.1	Test Samples and Temperature Measurement Probes	87
6.3.2	Maintenance of Constant Surface Water Activity	88
6.3.3	Air Tunnel	91
6.3.3.1	Air Velocities	91
6.3.3.2	Relative Humidity	91
6.4	MEASURING EQUIPMENT	92

6.4.1	Relative Humidity	92
6.4.2	Data Logging	93
6.4.3	Air Velocity	94
6.5	EXPERIMENTAL PROCEDURE	94
6.6	HEAT TRANSFER COEFFICIENTS	95
6.7	SUMMARY	97
7	TESTING OF SIMPLE MODEL AGAINST EXPERIMENTAL DATA FOR IDEALISED MODEL SYSTEMS	107
7.1	INTRODUCTION	107
7.2	EXPERIMENTAL DESIGN AND RESULTS	107
7.3	HEAT TRANSFER COEFFICIENTS	108
7.4	EQUILIBRIUM TEMPERATURE ANALYSIS	110
7.5	LINEARIZATION OF SEMI-LOG PLOTS	110
7.6	COOLING WITH EVAPORATIVE EFFECTS	111
7.7	CHILLING TIME PREDICTION	112
7.8	DISCUSSION AND CONCLUSIONS	113
8	EXPERIMENTAL DESIGN AND METHODS FOR EXPERIMENTS WITH A REAL PRODUCT	149
8.1	INTRODUCTION	149
8.2	EVAPORATIVE COOLING OF REAL FOOD PRODUCTS	149
8.2.1	Products without Skin Resistance	150
8.2.2	Products with Skin Resistance	150
8.3	SELECTION OF TEST MATERIAL	151
8.4	EXPERIMENTAL METHODS - PEELED CARROT	151
8.4.1	Sample Preparation	151
8.4.2	Weight Loss, Water Content, and Surface Water Activity Measurement	152
8.4.3	Temperature and Relative Humidity Measurement	153
8.4.4	Cooling Trials	153
8.4.5	Heat Transfer Coefficient Measurement	154

8.4.6	Experimental Design	154
8.5	EXPERIMENTAL METHODS - UNPEELED CARROT	155
8.5.1	Sample Preparation	155
8.5.2	Weight Loss, Water Content, and Surface Water Activity Measurement	155
8.5.3	Experimental Design	156
8.6	THERMOPHYSICAL PROPERTIES OF CARROTS	156
8.7	HEAT TRANSFER COEFFICIENTS FOR PEELED AND UNPEELED CARROTS	156
8.8	FINISHING REMARKS	158
9	TESTING OF THE PROPOSED MODEL AGAINST EXPERIMENTAL DATA FOR A REAL PRODUCT WITHOUT SKIN RESISTANCE	163
9.1	INTRODUCTION	163
9.2	SURFACE WATER ACTIVITY AND EQUILIBRIUM TEMPERATURE ANALYSIS	163
9.3	LINEARIZATION OF SEMI-LOG PLOTS	164
9.4	COOLING WITH EVAPORATIVE EFFECTS	164
9.5	WEIGHT LOSS	166
9.6	DISCUSSION AND CONCLUSIONS	166
10	TESTING OF THE PROPOSED MODEL AGAINST EXPERIMENTAL DATA FOR A REAL PRODUCT WITH SKIN RESISTANCE	186
10.1	INTRODUCTION	186
10.2	SURFACE WATER ACTIVITY IN THE QUASI-EQUILIBRIUM STAGE	187
10.3	LINEARIZATION OF SEMI-LOG PLOTS	188
10.4	f AND j VALUES FOR ACTIVE CHILLING PHASE	188
10.4.1	a_{wf}	189
10.4.1	a_{wj}	189
10.5	COOLING WITH EVAPORATIVE EFFECTS AND CHILLING TIME PREDICTION	190
10.6	WEIGHT LOSS	192

11 DISCUSSION AND CONCLUSION	207
11.1 DISCUSSION	207
11.2 CONCLUSIONS AND RECOMMENDATIONS FOR FURTHER WORK	209
NOTATION	212
REFERENCES	217
APPENDICES	
1 COMPUTER PROGRAM USED FOR CHILLING PROCESS SIMULATION AND ANALYSIS	231
2 SAMPLE OF CALCULATION	243

LIST OF FIGURES

4.1	Example plot for convection-only cooling showing the approach of the centre, surface, and mass-average temperatures to the cooling medium temperature.	47
4.2	Example plots showing the effect of $(a_w - H_r)$ on the cooling process.	47
4.3	Example semi-plots of cooling by both convection and evaporation with $H_r = a_w$.	48
4.4	Example semi-plots of cooling by both convection and evaporation with $a_w < H_r$, $a_w > H_r$, and $a_w = H_r$.	48
5.1	Alignment chart to estimate the equilibrium temperature (T_{eq}) at $a_w = 0.6$.	70
5.2	Alignment chart to estimate the equilibrium temperature (T_{eq}) at $a_w = 0.8$.	71
5.3	Alignment chart to estimate the equilibrium temperature (T_{eq}) at $a_w = 1.0$.	72
5.4	Example plots of $\ln Y_c$ vs Fo for evaporative cooling.	73
5.5	Plot of numerically predicted f_{cEvap}/f_{cConv} vs Bi for an infinite cylinder.	73
5.6	Effect of Bi on the slope ratios of semi-log plots (centre position) at different T_a (predicted by finite difference simulations for an infinite cylinder).	74
5.7	Effect of T_a on the slope ratios of semi-log plots (centre position) at different Bi (predicted by finite difference simulations for an infinite cylinder).	74
5.8	Effect of T_a on the slope ratios of semi-log plots (centre position) at high Bi and different H_r (predicted by finite difference simulations for an infinite cylinder).	75
5.9	Effect of H_r on the slope ratios of semi-log plots (centre position) at high Bi and different a_w (predicted by finite difference simulations for an infinite cylinder).	75
5.10	Effect of T_a on the slope ratios of semi-log plots (centre position) at high Bi and different a_w (predicted by finite difference simulations for an infinite cylinder).	76
5.11	Effect of Bi on the slope ratios of semi-log plots (centre position) at different T_{in} (predicted by finite difference simulations for an infinite	76

	cylinder).	
5.12	Effect of a_w on the slope ratio of semi-log plots (centre position) at high Bi and different T_{in} (predicted by finite difference simulations for an infinite cylinder).	77
5.13	Effect of shape on the slope ratio of semi-log plots (centre position) (predicted by finite difference simulations for an infinite cylinder).	77
5.14	Plot of numerically predicted j_{cEvap}/j_{cConv} data for an infinite cylinder vs Bi .	78
5.15	Effect of Bi on the intercept ratios of semi-log plots (centre position) at different H_r (predicted by finite difference simulations for an infinite cylinder).	78
5.16	Effect of Bi on the intercept ratios of semi-log plots (centre position) at different T_a (predicted by finite difference simulations for an infinite cylinder).	79
5.17	Effect of Bi on the intercept ratios of semi-log plots (centre position) at different a_w (predicted by finite difference simulations for an infinite cylinder).	79
5.18	Effect of Bi on the intercept ratios of semi-log plots (centre position) at different T_{in} (predicted by finite difference simulations for an infinite cylinder).	80
5.19	Effect of H_r on the intercept ratios of semi-log plots (centre position) at different T_a (predicted by finite difference simulations for an infinite cylinder).	80
5.20	Effect of T_{in} on the intercept ratios of semi-log plots (centre position) at different T_a (predicted by finite difference simulations for an infinite cylinder).	81
5.21	Effect of shape on the intercept ratios of semi-log plots (centre position) (predicted by finite difference simulations for an infinite cylinder).	81
5.22	Plot of numerically predicted j_{cEvap}/j_{cConv} data for an infinite cylinder vs Bi .	82
5.23	Effect of Bi on the intercept ratios of semi-log plots (mass-average position) at different T_a (predicted by finite difference simulations for an infinite cylinder).	82
5.24	Effect of Bi on the intercept ratios of semi-log plots (mass-average position)	83

	at different T_{in} (predicted by finite difference simulations for an infinite cylinder).	
5.25	Effect of T_a on the intercept ratios of semi-log plots (mass-average position) at different H , (predicted by finite difference simulations for an infinite cylinder).	83
5.26	Effect of shape on the intercept ratios of semi-log plots (mass-average position), (predicted by finite difference simulations for an infinite cylinder).	84
5.27	Shape of cooling curve for centre and mass-average temperature during convective plus evaporative cooling under conditions where the evaporative effect is very small.	84
5.28	Shape of cooling curve for centre and mass-average temperature during convective plus evaporative cooling under conditions where the evaporative effect is substantial.	85
6.1	Schematic diagram of experimental apparatus installed in the air tunnel showing sample oscillator and wetting agent supply system.	103
6.2	The apparatus inside the air tunnel.	103
6.3	Example of measured and predicted cylinder temperatures for a run in which the reservoir temperature was too cold.	104
6.4	Example of measured and predicted cylinder temperatures for a run in which the reservoir temperature was too hot.	104
6.5	Results of an experiment for the large cylinder (with finite difference prediction) in which the reservoir temperature was ideal.	105
6.6	Results of an experiment for the small cylinder (with finite difference prediction) in which the reservoir temperature was ideal.	105
6.7	Experimental air tunnel used in experiments.	106
7.1	Plots of h_c vs air velocity for heat transfer coefficient measurement runs in which the wetting fluid was water.	129
7.2	Plots of h_c vs air velocity for heat transfer coefficient measurement runs in which the wetting fluid was a saturated solution of NaCl.	129
7.3	Plots of h_c vs air velocity for heat transfer coefficient measurement runs in which the wetting fluid was a saturated solution of KCl.	130
7.4	Plots of difference between $T_{eq,pred}$ and $T_{eq,exp}$ vs a_w for all experimental runs.	130

7.5	Plots of difference between $T_{eq,pred}$ and $T_{eq,exp}$ vs H_r for all experimental runs.	131
7.6	Plots of difference between $T_{eq,pred}$ and $T_{eq,exp}$ vs Bi for all experimental runs.	131
7.7	Plots of difference between $T_{eq,pred}$ and $T_{eq,exp}$ vs v_a for all experimental runs.	132
7.8	Plots of difference between $T_{eq,pred}$ and $T_{eq,exp}$ vs T_a for all experimental runs.	132
7.9	Plots of difference between $T_{eq,pred}$ and $T_{eq,exp}$ vs T_{in} for all experimental runs.	133
7.10	Typical plot of temperature vs time for cooling without evaporation ($T_{eq,exp} = T_a$).	133
7.11	Typical plot of temperature vs time for cooling with evaporation ($T_{eq,exp} > T_a$ and $a_w < H_r$).	134
7.12	Typical plot of temperature vs time for cooling with evaporation ($T_{eq,exp} < T_a$ and $a_w > H_r$).	134
7.13	Typical plot of temperature vs time for cooling with evaporation ($T_{eq,exp} = T_a$ and $a_w = H_r$).	135
7.14	Plot of $\ln Y_{c,exp}$ vs FO using $T_{eq,exp}$ as the reference temperature for the conditions in Fig. 7.11.	135
7.15	Plot of $\ln Y_{c,exp}$ vs FO using $T_{eq,exp}$ as the reference temperature for the conditions in Fig. 7.12.	136
7.16	Plot of $\ln Y_{c,exp}$ vs FO using $T_{eq,exp}$ as the reference temperature for the conditions in Fig. 7.13.	136
7.17	Comparisons of the % differences in f_{cEvap}/f_{cConv} between the simple model and the finite difference model.	137
7.18	Comparisons of the % differences in j_{cEvap}/j_{cConv} between the simple model and the finite difference model.	137
7.19	Comparisons of the values of f_{cEvap}/f_{cConv} between the simple model and the experimental results.	138
7.20	Comparisons of the values of j_{cEvap}/j_{cConv} between the simple model and the experimental results.	138
7.21	Plots of % difference in f_{cEvap}/f_{cConv} values calculated by the simple model compared to experimental values at different a_w .	139
7.22	Plots of % difference in f_{cEvap}/f_{cConv} values calculated by the simple model compared to experimental values at different H_r .	139
7.23	Plots of % difference in f_{cEvap}/f_{cConv} values calculated by the simple model	140

	compared to experimental values at different T_a .	
7.24	Plots of % difference in f_{cEvap}/f_{cConv} values calculated by the simple model compared to experimental values at different T_{in} .	140
7.25	Plots of % difference in f_{cEvap}/f_{cConv} values calculated by the simple model compared to experimental values at different Bi .	141
7.26	Plots of % difference in f_{cEvap}/f_{cConv} values calculated by the simple model compared to experimental values at different v_a .	141
7.27	Plots of % difference in j_{cEvap}/j_{cConv} values calculated by the simple model compared to experimental values at different a_w .	142
7.28	Plots of % difference in j_{cEvap}/j_{cConv} values calculated by the simple model compared to experimental values at different H_r .	142
7.29	Plots of % difference in j_{cEvap}/j_{cConv} values calculated by the simple model compared to experimental values at different T_a .	143
7.30	Plots of % difference in j_{cEvap}/j_{cConv} values calculated by the simple model compared to experimental values at different T_{in} .	143
7.31	Plots of % difference in j_{cEvap}/j_{cConv} values calculated by the simple model compared to experimental values at different Bi .	144
7.32	Plots of % difference in j_{cEvap}/j_{cConv} values calculated by the simple model compared to experimental values at different v_a .	144
7.33	Comparisons of % differences in time to reach the temperature corresponding to $Y_{c,exp} = 0.10$ between the simple model and the finite difference model.	145
7.34	Comparisons of % differences in time to reach the temperature corresponding to $Y_{c,exp} = 0.35$ between the simple model and the finite difference model.	145
7.35	Comparisons of % differences in time to reach the temperature corresponding to $Y_{c,exp} = 0.70$ between the simple model and the finite difference model.	146
7.36	Comparisons of time (hrs.) to reach the temperature corresponding to $Y_{c,exp} = 0.10$ between the simple model and the experimental results.	146
7.37	Comparisons of time (hrs.) to reach the temperature corresponding to $Y_{c,exp} = 0.35$ between the simple model and the experimental results.	147

7.38	Comparisons of time (hrs.) to reach the temperature corresponding to $Y_{c,exp} = 0.70$ between the simple model and the experimental results.	147
7.39	The best result of comparisons between the simple model, the finite difference with evaporation and without evaporation, and the experimental data.	148
7.40	The worst result of comparisons between the simple model, the finite difference with evaporation and without evaporation, and the experimental data.	148
8.1	A typical infinite cylindrical carrot sample used in experimental work.	160
8.2	Plot of Nu vs Re for runs with peeled carrots.	160
8.3	Plot of percentage difference in h_c (between calculated results using equation 8.4 and experimental results) for peeled carrots vs Re .	161
8.4	Plot of Nu vs Re for runs with unpeeled carrots.	161
8.5	Plots of percentage difference in h_c (between calculated results using equation 8.5 and experimental results) for unpeeled carrots vs Re .	162
8.6	Plot of Nu vs Re for runs with peeled & unpeeled carrots.	162
9.1	Plot of measured a_w and back-calculated a_w vs H_r .	173
9.2	Plot of difference between $T_{eq,pred}$ and $T_{eq,exp}$ vs H_r for all experimental runs.	173
9.3	Plot of difference between $T_{eq,pred}$ and $T_{eq,exp}$ vs Bi for all experimental runs.	174
9.4	Plot of difference between $T_{eq,pred}$ and $T_{eq,exp}$ vs v_a for all experimental runs.	174
9.5	Plot of difference between $T_{eq,pred}$ and $T_{eq,exp}$ vs T_a for all experimental runs.	175
9.6	Plot of difference between $T_{eq,pred}$ and $T_{eq,exp}$ vs T_{in} for all experimental runs.	175
9.7	Typical plot of temperature vs time for cooling of a peeled carrot without evaporation ($T_{eq,exp} = T_a$).	176
9.8	Typical plot of temperature vs time for cooling of a peeled carrot with evaporation at the product surface.	176
9.9	Plot of $\ln Y_c$ vs FO using $T_{eq,exp}$ as the reference temperature for the conditions in Fig. 9.7.	177
9.10	Plot of % difference in f_{cEvap}/f_{cConv} values calculated by the simple model compared to experimental values vs H_r .	177
9.11	Plot of % difference in f_{cEvap}/f_{cConv} values calculated by the simple model compared to experimental values vs T_a .	178

9.12	Plot of % difference in f_{cEvap}/f_{cConv} values calculated by the simple model compared to experimental values vs T_{in} .	178
9.13	Plot of % difference in f_{cEvap}/f_{cConv} values calculated by the simple model compared to experimental values vs Bi .	179
9.14	Plot of % difference in f_{cEvap}/f_{cConv} values calculated by the simple model compared to experimental values vs v_a .	179
9.15	Plot of % difference in j_{cEvap}/j_{cConv} values calculated by the simple model compared to experimental values vs H_r .	180
9.16	Plot of % difference in j_{cEvap}/j_{cConv} values calculated by the simple model compared to experimental values vs T_a .	180
9.17	Plot of % difference in j_{cEvap}/j_{cConv} values calculated by the simple model compared to experimental values vs T_{in} .	181
9.18	Plot of % difference in j_{cEvap}/j_{cConv} values calculated by the simple model compared to experimental values vs Bi .	181
9.19	Plot of % difference in j_{cEvap}/j_{cConv} values calculated by the simple model compared to experimental values vs v_a .	182
9.20	Comparisons of the values of f_{cEvap}/f_{cConv} between the simple model and the experimental results.	182
9.21	Comparisons of the values of j_{cEvap}/j_{cConv} between the simple model and the experimental results.	183
9.22	Comparisons of time (min.) to reach the centre temperature corresponding to $Y_{c,exp} = 0.10$ between the simple model and the experimental results.	183
9.23	Comparisons of time (min.) to reach the centre temperature corresponding to $Y_{c,exp} = 0.35$ between the simple model and the experimental results.	184
9.24	Comparisons of time (min.) to reach the centre temperature corresponding to $Y_{c,exp} = 0.70$ between the simple model and the experimental results.	184
9.25	Weight loss of peeled carrots vs air velocity.	185
10.1	Comparison of the cooling curves of peeled and unpeeled carrot under the same environmental conditions (Runs 15 of Table 9.1 and 10.1).	202
10.2	Plot of a_w vs time during a typical chilling experiment in which internal water movement rate to the product cannot always exceed evaporation rate.	202
10.3	Relationship between a_w back-calculated from $T_{eq,exp}$ using equation (5.4) and	203

	H_r for runs with unpeeled carrot.	
10.4	Typical plot of temperature vs time for cooling of an unpeeled carrot without evaporation ($T_{eq,exp} = T_a$).	203
10.5	Typical plot of temperature vs time for cooling of an unpeeled carrot with evaporation at the product surface.	204
10.6	Plot of $\ln Y_c$ (using $T_{eq,exp}$ as the reference temperature) vs FO for the conditions in Figure 10.5.	204
10.7	Plot of a_{wf} vs H_r during the active chilling phase.	205
10.8	Plot of a_{wf} vs Bi during the active chilling phase.	205
10.9	Plot of a_{wj} vs H_r during the active chilling phase.	206
10.10	Plot of a_{wj} vs Bi during the active chilling phase.	206

LIST OF TABLES

5.1	Percentage differences between results calculated by the proposed curve-fit algebraic equations and results calculated by finite differences for the centre temperature of all three shapes.	67
5.2	Percentage differences between results calculated by the proposed curve-fit algebraic equations and results calculated by finite differences for the mass-average temperature of all three shapes. Equation (5.23) was used to calculate f_{avEvap} .	68
5.3	Percentage differences between results calculated by the proposed curve-fit algebraic equations and results calculated by finite differences for the mass-average temperature of all three shapes. Equation (5.24) was used to calculate f_{avEvap} .	69
6.1	Ranges of experimental conditions used for model testing.	98
6.2	Experimental conditions used for the half-factorial experiment (v_h = high velocity, v_l = low velocity, v_m = mid-range velocity, L = large size, S = small size).	99
6.3	Experimental conditions for the runs used to extend the half-factorial experiment to a plan approximating a central composite design.	100
6.4	Experimental conditions for the 'centre point' runs in the central composite experimental design.	100
6.5	Water activity of saturated salt solutions used in the experiments.	101
6.6	The solubility of salts used in the experiments at different temperature.	101
6.7	Conditions used to obtain required relative humidities.	102
7.1	Designation of ranges of Biot number in the experimental described in Chapter 6.	115
7.2	95% confidence bounds on h_c ($W m^{-2} K^{-1}$) at the midrange value of v_a ($2 m s^{-1}$).	115
7.3	Experimental data and predicted results for runs using water as the wetting agent.	116
7.4	Experimental data and predicted results for runs using saturated salt sodium	118

	chloride as the wetting agent.	
7.5	Experimental data and predicted results for runs using saturated salt potassium chloride as the wetting agent.	120
7.6	Differences between results calculated by the finite difference method and results from the experiments (all data).	122
7.7	Difference between results calculated by the proposed curve-fitted algebraic equations (simple model) and results from the experiments (all data).	122
7.8	Prediction and measured chilling times to $Y_{c,exp} = 0.10, 0.35, \text{ and } 0.70$ for runs using water as the wetting agent.	123
7.9	Prediction and measured chilling times to $Y_{c,exp} = 0.10, 0.35, \text{ and } 0.70$ for runs using saturated salt sodium chloride as the wetting agent.	125
7.10	Prediction and measured chilling times to $Y_{c,exp} = 0.10, 0.35, \text{ and } 0.70$ for runs using saturated salt potassium chloride as the wetting agent.	127
8.1	Experimental plan for cooling trials with carrots.	159
9.1	Experimental data and predicted results for runs using peeled carrot as the product with $a_w = 0.977$.	167
9.2	Predicted and measured chilling times to reach certain centre temperatures which corresponded to $Y_{c,exp} = 0.10, 0.35, \text{ and } 0.70$ for runs using peeled carrot as the product.	170
9.3	Differences between results calculated by the finite difference method (assuming $a_w = 0.977$) and results from the experiments (for peeled carrots).	172
9.4	Differences between results calculated by the proposed curve-fit equations (simple model) and results from the experiments (for peeled carrots).	172
10.1	Experimental data for experiments with unpeeled carrot and comparisons of measured quasi-equilibrium temperature ($T_{eq,exp}$) to predictions of T_{eq} calculated using (A) $a_w = 0.977$, (B) $a_w = H_r$, (C) a_w calculated from equation (10.1).	193
10.2	Comparisons between experimental results and model predictions of f_{cEvap}/f_{cConv} (at $a_w = 0.30$ and 0.16) and j_{cEvap}/j_{cConv} (at $a_{wj} = 0.977$).	195
10.3	Comparisons of time (to the temperature that corresponds to $Y_{c,exp} = 0.10, 0.35, \text{ and } 0.70$) between the experimental results and simple model using $a_{wf} = 0.16$ & $a_{wj} = 0.977$, $a_{wf} = 0.30$ & $a_{wj} = 0.977$, and $T_{eq,pred}$ at (A) $a_w =$	197

0.977, (B) $a_w = H_r$, and (C) $a_w = 0.792H_r + 0.215$.

- 10.4 Predicted (using $a_{wf} = 0.30$, $a_{wj} = 0.977$, and a_w from equation 10.1) and measured chilling time to the time that corresponds to $Y_{c,exp} = 0.10, 0.35,$ and 0.70 for an unpeeled carrot. 199
- 10.5 Predicted (using $a_{wf} = 0.16$, $a_{wj} = 0.977$, and a_w from equation 10.1 in equation 10.2) and measured chilling time to the time that corresponds to $Y_{c,exp} = 0.10, 0.35,$ and 0.70 for an unpeeled carrot. 200

1. INTRODUCTION

The food market is facing enormous changes and challenges internationally. Export of food is important for Agro-Industrial countries. Much of the fresh food supply is perishable because of its moderate to high water content and its nutritious nature. A great need exists for more effective and more widely used methods of food preservation to fulfill future needs and reduce the problem of food wastage.

The aim of commercial food preservation is to prevent undesirable changes in the wholesomeness, nutritive value, or sensory quality of food by economical methods which control growth of microorganism, reduce chemical, physical, and physiological changes of an undesirable nature, and obviate contamination of moderately or highly perishable foods.

There are many methods of food preservation but most of them change the product characteristics. Frozen and chilled fresh foods are replacing many traditionally preserved products because product quality loss is relatively slow under refrigerated storage conditions.

Chilling involves removal of heat from fresh products in sufficient time to prevent spoilage, and to keep the product in a condition closely resembling its fresh state (to maintain texture and flavour). Food products are often precooled before they are transported for further processing. Rapid cooling is desirable on economic grounds, and would normally lead to least quality deterioration.

Accurate prediction of chilling rates is essential for efficient execution of the process, plus optimal design and operation of chilling facilities. A knowledge of the heat transfer characteristics of the food product being precooled is required. However, transient heat conduction in food products is a complicated problem because of inherent loss of free water at the surface and from within the product if the conditions are favourable for moisture diffusion to take place. The influence of this moisture loss on the overall transfer of energy and on product weight, can be significant, and it is one of the important factors that affects quality of food products.

Detailed modelling of coupled heat and mass transfer effects results in a non-linear boundary condition, necessitating the use of approximate or numerical techniques for the solution of the problem, unless simplifying assumptions are made. Simpler, but approximate chilling calculation methods have been developed, but many of these have practical shortcomings particularly in situations in which evaporative cooling during chilling is significant. Thus there is a further need to research methods for predicting the rates of chilling processes involving water evaporation from the product surface.

2. LITERATURE SURVEY

2.1 INTRODUCTION

Historically, the most commonly used method of chilling food products has been air chilling in refrigerated rooms. However, slow air cooling can lead to a number of problem such as increased weight loss or shrinkage, and more rapid increases in microbial flora. Rapid air cooling can reduce weight loss by cooling the surface of the product faster and thus reducing the potential for evaporation. Rapid air cooling often results in a higher quality product with longer shelf life, reductions in space requirements for refrigeration, and shipment of product on the day of slaughter or harvesting (Stermer *et al.*, 1984, 1986; Drumm *et al.*, 1992). In the cooling of food products, heat transfer does not always involves single solid particles, but the single particle situation is usually analyzed before describing the multi-particle or bulk condition (Gaffney *et al.*, 1985a).

2.2 CHILLING WITHOUT INTERNAL HEAT GENERATION OR EVAPORATION

Where the effects of evaporation, radiation, and internal heat generation are neglected, transient heat transfer can be analysed as follows.

2.2.1 Analytical Solutions

Chilling with cool air introduces a boundary layer which is a thin layer of fluid at the product surface that controls interfacial transport. When heat is the only transferred property, a measure of the interfacial transport compared to the heat conduction inside a solid body is the Biot number ($Bi = h_c R/k$). Thus, the Biot number is used in the boundary conditions of the heat transport equation. The higher the Biot number, the less important the interfacial resistance to the overall rate of cooling within the solid body.

2.2.1.1 Low Biot Number (typically $Bi < 0.2$)

Situation can arise in which the products are good thermal conductors or cooled in air with

a low velocity so that the convective heat transfer coefficient at the surface is very low. The resistance to heat transfer at the surface is high compared to the internal resistance to conduction. Under such conditions, there will be a negligible temperature gradient within the object, and the temperature at any point within the object, at a particular time, will not differ appreciably from the surface temperature. The rate of cooling as described by the convection boundary condition (third kind of boundary condition) or Newton's law of cooling:

$$C \rho V \frac{dT}{dt} = h_c A (T_a - T) \quad (2.1)$$

- where C = specific heat of solid ($\text{J kg}^{-1} \text{K}^{-1}$)
 ρ = density of solid (kg m^{-3})
 V = volume of solid (m^3)
 T = temperature of solid (K or $^{\circ}\text{C}$)
 T_a = surrounding cooling medium temperature (K or $^{\circ}\text{C}$)
 h_c = surface heat transfer coefficient ($\text{W m}^{-2} \text{K}^{-1}$)
 A = surface area of solid (m^2)
 t = time (s)

If product thermal properties do not change with temperature, and the surrounding air temperature is constant, equation (2.1) can be integrated with $T = T_{in}$ at $t = 0$, giving the following result:

$$\frac{T - T_a}{T_{in} - T_a} = e^{-\left(\frac{h_c A}{\rho C V}\right)t} \quad (2.2)$$

$$T_{av} = T_c = T \quad (2.3)$$

- where T_{in} = initial uniform temperature of solid (K or $^{\circ}\text{C}$)
 T_c = centre temperature of solid (K or $^{\circ}\text{C}$)
 T_{av} = mass average temperature of solid (K or $^{\circ}\text{C}$)

In practice, this equation is valid only for conditions of very slow cooling, constant surrounding temperature and homogeneous products of any shape.

2.2.1.2 Higher Biot Number (typically $Bi > 0.2$)

When food products are cooled in air with a high velocity the surface temperature changes faster than the interior. There is a temperature gradient within the object, and the centre temperature will be different from the mass average temperature. This situation is common in the cooling of horticultural produce which are poor conductors, where h_c , the surface heat transfer coefficient, is usually large relative to k , the thermal conductivity. The rate of change of internal temperature can be described by the energy balance equation (Fourier's law):

$$\rho C \frac{\partial T}{\partial t} = \frac{\partial}{\partial x} \left(k \frac{\partial T}{\partial x} \right) + \frac{\partial}{\partial y} \left(k \frac{\partial T}{\partial y} \right) + \frac{\partial}{\partial z} \left(k \frac{\partial T}{\partial z} \right) \quad (2.4)$$

Where the thermal properties can be assumed to be constant with respect to both temperature and time this simplifies to:

$$\frac{\partial T}{\partial t} = \frac{k}{\rho C} \left(\frac{\partial^2 T}{\partial x^2} + \frac{\partial^2 T}{\partial y^2} + \frac{\partial^2 T}{\partial z^2} \right) = \alpha \left(\frac{\partial^2 T}{\partial x^2} + \frac{\partial^2 T}{\partial y^2} + \frac{\partial^2 T}{\partial z^2} \right) \quad (2.5)$$

where x, y, z = space position within solid (m)
 k = thermal conductivity of solid ($\text{W m}^{-1} \text{K}^{-1}$)
 α = thermal diffusivity of solid, $k / (\rho C)$ ($\text{m}^2 \text{s}^{-1}$)

With appropriate boundary and initial conditions, equation (2.4) can be solved analytically for one dimensional heat flow in regularly shaped objects (i.e., sphere, infinite cylinder, or infinite slab) subject to the following restrictions (Carslaw & Jaeger, 1959; Gaffney *et al.*, 1985a):

- (1) The object is homogeneous;
- (2) The initial temperature of the object is uniform;
- (3) The temperature of the surroundings is constant with time;
- (4) There is no internal heat generation;
- (5) There is no mass transfer (evaporation) at the surface;
- (6) The thermal properties of the object are constant with time and temperature.

There are a number of boundary conditions that describe how the heat transfers from the solid to the cooling medium. The most common, and most practical boundary condition, is the so-called third kind of boundary condition (Cleland & Earle, 1977), which takes account of convection at the surface, and can be used wherever there is significant resistance to heat transfer between the surface of the object and the bulk external medium. For the one-dimensional solid with a surface at $r = R$, it is defined as:

$$h_c(T_a - T_{r=R}) = k \left(\frac{\partial T}{\partial r} \right)_{r=R} \quad (2.6)$$

Analytical solutions can be derived for this boundary condition provided neither h_c or T_a changes with time or temperature (Newman, 1936; Carslaw & Jaeger, 1959; Smith *et al.*, 1967):

$$Y_r \equiv \frac{T_r - T_a}{T_{in} - T_a} = \sum_{m=1}^{\infty} j_m(r) e^{-(\beta_m^2) \frac{\alpha t}{R^2}} \quad (2.7)$$

$$Y_{av} \equiv \frac{T_{av} - T_a}{T_{in} - T_a} = \sum_{m=1}^{\infty} j_m(av) e^{-(\beta_m^2) \frac{\alpha t}{R^2}} \quad (2.8)$$

(1) Sphere. The values of β are found by solving

$$Bi = 1 - \beta_m \cot(\beta_m) \quad (2.9)$$

and values of j_m are given by:

$$j_m(r) = \frac{2BiR}{r} \frac{(\beta_m^2 + (Bi - 1)^2)}{\beta_m^2(\beta_m^2 + (Bi - 1)Bi)} \sin(\beta_m) \sin(\beta_m \frac{r}{R}) \quad (2.10)$$

$$j_m(av) = \frac{6Bi^2}{\beta_m^2(\beta_m^2 + (Bi - 1)Bi)} \quad (2.11)$$

(2) Infinite cylinder. The values of β are found by solving

$$Bi = \frac{\beta_m J_1(\beta_m)}{J_0(\beta_m)} \quad (2.12)$$

and values of j_m are given by:

$$j_m(r) = \frac{2Bi J_0(\beta_m \frac{r}{R})}{(\beta_m^2 + Bi^2) J_0(\beta_m)} \quad (2.13)$$

$$j_m(av) = \frac{4 Bi^2}{\beta_m^2 (\beta_m^2 + Bi^2)} \quad (2.14)$$

(3) Infinite slab. The values of β are found by solving

$$Bi = \beta_m \tan(\beta_m) \quad (2.15)$$

and values of j_m are given by:

$$j_m(r) = \frac{2 Bi \cos(\beta_m \frac{r}{R}) \sec(\beta_m)}{Bi(Bi + 1) + \beta_m^2} \quad (2.16)$$

$$j_m(av) = \frac{2 Bi^2}{\beta_m^2 (Bi(Bi + 1) + \beta_m^2)} \quad (2.17)$$

- where Y_r = dimensionless temperature ratio as a function of time and position within the solid (fractional unaccomplished temperature change)
- Y_{av} = dimensionless temperature ratio as a function of time for the mass-average position in the solid (fractional unaccomplished temperature change for mass-average)
- T_r = temperature within the solid at position r (K or °C)
- $j_m(r)$ = function of β_m , geometry, and position within the solid but not time or temperature
- $j_m(av)$ = function of β_m , and geometry, but not time or temperature
- Bi = Biot number, $h_c R/k$
- $J_1(\beta_m)$ = first order Bessel function of first kind
- $J_0(\beta_m)$ = zero order Bessel function of first kind
- β_m = m^{th} root of the transcendental equation appropriate for the given geometry (equation 2.9, 2.12 or 2.15)
- R = characteristic length for solid (radius of sphere or cylinder and half-thickness of slab) (m)
- r = space position within solid relative to centre position (m)

These analytical solutions are complex, so graphical presentations have been developed by relating temperature ratio, to Fourier number, Biot number, and relative distance from the

center (Williamson & Adams, 1919; Gurney & Luries, 1923; Heisler, 1947; Boelter *et al.*, 1948; Carslaw & Jaeger, 1959; Schneider, 1963; Luikov, 1968).

A number of researchers have used the analytical solutions described by equation (2.7) to predict cooling rates of fruits and vegetables by considering the product to be essentially homogeneous and relatively regular in shape; for example, some varieties of apples, grapes, peaches, lettuces, cabbages, watermelons, radishes or tomatoes might be considered as relatively spherical; cucumbers, snaps, beans, bananas, carrots, and elonged varieties of watermelons might be approximated by an infinite cylinder. Bell peppers might be analyzed as an infinite slab, except for the region near the stem (Abdul Majeed, 1982; Gaffney *et al.*, 1985). Canned foods might be treated as a homogeneous mass because the container thickness is usually quite small (Abdul Majeed, 1982).

Nicholas *et al.* (1964) conducted experiments involving air and water cooling of apples at different flow rates. The experimental cooling curves agreed well with the analytical solution for a sphere. Hood (1964) carried out experiments involving air and water cooling of cucumbers and found good comparisons between experimental results and analytical solutions for an infinite cylinder. He also presented an analytical solution similar to equation (2.7) for situations in which the ambient temperature changes as a linear function of time. He found good agreement of this solution with experimental data. Akimoto (1975) conducted experiments involving cooling of a slab shaped sample of potato and found good comparisons between experimental results and analytical solutions for the infinite slab.

The solutions for infinite slab, infinite cylinder, and sphere can also be applied to other regular shapes using a product rule (Williamson & Adams, 1919; Newman, 1936). For the two-dimensional rectangular rod of dimensions L_x and L_y , the solution is the product of the solutions for infinite slabs in x and y directions. For the rectangular brick shape of dimensions L_x , L_y , and L_z , the solution is the product of the solutions for infinite slabs in x , y , and z directions. For a finite cylinder, the solution is the product of the solutions for an infinite slab and an infinite cylinder.

Cleland (1989) stated that the difference between analytical predictions and experimental results is due to the net effect of experimental error in data collection, thermal property data

error, and use of the prediction methods beyond their range of applicability (e.g. constant conditions, uniform initial temperature, homogeneous product, and regular shape are assumed). He suggested that factors that could introduce error should be identified, and quantitative guidelines relating the extent of error to the type of approximation used should be developed. Numerical methods could be used to supplement experimental data, so there was no need for an excessively large number of experiments when attempting to establish such guidelines (Cleland, 1989).

2.2.2 Empirical Solutions

The analytical methods often have limited value in industrial practice because the conditions imposed during their derivation cannot be satisfied by many products. For example, there are no exact analytical methods that apply to irregular shapes with the third kind of boundary condition. A number of researchers have proposed empirical prediction methods to extend the use of an analytical method beyond its range of applicability. The key to developing most such empirical methods is that after a certain amount of time has elapsed in a heating or cooling process (the lag phase), the infinite series solution of equation (2.7) converges rapidly and the dimensionless temperature ratio can be evaluated accurately by use of only the first term in the series. For common situations, this occurs if sufficient time has passed such that $Fo > 0.2$ ($Fo = \alpha t / R^2$) and thereafter the temperature at the thermal centre decreases with time in an exponential fashion, often called the 'regular regime' or 'constant half-life' period. The general form of the resulting equation is:

$$Y_c = \frac{(T_c - T_a)}{(T_{in} - T_a)} = j_c \exp\left(-\frac{2.303 t}{g}\right) = j_c \exp\left(-\frac{0.693 t}{t_{0.5}}\right) \quad (2.18)$$

$$Y_{av} = \frac{(T_{av} - T_a)}{(T_{in} - T_a)} = j_{av} \exp\left(-\frac{2.303 t}{g}\right) = j_{av} \exp\left(-\frac{0.693 t}{t_{0.5}}\right) \quad (2.19)$$

where Y_c = fractional unaccomplished temperature change at thermal centre
 Y_{av} = fractional unaccomplished temperature change for mass-average
 j_c = centre position lag factor
 j_{av} = mass average position lag factor
 g = time for a 90 % reduction in Y (s) = $3.3222 t_{0.5}$

$t_{0.5}$ = half life time, the time taken for Y to be halved (s)

The lag factor, j , is a function of the geometry, thermal conductivity, thermal diffusivity, surface heat transfer coefficient, Biot number, and Fourier number (Wade, 1984). The lag time is the time taken for the single term equation to reduce Y from j to 1.0 (Cleland & Earle, 1982). If $Bi > 0.2$, the product internal temperature gradient can be appreciable as well as varying with time (Mohsenin, 1980). The mean temperature of the interior is, therefore, quite different from the surface temperature. The lag factor, j , is greater than 1 towards the interior, and less than 1 near the surface. The surface value of j tends to 0 as h_c tends to ∞ (Hicks, 1955). The values of g and j_c are also a function of object weight and cooling medium velocity (Schneider *et al.*, 1982; Stermer *et al.*, 1984, 1986; Haas & Felsenstein, 1985; James & Bailey, 1986; Gigiel & Creed, 1987).

Equations (2.18) and (2.19) have been proposed as a generally applicable prediction method for irregularly shaped objects of homogeneous composition cooled with the third kind of boundary condition. For infinite slabs, infinite cylinders and spheres the values of g , $t_{0.5}$, j_c , and j_{av} , which are functions of Biot number and shapes, can be calculated from the analytical solutions (equation 2.7). For other shapes, the values of g , $t_{0.5}$, j_c , and j_{av} can be found from the experiments by plotting either $\ln Y_c$ or $\ln Y_{av}$ versus time. The slope yields a value of g or $t_{0.5}$, and the intercept, if extrapolated back to $t = 0$, a value of j_c or j_{av} . Values obtained in this manner apply only to that product, of the size, shape and composition used in the experiments, and for the particular surface heat transfer coefficient used experimentally.

Pflug and Kopelman (1966) used equations (2.18) and (2.19) to develop charts for estimating the g , j_c , and j_{av} values for spheres, infinite cylinders and infinite slabs, when Biot number and thermal diffusivity are known. Solutions for other finite shapes may be obtained from those of the sphere, infinite slab, and infinite cylinder. For a solid of finite shape with heat transfer in three directions after $Fo > 0.2$, the composite solutions are:

$$\frac{1}{g_{composite}} = \frac{1}{g_1} + \frac{1}{g_2} + \frac{1}{g_3} \quad (2.20)$$

$$j_{c,composite} = j_{c,1} j_{c,2} j_{c,3} \quad (2.21)$$

$$j_{av,composite} = j_{av,1} j_{av,2} j_{av,3} \quad (2.22)$$

where subscripts 1, 2 and 3 refer to the 3 space dimensions and *composite* refers to the overall shape.

However, use of the charts is limited to geometrically simple shapes. Since the values of g , $t_{0.5}$, j_c , j_{av} are functions of Biot number and shape to make equations (2.18) and (2.19) more general, there is a need for development of shape factors that allow values of g , $t_{0.5}$, j_c , j_{av} to be determined for any shape and Biot number combination (Cleland, 1989). A possible shape factor is the surface area to volume ratio, AR/V , which is applicable to all regular and irregular shapes. It comes from equations (2.18) and (2.19) for the case of $Bi \rightarrow 0$, but it is not Biot number dependent, as it would need to be accurate (Cleland, 1989).

Fikiin and Fikiina (1971) used AR/V as a shape factor, irrespective of the Biot number, in Fikiin's chilling time prediction method:

$$t = \frac{V}{AR} \frac{\rho CR^2}{k} \left(\left(\frac{2.3}{Bi} + 0.8 \right) \ln \left(\frac{T_{in} - T_a}{T - T_a} \right) + 0.12 \right) \quad (2.23)$$

This method had a similar form to those of Baehr (1953) and Rutov (1958). However, the method would lose accuracy at high values of Biot number (Cleland, 1989). For $Bi \rightarrow \infty$, Smith & Nelson plus co-worker (Smith *et al.*, 1967, 1968; Clary *et al.*, 1968, 1971; Smith & Nelson, 1969) introduced a geometry index, G , which was a ratio of the slopes of the semi-log plots of Y versus Fo for the real shape and a sphere at $Bi = \infty$. That is:

$$G = \frac{\beta_1^2}{\pi^2} \quad (2.24)$$

Use of the geometry index allowed charts based on the analysis for a sphere to be used to make predictions for other shapes. For rectangular bricks of dimension the G value is given by:

$$G = 0.25 \left(1 + \left(\frac{L_x}{L_y} \right)^2 + \left(\frac{L_x}{L_z} \right)^2 \right) \quad (2.25)$$

For elliptical shapes with axis lengths of L_x , L_y , and L_z (where L_x is the shortest diameter) the

G value is found using:

$$G = 0.25 \left(1 + 0.375 \left(\frac{L_x}{L_y} \right)^2 + 0.375 \left(\frac{L_x}{L_z} \right)^2 \right) \quad (2.26)$$

Irregular shapes were related to the nearest equivalent ellipsoidal model shape that had equal orthogonal cross-sectional areas. A shortcoming of G is that it is not Biot number dependent (Cleland, 1989).

Smith *et al.* (1967) and Clary *et al.* (1971) tested their method for cooling of hams at values of Reynolds Number from 4,000 to 46,000, and found good agreement. Lin (1994) found the performance deteriorated at low Bi .

Cleland & Earle (1982) introduced a shape factor called the equivalent heat transfer dimensionality (E) which was available as a variable, and was Biot number dependent. They used a half-life method ($t_{0.5}$ value) instead of the g method (g value). The Fourier number corresponding to the half-life time ($Fo_{0.5}$) was introduced and this parameter ($Fo_{0.5}$) was changed according to the geometry and Biot number. Empirical equations for calculating E for regular and irregular shapes were suggested. The method accuracy was assessed across widely ranging conditions and the 95% confidence bounds were $\pm 12\%$.

Lin (1994) developed relationships for E that covered a wide range of heat transfer environmental conditions and multi-dimensional regular and irregular geometries. He used actual measurements of the three dimensions of an irregular geometry to define the dimensional ratios for an equivalent ellipsoid. The empirical equation for calculating E fitted experimental data he collected within the experimental uncertainty.

Another alternative is to define an 'equivalent model shape'. The sphere, infinite cylinder or infinite slab which has the closest shape to the real shape can be chosen to be the analogous object and then an equivalent radius R is defined such that the predicted chilling time is close or equal to the experimental chilling time of the real shape. Earle & Fleming (1967) used a cylinder as the analogous shape for lamb carcasses. Wade (1984) used an infinite slab as the analogous shape for pallets of cartons, and spheres as analogues for individual fruit pieces. The disadvantage of this procedure is that some experimental work is required before any

prediction can be made and for some products (e.g. strawberries, pears, and kiwifruit) it might be difficult to define shortest dimension unambiguously (Cleland, 1989).

Hayakawa (1970, 1971) applied the concepts of g and j values to instances where the conditions of equation (2.7) could not be met (i.e., products of complex shape, variable ambient temperature), or where the thermophysical properties were not known. Since ambient temperature varied with time, he considered new g and j values at each time interval. Substantial computation effort for calculating the temperature change within each time interval was needed.

2.2.3 Numerical Solutions

Fourier's law (equation 2.4) can be solved numerically by finite difference or finite element techniques. Such solutions are not subject to any of the restrictions of the analytical solution, e.g. numerical methods can be applied to food products which are not truly regular in shape, are not perfectly homogeneous, and for which thermal properties change with temperature or time. Applications of numerical methods can be considered in two groups: situations with the third kind of boundary condition, and situations with other boundary conditions.

Cleland (1989) summarised five common finite difference schemes: explicit finite difference scheme, Crank-Nicolson scheme, Lees scheme, enthalpy transformation method, and the implicit method, all of which are applicable to chilling. Each scheme has its own advantages and disadvantages. The explicit finite difference scheme is straight forward but its use is limited by stability criteria which restrict the time increment. Fully implicit and Crank-Nicolson type finite difference schemes can result in sets of non-linear equations which require iterative methods of solution, but the Lees scheme can overcome these difficulties (Mannapperuma *et al.*, 1988). However, for all schemes, provided data are accurate and sensible time and space steps are chosen, the prediction can be very accurate. Similarly, finite element schemes, if correctly implemented, will be very accurate. If the change in thermal properties with temperature is sufficiently small to be ignored, the enthalpy transformation finite difference method simplifies to the explicit method and this scheme is as satisfactory as the Lees or Crank-Nicolson schemes (Cleland, 1989). Although finite difference schemes are potentially useful for chilling (or heating) of irregular shapes, the finite element method

is usually preferred because of the ease with which it handles irregular geometry (Cleland, 1989).

Lovett (1988) used the one-dimensional Lees scheme for a slab to predict the chilling times of sides of beef. The predictions were considered adequate, taking into account data uncertainties.

De Baerdemaeker *et al.* (1977) demonstrated the application of a two-dimensional axisymmetrical finite element scheme (giving a three-dimensional model) to the chilling of a pear. No experimental verification was given. Arce *et al.* (1983) used a two-dimensional finite element scheme with triangular simplex elements to model chilling of the loin of sides of beef. Six experimental temperature/time profiles for different sides were presented and the predictions were in good agreement.

2.3 CHILLING WITH INTERNAL HEAT GENERATION BUT NO EVAPORATION

2.3.1 Description of Internal Heat Generation by Respiration

Since horticultural products are still living after they are harvested, they continue to carry out their normal life process of respiration. This process involves the intake of oxygen which reacts with sugars in the product to produce carbon dioxide, water, and heat. This heat accumulates in the product and will raise the temperature of the product unless it is removed by heat transfer from the product. Even in stable storage conditions the temperature is not necessarily that of the surrounding air. It may be somewhat higher, depending on the relative magnitudes of internal heat generation, and heat loss from the product surface.

Hayakawa & Succar (1982) summarized models to describe how the rate of internal heat generation by respiration changes as a function of time after harvesting until it reaches an equilibrium rate, and how it changes with temperature within a range of temperature specific to each fresh produce (Lutz & Hardenburg, 1968; Willis & McGlasson, 1971; Wu & Salunke, 1975; Gaffney & Baird, 1975, 1977; Anon., 1977; Buescher, 1979; Fukushima *et al.*, 1980; Kusunose & Sawamura, 1980). It is possible that the produce ceases to generate heat at temperatures outside the range of applicability, because of metabolic damage to the tissue,

or the heat may be generated at abnormal rates when the produce suffers from cold injury.

2.3.2 Analysis of Cooling with Internal Heat Generation

In attempting to predict chilling rate, food products with residual biochemical activity may require different treatment to those in which residual biochemical activity is negligible. For products with a high rate of internal heat generation, and for conditions of very slow cooling, and for a desired final temperature very close to that of the cooling medium, considerations of the internal heat generation may be important for chilling rate to be accurately predicted (Hicks, 1955; Gaffney *et al.*, 1985b). The effects of internal heat generation are much less when the air flow rate past the product is high (Chau *et al.*, 1988). The internal heat generation is easily transferred out to the air so that the surface temperature of the product is usually close to the air temperature, regardless of the rate of respiration. Cleland (1989) stated that rates of heat removal during industrial food chilling processes are typically in excess of 2 W/kg of product, and can be 5-20 W/kg. In comparison, rates of heat generation by respiration are often as low as 0.01-0.05 W/kg. As a result there are few industrial situations in which the internal heat generation significantly slows the chilling process (Awberry, 1927; Hood, 1964).

Meffert *et al.* (1971) used a non-temperature-dependent heat generation description to allow derivation of an analytical solution for cooling of an infinite slab. Hayakawa (1978) observed that heat generation due to produce respiratory activity strongly influenced internal temperature distribution, but did not significantly affect surface heat transfer during a 20-hour cooling process. Alyamovski (1974) developed an analytical solution for cooling of an infinite slab with an internal heating rate described by an exponential law. The equation is not algebraic in form and requires numerical integration for solution.

Alternatively, temperature-dependent heat generation can be modelled using finite differences or finite elements. Jiang *et al.* (1987) developed an axisymmetric finite element model to simulate the temperature field of the stalk of broccoli in a forced-air cooling process. From the broccoli shape, the stalk had the smallest surface-to-volume ratio among other parts of the broccoli head, so it is assumed to be the critical part during cooling. The beads were assumed to be responsible for most of the moisture loss, therefore, moisture transfer from

the stalk was assumed to be zero. An equation for broccoli respiration (Hayakawa, 1978) was modified using data from Anon (1981) to establish a non-zero heat generation rate at 0 °C. The temperature, predicted by the simulation model (with experimentally determined property values), was within 1.1 °C of measured values. They commented that the simulation accuracy is affected by many factors (surface evaporative cooling, respiratory activity, axisymmetric simplification of stalk geometry in the model, variation of the thermal properties, and possible violation of the assumption of uniform initial stalk temperature).

Another alternative is to use the analytical or prediction methods for no heat generation, but with the data compensated to account for respiration. For example, the cooling medium temperature used in calculations can be raised by an amount denoted the 'approach temperature', for which data are given by Sainsbury (1985).

2.4 COOLING INCLUDING RADIATION

Although the third kind of boundary condition (equation 2.6) covers many situations in which objects are frozen or chilled, the major exceptions are those in which radiation and/or evaporative heat loss are major components of the total heat flow from the object surface (Cleland, 1989). In cases where the surface temperature is significantly different from the air temperature (e.g. products having high rates of moisture loss or high rates of internal heat generation), the effects of radiation transfer can be significant (Chau *et al.*, 1988). However radiation can often be combined with convection in the surface heat transfer coefficient rather than requiring separate consideration (Cleland, 1989).

2.5 COOLING INCLUDING EVAPORATION

2.5.1 Moisture Transport Phenomena

Moisture loss from a product can be considered as the result of two phenomena: (1) migration of moisture within the body to its surface; and (2) transfer of the vapour at the surface to the surrounding air (Bonacina & Comini, 1971). The moisture transfer mechanisms within a product are (Van Arsdel, 1963):

- (1) liquid movement under capillary forces;

- (2) vapour diffusion in air-filled pores caused by a partial pressure gradient; and
- (3) molecular diffusion due to a concentration gradient.

Where it occurs, capillary action is the dominant mechanism for products with higher moisture content (Krischer & Mahler, 1959; Van Arsdell, 1963; Luikov, 1966; King, 1968), because water transport is in the liquid phase only and relatively rapid. Vapour diffusion is usually significant only with lower product moisture contents. Molecular diffusion would, usually, be limited to capillaries with molecular dimensions and because it is slow, its contribution to the total moisture migration within the body would be small if capillary action also occurs to any significant extent. Since many food materials are solids with capillary structure, capillary action is often the leading mechanism (Bonacina & Comini, 1971). In contrast, diffusion is slow and typically all the water is lost from the outside few millimetres of the product (Lovett *et al.*, 1976; Fulton *et al.*, 1987).

At the surface, heat is required to provide the latent heat of evaporation for the water. The rate of heat flow and the rate of moisture loss depend on a variety of conditions. The evaporation rate also relates to the transport of water inside the product. Radford *et al.* (1976) found that the rate of evaporation from slabs of meat was initially the same as that from a fully wetted surface, but that the surface dried rapidly. The evaporation declined progressively until equilibrium was reached between the evaporation rate and the rate of movement of water to the surface from the underlying tissues. As cooling proceeded, the partial pressure driving force for evaporation diminished until the diffusion transport rate exceeded the evaporation. The surface progressively re-wetted and the evaporation rate then once more approached that for a wetted surface. Surface fat or skin acts as an effective barrier to the water diffusion and therefore restricts weight loss (Gigieli *et al.*, 1989).

2.5.2 Modelling of Evaporative Heat Transfer at the Product Surface

When evaporation is considered in the boundary condition for heat transfer, it is often necessary to include the mass transfer of water by diffusion or capillary action within the product as part of the model (Comini & Lewis, 1976; Radford *et al.*, 1976; Cleland, 1989). For regular shapes this can be accomplished by linking finite difference calculations for diffusion with finite difference calculations for heat conduction (Cleland, 1989).

Weight loss in a horticultural product is a combination of the rate of carbon loss due to the evolution of carbon dioxide arising from respiration particularly during storage and the rate of moisture loss. In cooling, the carbon loss is usually an insignificant part of the total weight loss, except in cases where moisture loss rates are very low. The rate of water vapour flow (the rate of moisture loss from the product) can be described as follows (Chau *et al.*, 1985; Cleland, 1989):

$$m = KA(p_J - p_a) \quad (2.27)$$

$$p_J = a_w p_{wJ} \quad (2.28)$$

$$p_a = p_{wa} H_r \quad (2.29)$$

- where m = evaporation rate ($\text{kg s}^{-1} \text{m}^{-2}$)
 K = overall mass transfer coefficient ($\text{kg s}^{-1} \text{m}^{-2} \text{Pa}^{-1}$)
 a_w = surface water activity (vapour pressure lowering effect due to the presence of solute in the product moisture)
 p_J = partial pressure of water vapour at evaporating surface (Pa)
 p_{wJ} = (saturation) vapour pressure of pure water at the evaporating surface temperature (Pa)
 p_a = partial pressure of water vapour in the surrounding air (Pa)
 p_{wa} = (saturation) vapour pressure of pure water at the surrounding air temperature (Pa)
 H_r = air relative humidity

The evaporation rate is normally numerically small in size (Lutz & Hardenberg, 1968; Bonacina & Comini, 1971). The partial pressure exerted by water vapour in the surrounding air is a direct function of the dry bulb temperature and relative humidity of the air. The partial pressure of water vapour in the boundary layer at the evaporating surface is a function of temperature at the product surface and the surface water activity.

If the ambient temperature is below the product temperature, a large vapour pressure difference exists, and the moisture loss may be expected to be rapid. In the early stages of chilling, air relative humidity has little effect on weight loss, and the temperature difference between the surface and the air is acting as the main driving force for evaporation. However,

during the later stages of cooling and in subsequent storage, the effect of humidity can be substantial (Brown & James, 1992; Pham & Willix, 1985).

An alternative description is a dew point model. If product temperature is the same as the air dew point temperature then there is no driving force for either water condensation or evaporation. If product temperature is below the air dew point, condensation occurs, whereas if it is above the air dew point, evaporation occurs (Patel *et al.*, 1988).

Water activity is closely related to physical, chemical and biological properties of products but also depends on moisture content (Troller & Christian, 1978; Chirife & Fontan, 1982). The water activity can be used to describe the variation of surface dryness throughout the cooling process. As evaporation proceeds the surface moisture becomes depleted, so the water activity changes with time (Comini & Lewis, 1976; Radford *et al.*, 1976; Sastry *et al.*, 1985; Balaban, 1989; Cleland, 1989). In modelling, the major difficulty is knowing how the product water activity varies with water concentration at the product surface and in obtaining accurate data for water movement through the solid (Cleland, 1989).

Van Beek (1983, 1985) stated that the mass transfer coefficient could not be considered as a constant product property. In his experience it changed with temperature and in circumstances with little air movement, it could vary with position on a surface. Since the skin of horticultural products is permeable to water vapour, Chau *et al.* (1985) proposed that the mass transfer coefficient (K) be determined from two variables, the skin coefficient (K_s) and the air film coefficient (K_a) as follows:

$$\frac{1}{K} = \frac{1}{K_s} + \frac{1}{K_a} \quad (2.30)$$

where K_s = skin mass transfer coefficient ($\text{kg s}^{-1} \text{m}^{-2} \text{Pa}^{-1}$)

K_a = air film mass transfer coefficient ($\text{kg s}^{-1} \text{m}^{-2} \text{Pa}^{-1}$)

It would be more general to include a packaging mass transfer coefficient, K_p , as well:

$$\frac{1}{K} = \frac{1}{K_s} + \frac{1}{K_a} + \frac{1}{K_p} \quad (2.31)$$

where K_p = packaging mass transfer coefficient ($\text{kg s}^{-1} \text{m}^{-2} \text{Pa}^{-1}$)

2.5.3 Evaluation of Mass Transfer Coefficients

The air film mass transfer coefficient, K_a , can be measured; for meat, James *et al.* (1988b) related it to air velocity. K_a is often determined from the convection heat transfer coefficient using the well-known Lewis relationship (Cleland, 1989). However, it is sometimes difficult to obtain accurate data for K_a because it is dependent upon the size of the product as well as the properties and flow rate of the surrounding air. There are situations where the resistance attributed to K_a may play only a minor role except in the initial stages of moisture loss (Pham & Willix, 1984), but it can be a significant portion of the total resistance for products with a relatively high skin mass transfer coefficient, K_s . However, for horticultural products with skins, at high airflow rate, the influence of K_a can be neglected (Chau *et al.*, 1988) and the overall mass transfer coefficient can be approximated by

$$\frac{1}{K} \approx \frac{1}{K_s} + \frac{1}{K_p} \quad (2.32)$$

The skin coefficient (K_s) is dependent upon the structure and properties of the product skin. It depends only on the condition of the product surface and is independent of the air flow rate or the air relative humidity. For fruit and vegetables measurements of K_s can be sensitive to internal heat generation at high temperature and humidity. Chau *et al.* (1985) suggested that at high airflow rate, K_s can be more accurately determined because the effect of internal heat generation is less and the surface temperature is very close to the air temperature due to high rates of convection.

Chau *et al.* (1988) used horticultural products to study effects of air flow rate and relative humidities on the mass transfer coefficient under conditions of still air and forced air flow. They presented data for K under still air conditions, and for K_s under forced-air flow conditions. Sastry (1985) studied factors affecting these two parameters.

Fockens and Meffert (1972) used a mathematical model to explain the relation between biophysical properties of the skin of products and the rate of moisture loss under difference ambient air conditions. However, they neglected the effect of evaporative cooling. They classified product surfaces as follows:

- (1) a wet surface, being a surface covered with a thin layer of water or air saturated with water vapour; (only K_a is being considered).

- (2) a wet surface covered by a porous layer, the pores being filled with air; (both K_a and K_s are considered).
- (3) a surface covered by a layer which is impervious to water vapour; (the overall mass transfer resistance is very high).
- (4) a surface which is a combination of the surfaces 1, 2 and 3.

Levy (1986) included in his model a 'resistance coefficient to evaporation' which had a value of 1.0 for a wetted surface, and greater than 1.0 for surface of a meat which was covered by fat or skin. This was an equivalent to K_s .

Patel *et al.* (1988) related mass transfer coefficient and microbial activity on the surface of selected perishables, as a function of storage temperature, relative humidity and time. At high humidity, an observed gradual increase in mass transfer coefficient with decreasing water vapour difference over time might have been due to increased microbial activity at the surface (Patel *et al.*, 1988).

2.5.4 Influence of Product Shape

The influence of product shape is primarily associated with the ratio of surface area to volume of the product. High surface-area products present more avenues for moisture loss than products with low surface areas, as noted by Apeland and Baugerod (1971). A secondary effect of product shape relates to its effect on boundary layer resistance, thereby affecting the contribution of this component to the overall resistance, as has been noted by Villa (1973). For products with skins, the alteration of boundary layer characteristics is likely to produce only a small effect, since the major portion of the resistance term is accounted for by the skin resistance. For products that approximate free water surfaces, the effect may be considerable. Pasternak & Gauvin (1960), Skelland & Cornish (1963), and Pham & Willix (1984) showed that, providing an appropriate value of the characteristic dimension is taken, the actual shape is of minor significance in modelling chilling with evaporation.

2.5.5 Contribution of Evaporation to Chilling Rate

When products are losing moisture, heat is required to provide the latent heat of evaporation

for the water, meaning that the temperature of the wet surface is affected not only by the temperature of the surrounding air, but also by the cooling effect due to evaporation (Chau *et al.*, 1985). The effect of surface evaporation on the overall energy transfer can be significant, especially at low air humidities (Srinivasa *et al.* 1976; Abdul Majeed *et al.*, 1980), since a high rate of moisture loss occurs resulting in increased evaporative cooling. Feldman (1976), working with spheres made of ice, found that water evaporation produced an additional cooling of 16 % when the air velocity was 2 ms^{-1} and 22 % when air velocity was 4 ms^{-1} .

2.5.6 Effect of Internal Heat Generation

Sastry & Buffington (1982) and Gaffney *et al.* (1985b) stated that the evaporative cooling effect at higher vapour pressure difference is generally much greater than that of respiratory heat generation. Thus the surface temperature for both respiring and nonrespiring products are generally lower than ambient temperature.

Under saturated storage conditions, nonrespiring commodities would lose no water or gain some moisture, depending on the water activity. Respiring commodities, however, could continue to lose water under saturated storage conditions due to the respiratory heat generation raising the surface temperature above the ambient value (Srinivasa Murthy *et al.*, 1976; Sastry *et al.*, 1978; Gaffney *et al.*, 1985b; Sastry, 1985).

2.5.7 Steady State Models for Moisture Loss with and without Internal Heat Generation

Products held in constant environmental surroundings will eventually reach a steady-state temperature condition, yet heat and mass transfer will continue to take place due to respiratory heat generation and evaporation of moisture at the product surface.

The steady state model developed by Chau *et al.* (1985) was stated earlier as equations (2.27)-(2.29). Chau & Gaffney (1985) developed a model to predict temperatures of products having shapes of a sphere, infinite cylinder or infinite slab:

$$T_J = \frac{QV}{h_c A} + T_a - \frac{\epsilon_{fg} m}{h_c} \quad (2.33)$$

where Q = respiration rate ($W\ m^{-3}$)
 T_J = surface temperature of solid (K or °C)
 T_a = surrounding cooling medium temperature (K or °C)
 ϵ_{fg} = latent heat of vaporisation of water ($J\ kg^{-1}$)
 m = rate of moisture transfer ($kg\ s^{-1}\ m^{-2}$)

They also presented equations to calculate the mean temperature in the product, and the temperature at any point in the product. An iterative procedure was used to calculate the final product surface temperature and resultant moisture loss rate as a function of product size, air velocity, temperature, and relative humidity of the surrounding air.

Sastry & Buffingtons (1982, 1983) developed a mathematical model for predicting evaporating surface temperature and the steady state evaporation rate of stored perishable commodities, particularly tomatoes. In their mathematical model, the effect of latent heat of vaporization was included and the rate of respiratory heat generation was added at the evaporating surface. For spherical products with skin (e.g. tomatoes, apples), the equations for the moisture transfer and surface temperature were:

$$m = \frac{(p_J - p_a)}{\frac{\tau}{\delta\Phi} + \frac{1}{K_a}} = \frac{(p_J - p_a)}{\frac{1}{K_x} + \frac{1}{K_a}} \quad (2.34)$$

$$T_J = T_a - \frac{(\epsilon_{fg} m_p - QR)}{C m_p} \left(\exp\left(\frac{C m_p \tau}{k}\right) - 1 \right) \quad (2.35)$$

For a spherical product with no skin (e.g. mushrooms, Brussels sprouts), the surface temperature was:

$$T_J = T_a - \frac{\left(\epsilon_{fg} m_p - \frac{QR}{3}\right)}{h_c} \quad (2.36)$$

where K_x	=	equivalent transpiration coefficient = $\delta\Phi/\tau$ ($\text{kg s}^{-1} \text{m}^{-2} \text{Pa}^{-1}$)
m_p	=	rate of moisture loss per unit pore area ($\text{kg s}^{-1}\text{m}^{-2}$)
τ	=	skin thickness (m)
δ	=	diffusion coefficient of water vapour in air ($\text{m}^2 \text{s}^{-1}$)
Φ	=	the fraction of fruit surface area covered by pores
R	=	radius of the spherical product (m)

2.5.8 Analytical and Empirical Models for Moisture Loss during Chilling

Pham (1987) developed a mathematical model to estimate moisture loss by using elementary psychrometry. The assumptions he made were uniform temperature (with no internal gradient) and wetted product surface ($a_w = 1$). He found from his model that if the temperature was not uniform, the surface temperature tended to change more rapidly than the mean temperature and the moisture loss would be reduced. If the surface was not fully wetted, the moisture loss would be reduced.

Patel & Sastry (1988) developed three-dimensional finite element models to predict moisture loss behaviour of apples, tomatoes, and mushrooms under fluctuating temperature conditions. To represent a fluctuating environmental temperature, they used time-dependent convective boundary condition and temperature-dependent heat generation.

2.5.9 Analytical and Empirical Chilling Time Prediction Methods

Although the amounts of moisture lost by evaporation may be small compared with the total moisture contents of product, a large amount of heat is consumed for the evaporation of the moisture (Hayakawa, 1978). This evaporation significantly alters the rate of chilling, makes the cooling curves ($\ln Y$ versus Fo) non-linear and changes the slope and intercept of such plots. Some researchers (Schneider *et al.* 1982; James & Bailey, 1986; Gigiel & Creed, 1987), worked at very high relative humidity and a_w close to 1 to reduce these problems. Gigiel & Creed (1987) tried to correlate air velocity and carcass weight against the slope and intercept of a straight line transformation of the cooling curve but the predictions were not accurate. Schneider *et al.* (1982) used a similar technique to correlate weight and fat to slope and intercept. However, the result was still not accurate.

The effect of evaporation can be included indirectly in a solely heat transfer equation. For example, the analytical method for the third kind of boundary condition might be used with the adjusted values for the surface heat transfer coefficient and external medium temperature to predict chilling time. These adjusted values would be chosen to compensate for the evaporation (Cleland, 1989). Since the wet bulb temperature couples the effect of the dry bulb temperature and relative humidity in a single parameter, several researchers have used wet bulb temperature as the reference temperature in their work (Abdul Majeed *et al.*, 1980; Badari Narayana & Krishna Murthy, 1981; Abdul Majeed, 1982; Narasimha Rao *et al.*, 1993). Abdul Majeed *et al.* (1980) proposed that the factors affecting cooling rate were Biot number, wet bulb temperature, Fourier number, and initial product temperature. They developed curve-fitted correlations which yielded better agreement with experimental results than the conventional Heissler and Gurnie-Lurie charts given by McAdams (1954). Earle and Fleming (1967) used the air wet bulb temperature in place of dry bulb temperature in making predictions for chilling of lamb, based on the premise that the lamb surface water activity would remain close to 1.0.

Devres (1989) developed an analytical method that included the effects of evaporative cooling, product heat generation, and convection and radiation at the surface of the sphere. He used a lumped-heat-capacity method and turned the non-linear differential equation into a linear equation using regression analysis. The heat generation equation and the rate of weight loss were assumed to be functions of temperature only and were then curve -fitted by a second order polynomial. He used a_w of 0.98 (for fruit and vegetables) and storage conditions of 0 °C and 90 % air relative humidity. The analytical solutions were complicated by the variation of coefficients in different temperature regions and there was no experimental test.

Based on fit to finite element simulations, Mallikarjunan & Mittal (1995) developed regression equations to predict the centre temperature and mass loss of beef carcass as function of carcass fat cover thickness, initial carcass mass, air velocity, ambient temperature, and relative humidity. Temperature predictions were within ± 2 °C and mass loss prediction were within ± 1 %.

2.5.10 Numerical Chilling Time Prediction Methods

Radford *et al.* (1976) used explicit finite differences to simulate convective and diffusional transport of heat and mass in meat. They used the water activity as the 'availability' of water at the evaporating surface which depended on the water content of the product, then linked finite difference calculations for diffusion with finite calculations for heat conduction. The model gave close agreement between simulated and experimental results at various air flow rates. James *et al.* (1988a) used similar techniques and products. They found that changing the water diffusivity and the heat and mass transfer coefficient combination had a large effect on weight loss. Morley (1972) and Fulton *et al.* (1987) found that temperature and humidity fluctuations have far less effect on weight loss, and any apparent effect is caused by changes in the mean conditions.

The definition of enthalpy potential (Stoecker, 1977; Mannapperruma & Singh, 1988) uses the overall enthalpy change to include latent heat as well as sensible heat effects. Whenever a continuous water film is assumed to exist at the product surface (or $a_w = 1$), the energy transfer at the liquid-air interface is (Srinivasa Murthy *et al.*, 1974, 1976; Abdul Majeed *et al.*, 1980):

$$\phi = \frac{h_c A (\epsilon_a - \epsilon_s)}{C_{air} + H_{air} C_v} \quad (2.37)$$

- where ϕ = surface heat flow (W)
 ϵ_a = enthalpy of cooling air (J kg⁻¹)
 ϵ_s = enthalpy of saturated air evaluated at the product surface temperature (J kg⁻¹)
 C_{air} = specific heat of dry air (J kg⁻¹ K⁻¹)
 H_{air} = absolute humidity of the ambient air (kg water kg⁻¹ dry air)
 C_v = specific heat of water vapour (J kg⁻¹ K⁻¹)

The enthalpy of saturated air as a function of the temperature can be approximated by a second degree polynomial (Stoecker, 1977). Hence, the total evaporative and convective heat flow could be written in solely heat transfer terms.

Srinivasa Murthy *et al.* (1974) used this formulation to simulate simultaneous heat and mass transfer in slab-shaped moist food products. They considered the change in temperature with

time and with position within the product. Their model used the heat balance integral method of Goodman (1964) and Ozisik (1968). Srinivasa Murthy *et al.* (1976) also extended this kind of analysis to products of cylindrical and spherical shapes. The solution for the case of spherical products was obtained by converting the problem into that of an equivalent slab by suitable transformation and then applying Goodmans integral technique (Goodman, 1964; Ozisik, 1968). In the cylindrical case numerical evaluation, by using Crank-Nicolson finite difference schemes to generate data, was required to prepare look-up charts. Predictions were compared to experiments with a cylindrical model food gel, but agreement was not good. Abdul Majeed *et al.* (1980) adopted the enthalpy technique and used the finite difference technique to simulate the coupled effects of heat and mass transfer in rectangular, spherical and cylindrical objects. The enthalpy of unsaturated air was represented by the enthalpy of saturated air at the wet bulb temperature of the air. The cooling rates were presented in the form of charts. The theoretical predictions yielded good agreement with experimentally determined time-temperature histories but only limited testing was reported. Badari Narayana *et al.* (1981) used a similar enthalpy technique for a slab, and tested a proposed mathematical model in a simple experiment where one side of a moist product was exposed to constant heat flux and the other side to the ambient air. They used time-temperature curves to study the effects of dry bulb temperature, modified Biot number, wet bulb temperature, initial temperature, and Kirpichev number. A modified Grashof number was introduced to obviate the difficulty of surface temperature varying with time. A Crank-Nicolson implicit finite difference scheme was used to solved the equations, and a backward difference analog was used for the non-linear boundary condition to avoid oscillations (Von Rosenberg, 1969).

Anasari and Afaq (1986) suggested that whenever moisture evaporation was occurring from the product surface, its total heat loss would be a function of the enthalpy potential which existed between the product surface and the cooling air, since evaporation is significant during the initial stages but becomes negligible later. Computations were made with simultaneous heat and moisture transfer up to the half cooling time and with pure convection heat transfer afterwards. They used explicit finite differences to solve the model.

Abdul Majeed (1982) combined the advantages of the conventional air cooling and hydrocooling in a technique called air film cooling, to cool cylindrical food products. This technique resulted in faster cooling than hydrocooling. He neglected internal heat generation.

He used the enthalpy potential definition (equation 2.37) and polynomial expressions to relate air enthalpy to temperature. He used a backward difference scheme in a differential equation for a product and used an alternating direction implicit (ADI) scheme in a differential equation for a liquid film.

2.5.11 Incorporation of Internal Heat Generation in Numerical Prediction Methods

Hayakawa (1978) used the standard heat conduction equation with a term for internal heat generation. Convection and evaporation occurred at the surface of fresh produce assumed to be in the shape of an infinite slab. The rate of heat loss by evaporation was described in terms of parameters that could be related to the heat transfer analysis. He used an implicit finite difference method to solve the mathematical model, which was used to illustrate the influence of six physical and biological parameters on moisture loss and the transient temperature distribution within the product. These parameters were: rate of heat generation, surface conductance for heat transfer, mass transfer coefficient and environmental relative humidity, initial temperature, mean inactivation temperature, and local inactivation temperature (inactivation temperature is the temperature that all cells undergo irreversible damage and thus these cells do not produce internal heat generation).

Hayakawa and Succar (1982) used finite element techniques to develop a solution for cooling and moisture loss of spherically shaped produce with time-varying respiratory heat generation and temperature-variable density and thermal conductivity. The model also considered cases when condensation may occur on the product surface, and its effect on the mass transfer coefficient. They reported good agreement between the model and experimental results.

Chau and Gaffney (1990) included in their models, internal heat generation due to respiration, evaporative cooling due to evaporation, and radiative heat transfer due to a temperature gradient between the product and the surrounding. A non capacitance node at the surface was introduced and a finite difference method was utilized. The node allocation was illustrated using a spherical body. According to the investigators, the model is more accurate than currently used finite-difference models, could use larger time steps, and can be applied to non-spherical objects.

3. PRELIMINARY CONSIDERATIONS

The survey of the literature (Chapter 2) showed that methods taking into account the effect of evaporation on cooling do exist, but they often apply to only restricted circumstances. For example, many assume that the product surface is fully wetted ($a_w = 1$), and there is no skin resistance. To be realistic, a model should apply to a range of relative humidities, air temperatures, product thermal properties and product surface water activities. Whilst numerical methods can be applied widely, they are often less suitable for meeting the practical needs of food engineers than those methods which use only simple algebraic calculations based on easily understood variables such as air temperature, relative humidity and surface water activity. No method was found in the literature which covered a wide range of practical conditions, and could be applied using only simple algebraic calculations.

The objective of the present work was therefore to develop and test a simple prediction method with wide application. In practice the development of new methods is often incremental, each stage moving closer to the ideal goal. Therefore the programme for the present work was to conduct research in a set of in orderly steps as follows:

- (a) Development, on a theoretical basis, of an algebraic model that predicts chilling times for foods of simple geometry (one-dimensional heat transfer in an infinite slab, infinite cylinder, and sphere) subject to evaporative and convective cooling, but with constant surface water activity.
- (b) Independent environmental testing of this model in idealised systems in which the measurement environment could be closely controlled.
- (c) Investigation of means to extend the proposed model to situations that are less ideal. Possibilities included a wider range of geometries, variable surface water activity, presence of skins, and real rather than idealised food products. In practice there was only time to consider extension to one real food product, but this was investigated both with and without skin resistance. Variable surface water activity occurs in chilling of such products. Only one-dimensional (cylindrical) heat transfer was considered in this step.

The expected result of the research was an algebraic model that would accurately predict chilling times of foods in which only one-dimensional heat transfer occurred, subject to both convective and evaporative cooling (under constant conditions), and provided the surface water activity was either constant or varied within the range investigated experimentally.

Chapters 4 and 5 describe theoretical development for idealised conditions including assuming the surface water activity is constant. Chapters 6 and 7 describe independent experimental testing for model food systems. Chapter 8 describes experimental measurement in one real food system. Chapters 9, 10, and 11 describe how the test results for food were used to extend the model of Chapter 5 to less restricted circumstances.

4. THEORETICAL MODELLING OF IDEALISED SYSTEMS

4.1 INTRODUCTION

Whilst the overall aim of the work is to develop a simple chilling time prediction method, this does not preclude the use of numerical methods to help in the analysis. It was anticipated that accurate experimental data collection would be difficult so it was decided to use numerical methods to predict likely behaviour on a theoretical basis, and then base simple model development on fit to the numerically predicted results. The experimental data could then be used solely for model testing, and not for model development. Chapter 4 describes the numerical modelling carried out, the trends discovered, and discusses how the trends might provide insights for simple model development.

4.2 THEORETICAL DEVELOPMENT

4.2.1 Nonlinear Partial Differential Equations

Many, but not all, fruits and vegetables are cellular in structure and have homogeneous and uniform texture (Ansari, 1986). Many other products chilled industrially are also relatively homogeneous. Chilling of a homogeneous product can be considered as a heat transfer process with constant thermal properties, as the small variations in properties with temperature can usually be adequately handled by using averages (Cleland, 1989). Products can have a variety of shapes, and ideally any prediction methods should apply to a wide variety of possibilities. As has been outlined in Chapter 3, it was decided to limit the initial analysis to a small number of the most simple shapes, and to leave the possible extension to more complex shapes to a later time. Therefore, one dimensional analysis for three elementary shapes (infinite slab, infinite cylinder and sphere) was made. Further assumptions made were:

- (1) uniform initial product temperature
- (2) constant ambient conditions
- (3) constant thermal properties and surface water activity
- (4) no skin or packaging resistance.

These assumptions significantly simplify the modelling, but the model will have reduced ranges of applicability (as discussed in Chapter 3, the second part of the research sought to widen the range of applicability with respect to the two last assumptions).

4.2.1.1 Energy Balance

Because of the relatively poor thermal conductivity and considerable thickness of some products, conduction from the innermost tissues to the surface may be the controlling factor. At this condition ($Bi > 0.2$, especially at high air velocity), interior temperature varies with time and position. The basic law of heat transfer by conduction is given by Fourier's law:

(a) infinite slab ($-R \leq r \leq R$) with constant product thermal properties:

$$\rho C \frac{\partial T}{\partial t} = k \frac{\partial^2 T}{\partial r^2} \quad \text{for } t \geq 0 \quad (4.1)$$

(b) infinite cylinder ($0 \leq r \leq R$) with constant product thermal properties:

$$\rho C \frac{\partial T}{\partial t} = k \frac{\partial^2 T}{\partial r^2} + \frac{k}{r} \frac{\partial T}{\partial r} \quad \text{for } t \geq 0 \quad (4.2)$$

(c) sphere ($0 \leq r \leq R$) with constant product thermal properties:

$$\rho C \frac{\partial T}{\partial t} = k \frac{\partial^2 T}{\partial r^2} + \frac{2k}{r} \frac{\partial T}{\partial r} \quad \text{for } t \geq 0 \quad (4.3)$$

where ρC = volumetric specific heat capacity ($\text{J m}^{-3} \text{K}^{-1}$)
 k = thermal conductivity of solid ($\text{W m}^{-1} \text{K}^{-1}$)
 r = space position within solid (m)
 T = temperature of solid (K or °C)
 R = characteristic length for solid (radius of sphere or cylinder and half-thickness of slab) (m)
 t = time (s)

At the boundary $r = R$, for $t > 0$ energy transfer takes place due to the combined effect of heat and mass transfer. The temperature difference between the product surface and the free stream air acts as the driving force for the sensible heat transfer. The water vapour partial pressure difference between the bulk air and the boundary layer over the product surface causes evaporation of moisture at the surface resulting in the transfer of latent heat, and lowering of the surface temperature of the product (Gaffney *et al.*, 1985a). The boundary condition can be stated as:

$$\left(k \frac{\partial T}{\partial r} \right)_{r=R} = h_c (T_{r=R} - T_a) + K_a (p_{r=R} - p_a) \epsilon_{fg} \quad \text{at } r = R \text{ for } t \geq 0 \quad (4.4)$$

- where h_c = surface heat transfer coefficient ($\text{W m}^{-2} \text{K}^{-1}$)
 ϵ_{fg} = latent heat of vaporisation of water (J kg^{-1})
 K_a = air film mass transfer coefficient ($\text{kg s}^{-1} \text{m}^{-2} \text{Pa}^{-1}$)
 $p_{r=R}$ = partial pressure of water vapour in the boundary layer at the product surface (Pa)
 p_a = partial pressure of water vapour in the surrounding air (Pa)
 T_a = surrounding cooling medium temperature (K or $^{\circ}\text{C}$)
 $T_{r=R}$ = product surface temperature (K or $^{\circ}\text{C}$)

For the infinite slab, the temperature distribution is symmetrical around $r = 0$ so only half the thickness need be considered. Thus for all three shapes the other boundary condition can be stated at position $r = 0$.

$$\frac{\partial T}{\partial r} = 0 \quad \text{at } r = 0 \text{ for } t \geq 0 \quad (4.5)$$

For a uniform initial product temperature

$$T = T_{in} \quad 0 \leq r \leq R \text{ at } t = 0 \quad (4.6)$$

where T_{in} = initial uniform temperature (K or $^{\circ}\text{C}$)

To use equation (4.4) several terms require definition. The partial pressure of water vapour in the boundary layer over the product surface is defined by:

$$p_{r=R} = a_w p_{w(r=R)} \quad (4.7)$$

$$p_{w(r=R)} = f(T_{r=R}) \quad (4.8)$$

where a_w = water activity at product surface

$p_{w(r=R)}$ = (saturation) vapour pressure of pure water at product surface temperature $T_{r=R}$ (Pa)

The vapour pressure $p_{w(r=R)}$ is a function of the surface temperature only, and the surface water activity a_w is a function of the water concentration at the surface. The partial pressure of water vapour in the bulk air, p_a is given by:

$$p_a = H_r p_{wa} \quad (4.9)$$

where H_r = air relative humidity

p_{wa} = (saturation) vapour pressure of pure water at surrounding air temperature T_a (Pa)

4.2.1.2 Mass Balance

In practice a_w depends on the availability of water at the surface which is limited by the rate at which water can be transported from the underlying tissue (Radford, 1976). By assuming a_w is constant the model need not directly consider this water movement. Nevertheless, it was decided to formulate the model to include a description of diffusional mass transfer so that, if required at a later time, the assumption of constant a_w could be removed and replaced by a less restrictive alternative. The equations are:

(a) infinite slab ($-R \leq r \leq R$)

$$\frac{\partial c}{\partial t} = D \frac{\partial^2 c}{\partial r^2} \quad \text{for } t \geq 0 \quad (4.10)$$

(b) infinite cylinder ($0 \leq r \leq R$)

$$\frac{\partial c}{\partial t} = D \frac{\partial^2 c}{\partial r^2} + \frac{D}{r} \frac{\partial c}{\partial r} \quad \text{for } t \geq 0 \quad (4.11)$$

(c) sphere ($0 \leq r \leq R$)

$$\frac{\partial c}{\partial t} = D \frac{\partial^2 c}{\partial r^2} + \frac{2D}{r} \frac{\partial c}{\partial r} \quad \text{for } t \geq 0 \quad (4.12)$$

At the surface $r = R$

$$\left(D \frac{\partial c}{\partial r} \right)_{r=R} = K_a (p_{r=R} - p_a) \quad \text{for } t \geq 0 \quad (4.13)$$

For all three shapes, water concentration is symmetrical around $r = 0$.

$$\frac{\partial c}{\partial r} = 0 \quad \text{at } r = 0, t \geq 0 \quad (4.14)$$

For a uniform initial water concentration.

$$c = c_{in} \quad \text{at } t = 0 \quad (4.15)$$

where c = water concentration (kg m^{-3})
 c_{in} = initial water concentration (kg m^{-3})
 D = mass diffusivity ($\text{m}^2 \text{s}^{-1}$) (assumed constant)

Equation (4.13) uses both the concentration of the water at the surface ($c_{r=R}$) and the partial pressure of water vapour in the boundary layer over this surface ($p_{r=R}$). These relate to each other via equations (4.7), (4.8), and (4.16):

$$a_w = f(c_{r=R}) \quad (4.16)$$

It is primarily through these equations that the heat and mass transfer are linked, although D might be a function of temperature in some situations. In practice $a_w = \text{constant}$ was used to replace equation (4.16) in most analyses performed, so the results of the mass transfer calculations were ignored.

4.2.2 Finite Difference Schemes

For simplicity, the finite difference method was selected to solve equations (4.1) to (4.16). The simplest possible approximation is the so-called explicit finite difference formula. The

main disadvantage of explicit formulations is the limitations on time increments imposed by the stability criteria. The program used incorporated a routine to minimize the execution time by selecting the largest time increment that satisfied the stability criteria thus achieving reasonable computation times. The explicit finite difference schemes were derived by modelling the product as a stack of thin, uniform slices, Δr , with time divided into time steps of Δt . In the space description there were J nodes. The first node, $j = 0$, is at the center of the solid and the highest numbered node, J , is at the solid surface. The node in each volume element is placed at the midpoint between the two surfaces of the slice which has thickness, Δr , except for the outermost and innermost slice which have thicknesses of $\Delta r/2$, and where the node is at one edge of the element. Evaporative and convective heat transfer occur only from the outer surface of the J th slice. Conductive heat transfer takes place within the underlying slices.

4.2.2.1 Energy Transfer Equations

Heat balances for the various regions were performed with the following results.

Generalised region for $1 \leq j \leq J - 1$, $t > 0$

(a) infinite slab:

$$\frac{T_j^{i+1} - T_j^i}{\Delta t} = \alpha \frac{T_{j+1}^i - 2T_j^i + T_{j-1}^i}{\Delta r^2} \quad (4.17)$$

(b) infinite cylinder:

$$\frac{T_j^{i+1} - T_j^i}{\Delta t} = \alpha \frac{\left(1 + \frac{1}{2j}\right)T_{j+1}^i - 2T_j^i + \left(1 - \frac{1}{2j}\right)T_{j-1}^i}{\Delta r^2} \quad (4.18)$$

(c) sphere:

$$\frac{T_j^{i+1} - T_j^i}{\Delta t} = \alpha \frac{\left(1 + \frac{1}{j}\right)T_{j+1}^i - 2T_j^i + \left(1 - \frac{1}{j}\right)T_{j-1}^i}{\Delta r^2} \quad (4.19)$$

where Δr = thickness of slices (m)

- Δt = time step (s)
 i = number of time step or time level in numerical calculations
 j = space position in r direction in numerical calculations
 α = thermal diffusivity (m^2s^{-1})

Boundary condition at $r = R$ ($j = J$) for $t > 0$

(a) infinite slab:

$$\frac{\rho C}{2} \left(\frac{T_J^{i+1} - T_J^i}{\Delta t} \right) = \frac{1}{\Delta r} \left[\frac{k}{\Delta r} (T_{J-1}^i - T_J^i) - h_c (T_J^i - T_a^i) - K_a \epsilon_{fg} (p_J^i - p_a^i) \right] \quad (4.20)$$

(b) infinite cylinder:

$$\frac{\rho C}{2} \left(\frac{T_J^{i+1} - T_J^i}{\Delta t} \right) = \frac{1}{\Delta r} \left[\left(\frac{J - \frac{1}{2}}{J - \frac{1}{4}} \right) \frac{k}{\Delta r} (T_{J-1}^i - T_J^i) - \frac{J}{\left(J - \frac{1}{4} \right)} h_c (T_J^i - T_a^i) - \frac{J}{\left(J - \frac{1}{4} \right)} K_a \epsilon_{fg} (p_J^i - p_a^i) \right] \quad (4.21)$$

(c) sphere:

$$\frac{\rho C}{3} \left(\frac{T_J^{i+1} - T_J^i}{\Delta t} \right) = \frac{1}{\left(J^3 - \left(J - \frac{1}{2} \right)^3 \right) \Delta r} \left[\left(J - \frac{1}{2} \right)^2 \frac{k}{\Delta r} (T_{J-1}^i - T_J^i) - J^2 h_c (T_J^i - T_a^i) - J^2 K_a \epsilon_{fg} (p_J^i - p_a^i) \right] \quad (4.22)$$

where p_J = partial pressure of water vapour in the boundary layer at evaporating surface (Pa) ($\approx p_{r=R}$)

J = number of nodes = $R/(\Delta r)$

It should be noted that the above 3 equations assume that the mass of material in region J is not reduced by evaporation, and this allows only the latent heat and not the full enthalpy of the leaving water to be modelled.

For the boundary at $r = 0$ ($j = 0$) for $t > 0$ symmetry considerations suggest:

(a) infinite slab:

$$\frac{\rho C}{2} \left(\frac{T_0^{i+1} - T_0^i}{\Delta t} \right) = \frac{k}{\Delta r^2} (T_1^i - T_0^i) \quad (4.23)$$

(b) infinite cylinder:

$$\frac{\rho C}{4} \left(\frac{T_0^{i+1} - T_0^i}{\Delta t} \right) = \frac{k}{\Delta r^2} (T_1^i - T_0^i) \quad (4.24)$$

(c) sphere:

$$\frac{\rho C}{6} \left(\frac{T_0^{i+1} - T_0^i}{\Delta t} \right) = \frac{k}{\Delta r^2} (T_1^i - T_0^i) \quad (4.25)$$

The uniform initial condition at $t = 0$ is represented by:

$$T_j = T_{in} \quad \text{at } t = 0 \text{ for } 0 \leq j \leq J \quad (4.26)$$

The mass-average temperature is given by:

$$T_{av} = \frac{\sum (\text{volume of slice at node } j)(\text{temperature at node } j)}{\text{total volume}} \quad (4.27)$$

(a) infinite slab:

$$T_{av} = \frac{\frac{T_J}{2} + \frac{T_0}{2} + \sum_{j=1}^{J-1} T_j}{J} \quad (4.28)$$

(b) infinite cylinder:

$$T_{av} = \frac{\left(J - \frac{1}{4} \right) T_J + \frac{T_0}{4} + 2 \sum_{j=1}^{J-1} j T_j}{J^2} \quad (4.29)$$

(c) sphere:

$$T_{av} = \frac{\left[J^3 - \left(J - \frac{1}{2} \right)^3 \right] T_J + \frac{T_0}{8} + \sum_{j=1}^{J-1} \left[\left(j + \frac{1}{2} \right)^3 - \left(j - \frac{1}{2} \right)^3 \right] T_j}{J^3} \quad (4.30)$$

where T_{av} = mass-average temperature of solid (K or °C)
 T_0 = temperature of solid at node 0 (K or °C)
 T_j = temperature of solid at node j (K or °C)
 T_J = surface temperature of solid (K or °C)

4.2.2.2 Mass Transfer Equations

Generalised region for $t > 0$, $1 \leq j \leq J - 1$

(a) infinite slab:

$$\frac{c_j^{i+1} - c_j^i}{\Delta t} = D \frac{c_{j+1}^i - 2c_j^i + c_{j-1}^i}{\Delta r^2} \quad (4.31)$$

(b) infinite cylinder:

$$\frac{c_j^{i+1} - c_j^i}{\Delta t} = D \frac{\left(1 + \frac{1}{2j} \right) c_{j+1}^i - 2c_j^i + \left(1 - \frac{1}{2j} \right) c_{j-1}^i}{\Delta r^2} \quad (4.32)$$

(c) sphere:

$$\frac{c_j^{i+1} - c_j^i}{\Delta t} = D \frac{\left(1 + \frac{1}{j} \right) c_{j+1}^i - 2c_j^i + \left(1 - \frac{1}{j} \right) c_{j-1}^i}{\Delta r^2} \quad (4.33)$$

For the boundary at $r = R$ ($j = J$) for $t > 0$

(a) infinite slab:

$$\frac{c_J^{i+1} - c_J^i}{2\Delta t} = \frac{D}{\Delta r^2} (c_{j-1}^i - c_j^i) - \frac{K_a}{\Delta r} (p_j^i - p_a^i) \quad (4.34)$$

(b) infinite cylinder:

$$\frac{c_J^{i+1} - c_J^i}{2\Delta t} = \frac{\left(J - \frac{1}{2}\right)}{\left(J - \frac{1}{4}\right)} \frac{D}{\Delta r^2} (c_{j-1}^i - c_j^i) - \frac{J}{\left(J - \frac{1}{4}\right)} \frac{K_a}{\Delta r} (p_j^i - p_a^i) \quad (4.35)$$

(c) sphere:

$$\frac{c_J^{i+1} - c_J^i}{3\Delta t} = \frac{1}{\left(J^3 - \left(J - \frac{1}{2}\right)^3\right)} \left(\left(J - \frac{1}{2}\right)^2 \frac{D}{\Delta r^2} (c_{j-1}^i - c_j^i) - J^2 \frac{K_a}{\Delta r} (p_j^i - p_a^i) \right) \quad (4.36)$$

For the boundary at $r = 0$ ($j = 0$) for $t > 0$. Symmetry suggests:

(a) infinite slab:

$$\frac{c_0^{i+1} - c_0^i}{2\Delta t} = \frac{D}{\Delta r^2} (c_1^i - c_0^i) \quad (4.37)$$

(b) infinite cylinder:

$$\frac{c_0^{i+1} - c_0^i}{4\Delta t} = \frac{D}{\Delta r^2} (c_1^i - c_0^i) \quad (4.38)$$

(c) sphere:

$$\frac{c_0^{i+1} - c_0^i}{6\Delta t} = \frac{D}{\Delta r^2} (c_1^i - c_0^i) \quad (4.39)$$

The uniform initial water concentration is given by:

$$c_j = c_{in} \quad \text{for } t = 0, 0 \leq j \leq J \quad (4.40)$$

The mass-average water concentration is given by:

$$c_{av} = \frac{\sum (\text{volume of slice at node } j)(\text{concentration at node } j)}{\text{total volume}} \quad (4.41)$$

which was implemented as follows:

(a) infinite slab:

$$c_{av} = \frac{\frac{c_J}{2} + \frac{c_0}{2} + \sum_{j=1}^{J-1} c_j}{J} \quad (4.42)$$

(b) infinite cylinder:

$$c_{av} = \frac{\left(J - \frac{1}{4}\right)c_J + \frac{c_0}{4} + 2\sum_{j=1}^{J-1} jc_j}{J^2} \quad (4.43)$$

(c) sphere:

$$c_{av} = \frac{\left(J^3 - \left(J - \frac{1}{2}\right)^3\right)c_J + \frac{c_0}{8} + \sum_{j=1}^{J-1} \left(\left(j + \frac{1}{2}\right)^3 - \left(j - \frac{1}{2}\right)^3\right)c_j}{J^3} \quad (4.44)$$

where c_{av} = mass-average water concentration (kg m^{-3})
 c_J = water concentration at node J (kg m^{-3})
 c_j = water concentration at node j (kg m^{-3})
 c_0 = water concentration at node 0 (kg m^{-3})

4.2.3 Vapour Pressure Equations

As stated earlier the water partial pressure in the boundary layer at the surface of products is lower than that of pure water at the same temperature. Equation (4.7) can be rewritten as:

$$p_J = a_w p_{wJ} \quad (4.45)$$

where p_{wJ} = (saturation) vapour pressure of pure water at the evaporating surface temperature T_J (Pa)

The vapor pressure of water at the evaporating surface p_{wJ} , depends on the temperature of the surface. The following Antoine equation gives a satisfactory approximation:

$$p_{wJ} = \exp \left(23.4795 - \frac{3990.56}{(T_J + 233.833)} \right) \quad (4.46)$$

To implement equation (4.9) it is convenient to use the Antoine equation again:

$$p_{wa} = \exp \left(23.4795 - \frac{3990.56}{T_a + 233.833} \right) \quad (4.47)$$

The latent heat of vaporisation (ϵ_{fg} , J kg⁻¹) can be approximated by:

$$\epsilon_{fg} = 2.5 * 10^6 - 2.5 * 10^3 T_J \quad (4.48)$$

where T_J is in units of °C.

4.2.4 Use of the Lewis Relationship

The mass transfer coefficient (K_a) is not easily measured for conditions which exist during evaporation. A commonly used approximation involves the use of the Lewis number, Le , defined as (Heldman, 1975):

$$Le = \frac{h_c}{K_y C_a} \quad (4.49)$$

and

$$K_y \approx \frac{29 P_r K_a}{18} \quad (4.50)$$

where K_y = mass transfer coefficient in humidity units (kg m⁻² s⁻¹)

P_t = total air pressure (Pa)

which implies

$$K_a \approx \frac{18h_c}{29C_aP_t} \quad (4.51)$$

where C_a = air humid heat capacity on a dry air mass basis ($\text{J kg}^{-1} \text{K}^{-1}$)

Le is unity only if $Pr = Sc$ (which is approximately the case for air). It was thus assumed that equation (4.51) applied, although in its implementation the heat capacity of dry air was used instead of the humid heat capacity of air for convenience, since at chilling conditions the humidity is low, and hence the error is small. Thus, by use of the Lewis relationship the Biot number for heat transfer also defined the external mass transfer conditions.

4.3 Computer Program Development and Testing

A Turbopascal computer program was developed for equations (4.17) to (4.51) (Appendix A). A running energy balance was included to check for numerical error, and this rarely was out of balance by more than 0.01 %. By setting $K_a = 0$ the program was successfully checked against the analytical solutions for convective heat transfer only (equations 2.7 and 2.8).

4.4 Simulation Performed

Simulations were carried out across a wide range of conditions that might arise in industrial chilling practice. Initial temperature, T_{in} , was varied from 20 °C to 50 °C. Higher temperatures were unlikely for natural products and at temperatures below 20 °C the potential for evaporation is modest. Cooling medium temperature, T_c , was varied from 0 to 15 °C (higher temperatures are unlikely in practice, and temperatures much below 0 °C are only occasionally used for high water content foods). Relative humidity is typically about 0.85 (Schneider *et al.*, 1982) but a wide range (0.5 to 1.0) was investigated. Biot number was varied from 0.1 to 10, the most important range.

As discussed earlier, it was assumed that:

$$a_w = \text{constant} \neq F(c_j) \quad (4.52)$$

This effectively decommissioned the equations modelling the diffusional mass transfer, and the simulation was then expressed in largely heat transfer terms. A wide range of a_w (0.6 to 1.0) was investigated.

Numerical process simulations were carried out across most of the possible combinations of conditions:

shape :	infinite slab, infinite cylinder, sphere
$T_{in}(\text{°C})$:	20, 30, 40, 50
$T_a(\text{°C})$:	0, 5, 10, 15
a_w :	0.6, 0.8, 1.0
H_r :	0.50, 0.75, 1.00
Bi :	0.1, 0.316, 1.0, 3.16, 10 (even logarithmic steps)

Those combinations excluded were unlikely in practice e.g. $T_{in} = 20 \text{ °C}$ and $T_a = 15 \text{ °C}$.

4.5 Discussion of Simulation Behaviour

From the various numerically generated process simulations the effects of various parameters on centre and mass-average temperatures in particular could be summarised as follows:

4.5.1 Steady State (Equilibrium) Condition

For practical purposes, after some time had elapsed temperatures reached a steady state at which all of the centre, surface, and mass-average temperature became the same. This temperature was called the equilibrium temperature (Figure 4.1) and was independent of T_{in} and Bi but depended on T_a , H_r , and a_w . The steady state conditions could be classified according to the relationship between H_r and a_w as follows (Figure 4.2):

(1) $a_w = H_r$

For these simulations, no evaporation occurred at steady state and the equilibrium temperature was equal to the ambient air temperature. This was the same result as for the case of

convection only.

$$(2) a_w > H_r$$

For these simulations, evaporation still occurred at equilibrium and the equilibrium temperature was less than the ambient air temperature because heat removal by evaporation was being balanced by heat gain by convection.

$$(3) a_w < H_r$$

For these simulations, condensation on the product surface occurred and at equilibrium the equilibrium temperature was more than the ambient air temperature. This was because heat added by condensation balanced heat removed by convection from the product surface to the surrounding air.

4.5.2 Active Chilling Period (Unsteady State Condition)

During the cooling process, whenever a vapour pressure driving force existed ($p_j > p_a$), moisture loss occurred. High initial temperature differences (lower T_a or high T_{in}) resulted in a high initial partial pressure driving force, faster initial cooling, and greater rates of moisture loss, even with high relative humidity air. Other factors that affected the magnitude of the predicted cooling rate were the surface water activity (a_w), relative humidity (H_r), and Biot number (Bi). If $(a_w - H_r)$ was positive, the cooling process was faster to achieve a certain temperature than when the parameter was negative (Figure 4.2). It should be noted that in the simulation, effects of air velocity and K_a were included in the term h_c , which was a function of Bi by use of the Lewis relationship.

For the case of convection only ($K_a = 0$), no matter what other conditions existed, the characteristic cooling curve ($\ln Y$ versus Fo where Y is defined using equation 2.18 or 2.19) depends on Bi but not on a_w or H_r . The higher Bi is; the faster the cooling rate. In the cases with evaporation, plots of $\ln Y$ versus Fo gave straight lines as implied by equations (2.18) and (2.19) only at $a_w = H_r$. When Bi was held constant, the rate of cooling at $H_r = a_w$ was faster than the rate for convective cooling only (Figure 4.3), but its magnitude depended on other conditions. Figure 4.2 implies that the higher a_w was, the faster the cooling rate. This was because there was more water available at the product surface resulting in a stronger evaporative cooling effect. Whenever $a_w \neq H_r$, a straight semi-log cooling rate plot suggested

by equations (2.18) and (2.19) was not observed (e.g. Figure 4.4) and the curvature was greater the more different a_w and H_r were.

In summary, from the numerically generated data, it was found that Bi , H_r , a_w , T_a and T_{in} are the important parameters that influence the effect of evaporation on cooling rate at centre and mass-average positions. Their relationships were complicated because these factors affected each other and their effects were not equal.

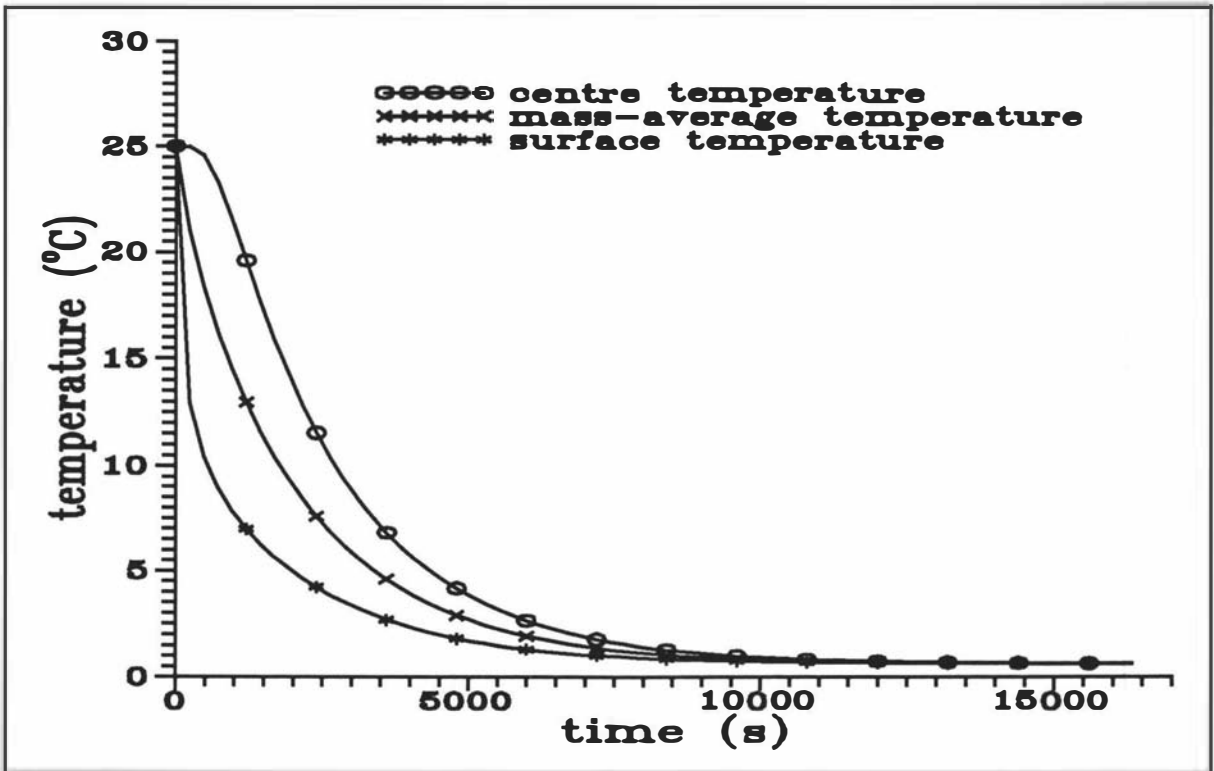


Figure 4.1 Example plot for convection-only cooling showing the approach of the centre, surface, and mass-average temperatures to the cooling medium temperature.

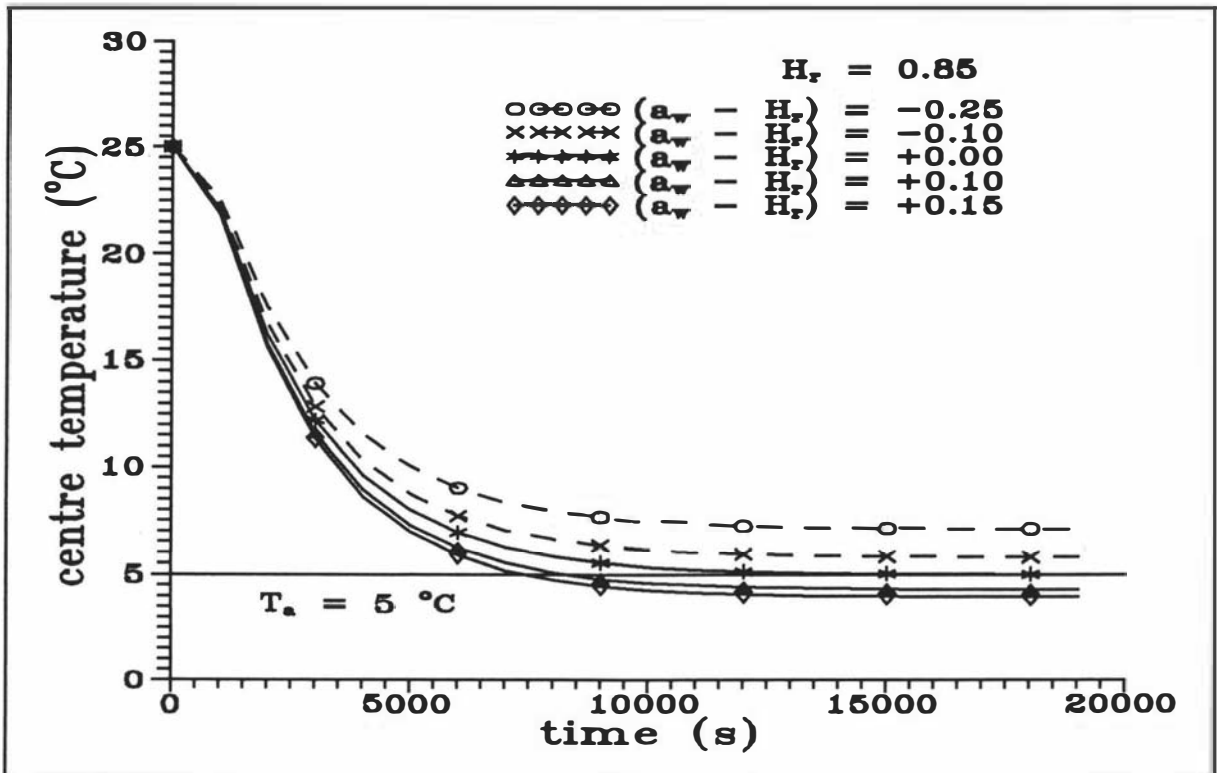


Figure 4.2 Example plots showing the effect of $(a_w - H_r)$ on the cooling process.

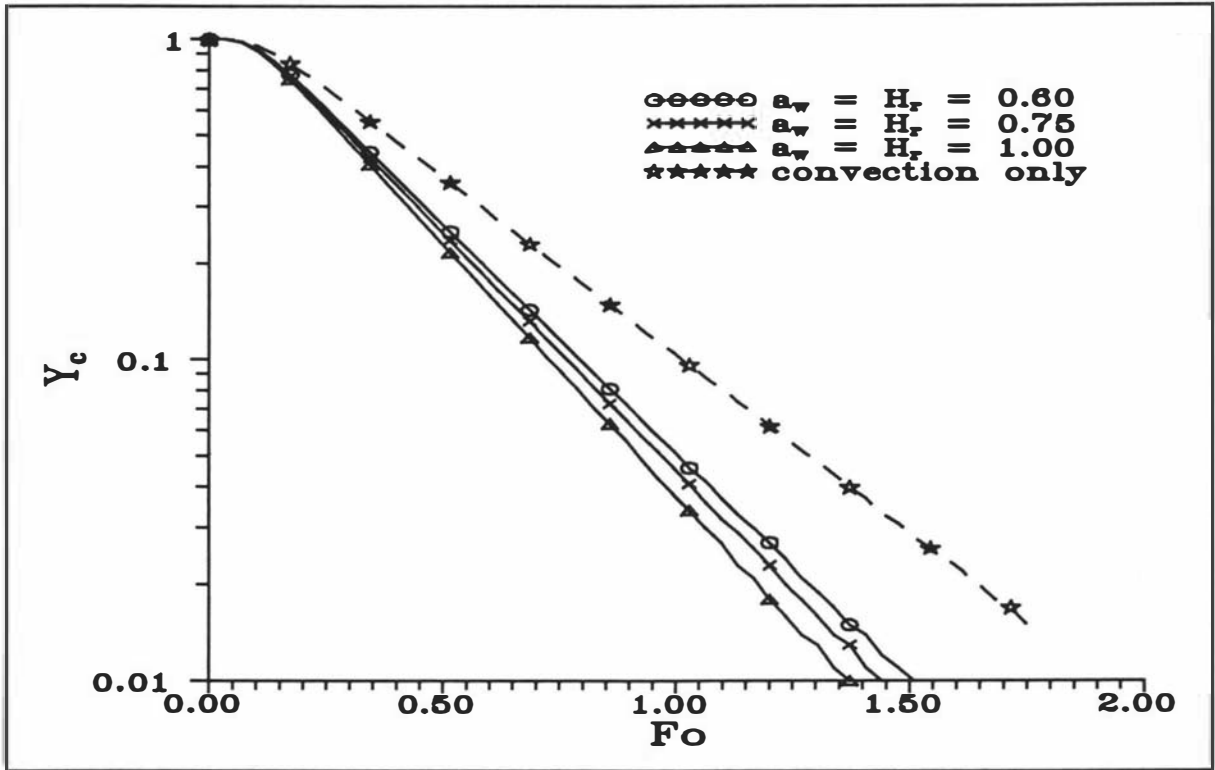


Figure 4.3 Example semi-log plots of cooling by both convection and evaporation with $H_r = a_w$.

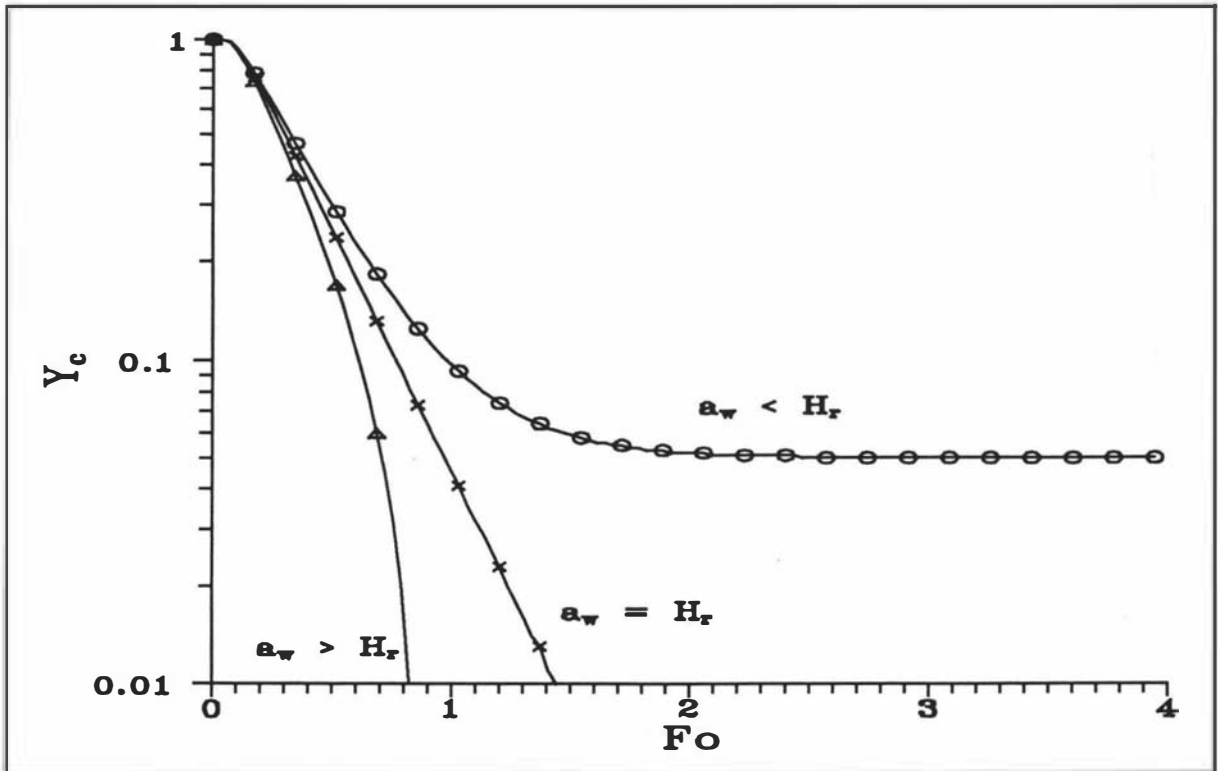


Figure 4.4 Example semi-log plots of cooling by both convection and evaporation with $a_w < H_r$, $a_w > H_r$, and $a_w = H_r$.

5. MODEL DEVELOPMENT & RESULT

5.1 INTRODUCTION

Chapter 4 described the model used to simulate simultaneous heat and mass transfer and how the finite difference method was used to implement the model to predict the likely behaviour of a sphere, infinite cylinder, and infinite slab cooled by both evaporation and convection. It was found that the extent to which evaporation affected cooling rate depended on the environmental (H_r , T_a , Bi) and product conditions (a_w , T_{in}). In this chapter their relationships will be further investigated, and simple empirical models to predict cooling rate at centre and mass-average positions for cooling with evaporation are developed.

5.2 DESCRIPTION OF CONVECTION-ONLY COOLING

In the case of no moisture transfer or radiation, the surface boundary condition is defined by the convection at the surface, or Newton's law of cooling. Heat loss is a function of the temperature difference between the product surface and the ambient air. The transient heat conduction and convection for an infinite slab, infinite cylinder and sphere can be solved analytically (Newman, 1936; Carslaw & Jaeger, 1959; Hodgson, 1966). Due to rapid exponential decay, only one term in each of the analytical series solutions is significant, except shortly after cooling commences. The temperatures at the thermal centre, T_c , and the mass-average temperature, T_{av} , are normally expressed as a function of the unaccomplished temperature change, Y . The analytical solutions can be written in the form which was first introduced as equations (2.18) and (2.19). However the practice of writing g in the bottom line was discontinued. The reason was that the study was concerned with cooling enhancement, and this is best measured as the slope of a line of $\ln Y$ versus t . Accordingly:

$$Y_c = \frac{(T_c - T_a)}{(T_{in} - T_a)} = j_{cConv} e^{-\beta_1^2 Fo} = j_{cConv} e^{f_{cConv} Fo} \quad (5.1)$$

$$Y_{av} = \frac{(T_{av} - T_a)}{(T_{in} - T_a)} = j_{avConv} e^{-\beta_1^2 Fo} = j_{avConv} e^{f_{avConv} Fo} \quad (5.2)$$

- where Y_c = fractional unaccomplished temperature change at centre position of the product
- Y_{av} = fractional unaccomplished temperature change at mass-average position of the product
- T_c = centre temperature of the product (K or °C)
- T_{av} = mass-average temperature of the product (K or °C)
- T_a = surrounding cooling medium temperature (K or °C)
- T_{in} = uniform initial temperature of the product (K or °C)
- j_{cConv} = j at centre position for convection-only cooling
= intercept of a plot of $\ln Y_c$ versus Fo
- j_{avConv} = j at mass-average position for convection-only cooling
= intercept of a plot of $\ln Y_{av}$ versus Fo
- β_1 = 1st root of the appropriate transcendental equation
- Fo = Fourier number = $\alpha t/R^2$
- R = characteristic length of the product (m)
- t = time (s)
- α = thermal diffusivity of the product = $k/\rho C$ ($m^2 s^{-1}$)
- f_{cConv} = f at centre position for convection-only cooling
= slope of a plot of $\ln Y_c$ versus Fo
- f_{avConv} = f at mass-average position for convection-only cooling
= slope of a plot of $\ln Y_{av}$ versus Fo

By analyzing a plot of $\ln Y$ versus Fo , the cooling performance data of a product is conveniently presented in terms of f (the slope which is dependent on shape and Bi) and j (the intercept or the lag factor which depends on shape, Bi , and position in the product). It should be noted that the f value represents the cooling rate once sufficient time has elapsed that the cooling rate follows exponential decay (typically for $Fo > 0.2$). For the thermal centre

temperature, the relationship between time and temperature is similar to that for the mass-average temperature in that the f values are the same although the intercepts are different. The lag factor, j , arises from the limiting effect of k on thermal diffusivity which results in a lag in the cooling of the interior. Thus the temperature changes more slowly at the centre than it does at the surface of the product, especially when $Bi > 0.2$. The lag factor, j , is thus > 1 towards the interior, and < 1 near the surface. The j value for the mass-average position is ≤ 1 .

For more complex shapes than the sphere, infinite cylinder and infinite slab the concepts of equations (5.1) and (5.2) are still often used where:

- f = the slope of $\ln Y$ versus $Fo = F(Bi, \text{shape, size})$
 j = the intercept of $\ln Y$ versus $Fo = F(Bi, \text{shape, size, internal position})$
 F = functional relationship

That is, the f and j values do not depend on environmental conditions or other physical properties (e.g. T_{in} , T_a , and a_w). The major limitation of the use of f and j values is that early on in the process, cooling is not accurately predicted.

5.3 COMPLICATIONS INTRODUCED BY EVAPORATIVE COOLING

When moisture transfer by evaporation is included in the analysis, some extra resulting problems arise:

- (1) two more mechanisms may have to be modelled: mass transfer inside the product (water diffusion) and mass transfer at the product surface (evaporation); (as discussed in Chapter 4, the former was avoided by assuming $a_w = \text{constant}$, but at the cost of representing reality less accurately).
- (2) the relative importance of evaporation and convection cannot easily be expressed in terms of dimensionless numbers. It depends on physical properties such as relative humidity, initial temperature, ambient air temperature, product water activity, and shape.
- (3) Plots of $\ln Y$ versus Fo are no longer necessarily linear, with the curves varying according to the environmental conditions especially at water activities less than one (as Figure 4.4 shows).

5.4 DEVELOPMENT OF AN EQUILIBRIUM REFERENCE TEMPERATURE

In seeking a model for cooling with evaporation it was decided to attempt to modify equations (5.1) and (5.2) rather than seek a new equation for the following reasons:

- (1) Convection is still the dominant mode of heat transfer. When considering the pattern of Y in equations (5.1) - (5.2), it can be seen that initially, the product is at T_{in} and $Y = 1$. If the product is left sufficiently long in the chiller with convection-only cooling, it will equilibrate to T_a , the steady temperature at which stage, $Y = 0$. Therefore the air temperature is what will be termed the steady state or reference temperature for Y values in convection-only cooling situations.
- (2) When considering the evaporative cooling curves in Chapter 4, it was found that at steady state conditions the product will eventually equilibrate to a temperature which differs from T_a . This equilibrium temperature is influenced by parameters such as relative humidity and surface water activity but was still close to T_a .

There is a need to find a means to linearise cooling curves of $\ln Y$ versus Fo if equations (5.1) and (5.2) are to be used. One possibility is to modify the definition of Y by developing a new reference temperature to replace T_a . If a new definition of reference temperature which linearizes the plots can be found, the f and j values for cooling with evaporation can then be evaluated.

In attempts to linearize $\ln Y_c$ or $\ln Y_{av}$ versus Fo plots three possibilities were tried. Firstly, as already stated, the surrounding air temperature was used as the reference temperature, but it did not linearize the curves (e.g. Figure 4.4). Secondly, since moisture loss depends on environmental factors and the wet-bulb temperature is the temperature that already includes the effect of dry bulb temperature and relative humidity, the wet-bulb temperature was tried as reference temperature. Although it reduced the non-linearity compared with using the air temperature as a reference, slopes for some situations were still non-linear, especially for $a_w < 1$. After investigating all the numerically generated data carefully, it was considered that the reference temperature might need to depend on a_w as well as H_r and T_a . Success in linearising plots was achieved when the equilibrium or reference temperature was derived using the energy balance at the product surface.

At steady state, by definition, heat lost from the product surface by evaporation is equal to heat gained by the product surface due to convection. Therefore from equations (4.4), (4.7), (4.9), and (4.45), it follows that:

$$K_a(a_w p_{wJ} - H_r p_{wa}) \epsilon_{fg} = h_c(T_a - T_{eq}) \quad (5.3)$$

- where h_c = surface heat transfer coefficient ($\text{W m}^{-2} \text{K}^{-1}$)
 ϵ_{fg} = latent heat of vapourisation of water (J kg^{-1})
 K_a = air film mass transfer coefficient ($\text{kg s}^{-1} \text{m}^{-2} \text{Pa}^{-1}$)
 T_a = ambient air temperature ($^{\circ}\text{C}$)
 T_{eq} = equilibrium or steady state temperature ($^{\circ}\text{C}$)
 a_w = water activity at product surface
 p_{wJ} = (saturation) vapour pressure of pure water at the evaporating surface temperature T_J (Pa)
 p_{wa} = (saturation) vapour pressure of pure water at surrounding air temperature T_a (Pa)
 H_r = air relative humidity

In section 4.2.4 where the Lewis relationship was introduced it was stated that for air:

$$K_y \approx \frac{h_c}{C_a} \quad (5.4)$$

where C_a = air humid heat capacity on a dry air mass basis ($\text{J kg}^{-1} \text{K}^{-1}$)
 K_y is a mass transfer coefficient written in humidity terms ($\text{kg m}^{-2} \text{s}^{-1}$). If equation (5.4) is to be used directly then equation (5.3) must be rewritten as:

$$K_y(H_J - H_{air}) \epsilon_{fg} = h_c(T_a - T_{eq}) \quad (5.5)$$

where H_J = absolute humidity in the boundary layer over the product surface ($\text{kg water kg dry air}^{-1}$)
 H_{air} = absolute humidity in the surrounding air ($\text{kg water kg dry air}^{-1}$)

The definitions of H_J and H_{air} are:

$$H_J = \frac{18p_J}{29(P_t - p_J)} \quad (5.6)$$

where p_J = partial pressure of water vapour in the boundary layer at evaporating surface (Pa)

P_t = total air pressure (Pa)

$$H_{air} = \frac{18p_a}{29(P_t - p_a)} \quad (5.7)$$

where p_a = partial pressure of water vapour in the surrounding air (Pa)

For chilling both T_{eq} and T_a are typically in the range of 0 - 15 °C, so p_a and p_J are usually 600 - 1700 Pa, compared to P_t which is atmospheric pressure (101,325 Pa). To reconcile equations (5.3) and (5.5) it would normally be assumed that

$$K_y \approx \frac{29p_{bm}K_a}{18} \quad (5.8)$$

where p_{bm} = mean partial pressure of dry air (Pa)

As p_J and p_a are small compared to P_t in chilling operations it is often assumed that $p_{bm} \approx P_t$, which leads to equation (4.50) which was presented earlier.

Depending on the assumptions made, equations of differing complexity for T_{eq} can be derived.

The simplest assuming $p_{bm} \approx P_t$ is

$$T_{eq} \approx T_a - \frac{18\epsilon_{fg}}{29C_a} \left(\frac{p_J - p_a}{P_t} \right) \quad (5.9)$$

or

$$T_{eq} \approx T_a - \frac{18\epsilon_{fg}}{29C_a} \left(\frac{a_w p_{wJ} - H_r p_{wa}}{P_t} \right) \quad (5.10)$$

At equilibrium the surface of the product is at temperature T_{eq} , so ϵ_{fg} can be evaluated approximately by substituting T_{eq} for T_J in equation (4.48). Similarly, p_{wJ} can be evaluated by substituting T_{eq} for T_J in equation (4.46). Lastly, substitution of T_a in equation (4.47) allows

p_{wa} to be evaluated. Making these substitutions, but recognising that they use approximations for thermodynamics properties of water one can derive:

$$T_{eq} \approx T_a - \frac{18(2.5 \times 10^6 - 2.5 \times 10^3 T_{eq})}{29 C_a P_t} \left(a_w e^{\left(\frac{23.4759 - \frac{3990.56}{T_a + 233.833}}{T_a + 233.833} \right)} - H_r e^{\left(\frac{23.4795 - \frac{3990.56}{T_a + 233.833}}{T_a + 233.833} \right)} \right) \quad (5.11)$$

T_{eq} is the only unknown and so equation (5.11) can be solved iteratively. Alternatively equation (5.10) could be solved using tabulated thermodynamic data for water. Whilst equation (5.11) is as complex an equation as one could reasonably expect a user to solve by hand, if a computer is used more complex arithmetic can be tolerated, and so the assumption that $p_{bm} \approx P_t$ can be relaxed. Figures 5.1, 5.2, and 5.3 were calculated by the more complex equations that result from using equation (5.8) rather than equation (4.50) in derivation of an equation for T_{eq} . In practice, as has been discussed, the differences are small and can be ignored for practical purposes, thus allowing equations (5.10) and (5.11) plus Figures 5.1, 5.2, and 5.3 to be used interchangeably. Interpolation of the Figures is required for $a_w \neq 0.6, 0.8$ or 1.0. (All Figures are located at end of chapter)

5.5 DEVELOPMENT OF A MODIFIED Y VALUE

In practical chilling situations the final value of Y is usually less than about 0.5, and if Y values are less than about 0.7 - 0.8, the error in neglecting the second and subsequent terms in the series solution (equations 5.1 and 5.2) is usually small. In this study, the range of interest for the Y_c and Y_{av} was set between 0.70 and 0.045 to effectively match the associated work of Lin (1994). When T_{eq} (equation 5.10) was used to replace T_a in equations (5.1) and (5.2), linear or close to linear plots were obtained for all conditions (e.g. Figure 4.4 leads to Figure 5.4), thus indicating that T_{eq} would be the appropriate reference temperature for the evaporation process. This was confirmed by checking across the full numerically-generated data. Using regression applied to the plots of $\ln Y_c$ or $\ln Y_{av}$ versus FO , it was found that R^2 values were in the range 0.999 - 1 at all conditions, indicating that T_{eq} had very satisfactorily linearised the plots. Therefore the equilibrium temperature was used to replace the dry bulb temperature (T_a) in the modified fractional unaccomplished temperature change as followed:

$$Y_c = \frac{(T_c - T_{eq})}{(T_{in} - T_{eq})} = j_{cEvap} e^{-\beta_1^2 Fo} = j_{cEvap} e^{f_{cEvap} Fo} \quad (5.12)$$

$$Y_{av} = \frac{(T_{av} - T_{eq})}{(T_{in} - T_{eq})} = j_{avEvap} e^{-\beta_1^2 Fo} = j_{avEvap} e^{f_{avEvap} Fo} \quad (5.13)$$

where f_{cEvap} = f at centre position for cooling with evaporation as well as convection
 j_{cEvap} = j at centre position for cooling with evaporation as well as convection
 f_{avEvap} = f at mass-average position for cooling with evaporation as well as convection
 j_{avEvap} = j at mass-average position for cooling with evaporation as well as convection

This completed the first stage of model development.

5.6 ISOLATION OF THE EVAPORATIVE EFFECT ON COOLING RATE

After all cooling curves were linearized, the f and j values were evaluated. The relative cooling rates with both evaporation and convection and convection only were considered for each set of conditions tested. It was proposed that the f_{Evap} and j_{Evap} values (from the evaporative cooling curve) be compared with the f_{Conv} and j_{Conv} values (from the analytical solutions for convection only) to derive formulae as follows:

$$f_{Evap} = f_{Conv} \cdot correction \quad (5.14)$$

$$j_{Evap} = j_{Conv} \cdot correction \quad (5.15)$$

The ratios of the f and j values with and without evaporation would be related to product conditions (a_w, T_{in}) and environmental conditions (H_r, Bi, T_a). That is:

$$correction = F(Bi, H_r, a_w, T_a, T_{in}) \quad (5.16)$$

It was convenient to re-express equations (5.14) and (5.15) as:

$$\frac{f_{Evap}}{f_{Conv}} - 1 = F(Bi, H_r, a_w, T_a, T_{in}) \quad (5.17)$$

$$\frac{j_{Evap}}{j_{Conv}} - 1 = F(Bi, H_r, a_w, T_a, T_{in}) \quad (5.18)$$

where $f_{Evap} = f$ for cooling with evaporation as well as convection
 $j_{Evap} = j$ for cooling with evaporation as well as convection
 $f_{Conv} = f$ for convection-only cooling
 $j_{Conv} = j$ for convection-only cooling

If there is no evaporation, the term on the right hand side of equations (5.17) and (5.18) should be zero (as this term arises as a result of evaporative effect only), and thus $f_{Evap} = f_{Conv}$ and $j_{Evap} = j_{Conv}$. The f_{Conv} and the j_{Conv} , which are termed the reference values, depend only on Bi and position in the object and can be found using the analytical solutions for convective cooling of spheres, infinite cylinders, and infinite slabs. The f_{Evap} and j_{Evap} are subject to the same limitations as their reference values in terms of their ranges of applicability.

The effect of product size is already included in FO and hence f_{Conv} & j_{Conv} (equations 5.1 and 5.2) so that equations (5.17) and (5.18) need not consider product size.

5.7 MODEL DEVELOPMENT OF EMPIRICAL EQUATIONS FOR f_{Evap}/f_{Conv} AND j_{Evap}/j_{Conv}

From the above techniques, using the numerically generated data described in Chapter 4, the next steps were:

- (1) Simple empirical equations (that can be applied without a computer) were developed to represent the functionality of six parameters ($H_r, T_a, Bi, a_w, T_{in}$, shape) using trend graphs to select appropriate variables, and then non-linear regression techniques to fit the parameters.
- (2) Quality of predictions, relative to the numerically-predicted results, was investigated. One concern was whether variables other than $a_w, H_r, T_a, T_{in}, Bi$, and shape affected f_{Evap}/f_{Conv} and j_{Evap}/j_{Conv} values.

5.7.1 The Effects of Product Properties on f_{Evap} and j_{Evap} Values

Common chilled food thermal properties are typically in the range of $\rho C = 2 \times 10^6 - 4 \times 10^6 \text{ J m}^{-3} \text{ K}^{-1}$ and $k = 0.3 - 0.6 \text{ W m}^{-1} \text{ K}^{-1}$. It was found that when thermal food properties were varied within these ranges, the ratio of the f and j values remained relatively constant. For example in numerical simulations, when ρC was changed from 2×10^6 to $4 \times 10^6 \text{ J m}^{-3} \text{ K}^{-1}$, f_{Evap}/f_{Conv} and j_{Evap}/j_{Conv} changed only 0.1 %. When k was changed from 0.3 to $0.6 \text{ W m}^{-1} \text{ K}^{-1}$, f_{Evap}/f_{Conv} and j_{Evap}/j_{Conv} changed only -0.05 %. Thus varying food thermal properties should not significantly affect the accuracy of the curve-fit algebraic equations for f_{Evap}/f_{Conv} and j_{Evap}/j_{Conv} .

5.7.2 The Reference Shape

It was uncertain whether shape would affect the form of the models. To investigate this effect of the ratios of f_{Evap}/f_{Conv} and j_{Evap}/j_{Conv} values for the 3 shapes were calculated from the numerical simulation results. The worst deviation from 1:1:1 (for infinite slab:infinite cylinder:sphere) was at $Bi = 1$ where the ratios were 0.95:1:1.04 for f_{Evap}/f_{Conv} and 0.94:1:1.08 for j_{Evap}/j_{Conv} . Ratios for the infinite slab/infinite cylinder data were slightly closer to unity than ratios for the sphere/infinite cylinder.

Since the geometry and the behaviour of an infinite cylinder was intermediate between an infinite slab and a sphere, it was chosen to be the initial reference shape in developing the models. However it was decided that there might be a need to introduce a shape factor to the model to improve accuracy for the other two shapes. To index shape, the equivalent heat transfer dimensionality, E , as defined by Lin (1994) was used.

5.7.3 Models for Centre Temperature Position

It was considered that a mechanistic basis for equations (5.17) and (5.18) was unlikely. Trends within the numerically-predicted results were investigated to establish possible relationships that should be included. The range of f_{cEvap}/f_{cConv} was 1.1 to 2.9 and that of j_{cEvap}/j_{cConv} was 0.8 to 1.1.

5.7.3.1 Model Development for f_{cEvap}/f_{cConv}

When $(f_{cEvap}/f_{cConv} - 1)$ was plotted against different parameters, the following trends were observed:

(1) Bi

Figure 5.5 shows the relationship between f_{cEvap}/f_{cConv} and Bi . For the full numerical data set, although the cooling rate is faster at higher Bi , the evaporative effect is stronger at lower Bi . The spread of data at low Bi shows that Bi interacts with other variables. For example, when $(f_{cEvap}/f_{cConv} - 1)$ is plotted against Bi with T_a as a third variable (Figure 5.6), the T_a effect increased at low Bi . When the same data are replotted (Figure 5.7) better insights into possible model form were obtained. It was decided that the effects of Bi would be classified into 2 terms: one covering the effect at high Bi and the other adding a variable increment at low Bi in which interactions with other variables would be included.

(2) H_r

Relative humidity had a greater effect on evaporative cooling than either air temperature or velocity. It was found that H_r interacted with T_a (e.g. Figure 5.8) and at high Bi , H_r interacted slightly with a_w (Figure 5.9).

(3) T_a

T_a interacted with a_w at high Bi (e.g. Figure 5.10). The effect of T_a was relatively independent of the effect of T_{in} .

(4) T_{in}

The effects of T_{in} showed up only at low Bi (e.g. Figure 5.11). The effect of T_{in} was relatively independent of a_w .

(5) a_w

At high Bi , a_w interacted with H_r , T_a and T_{in} (e.g. Figure 5.12). At low Bi , a_w was approximately linearly related to $(f_{cEvap}/f_{cConv} - 1)$.

(6) E (shape factor)

Figure 5.13 shows an example of the effect of shape on $(f_{cEvap}/f_{cConv} - 1)$. It was found that at $0.2 \leq Bi \leq 8$, the value of $(f_{cEvap}/f_{cConv} - 1)$ for an infinite cylinder was between that for a sphere and an infinite slab. As has been discussed the maximum difference between the infinite cylinder and the sphere was -5 % at $Bi = 1$, and for the infinite

slab the maximum difference was +4 %.

In summary, from visual inspection it was decided that the equation for $(f_{cEvap}/f_{cConv} - 1)$ would depend most strongly on the value of Bi . For high Bi it might only need to be a function of Bi , but for lower levels of Bi , it should also involve T_{in} , T_a , H_r and a_w . It was decided to ignore the small effect of shape.

Nonlinear regression was used to develop a form of the model on a trial and error basis guided by the above considerations. It was found that the best correlation ($R^2 = 0.996$) and most significant coefficients for f_{cEvap}/f_{cConv} came from the curve-fit algebraic equation:

$$\frac{f_{cEvap}}{f_{cConv}} - 1 = \frac{Bi}{15 (Bi^{1.5} + 1.5)} + \frac{T_a(H_r + 0.34) + (5H_r + 0.12T_{in} + 9.87)a_w^{0.8}}{19(Bi^{1.2} + 1.2)} \quad (5.19)$$

Since the term on the left hand side is dimensionless, the numerical coefficients on the right hand side have appropriate units to make this side dimensionless also.

5.7.3.2 Model Development for j_{cEvap}/j_{cConv}

When $(j_{cEvap}/j_{cConv} - 1)$ was plotted against different parameters, the following trends were observed:

(1) Bi

Figure 5.14 shows all numerically generated data for j_{cEvap}/j_{cConv} plotted versus Bi . All other parameters interacted with Bi but H_r and T_a had similar relationships to each other with Bi . The higher the value of H_r or T_a , the higher the $(j_{cEvap}/j_{cConv} - 1)$ value was (e.g. Figure 5.15 and 5.16). T_{in} and a_w had a similar relationship to each other with Bi . The lower the value of T_{in} or a_w , the higher the value of $(j_{cEvap}/j_{cConv} - 1)$ was (e.g. Figure 5.17 and 5.18).

(2) H_r

It was found that H_r had an approximately linear relationship with $(j_{cEvap}/j_{cConv} - 1)$. At low Bi , H_r did not interact significantly with T_a , T_{in} or a_w but at high Bi , there was

interaction but the overall effect on $(j_{cEvap}/j_{cConv} - 1)$ was small (Figure 5.19).

(3) a_w

It was found that the effect of a_w was small at high Bi . At low Bi , a_w did not interact significantly with T_a , T_{in} , or H_r , but did interact with Bi (Figure. 5.17).

(4) T_a

At low Bi , it was found that $(j_{cEvap}/j_{cConv} - 1)$ varied according to T_a (e.g. Figure 5.20). The effect of T_a at high Bi was weaker. T_a did not interact significantly with T_{in} or a_w .

(5) T_{in}

At low Bi , it was found that $(j_{cEvap}/j_{cConv} - 1)$ changed inversely with T_{in} (e.g. Figure 5.18). The effect of T_{in} was low at high Bi .

(6) E (shape factor)

Since the lag factor, j , was a function of geometry, efforts could be made to include this effect in the form of the equivalent heat transfer dimensionality, E , of Lin *et al.* (1993), into the model. It was found that $(j_{cEvap}/j_{cConv} - 1)$ varied according to shape (e.g. Figure 5.21).

After the likely relationships between $(j_{cEvap}/j_{cConv} - 1)$ and the other six parameters had been determined, nonlinear regression was used to find the most accurate form of the model. It was found that the best correlation ($R^2 = 0.981$) and most significant coefficients occurred for j_{cEvap}/j_{cConv} calculated using the curve-fit algebraic equation:

$$\begin{aligned} \frac{j_{cEvap}}{j_{cConv}} - 1 = & - \frac{0.0153 a_w^{2.4}}{Bi^{0.4}} + 0.0335 E e^{-(Bi-2.5)^2} + \\ & 0.0725 H_r e^{-(Bi-0.7)^2} + T_a (0.00338 H_r + 0.00413 e^{-(Bi-0.9)^2}) - \\ & T_{in} (0.00447 e^{-1.33Bi} + 0.000599) \end{aligned} \quad (5.20)$$

The product shape factor (E) is required. This is calculated using the methodology of Lin (1994) as follows:

$$E = \frac{Bi^{\frac{4}{3}} + 1.85}{\frac{Bi^{\frac{4}{3}}}{E_{\infty}} + \frac{1.85}{E_0}} \quad (5.21)$$

where E_o = 1 for infinite slab
= 2 for infinite cylinder
= 3 for sphere
and E_{∞} = 0.75 for infinite slab
= 1.76 for infinite cylinder
= 3.0 for sphere

5.7.4 Models for Mass-Average Temperature

The mass-average temperature is the temperature at which the product would equilibrate if insulated completely and left. The mass-average temperature might be used to calculate the refrigeration load during a cooling process. The numerically generated data for all 3 shapes suggest that the f_{avEvap}/f_{avConv} was in the range of 1.1 to 2.9 and j_{avEvap}/j_{avConv} was in the range 0.7 to 1.0.

5.7.4.1 Model Development for j_{avEvap}/j_{avConv}

When $(j_{avEvap}/j_{avConv} - 1)$ was plotted against different parameters, the following trends were observed:

(1) Bi

Figure 5.22 shows the numerically generated data for j_{avEvap}/j_{avConv} for the infinite cylinder plotted versus Bi . All the parameters interacted with Bi to some extent. H_r had only a small interaction with Bi but T_a had a critical point at about $Bi = 1$ which made the effect of the interaction reverse (e.g. Figure 5.23). T_{in} and a_w had similar interactions with Bi to each other. The higher the T_{in} or a_w values, the lower the value of $(j_{avEvap}/j_{avConv} - 1)$ was and the greater the Bi interaction (Figure 5.24). At high Bi , the effect of T_{in} was relatively small.

(2) H_r

The effects of H_r were relatively independent of T_{in} and a_w but interacted to some extent with T_a (e.g. Figure 5.25).

(3) T_a

Effects of T_a were relatively independent of T_{in} and a_w but interacted to some extent with H_r (e.g. Figure 5.25).

(4) a_w

Effects of a_w were relatively independent of T_a , H_r , and T_{in} .

(5) T_{in}

Effects of T_{in} were relatively independent of H_r , a_w , and T_a .

(6) E (shape)

Figure 5.26 shows the interaction of shape with Bi . The line for the infinite cylinder was between that for the sphere and infinite slab.

Using the results of the trend graphs, a trial and error process, and non-linear regression, it was found that the best correlation ($R^2 = 0.951$) and coefficient for j_{avEvap}/j_{avConv} came from the following curve-fit algebraic equation:

$$\frac{j_{avEvap}}{j_{avConv}} - 1 = \frac{(0.0345H_r + 0.00207(T_a - T_{in}) - 0.0228a_w^4)}{Bi^{\frac{1}{3}}} - \frac{0.0321H_r e^{-(Bi-2.5)^2} - (0.00169T_a + 0.0166E) e^{-(0.1Bi)^2}}{Bi^{\frac{1}{3}}} \quad (5.22)$$

5.7.4.2 Model Development for f_{avEvap}/f_{avConv}

Using a similar approach the best correlation ($R^2 = 0.996$) and most significant coefficient for f_{avEvap}/f_{avConv} arose from the following curve-fit algebraic equation.

$$\frac{f_{avEvap}}{f_{avConv}} - 1 = \frac{Bi}{15 (Bi^{1.5} + 0.5)} + \frac{T_a(H_r + 0.33) + (4.93H_r + 0.12T_{in} + 9.58)a_w^{0.8}}{19(Bi^{1.2} + 1.2)} \quad (5.23)$$

Because of the similarity between this equation and equation (5.19), the results of calculation using f_{avEvap} (equation 5.23) and j_{avEvap} (equation 5.22) were compared with f_{cEvap} (equation 5.19) and j_{cEvap} (equation 5.22). It was postulated that to reduce the number of the models, the same model as f_{cEvap}/f_{cConv} might be used for f_{avEvap}/f_{avConv} . That is:

$$\frac{f_{avEvap}}{f_{avConv}} - 1 = \frac{Bi}{15 (Bi^{1.5} + 1.5)} + \frac{T_a(H_r + 0.34) + (5H_r + 0.12T_{in} + 9.87)a_w^{0.8}}{19 (Bi^{1.2} + 1.2)} \quad (5.24)$$

5.7.5 Time and Temperature Prediction Equations

The j_{Conv} and f_{Conv} needed by equations (5.19) - (5.24) can be found from analytical solutions (equations 2.9 - 2.17 and equations 5.1 - 5.2). The equilibrium temperature is found from equation (5.11) and f_{Evap} and j_{Evap} can be used to predict chilling time or temperature by using the following equations:

$$t = \left(\frac{\ln Y - \ln j_{Evap}}{f_{Evap} \alpha} \right) R^2 \quad (5.25)$$

$$T = (T_{in} - T_{eq}) e^{(j_{Evap} Fo + \ln j_{Evap})} + T_{eq} \quad (5.26)$$

where Y = modified fractional unaccomplished temperature change as defined in equations (5.12) to (5.13)

T = product temperature (°C)

5.7.6 Quality of Prediction from The Simple Models Relative to The Numerical Simulations Results and Conclusions

Equations (5.19) to (5.24) were tested for a range of conditions $T_a = 0 - 15$ °C, $T_{in} = 20 - 50$ °C, $Bi = 0.1 - 10$, $a_w = 0.6 - 1.0$, and $H_r = 0.5 - 1.0$. The percentage differences between the results calculated by the curve-fit algebraic equation and the numerical model were determined as follows:

$$\% \text{ difference} = \frac{(\text{finite difference} - \text{simple model})}{(\text{simple model})} \times 100 \quad (5.27)$$

- (1) The percentage differences in the j_c value, f_c value, and time to reach $Y_c = 0.1, 0.35, 0.7$ are shown in Table 5.1. It was found that the 95% confidence bounds on the percentage difference in f_c and j_c value were within $\pm 5.8 \%$ and $\pm 4.3 \%$ respectively. The percentage difference in time to reach Y_c of 0.10, 0.35, and 0.70 were within about $\pm 5 \%$, $\pm 5 \%$, and $\pm 7 \%$ respectively at the 95% level of confidence.
- (2) The percentage differences in the j_{av} value, f_{av} value, and time to reach $Y_{av} = 0.10, 0.35, 0.55$ are shown in Table 5.2. The 95% confidence bounds on the percentage difference in f_{av} and j_{av} value were within $\pm 5.6 \%$ and $\pm 4.1 \%$ respectively. The percentage differences in time to reach Y_{av} of 0.10, 0.35, and 0.55 were within about $\pm 6 \%$, $\pm 7 \%$, and $\pm 10 \%$ respectively.

When equation (5.24) was used to replace equation (5.23) (Table 5.3) the results are little different, suggesting that equation (5.23) is unnecessary, and that a single equation for f_{Evap}/f_{Conv} is satisfactory.

One trend that all of Tables 5.1 to 5.3 show is poorer prediction at $Y_c = 0.7$ and $Y_{av} = 0.55$ than at lower Y values. Figures 5.27 and 5.28 show the main reason. As the evaporative effect becomes stronger (Figure 5.28), j_{cEvap} and j_{avEvap} can become close to 0.7 and 0.55 respectively, and then these Y values are passed before the semi-log plot has linearised.

In contrast, with convection-only cooling (Figure 5.27), j_{cConv} and j_{avConv} depend only on Bi , and irrespective of Bi , $j_{cConv} \geq 1$ and $j_{avConv} \geq 0.61$. Therefore at $Y_c = 0.7$ and $Y_{av} = 0.55$ the graph has linearised satisfactorily in even the most extreme conditions.

Without moving to a more complex model than the one term approximation to the series analytical solution for convection cooling there is no easy way to make the methodology more accurate at higher Y values. However at the end of chilling, target Y values are usually 0.1 to 0.3 so the final chilling time will be accurately predicted. The problem does limit the ability of the methodology to accurately predict the temperature/time history early in a chilling process.

5.8 SUMMARY

The temperature histories were described in the form of f and j values. The plots of $\ln Y$ versus FO were linearized using a reference temperature. The equilibrium temperature used as reference temperature depends on the ambient air temperature, the relative humidity, and the product surface water activity and is defined by equation (5.11) or Figures 5.1 to 5.3. The existence of the equilibrium surface temperature will be experimentally tested in Chapter 6.

The magnitude of the evaporative cooling effects depends on the environmental conditions (Bi , T_a , and H_r) and product physical properties (T_{in} , E , and a_w) which alter the values of f and j . Across the ranges tested, the rate of evaporative cooling lies between 1.1 and 2.9 times that of the convection-only cooling. The values of j_{cEvap} and j_{avEvap} are 0.7 to 1 times the j value for convective only cooling.

When compared with the numerically-calculated results, all curve-fit equations generally give good agreement (95% confidence bound of about $\pm 5\%$ with the mean difference close to 0%). It is postulated that these empirical equations can be used (with high accuracy) for quick estimation of the chilling rate of simple shapes undergoing evaporative and convective cooling with constant surface water activity.

Table 5.1 Percentage differences between results calculated by the proposed curve-fit algebraic equations and results calculated by finite differences for the centre temperature of all three shapes.

shape		% difference in $f_{c,Evap}/f_{c,Conv}$	% difference in $j_{c,Evap}/j_{c,Conv}$	% difference in time to $Y_c =$		
				0.10	0.35	0.70
infinite cylinder	mean	+0.27	+0.04	-0.2	-0.2	-0.1
	std.	1.52	0.97	1.4	1.6	2.6
	95% conf. interval	-2.7 to +3.2	-1.8 to +1.9	-3.1 to +2.7	-3.3 to +2.9	-5.2 to +5.0
sphere	mean	+1.7	+0.5	-1.4	-1.3	-0.8
	std.	2.1	1.9	1.8	1.8	2.9
	95% conf. interval	-2.4 to +5.8	-3.3 to 4.3	-4.9 to +2.1	-4.9 to +2.3	-6.6 to +5.0
infinite slab	mean	-1.6	-0.8	+1.3	+0.9	-0.1
	std.	1.7	1.7	1.5	1.6	3.7
	95% conf. interval	-5.0 to +1.8	-4.2 to +2.6	-1.7 to +4.2	-2.1 to +3.9	-7.4 to +7.4

Table 5.2 Percentage differences between results calculated by the proposed curve-fit algebraic equations and results calculated by finite differences for the mass-average temperature of all three shapes. Equation (5.23) was used to calculate f_{avEvap} .

shape		% difference in f_{avEvap}/f_{avConv}	% difference in j_{avEvap}/j_{avConv}	% difference in time to $Y_{av} =$		
				0.10	0.35	0.55
infinite cylinder	mean	+0.0	+0.1	+0.0	+0.1	+0.3
	std.	1.3	1.1	1.4	1.8	3.0
	95% conf. interval	-2.5 to +2.5	-2.1 to +2.3	-2.7 to +2.7	-3.4 to +3.6	-5.6 to +6.2
sphere	mean	+2.0	+0.6	-1.7	-1.3	-0.6
	std.	1.7	1.8	2.0	2.8	5.0
	95% conf. interval	-1.3 to +5.3	-2.9 to +4.1	-5.6 to +2.2	-6.8 to +4.2	-10.4 to +9.2
infinite slab	mean	-2.3	0.2	2.5	2.6	2.9
	std.	1.7	1.3	1.9	2.5	3.6
	95% conf. interval	-5.6 to +1.0	-2.3 to +2.7	-1.2 to +6.2	-2.4 to +7.4	-4.2 to +10.0

Table 5.3 Percentage differences between results calculated by the proposed curve-fit algebraic equations and results calculated by finite differences for the mass-average temperature of all three shapes. Equation (5.24) was used to calculate f_{avEvap} .

shape		% difference in f_{avEvap}/f_{avConv}	% difference in j_{avEvap}/j_{avConv}	% difference in time to $Y_{av} =$		
				0.10	0.35	0.55
infinite cylinder	mean	+0.8	+0.1	-0.7	-0.7	-0.5
	std.	1.5	1.1	1.6	2.0	3.1
	95% conf. interval	-2.1 to +3.7	-2.1 to +2.3	-3.8 to 2.4	-4.6 to +3.2	-6.6 to +5.6
sphere	mean	+2.7	+0.6	-2.3	-1.9	-1.2
	std.	2.0	1.8	2.3	3.1	5.2
	95% conf. interval	-1.2 to +6.6	-2.9 to +4.1	-6.8 to +2.2	-8.0 to +4.2	-11.4 to +9.0
infinite slab	mean	-1.6	0.2	1.8	1.9	2.1
	std.	1.8	1.3	1.9	2.4	3.5
	95% conf. interval	-5.1 to +1.9	-2.3 to +2.7	-1.9 to +5.5	-2.8 to +6.6	-4.8 to +9.0

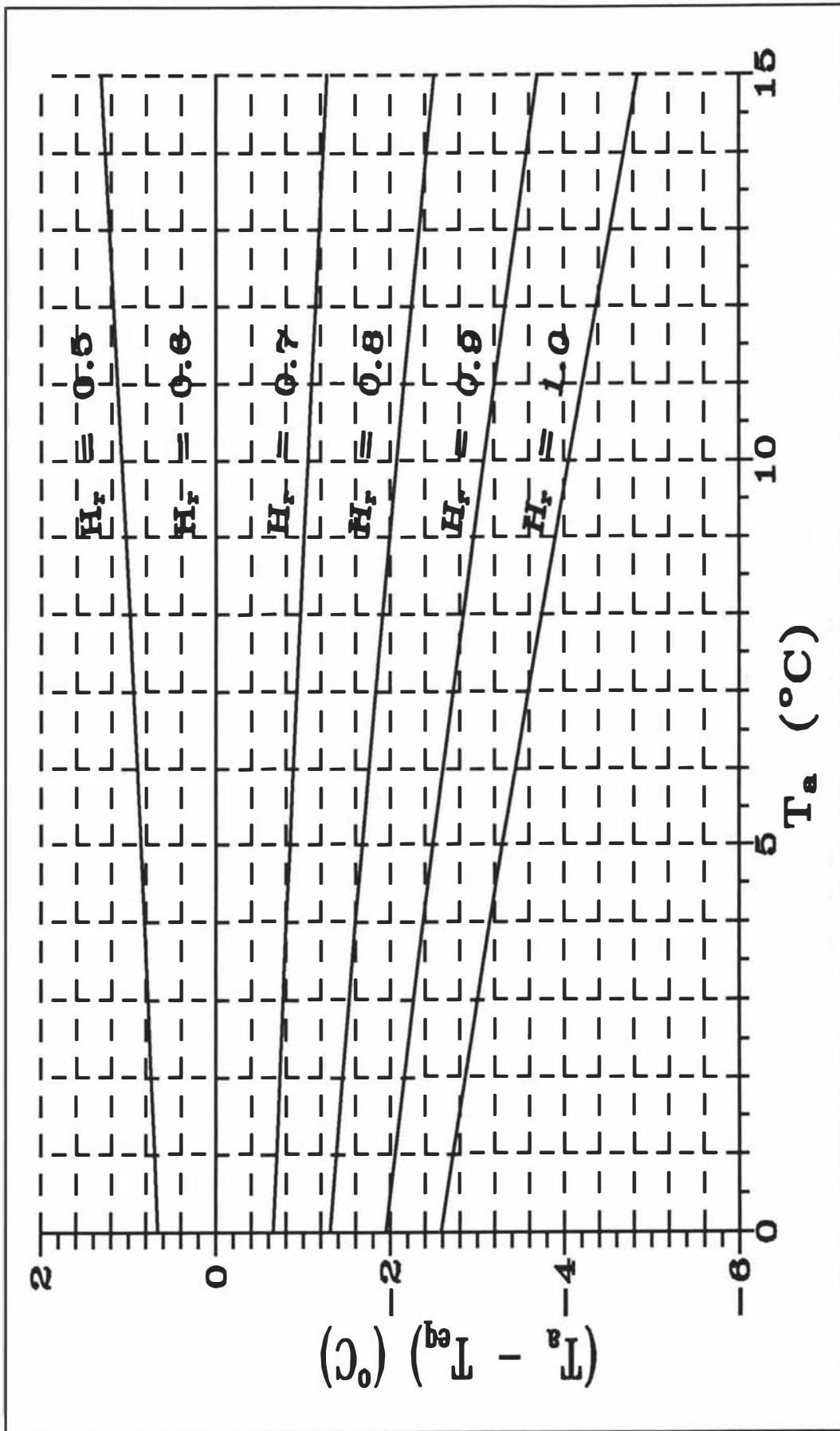


Figure 5.1 Alignment chart to estimate the equilibrium temperature (T_{eq}) at $a_w = 0.6$.

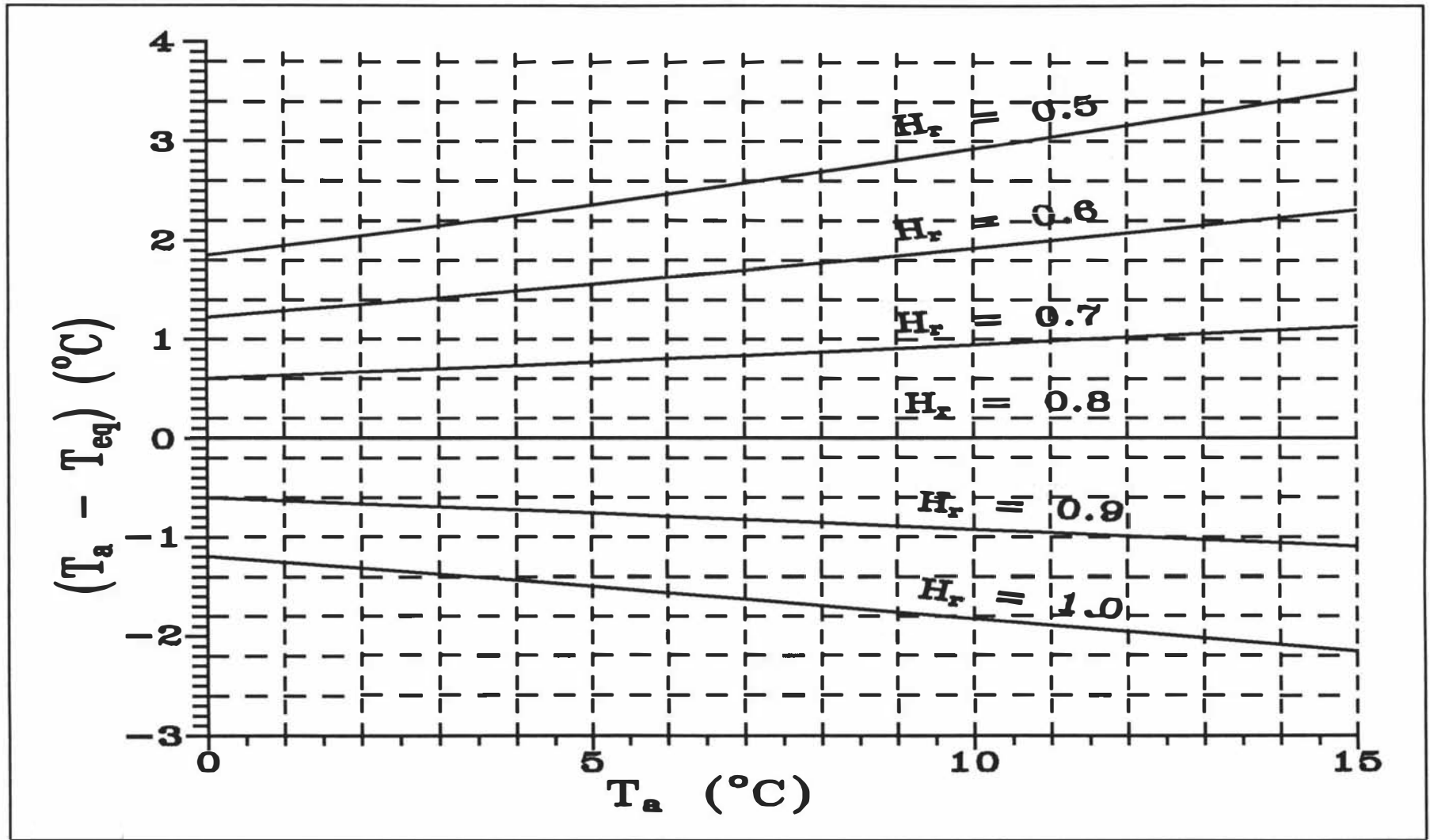


Figure 5.2 Alignment chart to estimate the equilibrium temperature (T_{eq}) at $a_w = 0.8$.

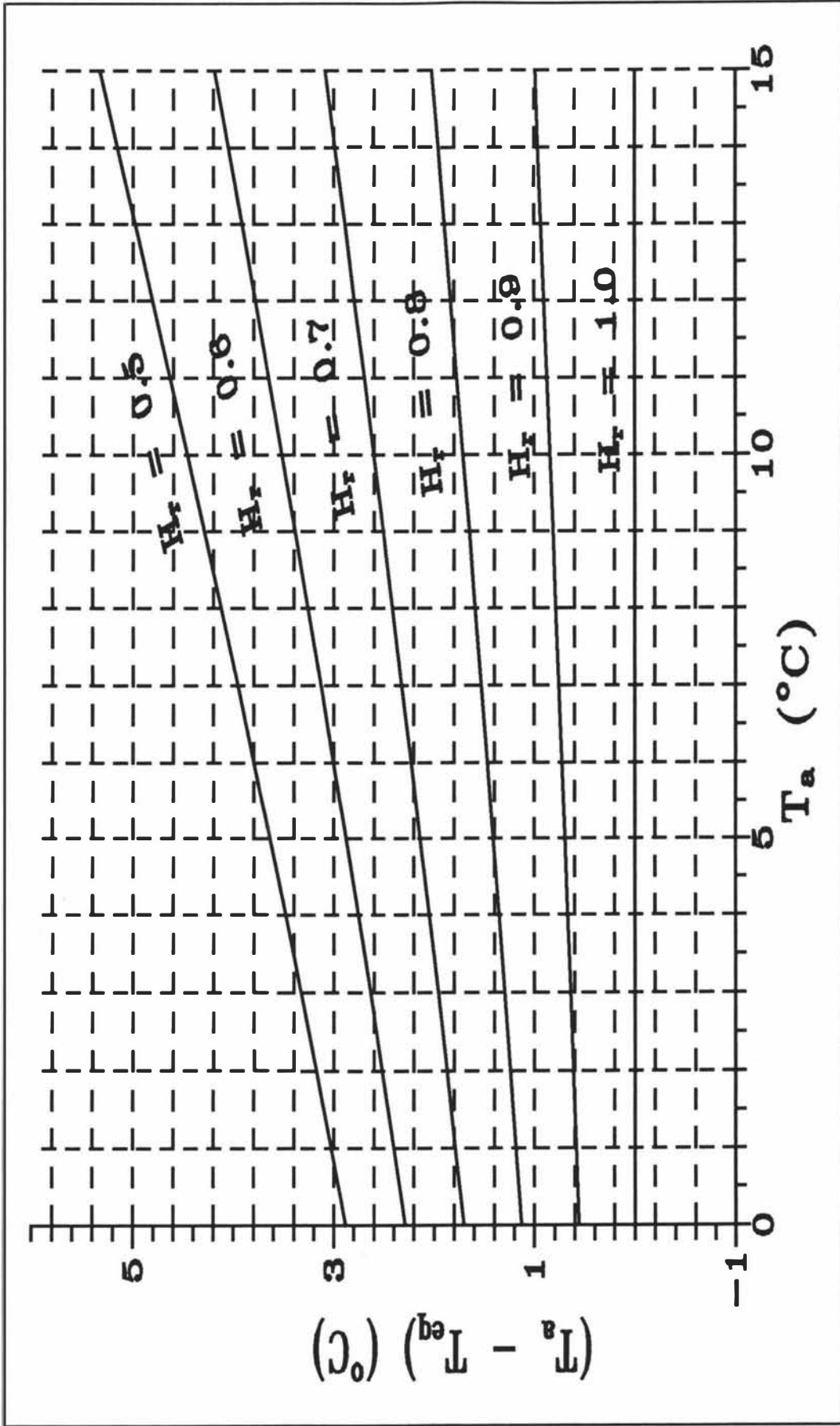


Figure 5.3 Alignment chart to estimate the equilibrium temperature (T_{eq}) at $a_w = 1.0$.

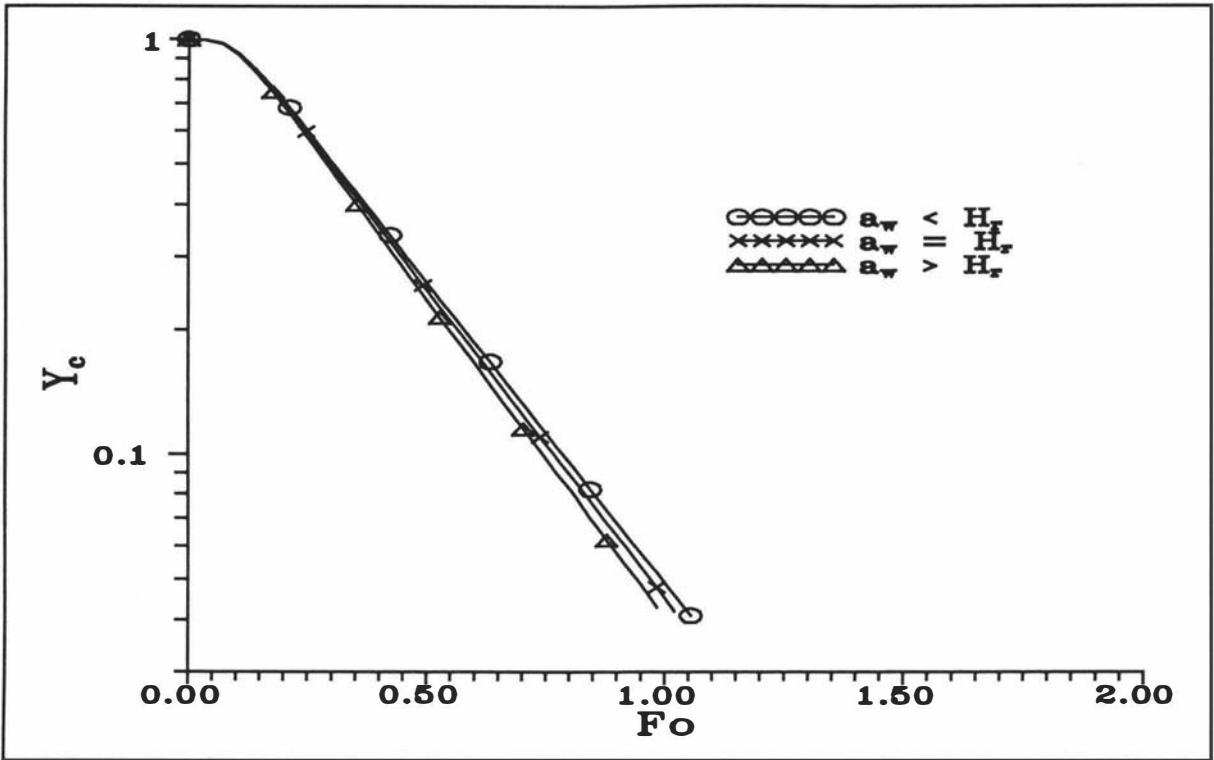


Figure 5.4 Example plots of $\ln Y_c$ vs Fo for evaporative cooling.

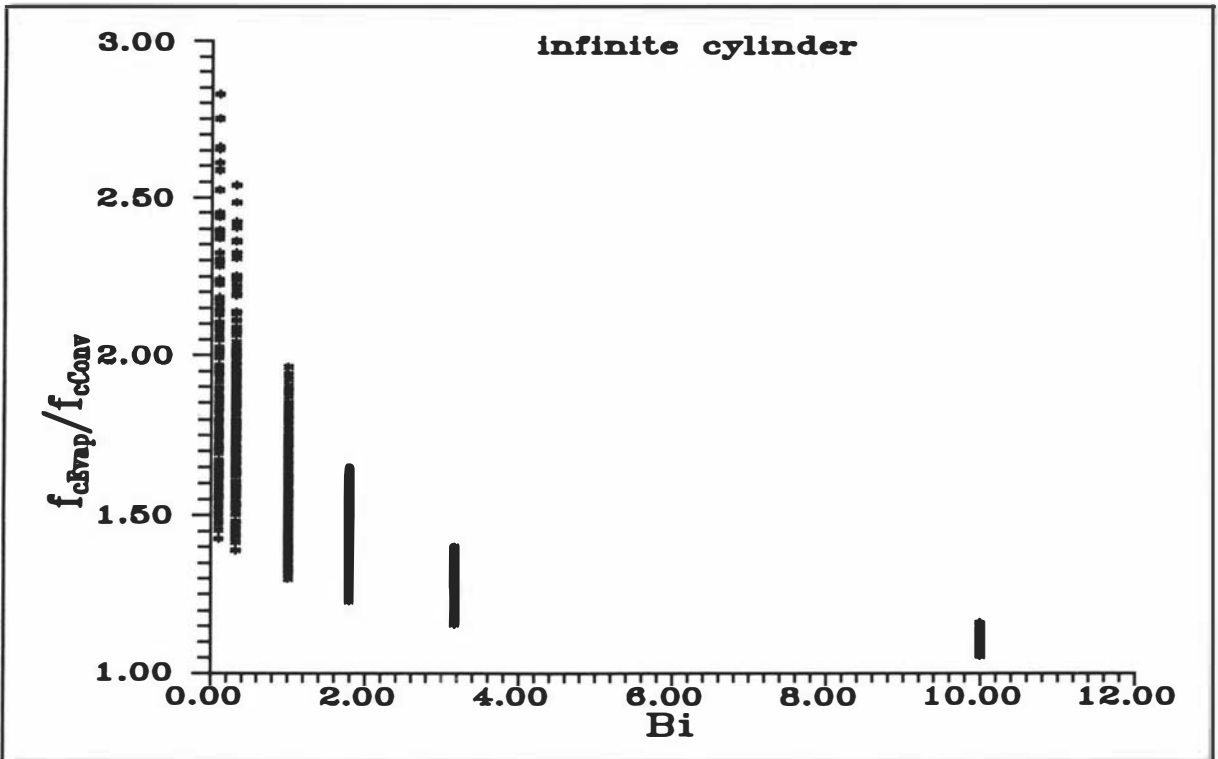


Figure 5.5 Plot of numerically predicted f_{cEvap}/f_{cConv} vs Bi for an infinite cylinder. All data in the ranges stated in Chapter 4 are plotted.

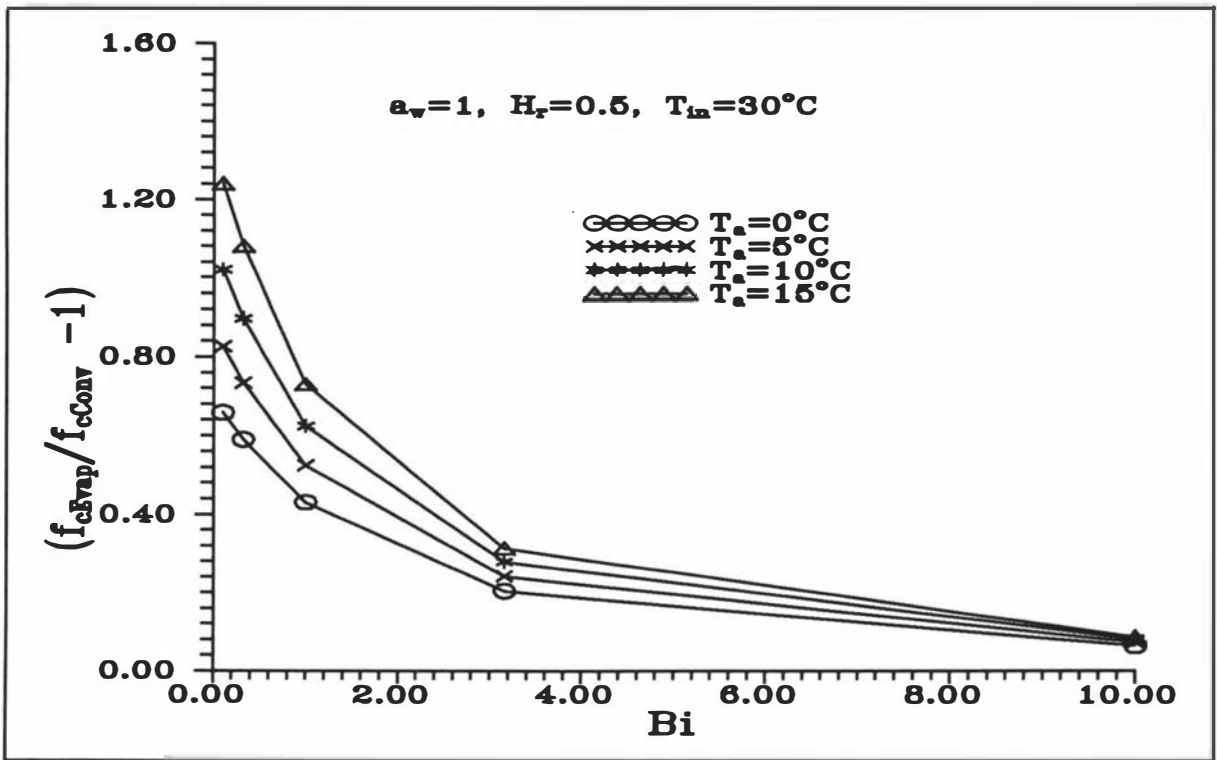


Figure 5.6 Effect of Bi on the slope ratios of semi-log plots (centre position) at different T_a (predicted by finite difference simulations for an infinite cylinder).

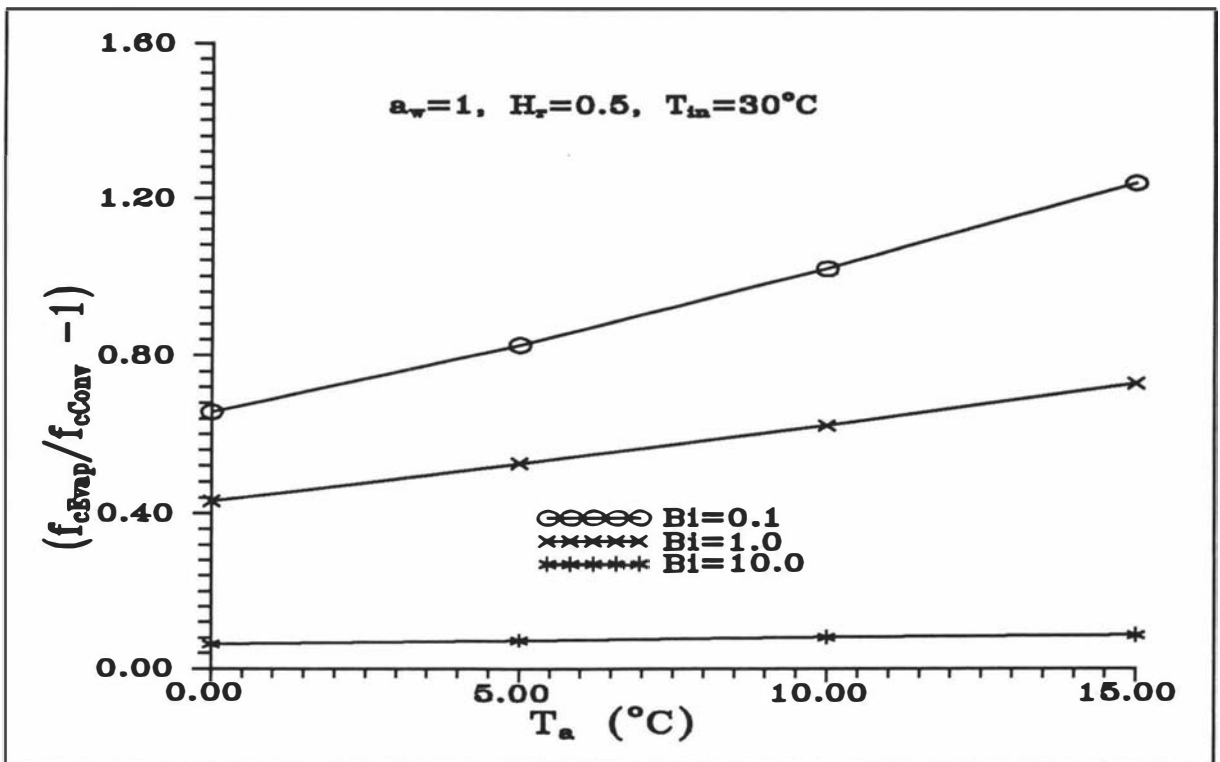


Figure 5.7 Effect of T_a on the slope ratio of semi-log plots (centre position) at different Bi (predicted by finite difference simulations for an infinite cylinder).

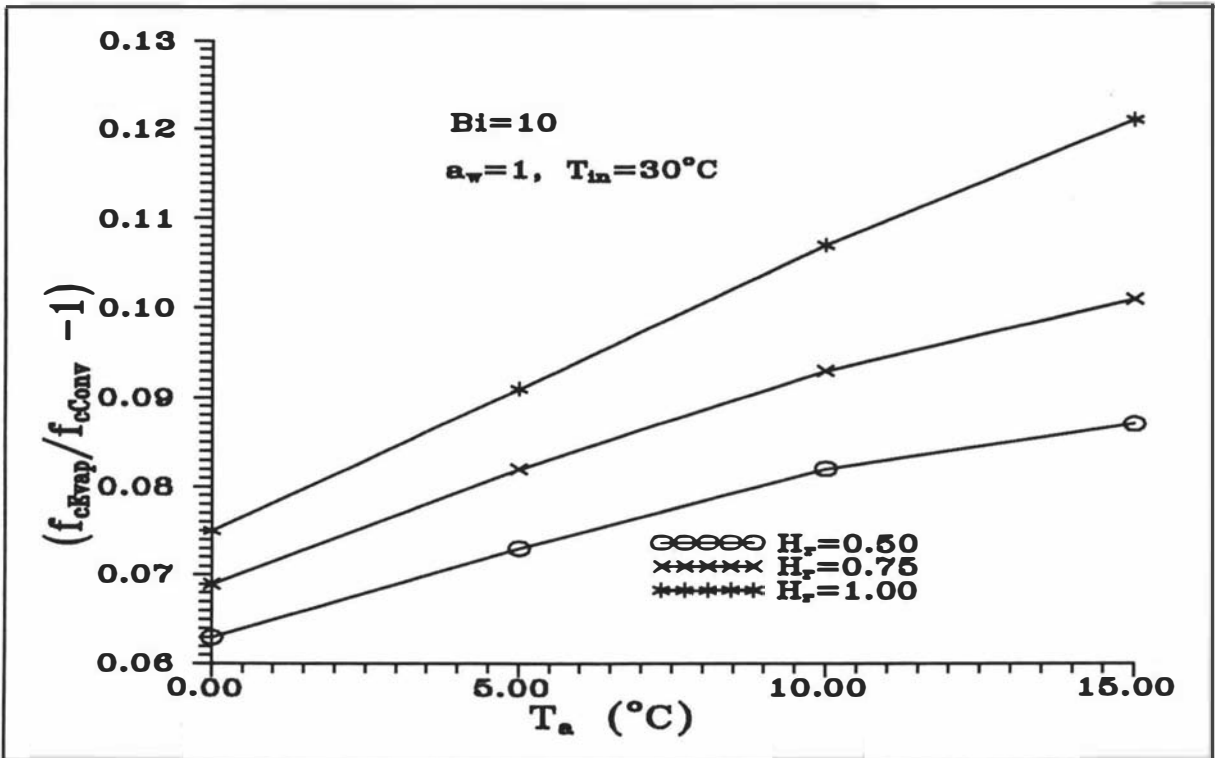


Figure 5.8 Effect of T_a on the slope ratio of semi-log plots (centre position) at high Bi and different H_r (predicted by finite difference simulations for an infinite cylinder).

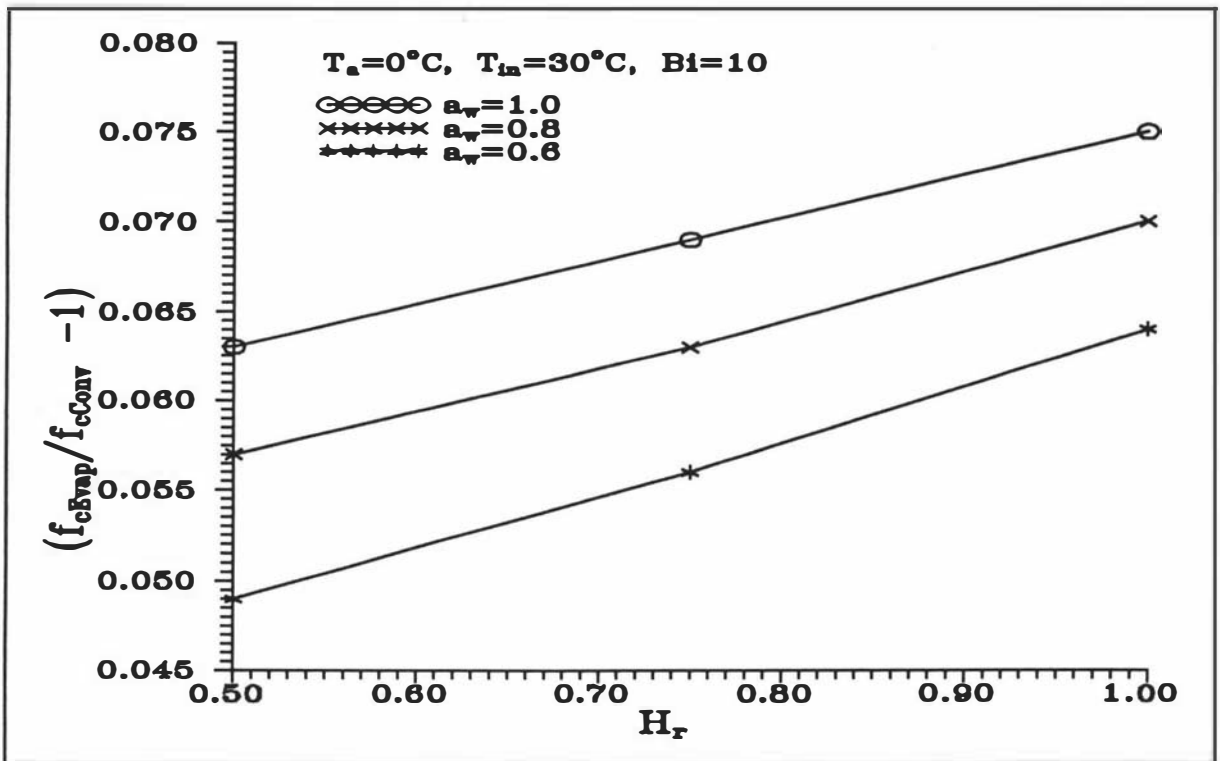


Figure 5.9 Effect of H_r on the slope ratio of semi-log plots (centre position) at high Bi and different a_w (predicted by finite difference simulations for an infinite cylinder).

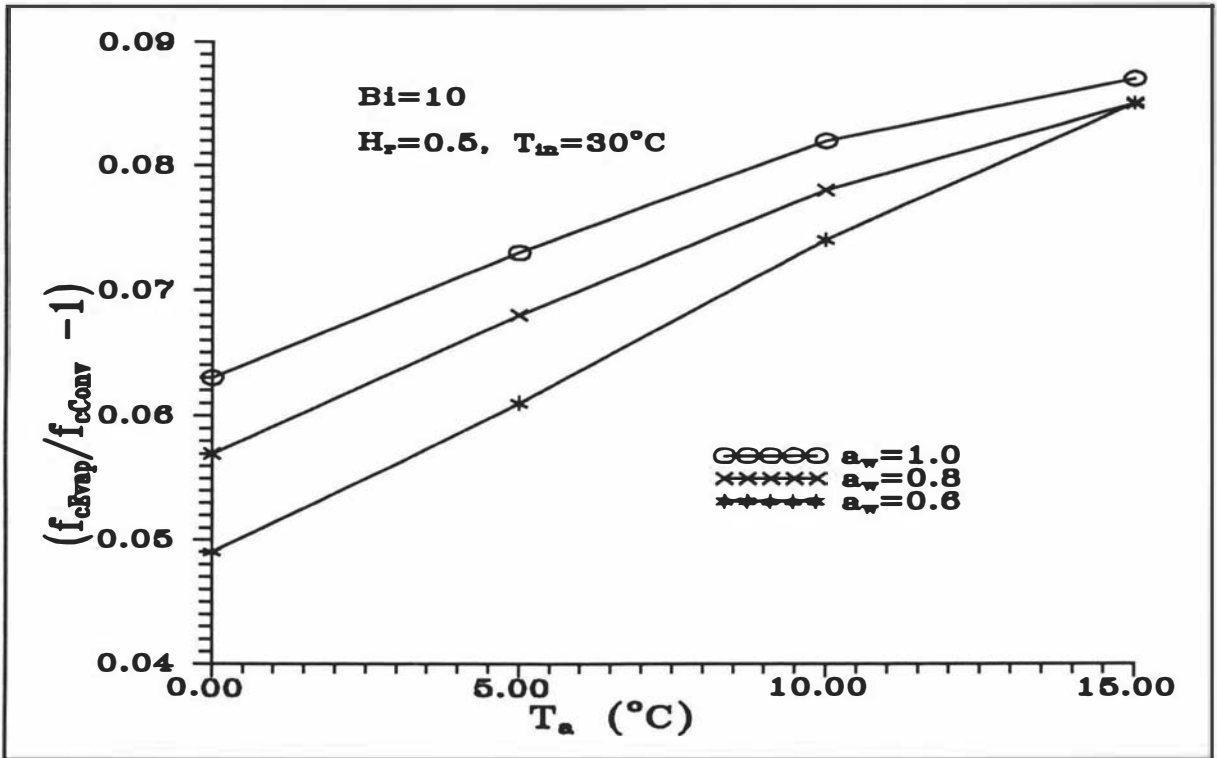


Figure 5.10 Effect of T_a on the slope ratio of semi-log plots (centre position) at high Bi and different a_w (predicted by finite difference simulations for an infinite cylinder).

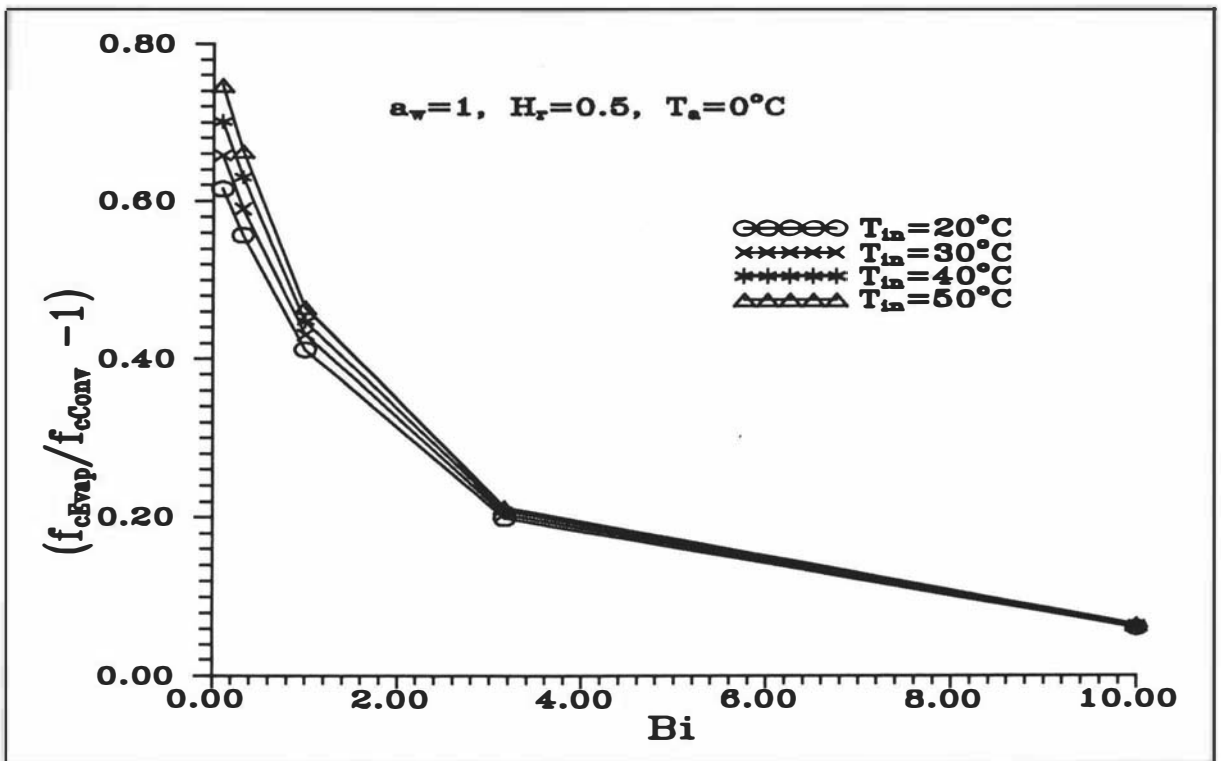


Figure 5.11 Effect of Bi on the slope ratio of semi-log plots (centre position) at different T_{in} (predicted by finite difference simulations for an infinite cylinder).

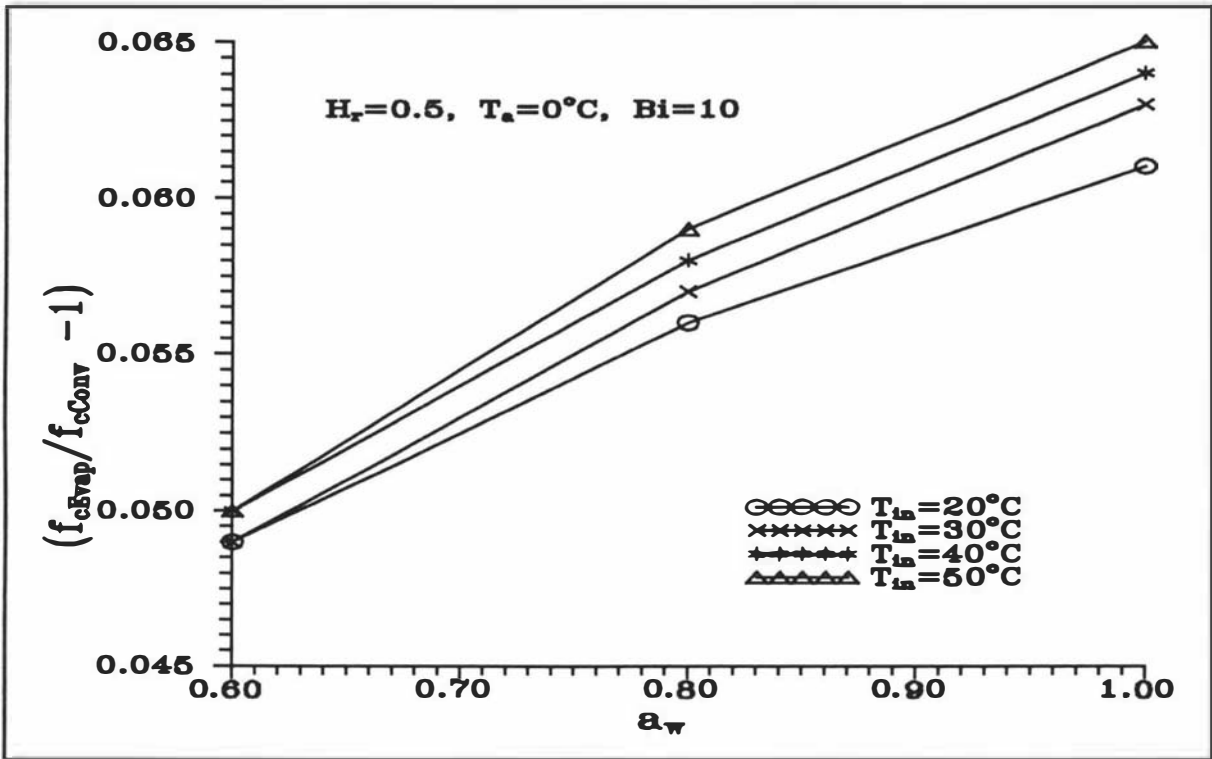


Figure 5.12 Effect of a_w on the slope ratio of semi-log plots (centre position) at high Bi and different T_{in} (predicted by finite difference simulations for an infinite cylinder).

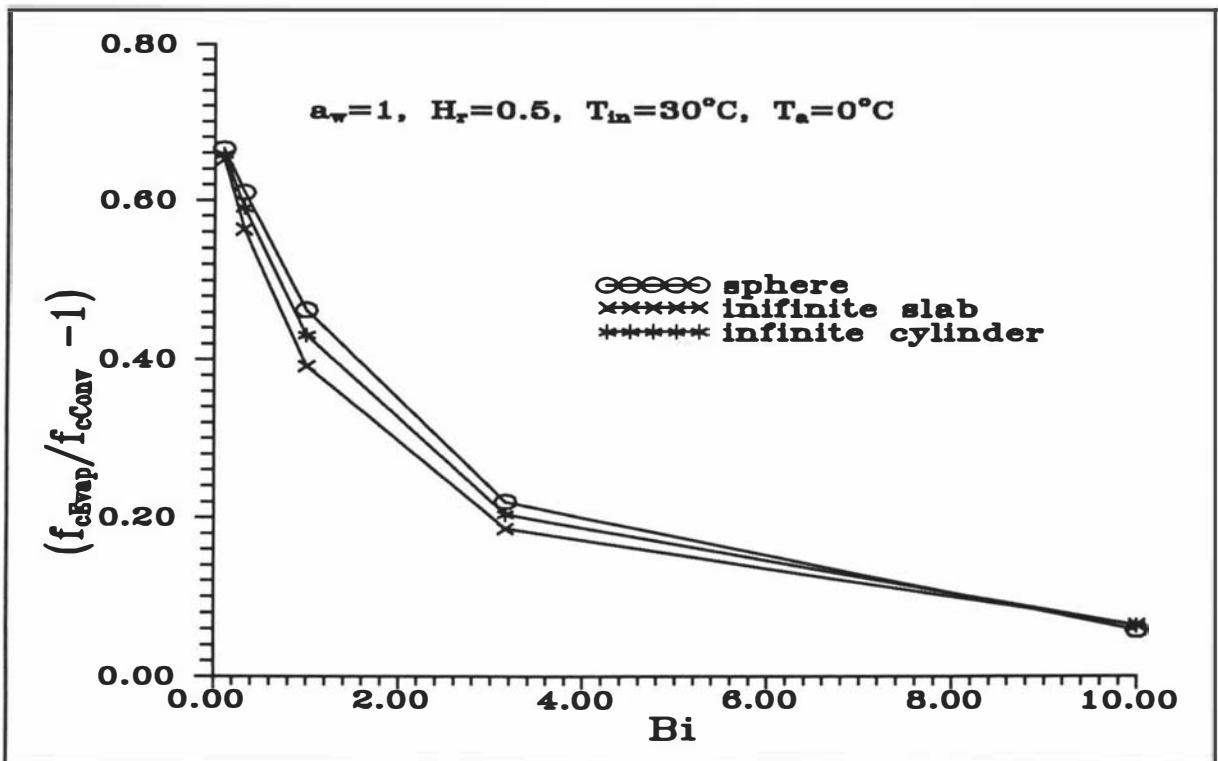


Figure 5.13 Effect of shape on the slope ratio of semi-log plots (centre position) (predicted by finite difference simulations for an infinite cylinder).

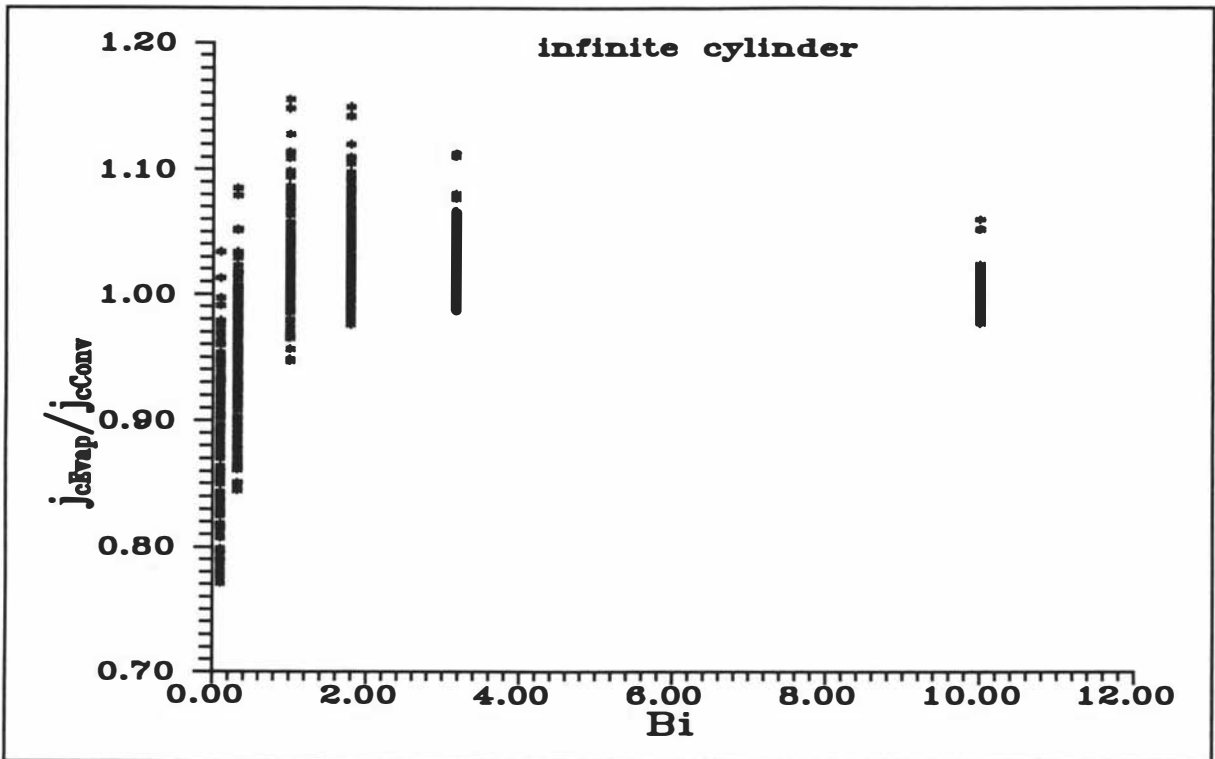


Figure 5.14 Plot of numerically predicted j_{cEvap}/j_{cConv} data for an infinite cylinder vs Bi .

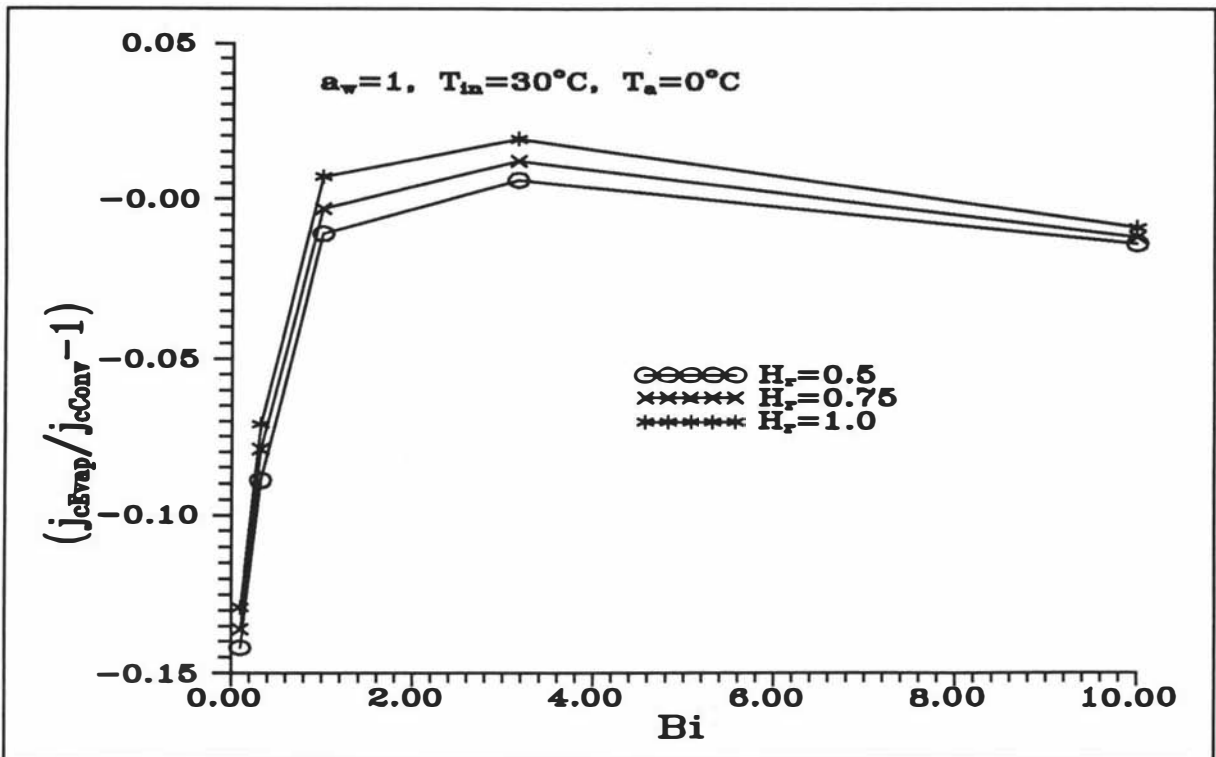


Figure 5.15 Effect of Bi on the intercept ratio of semi-log plots (centre position) at different H_r , (predicted by finite difference simulations for an infinite cylinder).

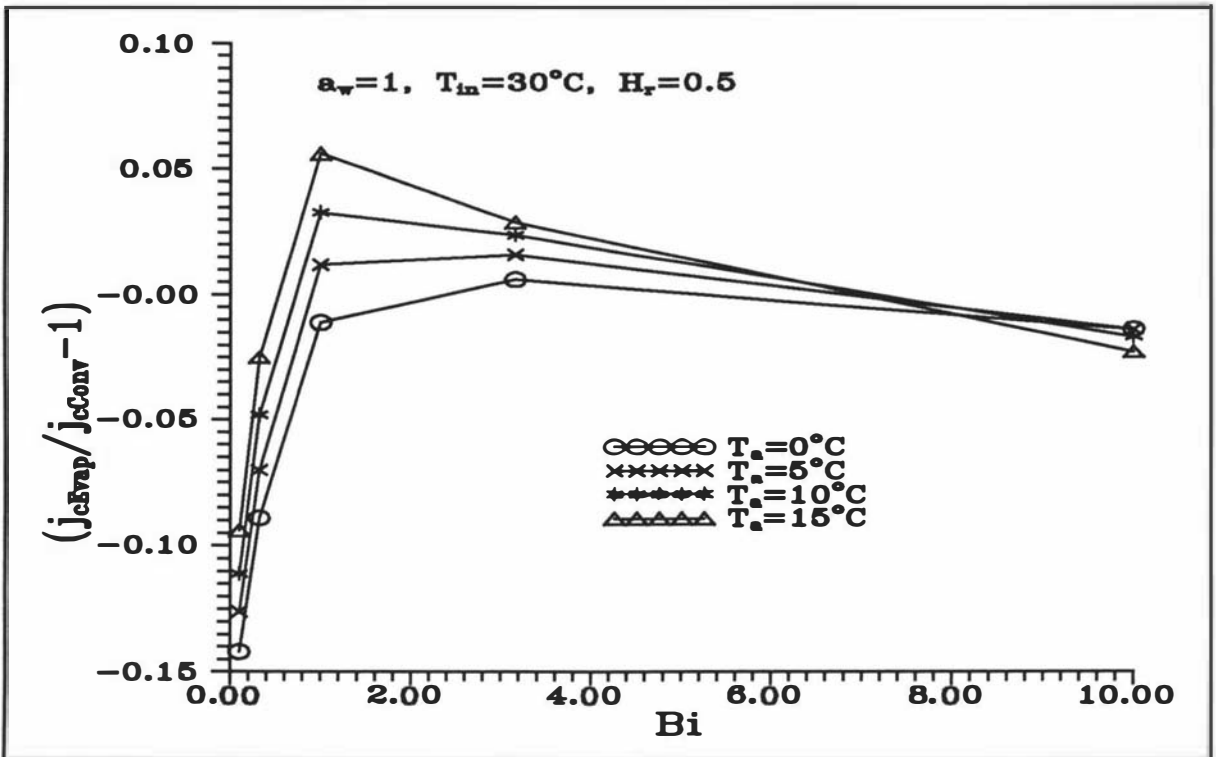


Figure 5.16 Effect of Bi on the intercept ratio of semi-log plots (centre position) at different T_a (predicted by finite difference simulations for an infinite cylinder).

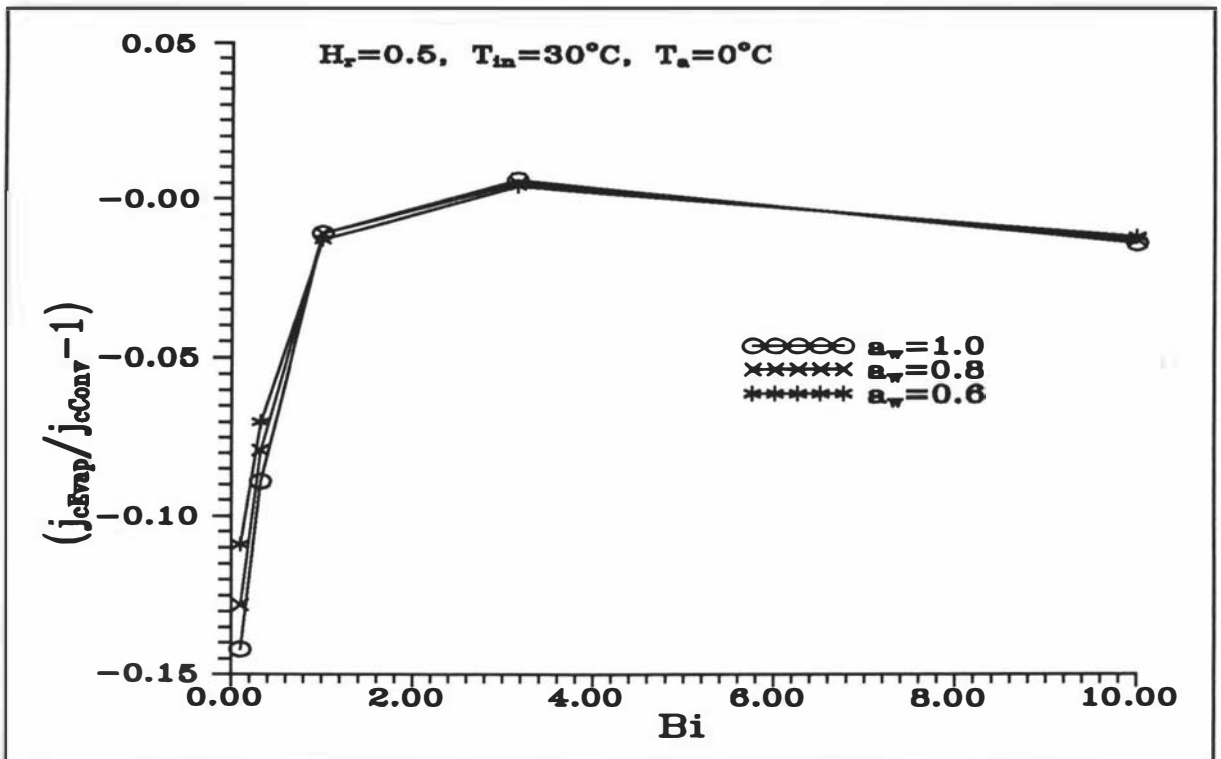


Figure 5.17 Effect of Bi on the intercept ratio of semi-log plots (centre position) at different a_w (predicted by finite difference simulations for an infinite cylinder).

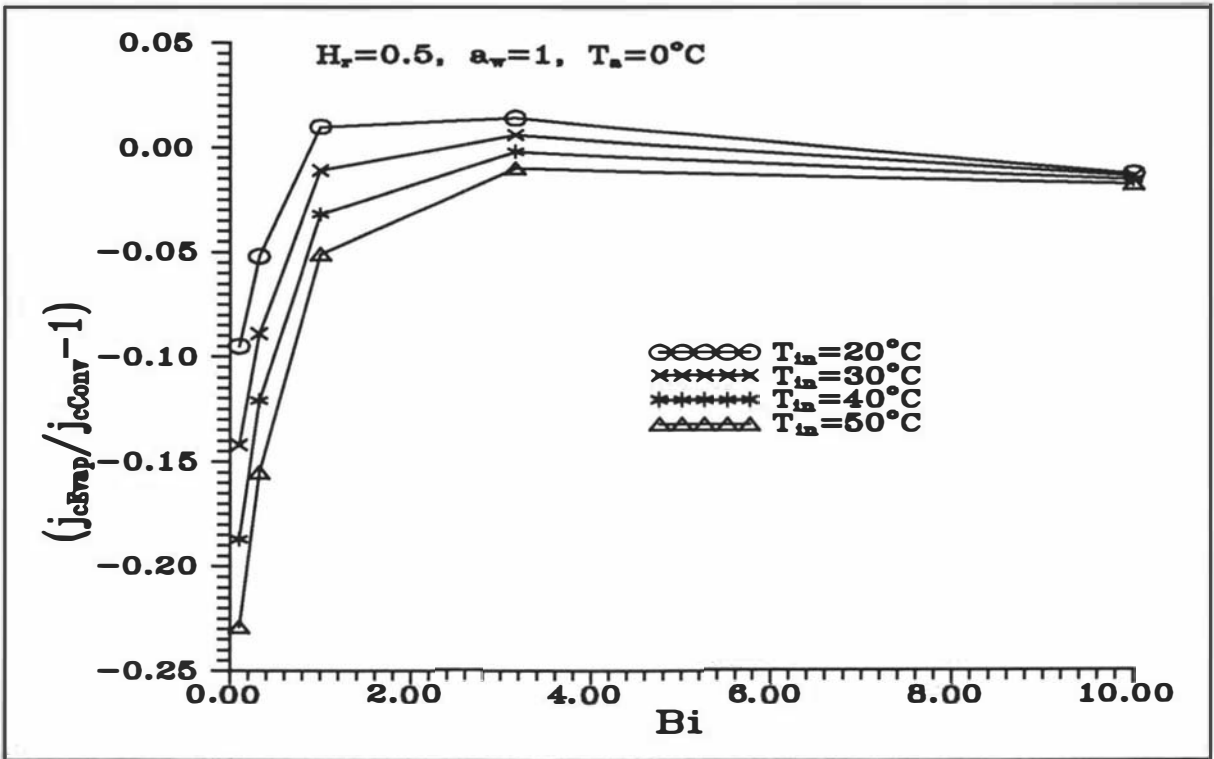


Figure 5.18 Effect of Bi on the intercept ratio of semi-log plots (centre position) at different T_{in} (predicted by finite difference simulations for an infinite cylinder).

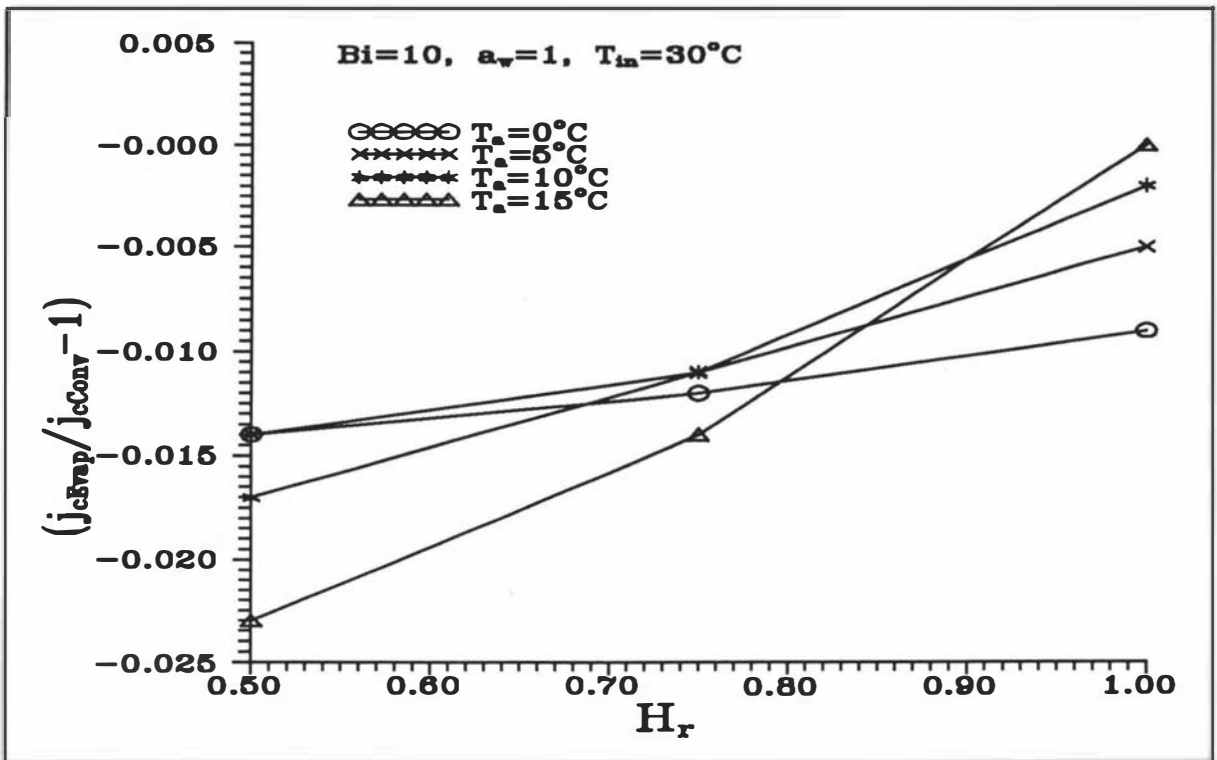


Figure 5.19 Effect of H_r on the intercept ratio of semi-log plots (centre position) at high Bi and different T_a (predicted by finite difference simulations for an infinite cylinder).

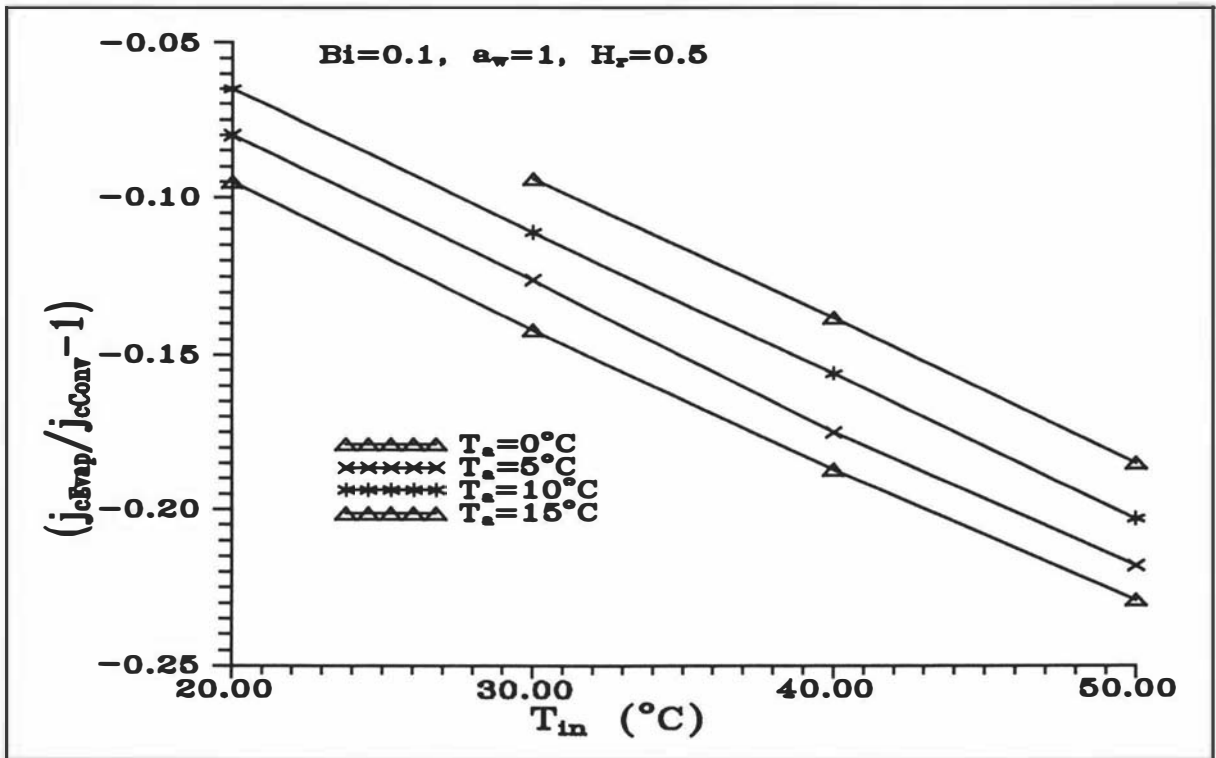


Figure 5.20 Effect of T_{in} on the intercept ratio of semi-log plots (centre position) at different T_a (predicted by finite difference simulations for an infinite cylinder).

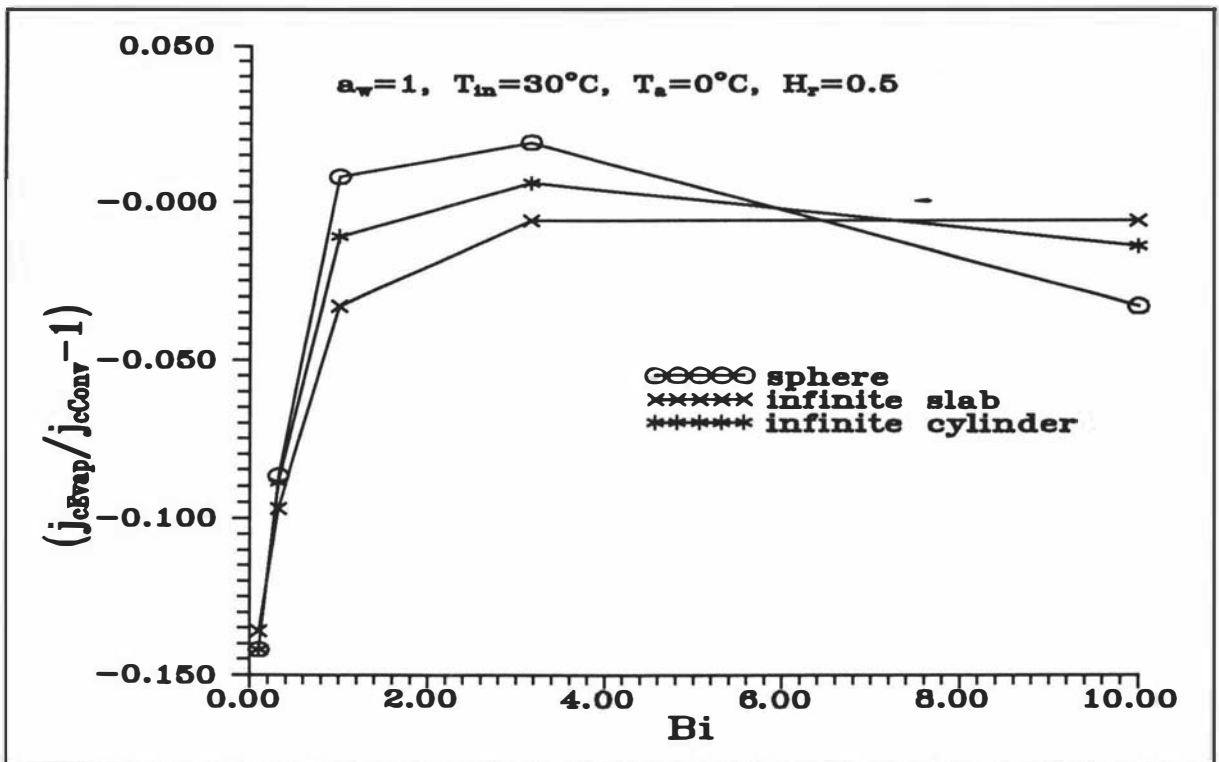


Figure 5.21 Effect of shape on the intercept ratio of semi-log plots (centre position) (predicted by finite difference simulations for an infinite cylinder).

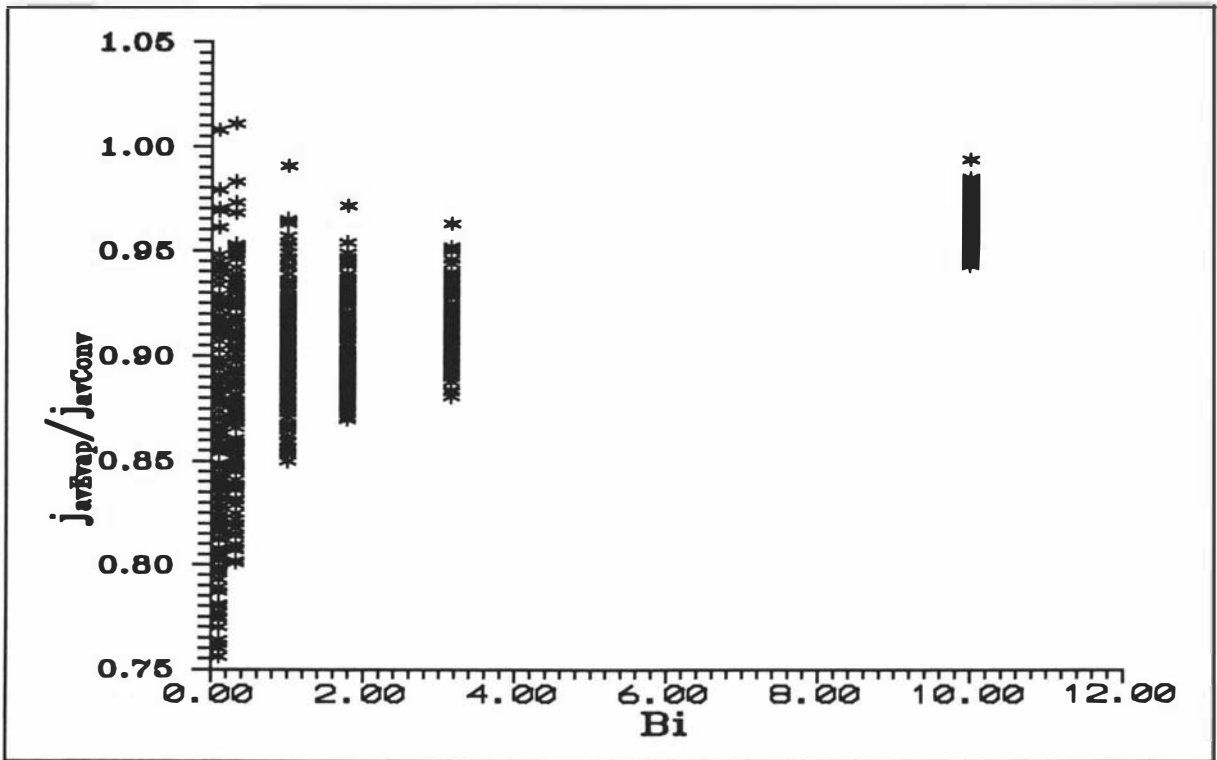


Figure 5.22 Plot of numerically predicted j_{avEvap}/j_{avConv} data for an infinite cylinder vs Bi .

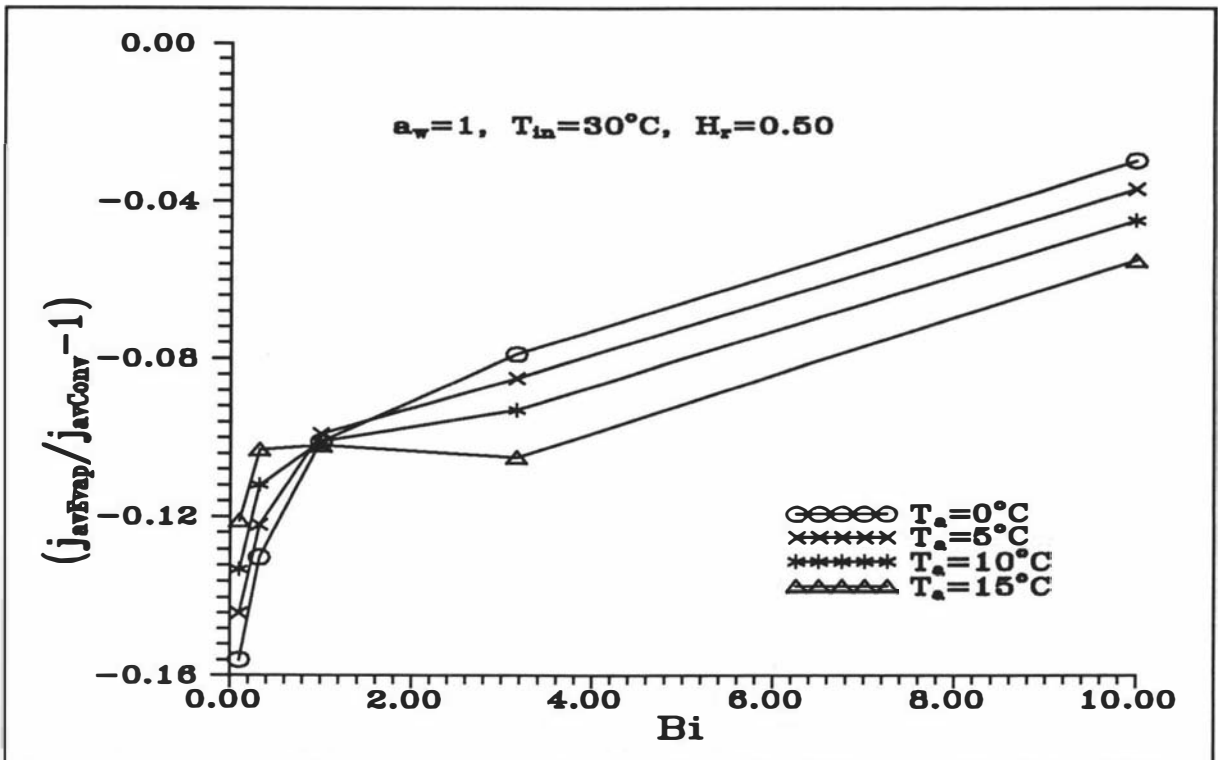


Figure 5.23 Effect of Bi on the intercept ratio of semi-log plots (mass-average position) at different T_a (predicted by finite difference simulations for an infinite cylinder).

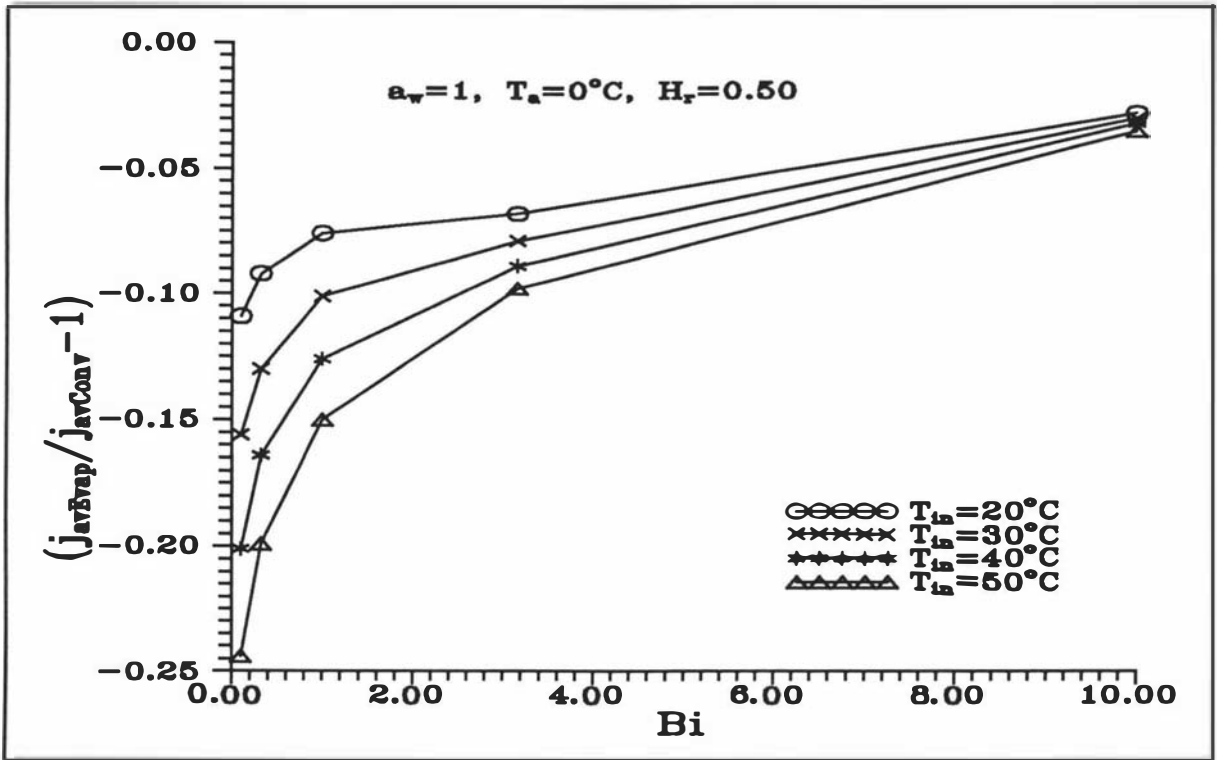


Figure 5.24 Effect of Bi on the intercept ratio of semi-log plots (mass-average position) at different T_{in} (predicted by finite difference simulations for an infinite cylinder).

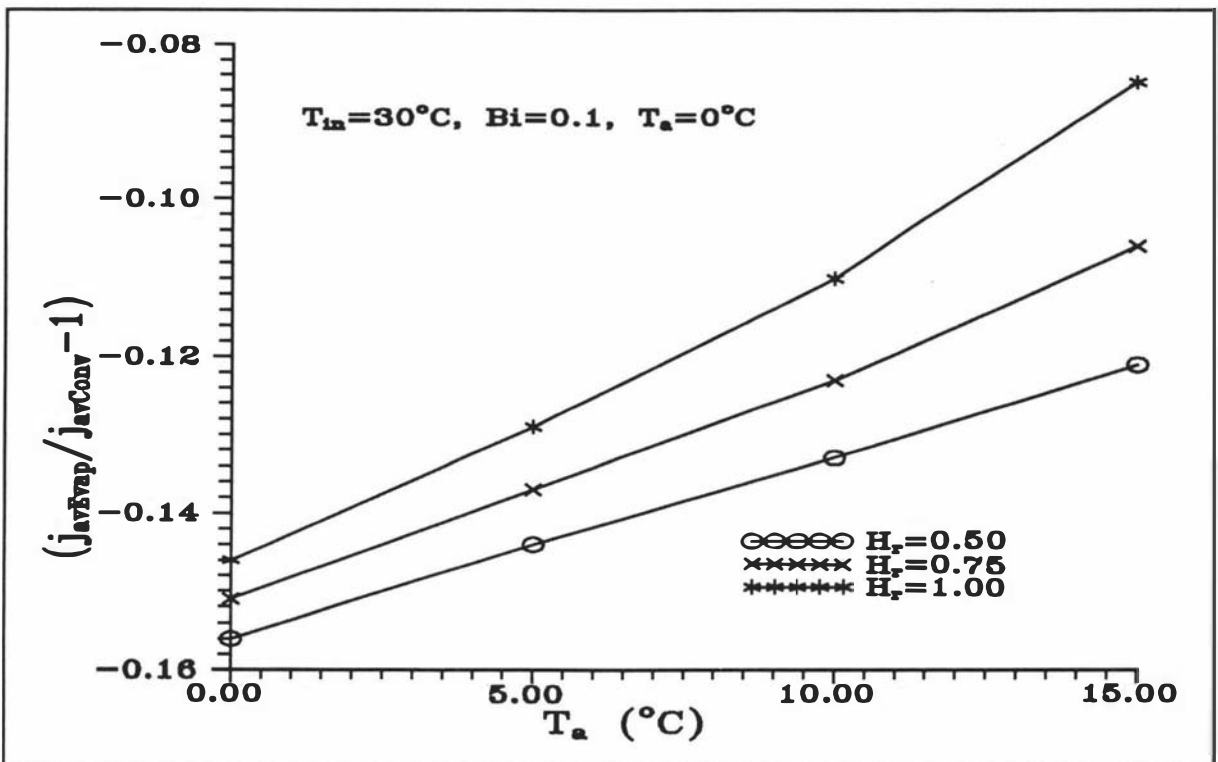


Figure 5.25 Effect of T_a on the intercept ratio of semi-log plots (mass-average position) at different H_r (predicted by finite difference simulations for an infinite cylinder).

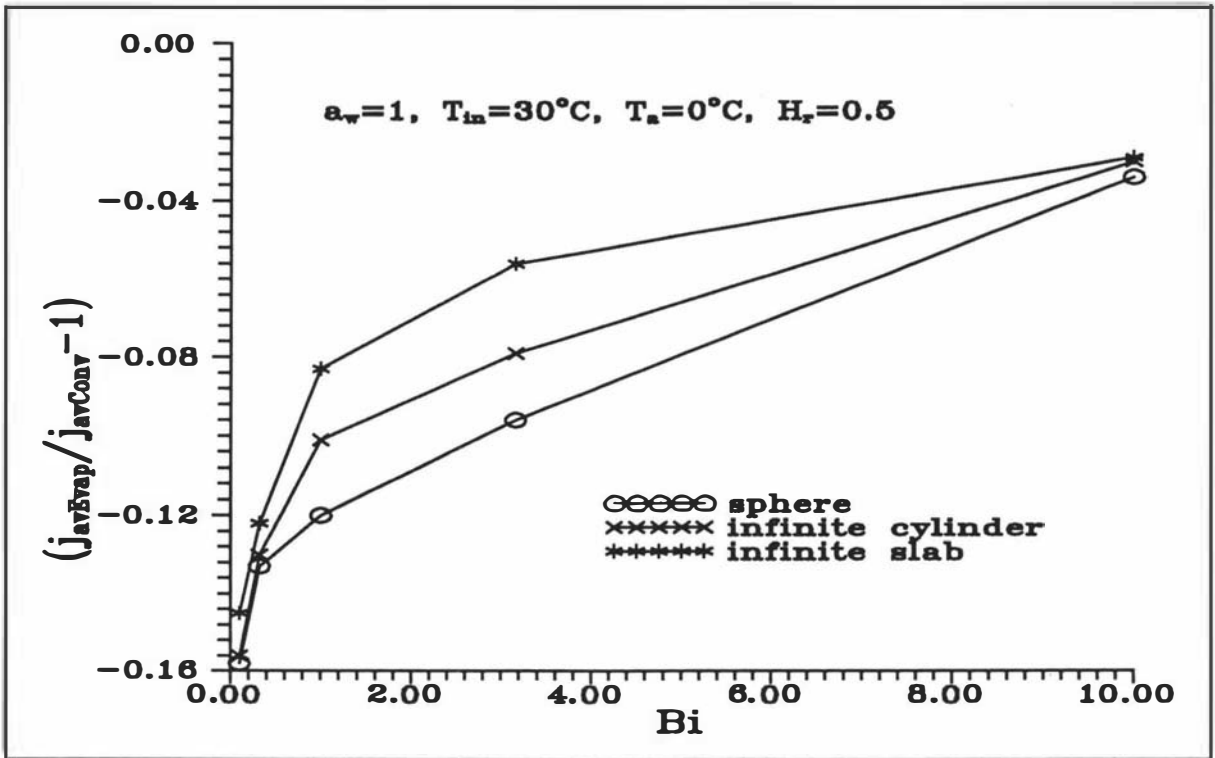


Figure 5.26 Effect of shape on the intercept ratio of semi-log plots (mass-average position) (predicted by finite difference simulations for an infinite cylinder).

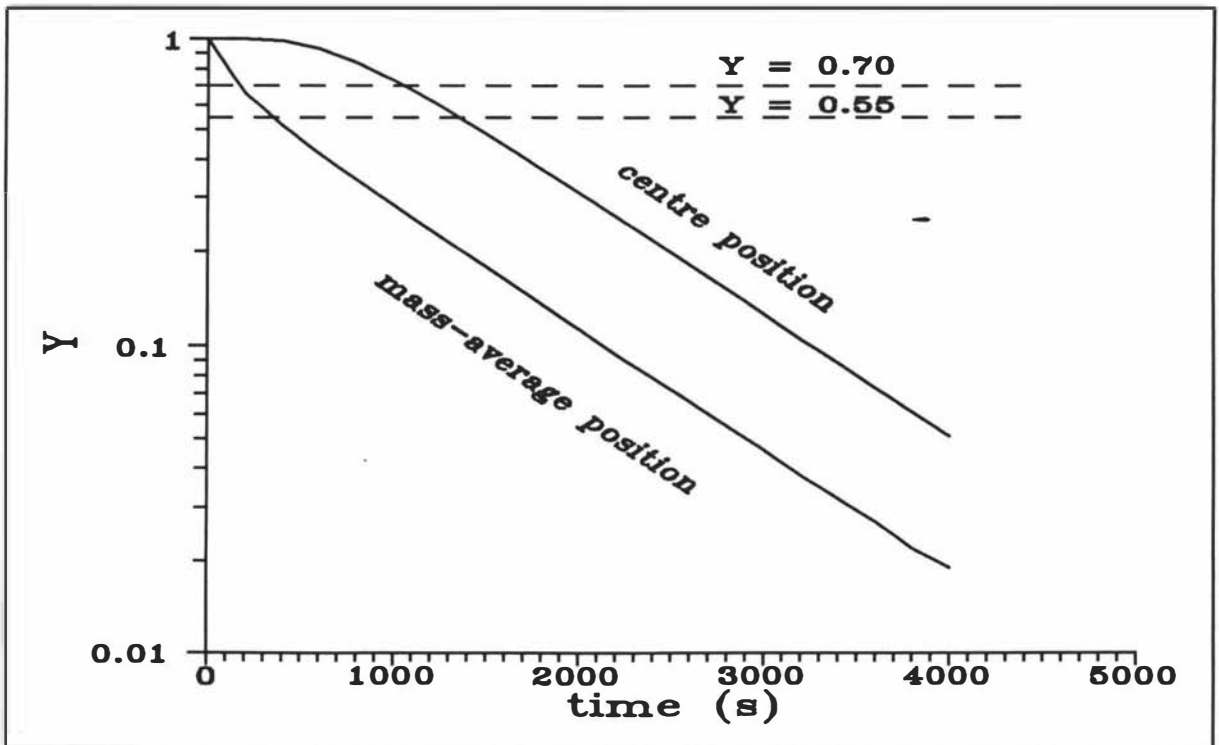


Figure 5.27 Shape of cooling curve for centre and mass-average temperatures during convective plus evaporative cooling under conditions where the evaporative effect is very small.

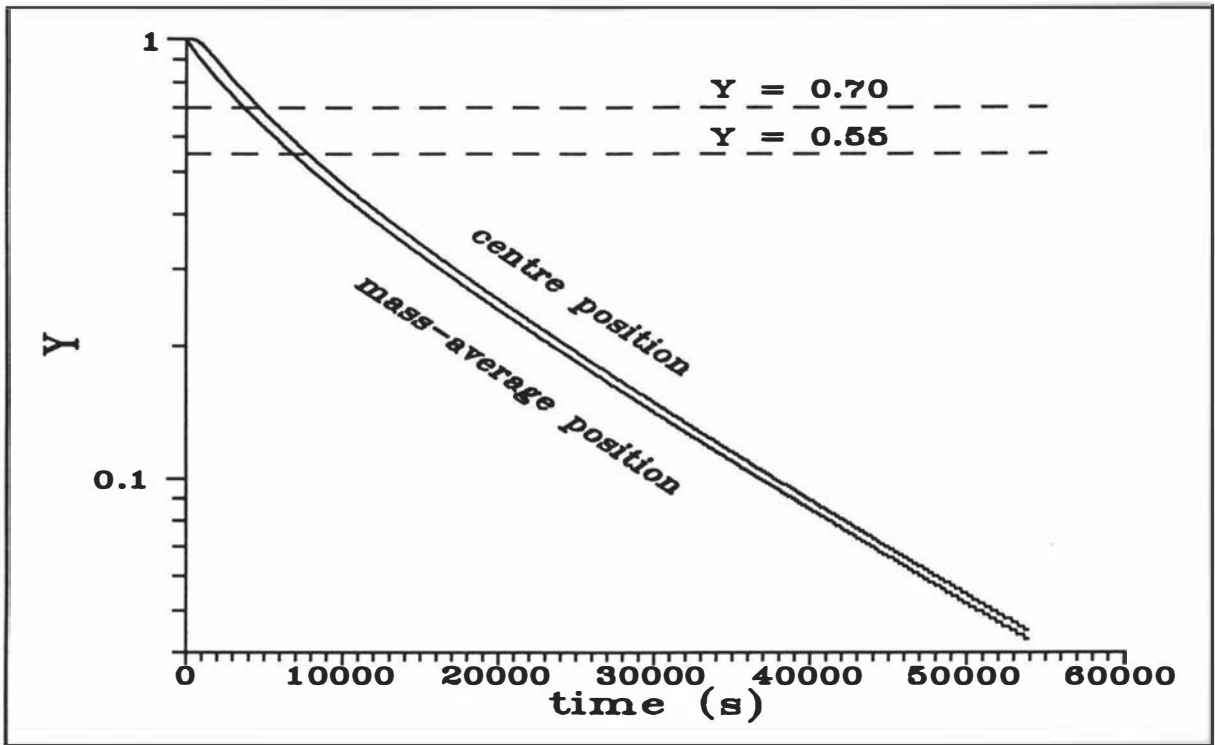


Figure 5.28 Shape of cooling curve for centre and mass-average temperatures during convective plus evaporative cooling under conditions where the evaporative effect is substantial.

6. EXPERIMENTAL DESIGN AND METHODS - IDEALISED PRODUCTS

6.1 INTRODUCTION

In this chapter, the methods used to obtain experimental data for testing whether the effects of evaporation on f_{cEvap}/f_{cConv} and j_{cEvap}/j_{cConv} are accurately predicted by the proposed models across likely practical chilling conditions, are described.

6.2 EXPERIMENTAL DESIGN

As discussed earlier, it had been anticipated that accurate experimental data collection would be difficult so numerical methods were used to predict likely behaviour, and a simple model developed by fitting the numerically-predicted results. The experimental data could then be used solely for model testing. Ideally, to test the full range of likely practical conditions an experimental design with five variables was seen as desirable. To match the numerical data, ideal ranges of conditions were:

a_w	:	0.6, 0.8, 1.0
H_r	:	0.5, 0.75, 1.0
T_{in} (°C)	:	20, 30, 40, 50
T_a (°C)	:	0, 5, 10, 15
Bi	:	0.1, 0.316, 3.16, 10

In practice, experimental limitations meant that the ranges covered were narrower as shown in Table 6.1 (All tables at end of chapter). In particular, there were difficulties in achieving desirable values of relative humidity and Biot number.

The conditions possible in the air tunnel used were limited to relative humidities of 0.78 or 0.90 as will be explained in Section 6.3.3.2. The Biot number depends on sample size and surface heat transfer coefficient. The latter depends on air velocity. In practice, the four conditions achievable were:

- (1) small sample, low air velocity (Bi_l)
- (2) large sample, high air velocity (Bi_h)
- (3) small sample, mid range air velocity (Bi_{m1})
- (4) large sample, low air velocity (Bi_{m2})

Using a normal factorial design, for five variables, there would be 32 runs. However, by using only a half replicate experiment, the number of runs at the high (+) and low (-) level was 16 (Table 6.2). To create a broader range of test condition a central composite design was used. In this, each variable was set to the high (+) and low (-) level with all others at the intermediate (0). The numbers of additional runs was 10 (Table 6.3). At the centre point of the design, the number of runs selected was 4 (Table 6.4).

In practice, a true central composite design was not possible because there were not true 0 levels for two variables (H , and Bi). In the case of H , half the planned 0 level runs were run at the + conditions and half at the - level. For Bi , half the planned 0 level runs were done at Bi_{m1} and half at Bi_{m2} . Thus, in total there were 30 runs covering as wide a range of conditions as the equipment available allowed, and the experimental design was close to central composite.

6.3 EXPERIMENTS

6.3.1 Test Samples and Temperature Measurement Probes

The proposed prediction method is in theory equally applicable to infinite slabs, infinite cylinders, and spheres. In selecting the geometry of the measuring apparatus, the sphere and infinite cylinder have advantages because heat transfer from the air stream to these bodies is easier to control than it would be for an infinite slab. The infinite cylinder was chosen as the shape to be investigated because it permitted the insertion of thermocouples parallel to its axis along zones of constant temperature. Further, it is the 'central' shape of the three possibilities, and as will be shown later it is easier to achieve a wetted surface with this shape than the others.

The product was made from a hollow aluminium cylinder filled with Tylose, a common food analogue material which had thermal properties similar to foods of about 75% water by composition (Riedel, 1960). By choosing a high ratio of length to radius and by insulating the ends of the cylinder with expanded polystyrene, which has low thermal conductivity, a good approximation to the infinite cylinder is attained (Poulsen, 1982). Two sizes of infinite cylinder were used. The large cylinder (L), had an inside diameter of 14.2 cm, length of 36 cm and ratio of length to radius of 5.1, and the small cylinder (S), had an inside diameter of 7.2 cm, length of 36 cm and ratio of length to radius of 10. As Cleland *et al.* (1994) showed this should ensure negligible edge effects provided there are good quality insulated end caps. Figure 6.1 shows a typical sample with end caps in place.

Aluminium was used as the cylinder material because its high thermal conductivity ensured that any local variations in air heat transfer coefficient would be equalised and because the material itself would impose a negligible heat transfer resistance. Good thermal contact between the aluminium-tylose interface was ensured by careful packing of the Tylose, so the surface temperature of the Tylose was the same as the temperature of the aluminium.

Thermocouples were inserted from the cylinder end to midpoint region of the cylinder length, each lead passing parallel to the axis through zones of constant temperature. At the central axis, two thermocouples were placed 4-5 cm apart. At the surface, three thermocouples were positioned equal distances apart around the cylinder. Copper-constantan thermocouples (28-30 SWG) were used. The thermocouple leads were connected to a data logger and temperature measurements were recorded at time intervals of 6 seconds.

6.3.2 Maintenance of Constant Surface Water Activity

The surface water activity of substances is a measure of the degree of water vapour saturation at the product surface. It represents how 'freely' water in a wet solid can evaporate and is determined by the nature and concentration of the dissolved chemical species naturally occurring in it, such as sugars, organic acids, inorganic salts, and other soluble substances. To maintain a uniform surface water activity at the product surface in the experiment, a cloth was wrapped around the cylinder and this was continuously wetted by dripping liquid from

a reservoir onto the cloth at different positions around the cylinder upper region (Figure 6.1). Only a very small quantity of surface wetting liquid (around 0.6 mL/min for the large cylinder and 0.3 mL/min for the small cylinder) was supplied, just enough to fully wet the product surface. The surface wetting liquid was either a saturated salt solution for which $a_w < 1$ (Table 6.5), or water for which $a_w = 1$.

Sulphuric acid, glycerol, or saturated salt solutions are employed most frequently for water activity adjustment. Saturated salt solutions are generally the most useful, as the three phase (vapor-liquid-solid) system is independent of changes in moisture content. Several of these salt solutions have low temperature coefficients and give essentially invariable water activities at ordinary laboratory temperature (Rockland, 1960). By providing excess solute, the solution will remain saturated even in the presence of modest sources or sinks of water (Greenspan, 1976). Table 6.5 shows the equilibrium relative humidity or water activity at various temperature of the stable saturated salt solutions, NaCl and KCl (Greenspan, 1976; Rockland, 1960). Safety and cost considerations as well as their a_w range, led to their selection for the present work.

To prepare a saturated salt solution, salt was dissolved in hot water and boiled until the supersaturated salt solution was obtained. Then it was seeded by an amount of salt crystal to turn it into the saturated salt solution. Tables 6.5 and 6.6 show that the water activity and solubility of sodium chloride were insensitive to air temperature in the range of interest. However, the water activity and solubility of potassium chloride does show some sensitivity to air temperature and this was a source of experimental error. In calculations, $a_w = 0.75$ was used for NaCl and a_w for KCl was selected as the mean for the temperature range traversed.

To collect accurate experimental data the temperature of the liquid film supplied must be the same as the surface temperature of the product at that time. This meant that the wetting liquid must be supplied at the same temperature as the surface, even though the latter continually changes. During the cooling period, it was difficult to maintain this condition. Considerable preliminary experimentation was carried out. The principle adopted was to place a reservoir of feed liquid inside the air cooling tunnel as shown in Figures 6.1 and 6.2. The initial temperature of this liquid was critical. Figures 6.3 and 6.4 show a comparison

between experimental results and the finite difference model at different initial feed liquid temperatures. If the feed liquid is colder than the product surface, this accentuates cooling slightly (Figure 6.3), if it is hotter cooling is retarded (Figure 6.4).

After approximately 10 trials the following conditions were determined to minimise errors:

(a) Water and sodium chloride

Initial liquid temperature was 4 - 6 °C above air temperature for large infinite cylinder (e.g. Figure 6.5) or 8 - 12 °C above air temperature for small infinite cylinder (e.g. Figure 6.6). The measured surface and reservoir temperature are similar to each other. However, the cooling rate of the product surface depended on the other environmental conditions and so was not constant. During a trial, if the liquid reservoir temperature remained too high relative to the surface temperature, the reservoir temperature was sometimes manually cooled by placing the whole reservoir tank in an ice tank at the appropriate time. The judgement of this time depended on experience gained after a few runs before each trial at the earlier stage of the experiments.

(b) Potassium chloride

Potassium chloride started to crystallize as the reservoir temperature became lower and this blocked the feeding tube when the saturated salt solution was pumped to the feeding system. To avoid this problem, the feeding system had to be run at the same or a little higher than the temperature of the air. Addition of liquid to the surface, above the surface temperature, could have affected the cooling rate. This provided an additional source of experimental error for runs with this salt solution.

It must be remembered that any net heat loss or gain from the wetting fluid would mainly affect the top of the cylinders, and by the time the liquid had percolated down, the effect on the central measurement region would be less.

The performance of the feeding system was checked using temperature readings from groups of thermocouples at different heights in the cylinders. There were two thermocouples at the center and three thermocouples at the surface. Irrespective of height the thermocouples gave similar readings to each other. This suggests that during the cooling period, the liquid distribution around the cylinder was sufficiently uniform and with the precautions taken, the

failure of reservoir temperature to match surface temperature was not a major source of experimental error.

6.3.3 Air Tunnel

The experiments were carried out in a small experimental chiller plant (Figure 6.7). The fans drew air horizontally over the evaporator coils (with 4 refrigerant circuits) and then discharged into the chiller plant in order to cool the product. Air temperatures in the air tunnel were automatically controlled and could be varied from 0°C to 20°C. Mesh screens were installed as shown to reduce air velocity variation with position. Measured data showed that variations in the vicinity of the test samples generally ranged $\pm 0.3 \text{ m s}^{-1}$ around the mean velocity.

6.3.3.1 Air Velocities

Air velocities outside the 0.5 to 3 m s^{-1} range are unlikely to be used in commercial chill rooms (Gigiel & Creed, 1987; Self & Burfoot, 1986). In this study, to ensure coverage of the range of air speeds measured in commercial chillers, the ideal range was set at $0.5 - 4.0 \text{ m s}^{-1}$. There were 2 variable speed fans in the air tunnel. The area for air flow could be reduced by putting a false back wall inside the working section of air tunnel to reduce the cross-sectional area for flow. The lowest air velocity (v_l , 0.5 m s^{-1}) was obtained at minimum fan speed and with 1 fan operating. The medium velocity (v_m , 1.1 m s^{-1}) was obtained at minimum fan speed and with 2 fans operating. The highest air velocity (v_h , 3.4 m s^{-1}) was obtained at full fan speed with 2 fans operating and with the false back wall installed.

6.3.3.2 Relative Humidity

The typical air relative humidity in a commercial chiller is about 0.85 (Schneider *et al.*, 1982). In this study, the range of interest was set at 0.75 - 0.95. The factors that influence relative humidity in an air tunnel of this type are as follows (Pham & Willix, 1985):

- (a) the evaporator coil area,
- (b) temperature difference between the evaporator coil and the air,

- (c) presence of products in the chiller plant.

Since the evaporator coils transfer heat from the air to the low pressure, low temperature refrigerant inside the coils, the degree of heat transfer achieved depends upon the temperature difference between the air and the refrigerant, the overall heat transfer coefficient of the coil and the area of the coil. Using an evaporator coil with a larger surface area requires a smaller temperature difference between the refrigerant and the air, and therefore less water vapour transfers from the air onto the coils. This keeps the relative humidity higher, and the evaporator coils needed to be defrosted less frequently.

In this study, relative humidity was reduced by:

- (1) reducing the number of the refrigerant circuits in the evaporator that were supplied with refrigerant. Since the evaporator coils are separated into 4 partitions (4 refrigerant circuits), it was possible to starve refrigerant from parts of it.
- (2) turning on heaters (there were 2 heaters, each of 2400 watts) to increase the sensible heat input in the air.
- (3) reducing the area of the evaporator coil by blocking the air flow to it with wooden sheets.

Although relative humidity could be kept constant during chilling, it was difficult to vary to achieve the pre-set design values. Ultimately, only two levels of relative humidity were used, $H_r \approx 0.78$ and 0.91 . The nature of the operation still depended on the air velocity and temperature as shown in Table 6.7.

6.4 MEASURING EQUIPMENT

In this section the various items of measuring equipment are described.

6.4.1 Relative Humidity

Two types of relative humidity measurement were used, and because they generally agreed within $\pm 3 - 5\%$ the results were averaged.

(1) Vaisala Series HMP 113Y

The Vaisala HUMICAP® type 1638 HM uses the capacitive principle of measurement. The sensor is covered by a thin polymer film which reacts quickly to changes in humidity. It is rated for operation from 0 to 100 % relative humidity, with an expected accuracy of ± 2 % from 0 to 80 %, and ± 3 % from 80 % to 100 %.

Humidity calibration was carried out using the known equilibrium relative humidity of saturated salt solutions of potassium chloride (86 % H_r) and sodium chloride NaCl (75 % H_r). It was considered that an accuracy of about ± 3 % was obtained with this instrument during the experiments, but at times it did fail due to moisture formation on it.

(2) Michell Series 3000 Dewpoint Hygrometer

The Michell Series 3000 is a precision optical dew point hygrometer which uses a three component optical system to sense condensation of water from an air sample. This system comprises an LED (Light Emitting Diode), the mirror surface and a photo-detector.

The operating range for dew point is -30 °C to $+30$ °C. Dew point is measured to an accuracy of ± 0.3 °C. At air temperatures of $0 - 15$ °C, and relative humidities of $75 - 90$ %, this translates to a measurement accuracy of about ± 3 %.

6.4.2 Data Logging

The FIX™ (Fully Integrated Control System) program was used to collect the temperature and relative humidity data. The FIX™ can perform all of the functions in a process control software package. It can monitor, control, generate alarms, and store data for the process. It uses a 12 bit analogue to digital converter. This has some round-off error. Total possible inaccuracy in temperature measurements considering probe quality and logging system shortcoming was considered to be about ± 0.2 to ± 0.3 °C.

6.4.3 Air Velocity

Air velocity was measured using a hot bulb anemometer. This consisted of a Dantec Low Velocity Transducer (Type 54R10) connected to a Dantec Low Velocity Flow Analyzer (Type 54N10). This had been recently calibrated, and its time integrated mean velocity readings were considered accurate to $\pm 0.02 \text{ m s}^{-1}$.

6.5 EXPERIMENTAL PROCEDURE

A typical 'run' consisted of the following steps:

- (1) Placement of a cloth on the product sample.
- (2) Placement of the product in a temperature-controlled room for at least 10 hours to equilibrate.
- (3) Stabilisation of the refrigeration system and fans in the air tunnel at the desired conditions.
- (4) Stabilisation of the relative humidity at the desired value
- (5) Measurement of the air velocity in the air tunnel after the conditions in the air tunnel are stable.
- (6) Placement of 6 kg of liquid that corresponds to a desired surface water activity in the reservoir.
- (7) Adjustment of the initial temperature of the reservoir to the desired value.
- (8) Transfer of the product from the controlled room in an insulated container.
- (9) Connection of the thermocouples from the product to the data logger.
- (10) Soaking of the cloth wrapping the product in the appropriate liquid at the same temperature as the product.
- (11) Placement of the product in the air tunnel and connection of the liquid feeding system from the reservoir to the product (the liquid was supplied to the product by a small pump).
- (12) Commencement of sample rotation by a sample oscillator to minimise position variation of heat transfer conditions.
- (13) The liquid feeding rate was set high for the first period of cooling and slowed down later.

- (14) Manual control of the reservoir temperature to make it as close as possible to the surface temperature. Since the cooling rate of the liquid in the reservoir was slow relative to the surface temperature, to speed up the cooling rate of the liquid, the reservoir was placed in an ice tank until the liquid temperature was close to the ambient air temperature. The ice tank was then taken away.
- (15) Continued chilling for at least 12 hours for the large infinite cylinder and at least 10 hours for the small one to achieve apparent equilibration.
- (16) Measurement of the air velocity in the air tunnel prior to sample removal.

6.6 HEAT TRANSFER COEFFICIENTS

There are many methods to estimate the surface heat transfer coefficient. In this study, heat transfer coefficients were determined by cooling the cylinders in separate trials. In those trials the cloth was wetted but to prevent evaporative water loss, the product was wrapped with a plastic film (which had a very low permeability to water vapour) before placing in the air tunnel. The resistance to heat transfer is made up of four components, as follows:

$$\frac{1}{h_c} = \frac{1}{h_a} + \frac{x_1}{k_1} + \frac{x_2}{k_2} + \frac{x_3}{k_3} + \frac{x_4}{k_4} \quad (6.1)$$

- where h_c = surface heat transfer coefficient ($\text{W m}^{-2} \text{K}^{-1}$)
- h_a = air convection heat transfer coefficient ($\text{W m}^{-2} \text{K}^{-1}$)
- k_1, k_2, k_3, k_4 = thermal conductivity of plastic film, aluminium, cloth, and liquid respectively ($\text{W m}^{-1} \text{K}^{-1}$)
- x_1, x_2, x_3, x_4 = thickness of plastic film, aluminium, cloth, and liquid respectively (m)

The air convection heat transfer coefficient, h_a , takes account of resistance to heat transfer in the air itself. Its value is related to the rate of air movement, its orientation to the air flow and dimensions and shape of the object. These effects are normally expressed as dimensionless correlations of the Nusselt number and Reynolds number.

The heat transfer resistance of the aluminium and wet cloth layer was assumed to be the same

in both the wrapped and unwrapped cases.

Because the plastic film was very thin (<0.1 mm.) and fitted tightly it was assumed that it did not change the overall heat transfer coefficient significantly.

The temperature response as a function of time at the centre position within an infinite cylinder undergoing convection cooling takes the following form (Luikov, 1968) which was previously stated in Chapter 2:

$$Y_c = \frac{(T_c - T_a)}{(T_{in} - T_a)} = \sum_{m=1}^{\infty} \frac{2Bi}{(\beta_m^2 + Bi^2)J_0(\beta_m)} e^{-\beta_m^2 \frac{kt}{\rho C R^2}} \quad (6.2)$$

where k = thermal conductivity of product (W m⁻¹ K⁻¹)
 t = time (s)
 ρC = volumetric specific heat capacity (J m⁻³ K⁻¹)
 R = radius of product (m)
 β_m = m^{th} root of the transcendental equation

The transcendental equation to be solved for β_m values is :

$$\beta_m J_1(\beta_m) - Bi J_0(\beta_m) = 0 \quad (6.3)$$

and J_0 and J_1 are Zero- and first-order Bessel's functions, respectively:

$$J_0(\beta_m) = 1 - \frac{\beta_m^2}{2^2(1!)^2} + \frac{\beta_m^4}{2^4(2!)^2} - \frac{\beta_m^6}{2^6(3!)^2} \dots + \frac{(-1)^n \beta_m^{2n}}{2^{2n}(n!)^2} \quad (6.4)$$

$$J_1(\beta_m) = \frac{\beta_m}{2} - \frac{\beta_m^3}{2^3 1! 2!} + \frac{\beta_m^5}{2^5 2! 3!} - \frac{\beta_m^7}{2^7 3! 4!} \dots + \frac{(-1)^n \beta_m^{2n+1}}{2^{2n+1} n! (n+1)!} \quad (6.5)$$

The technique to evaluate h_c from the cooling curves involves the assumption that the second and higher terms in the summation of Equation (6.2) are negligible after some time has elapsed and thus Y_c can be evaluated accurately by the use of the first term only. Therefore equation (6.2) (at $m = 1$) becomes:

$$Y_c = \frac{(T_c - T_a)}{(T_{in} - T_a)} = j_c e^{-\beta_1^2 \frac{kt}{\rho C R^2}} = j_c e^{-\beta_1^2 Fo} \quad (6.6)$$

where j_c = j at centre position

$$Fo = \frac{kt}{\rho C R^2}$$

When $\ln Y_c$ is plotted versus Fo , a straight line with a slope of $-\beta_1^2$ is obtained. From the slope and recently measured product properties of Tylose ($k = 0.500 \text{ W m}^{-1} \text{ K}^{-1}$, $\rho C = 3.889 \times 10^6 \text{ J m}^{-3} \text{ K}^{-1}$; data supplied by the Meat Industry Research Institute of NZ), Bi or h_c can be evaluated using an iterative method to solve equation (6.3). Any contribution of radiation to the heat transfer is also included in the estimation of this heat transfer coefficient. Chapter 7 discusses heat transfer coefficient data processing further.

6.7 SUMMARY

The methods used for experimental data collection have been described. To ensure experiments covered a wide range of conditions, a pseudo central composite design with five variables was used. The infinite cylinder was chosen as sample shape and the required water activity at the sample surface was created by feeding with a wetting liquid of constant water activity. The feeding system was carefully controlled to provide only the necessary amount of liquid. The saturated potassium chloride solution was the most difficult liquid to use because it crystallised at lower temperature. Relative humidity was difficult to control. It could be kept constant throughout the cooling process but was difficult to vary between runs. Overall, it was considered that the techniques described would lead to data of good quality.

Table 6.1 Ranges of experimental conditions used for model testing.

symbol	low	intermediate	high
a_w	0.75	0.88	1.00
$T_{in}(^{\circ}\text{C})$	20	30	40
$T_a(^{\circ}\text{C})$	0	5	10
H_r	0.78	-	0.90
Bi	Bi_l	Bi_{m1}, Bi_{m2}	Bi_h

Table 6.2 Experimental conditions for the half-factorial experiment (v_h = high velocity, v_l = low velocity, v_m = mid-range velocity, L = large size, S = small size).

Run	a_w	T_{in} (°C)	T_a (°C)	H_r	Bi	v_a (m s ⁻¹)	size
1	0.75 (-)	20(-)	0(-)	0.78(-)	(+)	v_h	L
2	0.75(-)	20(-)	0(-)	0.90(+)	(-)	v_l	S
3	0.75(-)	20(-)	10(+)	0.78(-)	(-)	v_l	S
4	0.75(-)	40(+)	0(-)	0.78(-)	(-)	v_l	S
5	1.0(+)	20(-)	0(-)	0.78(-)	(-)	v_l	S
6	0.75(-)	20(-)	10(+)	0.90(+)	(+)	v_h	L
7	0.75(-)	40(+)	0(-)	0.90(+)	(+)	v_h	L
8	1.0(+)	20(-)	0(-)	0.90(+)	(+)	v_h	L
9	1.0(+)	40(+)	0(-)	0.78(-)	(+)	v_h	L
10	1.0(+)	40(+)	0(-)	0.90(+)	(-)	v_l	S
11	1.0(+)	40(+)	10(+)	0.78(-)	(-)	v_l	S
12	0.75(-)	40(+)	10(+)	0.90(+)	(-)	v_l	S
13	1.0(+)	20(-)	10(+)	0.90(+)	(-)	v_l	S
14	0.75(-)	40(+)	10(+)	0.78(-)	(+)	v_h	L
15	1.0(+)	20(-)	10(+)	0.78(-)	(+)	v_h	L
16	1.0(+)	40(+)	10(+)	0.90(+)	(+)	v_h	L

Table 6.3 Experimental conditions for the runs used to extend the half-factorial experiment to a plan approximating a central composite design. Codes as in Table 6.2.

Run	a_w	T_{in} (°C)	T_a (°C)	H_r	Bi	v_a (m s ⁻¹)	size
17	0.75(-)	30(0)	5(0)	0.78(-)	(0)	v_m	S
18	1.0(+)	30(0)	5(0)	0.78(-)	(0)	v_m	S
19	0.88(0)	20(-)	5(0)	0.90(+)	(0)	v_m	S
20	0.88(0)	40(+)	5(0)	0.90(+)	(0)	v_m	S
21	0.88(0)	30(0)	0(-)	0.78(-)	(0)	v_l	L
22	0.88(0)	30(0)	10(+)	0.78(-)	(0)	v_l	L
23	0.88(0)	30(0)	5(0)	0.78(-)	(0)	v_l	L
24	0.88(0)	30(0)	5(0)	0.90(+)	(0)	v_l	L
25	0.88(0)	30(0)	5(0)	0.90(+)	(-)	v_l	S
26	0.88(0)	30(0)	5(0)	0.90(+)	(+)	v_h	L

Table 6.4 Experimental conditions for the 'centre point' runs in the central composite experimental design. Codes as in Table 6.2.

Run	a_w	T_{in} (°C)	T_a (°C)	H_r	Bi	v_a (m s ⁻¹)	size
27	0.88(0)	30(0)	5(0)	0.78(-)	(0)	v_m	S
28	0.88(0)	30(0)	5(0)	0.78(-)	(0)	v_m	S
29	0.88(0)	30(0)	5(0)	0.90(+)	(0)	v_l	L
30	0.88(0)	30(0)	5(0)	0.90(+)	(0)	v_l	L

Table 6.5 Water activity of saturated salt solutions used in the experiments.

saturated salt solution	water activity at °C									
	0	5	10	15	20	25	30	35	40	
sodium chloride	0.75	0.75	0.75	0.75	0.75	0.75	0.75	0.75	0.75	0.75
potassium chloride	0.88	0.88	0.87	0.87	0.86	0.86	0.84	0.84	0.83	

Table 6.6 The solubility of salts used in the experiments at different temperatures.

salts	solubility at 20° C g per 100 mL	solubility at 100° C g per 100 mL
sodium chloride	35.7	39.12
potassium chloride	62.9	79.2

Table 6.7 Conditions used to obtain required relative humidities.

Type	T_a (°C)	no. of fans	false wall	no. of evap. passes active	area blocked (%)	no. heaters on (2400 watt)	H_r	v_a (m s ⁻¹)
A	0	2	yes	2	50	0	0.78	3.4
	10	2	yes	2	50	0	0.81-0.82	3.4
B	5	2	no	2	50	1	0.80-0.82	1.1-1.5
C	0	1	no	2	50	1	0.74-0.79	0.5
	5	1	no	2	50	1	0.80-0.82	0.5
	10	1	no	2	50	2	0.78	0.5
D	0	2	yes	6	0	0	0.90-0.91	3.4
	5	2	yes	6	0	0	0.90-0.92	3.4
	10	2	yes	6	0	0	0.92-0.94	3.4
E	5	2	no	6	0	0	0.93	1.35-1.6
F	0	1	no	6	0	0	0.90-0.91	0.5
	5	1	no	6	0	0	0.91-0.92	0.5
	10	1	no	6	0	0	0.93-0.94	0.5

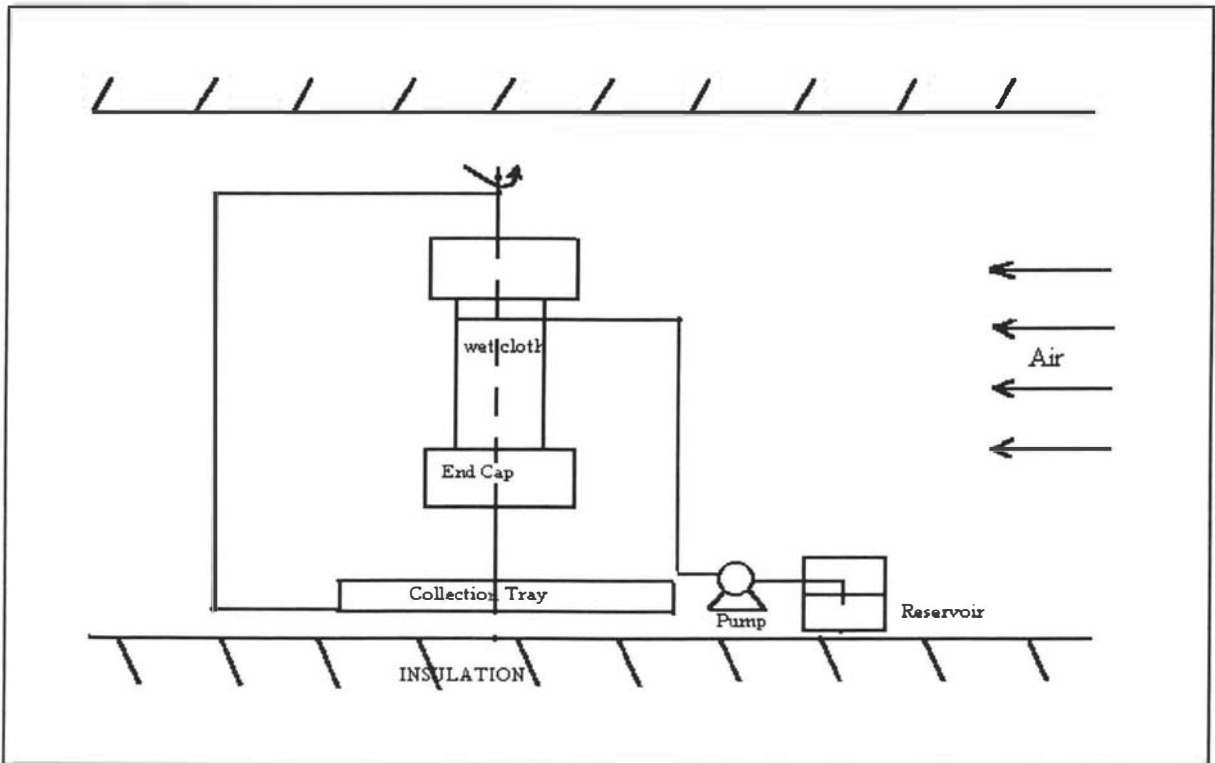


Figure 6.1 Schematic diagram of experimental apparatus installed in the air tunnel showing sample oscillator and wetting agent supply system.

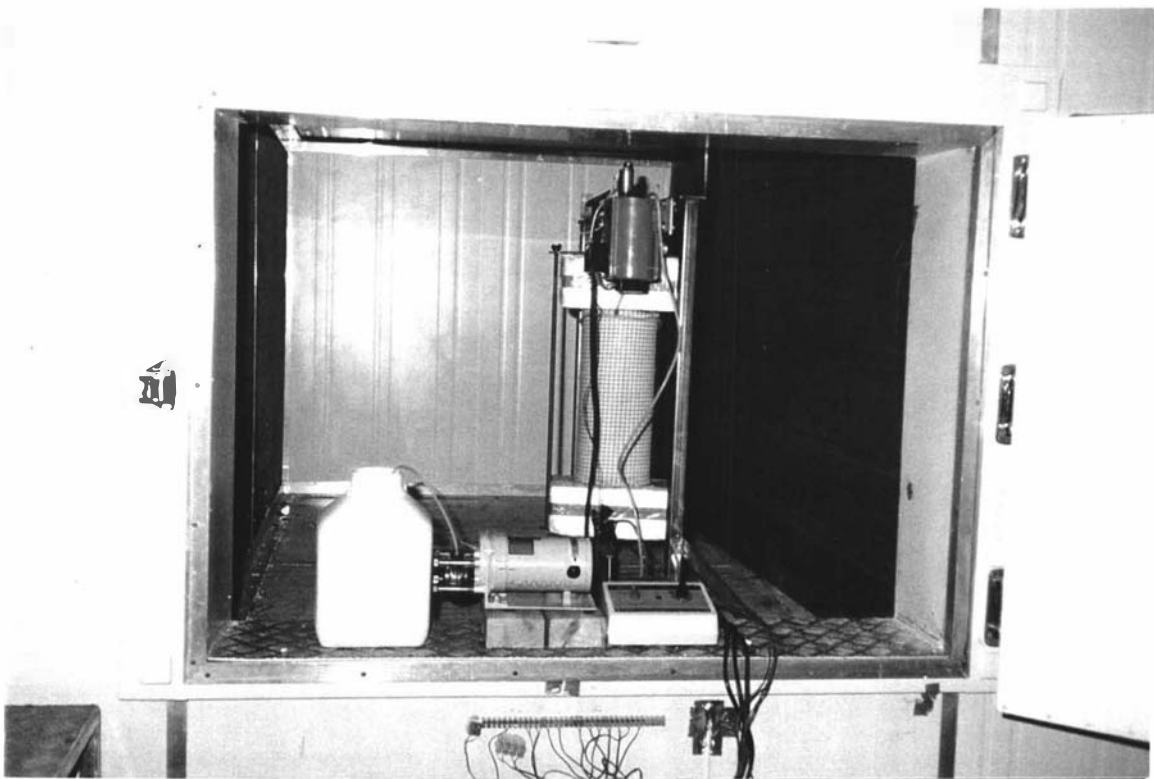


Figure 6.2 The apparatus inside the air tunnel.

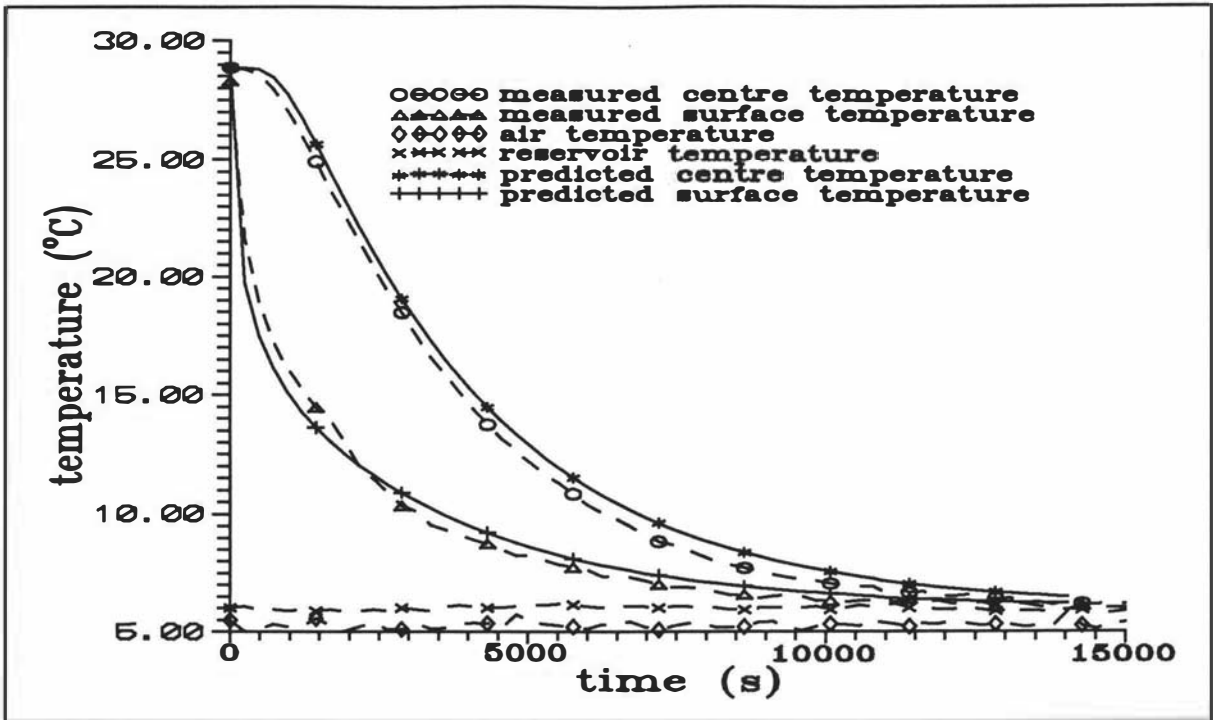


Figure 6.3 Example of measured and predicted cylinder temperatures for a run in which the reservoir temperature was too cold.

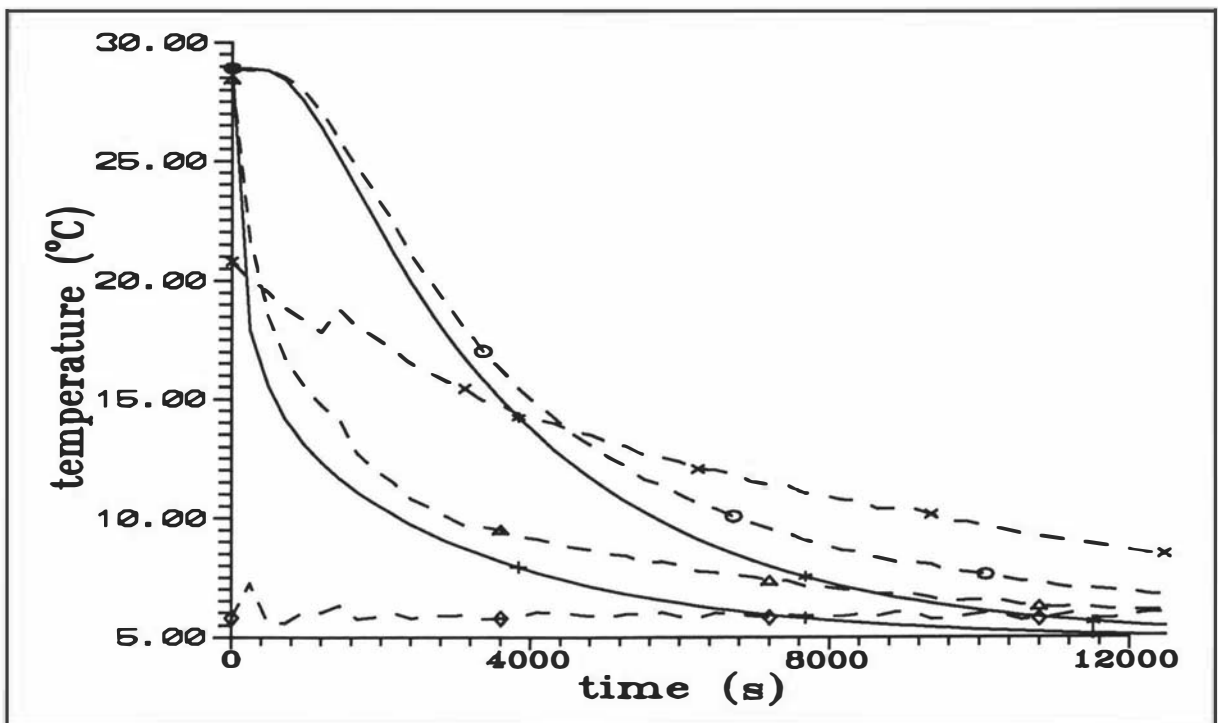


Figure 6.4 Example of measured and predicted cylinder temperatures for a run in which the reservoir temperature was too hot. Key as in Figure 6.3.

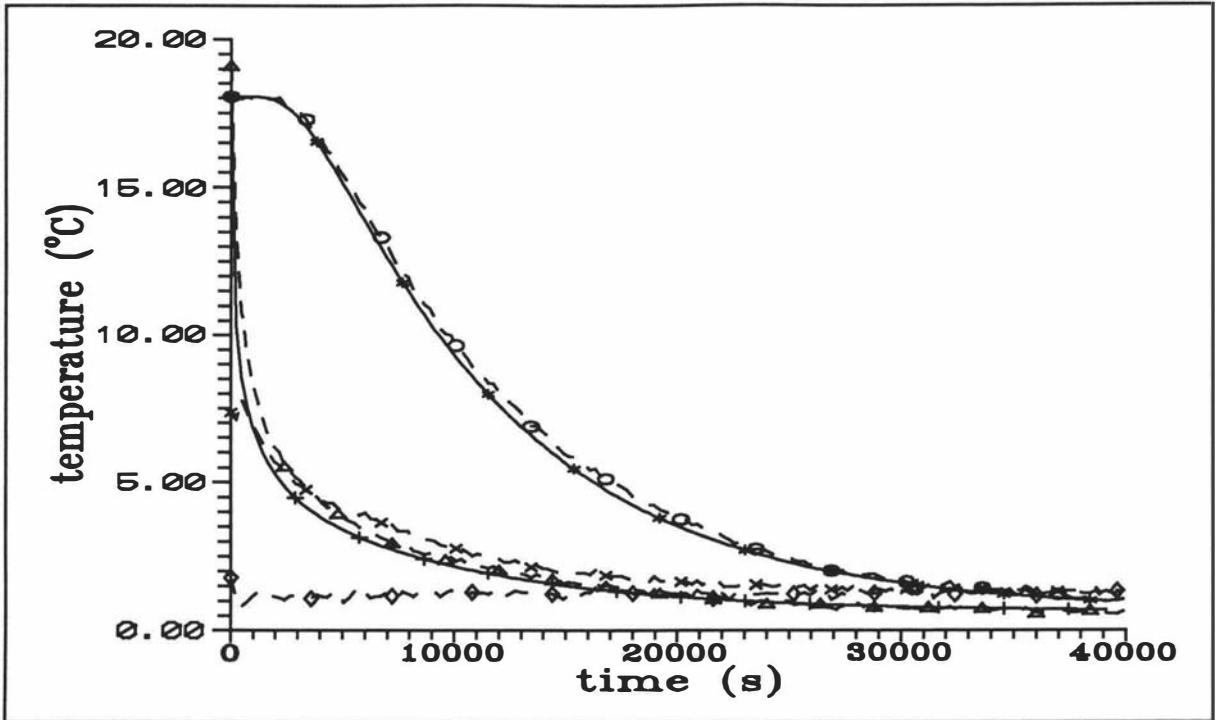


Figure 6.5 Results of an experiment for the large cylinder (with finite difference predictions) in which the reservoir temperature was ideal. Key as in Figure 6.3.

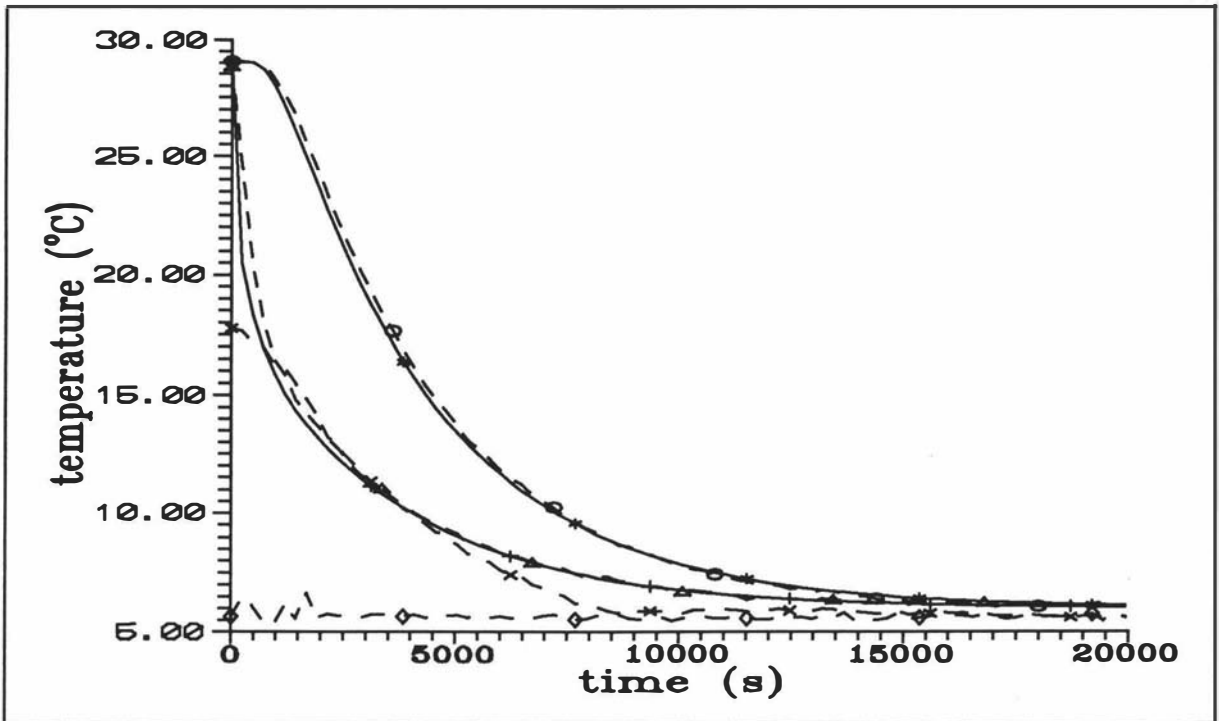


Figure 6.6 Results of an experiment for the small cylinder (with finite difference predictions) in which the reservoir temperature was ideal. Key as in Figure 6.3.

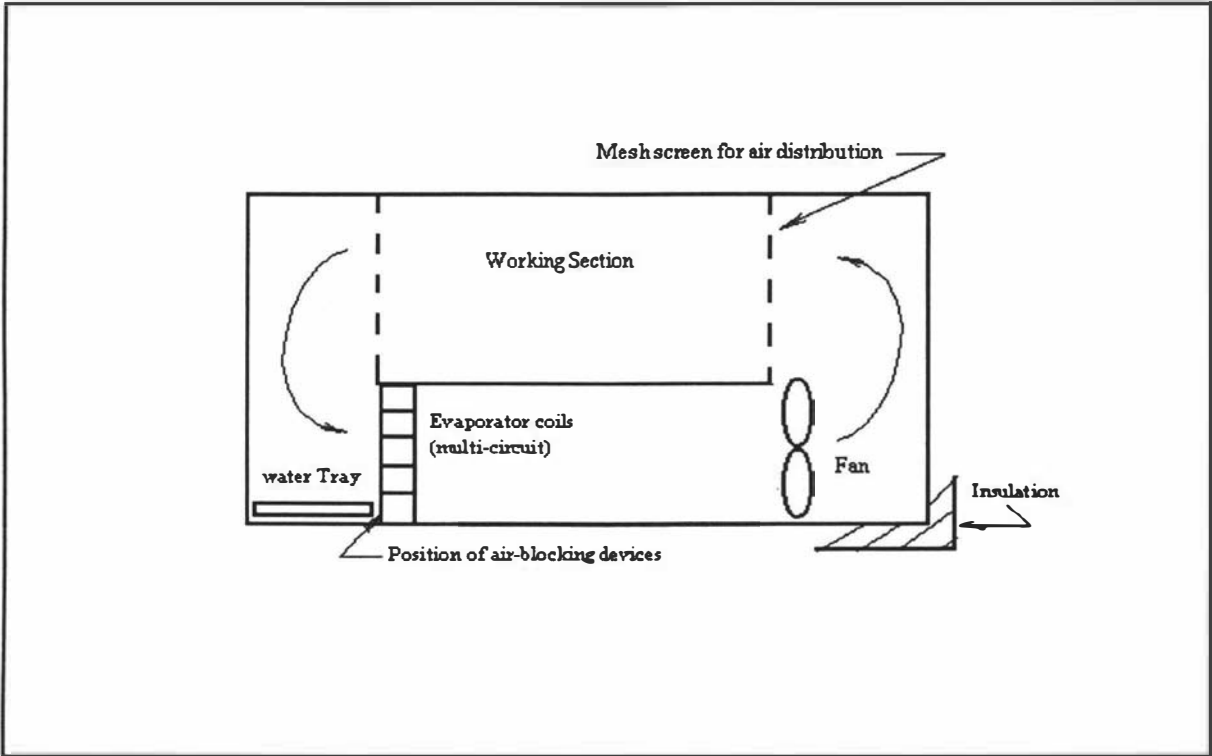


Figure 6.7 Experimental air tunnel used in experiments.

7. TESTING OF SIMPLE MODEL AGAINST EXPERIMENTAL DATA FOR IDEALISED MODEL SYSTEMS

7.1 INTRODUCTION

In Chapter 4, heat and mass transfer were simulated and numerical methods were used to predict likely chilling behaviour. The numerically-predicted results were investigated to find the factors that influenced evaporation. Simple model, based on the numerically-predicted results, was developed in Chapter 5 and gave similar predictions to the numerical method. Chapter 6 described experimental methods used to collect data across a wide range of conditions for testing the simple model. In Chapter 7 the qualities of the simple model relative to the experimental results are evaluated.

7.2 EXPERIMENTAL DESIGN AND RESULTS

In Chapter 6, the different techniques to control the environmental conditions in the air tunnel were described. The design conditions used were:

H_r	:	0.78, 0.91
$T_a(^{\circ}\text{C})$:	0, 5, 10
$T_{in}(^{\circ}\text{C})$:	20, 30, 40

Different Biot numbers were obtained by varying product sizes and air velocity. Since there were two sizes of infinite cylinder and three velocities, two Biot numbers at the intermediate level (which were between 1.3 to 1.8), one Biot number at the highest level (3.5 - 4.1) and another at the lowest level (0.9 - 1) were possible (Table 7.1). In total, 30 runs were carried out as defined in Tables 6.2 - 6.4. One extra trial not in the plan, run 31 was conducted. The results are listed in Tables 7.3, 7.4, and 7.5. In these Tables the run numbers listed are those from Tables 6.2 - 6.4. Runs 5, 27, and 29 were repeated because, at the time, there was doubt that the wetting liquid reservoir temperature was correct. Both the first attempt and second are reported here and used in the analysis but, as will be shown, the first attempt, for runs 27 and 29 were less well modelled than the second.

7.3 HEAT TRANSFER COEFFICIENTS

As described in Chapter 6, heat transfer coefficients (h_c) were determined by cooling the infinite cylinders in separate trials where the cloth was wetted but a thin plastic film covered the wet cloth to avoid evaporation. The analytical solutions for heat conduction were used to back-calculate h_c values from the temperature-time data in such trials. As expected, the heat transfer coefficient depended primarily on the air velocity. Nonlinear regression analysis to fit power law equations for samples of 2 sizes and the 3 kinds of wetting liquids were performed with the following results.

A. The Small Infinite Cylinder (Diameter = 0.072 m.)

(1) water (Figure 7.1)

$$h_c = 19.52 v_a^{0.416} \quad (R^2 = 0.993) \quad (7.1)$$

(2) sodium chloride (Figure 7.2)

$$h_c = 18.09 v_a^{0.438} \quad (R^2 = 0.989) \quad (7.2)$$

(3) potassium chloride (Figure 7.3)

$$h_c = 18.24 v_a^{0.433} \quad (R^2 = 0.985) \quad (7.3)$$

B. The Large Infinite Cylinder (Diameter= 0.142 m.)

(1) water (Figure 7.1)

$$h_c = 15.55 v_a^{0.501} \quad (R^2 = 0.980) \quad (7.4)$$

(2) sodium chloride (Figure 7.2)

$$h_c = 15.16 v_a^{0.457} \quad (R^2 = 0.992) \quad (7.5)$$

(3) potassium chloride (Figure 7.3)

$$h_c = 15.48 v_a^{0.472} \quad (R^2 = 0.988) \quad (7.6)$$

Table 7.2 shows heat transfer coefficients and 95% confidence bounds for individual data points at the mid-range value of air velocity. The bounds were calculated assuming normally distributed errors.

Variations in the measured heat transfer coefficients could be caused by any air or excess saturated salt solution trapped between the wet cloth and the plastic film. The amount of saturated salt solution trapped might have affected the thickness of the salt layer deposited on the cloth, and the amount of solution present might have been different for different trials. Therefore some variation in h_c for the same kind of salt is possible at any air velocity. The heat transfer coefficients also depended slightly on kinds of the liquids used, probably because different salt solutions had different thermal conductivity and where deposition occurred different kinds of crystal resulted. For example, NaCl crystals were coarser than KCl crystals. These effects probably explain why h_c for the salt solutions is lower than for water. Whilst it could be argued that the differences between equations (7.1), (7.2), and (7.3) in one group and equations (7.4), (7.5), and (7.6) in the other were not statistically significant it was decided to use the equations specific to the different wetting fluids in further analysis because there were sensible physical reasons for differences to occur, and because each equation is based on 8 -11 points, a significant number.

The range of air temperatures used during cooling trials was 0 to 10 °C. Although temperature affects the thermal and physical properties of air (which in turn affect Reynolds number (Re), Prantl number (Pr), and Nusselt number (Nu)), the effect of temperature (in the interested range of 0 °C to 10 °C) on the surface heat transfer coefficient through the property changes was probably negligibly small compared to uncertainties in the measurement systems e.g. Pr changes from 0.707 at 0 °C to 0.705 at 10 °C and Re by 6.2 % due to ν (kinetic viscosity). The h_c values represent the effects of both convective and radiation heat transfer at the product surface.

7.4 EQUILIBRIUM TEMPERATURE ANALYSIS

At the equilibrium temperature (T_{eq}), the convective cooling rate and water vaporisation rate are in balance. In Chapter 5, equations for the equilibrium temperature were derived theoretically. In this chapter, the practical existence of the equilibrium temperature is tested. In theory it takes an infinitely long time to reach an equilibrium state. In practice, the apparent steady state condition at 15 hours was used as an approximation as all runs had reached steady state within the sensitivity of the measurement system in less than 15 hours. As Tables 7.3 to 7.5 show, the experimental steady state temperature ($T_{eq,exp}$) closely matched the calculated equilibrium temperature ($T_{eq,pred}$, determined using equation 5.11). Figures 7.4 - 7.9 plot the difference between the calculated equilibrium temperature ($T_{eq,pred}$) and the experimental steady state temperature (assumed experimental equilibrium temperature, $T_{eq,exp}$) against different parameters. Figure 7.5 suggests that there may be a trend with respect to H_r , but the evidence is relatively weak. Otherwise, no significant trends were noted although the spread of results was greater at low velocities. The 95% confidence bounds were $-0.4\text{ }^{\circ}\text{C}$ to $+0.3\text{ }^{\circ}\text{C}$ (Tables 7.6 and 7.7) which is of the same magnitude as the estimated measurement uncertainty. It was concluded that within the limits of the methods used for verification the model is valid and the Lewis relationship held adequately down to velocities of about 0.4 ms^{-1} .

7.5 LINEARIZATION OF SEMI-LOG PLOTS

As expected when the product was wrapped with the plastic film (no evaporation), it was found that at the steady state condition, $T_{eq,exp}$ equalled T_a (e.g. Figure 7.10). When evaporation occurred, it was found that

$$T_{eq,exp} > T_a \text{ if } a_w < H_r \quad (\text{e.g. Figure 7.11})$$

$$T_{eq,exp} < T_a \text{ if } a_w > H_r \quad (\text{e.g. Figure 7.12})$$

$$T_{eq,exp} = T_a \text{ if } a_w = H_r \quad (\text{e.g. Figure 7.13})$$

When modified $Y_{c,exp}$ values were calculated using $T_{eq,exp}$ to replace T_a as discussed in Chapter 5 it was observed that the modified $Y_{c,exp}$ and the measured equilibrium temperature linearized the plots of $\ln Y_{c,exp}$ versus Fo successfully. For example Figures 7.14 - 7.16 are the results of linearization from Figures 7.11 - 7.13 respectively using $T_{eq,exp}$. The jagged appearance of

the lines at lower $Y_{c,exp}$ arises from analogue to digital conversion accuracy in the data logging system. The portion of the line below modified $Y_{c,exp} = 0.70$ could be best-fitted by a straight line with $R^2 > 0.99$ for all runs. This verified that T_{eq} satisfactorily linearised the cooling curves.

7.6 COOLING WITH EVAPORATIVE EFFECTS

In Chapter 5, the technique to model the evaporation effect was proposed in the form of relative values of f and j for evaporation plus convection versus convection only. The experimental results and comparisons to model predictions are shown in Tables 7.3 - 7.5. In the most extreme cases, the relative rate of cooling with evaporation to convection only is about 2 to 1. In deriving the tabulated results, experimental values of f_{cEvap} and j_{cEvap} were derived from plots of $\ln Y_{c,exp}$ versus FO where $Y_{c,exp}$ was defined as:

$$Y_{c,exp} = \frac{(T_{c,exp} - T_{eq,exp})}{(T_{in} - T_{eq,exp})} \quad (7.7)$$

where $T_{eq,exp}$ = the equilibrium temperature measured experimentally (°C)
 $T_{c,exp}$ = the centre temperature measured experimentally (°C)

Calculated values of f_{cEvap} and j_{cEvap} were obtained from equation (5.19) and (5.20) respectively.

There was probably more experimental error for runs with saturated salt solutions, especially KCl, than with water. Also, it can be seen in Table 7.5 that the first attempts at Runs 27 and 29 are less well predicted than the second. In Tables 7.3 to 7.5 comparisons were made to the finite difference model of Chapter 4 as well as the proposed model. Tables 7.6 and 7.7 summarise the results in Tables 7.3 to 7.5. The calculated values of f_{Evap} and j_{Evap} from the finite difference method, agreed within -6 to +10 % of the experimental data (Table 7.6). The mean offset for the f values was +2.1 %, whereas for the j values the mean error in predicting the experimental values was -0.2 %. When the calculated values of f_{Evap} and j_{Evap} from the simple model are compared to the experimental data, it was found that the agreement is within -7 % to +10 % (Table 7.7). The mean offset for the f values was +1.7 %, and for the

j values -0.4 %. Figures 7.17 and 7.18 show plots of the percentage differences resulting from the simple model against those resulting from the finite difference model. All data are clustered around the diagonal lines. This shows that relative to the experimental results the finite difference and simple model gave similar predictions.

Plots of f_{cEvap}/f_{cConv} and j_{cEvap}/j_{cConv} values predicted by the simple model against the experimental results are shown in Figures 7.19 and 7.20 respectively. Most data are clustered around the diagonal line, although the j data are less well correlated. After investigating the differences between the calculated results (simple model) and the experimental results (Figures 7.21 - 7.32), it was concluded that there were no significant systematic errors in the models. Overall, the agreement between the simple model and the experimental results was considered acceptable taking into consideration likely data uncertainties, especially in heat transfer coefficients, and the possibility of thermocouples not being positioned exactly at the centre of the products.

7.7 CHILLING TIME PREDICTION

The major interest was in chilling time prediction so the f_{Evap} and j_{Evap} values were used to estimate chilling times at different Y using the simple model. Chilling times to reach certain temperatures ($T_{c,exp}$) which corresponded to $Y_{c,exp} = 0.10, 0.35, \text{ and } 0.70$ were calculated (Tables 7.8 - 7.10). The value of $Y_{c,exp}$ was substituted in equation (7.7) to find $T_{c,exp}$ for each run. The corresponding $Y_{c,pred}$ value at which to make predictions was:

$$Y_{c,pred} = \frac{(T_{c,exp} - T_{eq,pred})}{(T_{in} - T_{eq,pred})} \quad (7.8)$$

where $T_{eq,pred}$ = temperature at equilibrium state calculated from equation (5.11) using a_w of the wetting liquid

$Y_{c,pred}$ = predicted value of Y_c corresponding to $T_{c,exp}$ and $T_{eq,pred}$

From equation (5.25), the predicted chilling time (t_{pred}) to reach $T_{c,exp}$ was then:

$$t_{pred} = \left(\frac{\ln Y_{c,pred} - \ln j_{cEvap,pred}}{k f_{cEvap,pred}} \right) \rho C R^2 \quad (7.9)$$

where $f_{cEvap,pred}$ = predicted value of f_{cEvap}

$j_{cEvap,pred}$ = predicted value of j_{cEvap}

The finite difference and simple model failed to predict experimental data in similar ways (Figures 7.33 - 7.35) because the correlation coefficients between % difference of two models were close to 1.0 (Table 7.7). Tables 7.6 and 7.7 summarise results. The mean offset for time of both models were close to zero. The agreement at $Y_{c,exp} = 0.10$ and $Y_{c,exp} = 0.35$ were within about $\pm 10\%$, and at $Y_{c,exp} = 0.70$ was within about $\pm 11\%$. The reason for the poorer agreements at $Y_{c,exp} = 0.70$ is that the exponential cooling regime is not always well established before this $Y_{c,exp}$ is reached. This was discussed earlier, and is a well-known weakness of any model based on exponential behaviour. When times predicted by the simple model were plotted against those from the experiments (Figures 7.36 - 7.38), it was found that the agreement is good. The slightly worse agreement at $Y_{c,exp} = 0.10$ compared to $Y_{c,exp} = 0.35$ arises because the former is more influenced by any uncertainty in $T_{eq,exp}$.

To illustrate the overall benefit of the new models, Figures 7.39 - 7.40 show plots of centre temperatures versus time for the finite difference model with and without evaporation, for the experimental results, and the simple model. Figure 7.39 shows one of the more closely predicted runs (Run 23) and Figure 7.40 shows the worst predicted run (Run 29). It can be seen that evaporation makes the cooling rate faster than for convection only, and that the simple model and the finite difference models gave the same results in even the worst case. Overall, the confidence in the model is increased by these results.

7.8 DISCUSSION AND CONCLUSIONS

The model of the equilibrium temperature and the modified unaccomplished temperature change successfully linearised the experimental cooling curves. The finite difference method, the simple model, and the experimental results were generally similar (Table 7.7) and

disagreement could be largely explained by experimental uncertainty, thus indicating that the simple model can be used with confidence across the ranges of conditions for which it was derived and tested.

It must be remembered that both model derivation and model testing were limited to conditions of:

- (1) uniform initial product temperature
- (2) constant ambient condition
- (3) constant thermal properties and surface water activity
- (4) no skin resistance
- (5) one dimensional heat transfer

For the simple method to be further developed, there is a wide choice of possibilities. That selected was extension to real food products in which the assumption of constant surface water activity may not be valid.

Table 7.1 Designation of ranges of Biot number used in the experiments described in Chapter 6.

Biot number	
Bi_i	0.9 - 1.0
Bi_{m1}	1.3 - 1.6
Bi_{m2}	1.7 - 1.8
Bi_h	3.5 - 4.1

Table 7.2 95% confidence bounds on h_c ($W m^{-2} K^{-1}$) at the midrange value of v_a ($2 m s^{-1}$).

cylinder size	water	NaCl	KCl
S	26.0 ± 1.5 (5.7%)	24.5 ± 2.0 (8.0%)	24.6 ± 1.9 (7.5%)
L	22.0 ± 2.0 (9.1%)	21.5 ± 1.6 (7.4%)	20.8 ± 1.3 (6.3%)

Table 7.3 Experimental data and predicted results for runs using water as the wetting agent.

Run	T_{in} (°C)	T_a (°C)	H_r (%)	v_a (ms ⁻¹)	h_c (Wm ⁻² K ⁻¹)	Bi	f_{cEvap} (exp.)	f_{cConv} (anal. soln.)	j_{cEvap} (exp.)	j_{cConv} (anal. soln.)	type	f_{cEvap}/f_{cConv}	j_{cEvap}/j_{cConv}	$\Delta f_{cEvap}/f_{cConv}$ (%)		$\Delta j_{cEvap}/j_{cConv}$ (%)		T_{eq} (°C)			T_{wb} (°C)
														simple model	finite diff.	simple model	finite diff.	exp.	model	ΔT_{eq} (°C)	
8	18.1	1.2	90	3.12	27.4	3.90	-4.10	-3.60	1.50	1.47	simple model	1.18	0.99	+3.5	+5.3	-2.9	-0.0	0.5	0.6	+0.1	0.7
											experiment	1.14	1.02								
											finite diff.	1.20	1.02								
31	40.8	1.2	90	3.34	28.5	4.04	-4.15	-3.66	1.40	1.47	simple model	1.19	0.98	+4.4	+5.3	+3.2	+6.3	0.5	0.7	+0.2	0.7
											experiment	1.14	0.95								
											finite diff.	1.20	1.01								
15	20.6	10.8	81	3.39	28.7	4.07	-4.65	-3.67	1.52	1.47	simple model	1.26	1.01	-0.8	-1.6	-1.9	-0.0	9.3	9.2	-0.1	9.2
											experiment	1.27	1.03								
											finite diff.	1.25	1.03								
9	41.2	1.1	83	3.41	28.8	4.08	-4.12	-3.67	1.40	1.47	simple model	1.19	0.98	+6.3	+6.3	+3.2	+5.3	0.1	0.1	+0.0	0.3
											experiment	1.12	0.95								
											finite diff.	1.19	1.0								
16	41.3	11.3	92	3.21	27.9	3.96	-4.47	-3.63	1.42	1.47	simple model	1.30	1.01	+5.7	+4.1	+4.1	+6.2	10.6	10.8	+0.2	10.7
											experiment	1.23	0.97								
											finite diff.	1.28	1.03								
10	41.2	1.4	91	0.50	14.6	1.05	-2.57	-1.64	1.22	1.22	simple model	1.52	0.99	-3.2	-2.6	-1.0	-1.0	1.1	0.9	-0.2	0.9
											experiment	1.57	1.00								
											finite diff.	1.53	0.99								
11	41.4	7.2	78	0.47	14.3	1.03	-2.50	-1.61	1.22	1.21	simple model	1.66	1.02	+7.1	+6.1	+1.0	+1.0	5.7	5.5	-0.2	5.6
											experiment	1.55	1.01								
											finite diff.	1.65	1.02								

Table 7.3 Experimental data and predicted results for runs using water as the wetting agent. (continued)

Run	T_{in} (°C)	T_a (°C)	H_r (%)	v_a (ms ⁻¹)	h_c (Wm ⁻² K ⁻¹)	Bi	f_{cEvap} (exp.)	f_{cCom} (anal. soln.)	j_{cEvap} (exp.)	j_{cCom} (anal. soln.)	type	f_{cEvap}/f_{cCom}	j_{cEvap}/j_{cCom}	$\Delta f_{cEvap}/f_{cCom}$ (%)		$\Delta j_{cEvap}/j_{cCom}$ (%)		T_{eq} (°C)			T_{wb} (°C)
														simple model	finite diff.	simple model	finite diff.	exp.	model	ΔT_{eq} (°C)	
13	20.6	7.9	94	0.50	14.6	1.05	-2.60	-1.64	1.30	1.22	simple model	1.66	1.07	+5.1	+5.1	+0.5	+0.8	7.4	7.4	+0.0	7.3
											experiment	1.58	1.07								
											finite diff.	1.66	1.08								
5	20.6	1.3	84	0.51	14.7	1.06	-2.39	-1.65	1.25	1.22	simple model	1.45	1.02	-0.0	+2.1	-1.0	+0.0	0.6	0.4	-0.2	0.5
											experiment	1.45	1.03								
											finite diff.	1.48	1.03								
5*	20.5	1.0	80	0.45	14.0	1.01	-2.26	-1.59	1.21	1.21	simple model	1.44	1.01	+1.4	+4.2	+1.0	+3.0	0.0	-0.2	-0.2	0.0
											experiment	1.42	1.00								
											finite diff.	1.48	1.03								
18	29.0	5.8	93	1.35	22.5	1.61	-3.13	-2.23	1.39	1.30	simple model	1.48	1.04	+4.2	+4.9	-2.8	-1.9	5.3	5.3	+0.0	5.2
											experiment	1.42	1.07								
											finite diff.	1.49	1.05								

note: * repeated run

Table 7.4 Experimental data and predicted results for runs using saturated salt sodium chloride as the wetting agent.

Run	T_{in} (°C)	T_a (°C)	H_r (%)	v_a (ms ⁻¹)	h_c (Wm ⁻² K ⁻¹)	Bi	f_{cSvap} (exp.)	f_{cCom} (anal. soln.)	j_{cSvap} (exp.)	j_{cCom} (anal. soln.)	type	f_{cSvap}/f_{cCom}	j_{cSvap}/j_{cCom}	$\Delta f_{cSvap}/f_{cCom}$ (%)		$\Delta j_{cSvap}/j_{cCom}$ (%)		T_{eq} (°C)			T_{wb} (°C)
														simple model	finite diff.	simple model	finite diff.	exp.	model	ΔT_{eq} (°C)	
7	41.4	1.4	91	3.24	25.9	3.68	-4.24	-3.52	1.50	1.46	simple model	1.19	0.99	-1.7	-1.7	-2.9	-1.0	2.4	2.4	+0.0	0.9
											experiment	1.21	1.02								
											finite diff.	1.19	1.01								
1	20.8	1.4	80	2.93	24.7	3.51	-3.74	-3.45	1.40	1.45	simple model	1.16	1.01	+7.4	+9.3	+4.1	+5.2	1.5	1.7	+0.2	0.4
											experiment	1.07	0.97								
											finite diff.	1.19	1.02								
14	41.3	10.7	80	2.93	24.8	3.51	-4.42	-3.45	1.48	1.45	simple model	1.28	1.02	-0.0	-0.0	-0.0	+1.0	11.1	11.2	+0.1	8.9
											experiment	1.28	1.02								
											finite diff.	1.28	1.03								
6	18.7	9.8	81	2.94	24.6	3.50	-4.05	-3.44	1.48	1.45	simple model	1.25	1.03	+6.8	+7.7	+1.0	+2.9	10.1	10.4	+0.3	8.2
											experiment	1.17	1.02								
											finite diff.	1.27	1.05								
17	29.1	5.6	80	1.05	18.9	1.36	-2.83	-1.98	1.35	1.26	simple model	1.44	1.04	-0.7	+0.7	-2.8	-2.8	5.9	6.0	+0.1	4.3
											experiment	1.45	1.07								
											finite diff.	1.46	1.04								
3	19.4	9.7	79	0.42	12.4	0.90	-2.19	-1.44	1.26	1.19	simple model	1.63	1.08	+7.2	+7.9	+1.9	+1.9	10.1	10.0	-0.1	7.9
											experiment	1.52	1.06								
											finite diff.	1.64	1.08								

Table 7.4 Experimental data and predicted results for runs using saturated salt sodium chloride as the wetting agent. (continued)

Run	T_{in} (°C)	T_a (°C)	H_r (%)	v_a (ms ⁻¹)	h_c (Wm ⁻² K ⁻¹)	Bi	f_{cSvap} (exp.)	f_{cCom} (anal. soln.)	j_{cSvap} (exp.)	j_{cCom} (anal. soln.)	type	f_{cSvap}/f_{cCom}	j_{cSvap}/j_{cCom}	$\Delta f_{cSvap}/f_{cCom}$ (%)		$\Delta j_{cSvap}/j_{cCom}$ (%)		T_{eq} (°C)			T_{sub} (°C)
														simple model	finite diff.	simple model	finite diff.	exp.	model	ΔT_{eq} (°C)	
4	41.3	0.8	74	0.46	12.9	0.93	-2.16	-1.49	1.13	1.20	simple model	1.42	0.97	-2.1	-0.7	+2.1	+2.1	1.0	0.7	-0.3	-0.6
											experiment	1.45	0.95								
											finite diff.	1.44	0.97								
2	21.5	1.7	91	0.53	13.7	0.99	-2.33	-1.56	1.23	1.21	simple model	1.41	1.03	-5.4	-2.7	+1.1	+1.0	2.6	2.7	+0.1	1.1
											experiment	1.49	1.02								
											finite diff.	1.45	1.03								
12	40.1	10.8	94	0.48	13.1	0.94	-2.77	-1.51	1.26	1.20	simple model	1.75	1.06	-4.9	-4.9	+1.0	+0.0	12.3	12.6	+0.3	10.1
											experiment	1.84	1.05								
											finite diff.	1.75	1.05								

Table 7.5 Experimental data and predicted results for runs using saturated salt potassium chloride as the wetting agent.

Run	T_{in} (°C)	T_a (°C)	H_r (%)	v_a (ms ⁻¹)	h_c (Wm ⁻² K ⁻¹)	Bi	f_{cExp} (exp.)	f_{cCom} (anal. soln.)	j_{cExp} (exp.)	j_{cCom} (anal. soln.)	type	f_{cExp}/f_{cCom}	j_{cExp}/j_{cCom}	$\Delta f_{cExp}/f_{cCom}$ (%)		$\Delta j_{cExp}/j_{cCom}$ (%)		T_{eq} (°C)			T_{wb} (°C)
														simple model	finite diff.	simple model	finite diff.	exp.	model	ΔT_{eq} (°C)	
26	27.7	5.7	91	3.29	27.1	3.85	-4.29	-3.58	1.52	1.46	simple model	1.22	1.00	+1.7	+2.5	-4.0	-1.0	6.0	6.0	+0.0	5.0
											experiment	1.20	1.04								
											finite diff.	1.23	1.03								
29	29.7	6.0	92	0.65	12.6	1.80	-3.10	-2.39	1.36	1.32	simple model	1.42	1.05	+9.2	+9.2	+1.5	+1.9	6.0	6.4	+0.4	5.4
											experiment	1.30	1.03								
											finite diff.	1.42	1.05								
29*	28.6	5.7	92	0.59	12.0	1.70	-3.30	-2.31	1.35	1.31	simple model	1.43	1.05	-0.0	+0.7	+1.9	+1.9	6.1	6.0	-0.1	5.1
											experiment	1.43	1.03								
											finite diff.	1.44	1.05								
30	29.4	5.7	92	0.59	12.2	1.70	-3.39	-2.33	1.43	1.31	simple model	1.43	1.05	-2.1	-1.4	-3.7	-3.7	6.1	6.0	-0.1	5.1
											experiment	1.46	1.09								
											finite diff.	1.44	1.05								
23	29.3	4.9	80	0.60	12.2	1.73	-3.23	-2.33	1.35	1.31	simple model	1.39	1.04	+0.0	+0.7	+1.0	+1.0	4.6	4.4	-0.2	3.6
											experiment	1.39	1.03								
											finite diff.	1.40	1.04								
21	28.3	0.7	74	0.63	12.4	1.77	-3.09	-2.37	1.34	1.31	simple model	1.30	1.02	-0.7	+1.5	+0.0	+0.0	0.2	-0.1	+0.3	-0.4
											experiment	1.31	1.02								
											finite diff.	1.33	1.02								
22	29.4	10.6	81	0.60	12.2	1.73	-3.64	-2.33	1.46	1.31	simple model	1.50	1.07	-3.8	-3.8	-4.5	-4.5	10.3	10.0	-0.3	8.9
											experiment	1.56	1.12								
											finite diff.	1.50	1.07								
24	28.8	5.7	92	1.59	22.3	1.60	-3.03	-2.22	1.40	1.29	simple model	1.44	1.05	+5.9	+6.6	-2.8	-2.8	5.9	6.0	+0.1	5.1
											experiment	1.36	1.08								
											finite diff.	1.45	1.05								

note: * repeated run

Table 7.5 Experimental data and predicted results for runs using saturated salt potassium chloride as the wetting agent. (continued)

Run	T_{in} (°C)	T_a (°C)	H_r (%)	v_a (ms ⁻¹)	h_c (Wm ⁻² K ⁻¹)	Bi	$f_{c\delta vap}$ (exp.)	f_{cCom} (anal. soln.)	$j_{c\delta vap}$ (exp.)	j_{cCom} (anal. soln.)	type	$f_{c\delta vap}/f_{cCom}$	$j_{c\delta vap}/j_{cCom}$	$\Delta f_{c\delta vap}/f_{cCom}$ (%)		$\Delta j_{c\delta vap}/j_{cCom}$ (%)		T_{eq} (°C)			$T_{\delta\delta}$ (°C)
														simple model	finite diff.	simple model	finite diff.	exp.	model	ΔT_{eq} (°C)	
19	20.6	5.7	92	1.54	22.0	1.58	-3.06	-2.20	1.38	1.29	simple model	1.43	1.06	+2.9	+4.3	-0.9	-0.0	6.1	6.1	-0.0	5.1
											experiment	1.39	1.07								
											finite diff.	1.45	1.07								
20	39.0	5.7	92	1.54	22.0	1.58	-3.43	-2.20	1.47	1.29	simple model	1.47	1.04	-5.8	-5.8	-8.8	-8.8	6.2	6.1	-0.1	5.12
											experiment	1.56	1.14								
											finite diff.	1.47	1.04								
27	29.2	5.3	82	1.46	21.5	1.55	-2.93	-2.17	1.41	1.29	simple model	1.43	1.05	+5.9	+6.3	-4.5	-5.5	5.1	5.0	-0.1	4.2
											experiment	1.35	1.10								
											finite diff.	1.44	1.04								
27*	29.1	5.5	81	1.49	21.7	1.56	-3.18	-2.18	1.32	1.29	simple model	1.43	1.04	-2.1	-1.4	+1.0	+1.0	5.1	5.1	-0.0	4.3
											experiment	1.46	1.03								
											finite diff.	1.44	1.04								
28	29.0	5.4	82	1.66	22.9	1.63	-3.19	-2.26	1.41	1.30	simple model	1.41	1.04	-0.7	+0.7	-4.6	-3.7	5.1	5.0	-0.1	4.2
											experiment	1.42	1.09								
											finite diff.	1.43	1.05								
25	30.1	5.7	92	0.56	14.2	1.02	-2.59	-1.61	1.27	1.21	simple model	1.58	1.04	-2.5	-1.9	-1.0	-1.0	6.0	6.1	0.1	5.1
											experiment	1.62	1.05								
											finite diff.	1.59	1.04								

note: * repeated run

Table 7.6 Differences between results calculated by the finite difference method and results from the experiments (all data).

	% difference in f_{cEvap}/f_{cConv}	% difference in j_{cEvap}/j_{cConv}	% difference in time to $Y_c =$			error in T_{eq} (°C)
			0.10	0.35	0.70	
mean	+2.1	-0.2	-2.2	-2.1	-1.9	0.0
std.	4.1	3.2	4.1	3.6	4.5	0.2
95% conf. interval	-6.2 to +10.5	-6.7 to +6.3	-10.6 to +6.2	-9.5 to +5.3	-11.0 to 7.2	-0.4 to +0.3

Table 7.7 Differences between results calculated by the proposed curve-fitted algebraic equations (simple model) and results from the experiments (all data).(* Correlation coefficient between (a) % difference between simple method prediction and experiment, and (b) % difference between finite difference predictions and experiments).

	% difference in f_{cEvap}/f_{cConv}	% difference in j_{cEvap}/j_{cConv}	% difference in time to $Y_c =$			error in T_{eq} (°C)
			0.10	0.35	0.70	
mean	+1.7	-0.4	-1.7	-1.8	-2.2	0.0
std.	4.0	2.9	4.2	3.8	4.7	0.2
95% conf. interval	-6.5 to +9.9	-6.3 to +5.6	-10.2 to +6.9	-9.6 to +6.0	-11.9 to +7.5	-0.4 to +0.3
R ^{2*}	0.944	0.900	0.932	0.890	0.862	-

Table 7.8 Predicted and measured chilling times to reach certain centre temperatures which corresponded to $Y_{c,exp} = 0.10, 0.35, \text{ and } 0.70$ for runs using water as the wetting agent.

Run	a_w	size	time (hrs.) to $Y_{c,exp} = 0.10$					time (hrs.) to $Y_{c,exp} = 0.35$					time (hrs.) to $Y_{c,exp} = 0.70$				
			simple model	exp.	finite diff.	Δ (%)		simple model	exp.	finite diff.	Δ (%)		simple model	exp.	finite diff.	Δ (%)	
						simple model	finite diff.				simple model	finite diff.				simple model	finite diff.
			simple model	exp.	finite diff.	simple model	finite diff.	simple model	exp.	finite diff.	simple model	finite diff.	simple model	exp.	finite diff.	simple model	finite diff.
8	1.0	L	6.99	7.19	6.96	-2.8	-3.2	3.68	3.86	3.70	-4.7	-4.1	1.88	2.02	1.93	-6.4	-4.5
33	1.0	L	6.72	6.92	6.79	-2.9	-1.9	3.53	3.64	3.61	-3.0	-0.8	1.79	1.82	1.87	-1.6	+2.7
15	1.0	L	6.28	6.37	6.36	-1.4	-0.2	3.40	3.44	3.46	-1.2	+0.6	1.78	1.82	1.83	-2.2	+0.5
9	1.0	L	6.64	6.97	6.71	-4.7	-3.7	3.52	3.66	3.59	-3.8	-1.9	1.79	1.83	1.86	-2.2	+1.6
16	1.0	L	6.34	6.46	6.50	-1.9	+0.6	3.35	3.41	3.46	-1.8	+1.5	1.73	1.72	1.81	+0.6	+5.7
10	1.0	S	2.74	2.72	2.73	+0.7	+0.4	1.38	1.36	1.37	+1.5	+0.7	0.61	0.60	0.60	+1.7	-0.0
11	1.0	S	2.59	2.80	2.60	-7.5	-7.1	1.31	1.40	1.32	-6.4	-5.7	0.59	0.62	0.59	-4.8	-4.8

Table 7.8 Predicted and measured chilling times to reach certain centre temperatures which corresponded to $Y_{c,exp} = 0.10, 0.35, \text{ and } 0.70$ for runs using water as the wetting agent. (continued)

Run	a_w	size	time (hrs.) to $Y_{c,exp} = 0.10$					time (hrs.) to $Y_{c,exp} = 0.35$					time (hrs.) to $Y_{c,exp} = 0.70$				
			simple model	exp.	finite diff.	Δ (%)		simple model	exp.	finite diff.	Δ (%)		simple model	exp.	finite diff.	Δ (%)	
						simple model	finite diff.				simple model	finite diff.				simple model	finite diff.
13	1.0	S	2.65	2.76	2.65	-4.0	-4.0	1.36	1.41	1.36	-3.5	-3.5	0.64	0.67	0.64	-4.5	-4.5
5	1.0	S	2.86	2.96	2.81	-3.4	-5.1	1.46	1.49	1.44	-2.0	-3.4	0.67	0.68	0.66	-1.5	-2.9
5*	1.0	S	2.92	3.09	2.87	-5.5	-7.1	1.50	1.54	1.48	-2.6	-3.9	0.68	0.68	0.68	+0.0	+0.0
18	1.0	S	2.23	2.35	2.23	-5.1	-5.1	1.15	1.23	1.16	-6.5	-5.7	0.56	0.61	0.57	-8.2	-6.6

note: * repeated run

Table 7.9 Predicted and measured chilling times to reach certain centre temperatures which corresponded to $Y_{c,exp} = 0.10, 0.35,$ and 0.70 for runs using saturated salt sodium chloride as the wetting agent.

Run	a_w	size	time (hrs.) to $Y_{c,exp} = 0.10$					time (hrs.) to $Y_{c,exp} = 0.35$					time (hrs.) to $Y_{c,exp} = 0.70$				
			simple model	exp.	finite diff.	Δ (%)		simple model	exp.	finite diff.	Δ (%)		simple model	exp.	finite diff.	Δ (%)	
						simple model	finite diff.				simple model	finite diff.				simple model	finite diff.
7	0.76	L	7.01	6.95	6.98	+0.9	+0.4	3.71	3.74	3.72	-0.8	-0.5	1.89	1.96	1.92	-3.6	-2.0
1	0.76	L	7.49	7.68	7.37	-2.5	-4.0	3.92	4.04	3.87	-3.0	-4.2	2.0	2.02	2	-1.0	-1.0
14	0.76	L	6.70	6.64	6.74	+0.9	+1.5	3.56	3.55	3.60	+0.3	+1.4	1.84	1.84	1.88	-0.0	+2.2
6	0.76	L	7.52	7.24	7.47	+3.9	+3.1	3.79	3.88	3.79	-2.3	-2.3	1.94	2.01	1.96	-3.5	-2.5
17	0.76	S	2.58	2.57	2.54	+0.4	-1.2	1.32	1.33	1.30	-0.8	-2.3	0.63	0.65	0.62	-3.1	-4.6

Table 7.9 Predicted and measured chilling times to reach certain centre temperatures which corresponded to $Y_{c,exp} = 0.10, 0.35,$ and 0.70 for runs using saturated salt sodium chloride as the wetting agent. (continued)

Run	a_w	size	time (hrs.) to $Y_{c,exp} = 0.10$					time (hrs.) to $Y_{c,exp} = 0.35$					time (hrs.) to $Y_{c,exp} = 0.70$				
			simple model	exp.	finite diff.	Δ (%)		simple model	exp.	finite diff.	Δ (%)		simple model	exp.	finite diff.	Δ (%)	
						simple model	finite diff.				simple model	finite diff.				simple model	finite diff.
3	0.76	S	2.84	3.24	2.82	-12.3	-13.0	1.50	1.64	1.49	-8.5	-9.1	0.71	0.75	0.71	-5.3	-5.3
4	0.76	S	3.19	3.14	3.12	+1.6	-0.6	1.58	1.52	1.55	+3.9	+2.0	0.67	0.62	0.65	+8.1	+4.8
2	0.76	S	3.23	3.01	3.13	+7.3	+4.0	1.62	1.51	1.57	+7.3	+4.0	0.73	0.68	0.71	+7.4	+4.4
12	0.76	S	2.81	2.56	2.81	+9.8	+9.8	1.39	1.29	1.39	+7.8	+7.8	0.64	0.59	0.63	+8.5	+6.8

Table 7.10 Predicted and measured chilling times to reach certain centre temperatures which corresponded to $Y_{c,exp} = 0.10, 0.35,$ and 0.70 for runs using saturated salt potassium chloride as the wetting agent.

Run	a_w	size	time (hrs.) to $Y_{c,exp} = 0.10$					time (hrs.) to $Y_{c,exp} = 0.35$					time (hrs.) to $Y_{c,exp} = 0.70$				
			simple model	exp.	finite diff.	Δ (%)		simple model	exp.	finite diff.	Δ %		simple model	exp.	finite diff.	Δ (%)	
						simple model	finite diff.				simple model	finite diff.				simple model	finite diff.
26	0.87	L	6.67	6.91	6.70	-3.5	-3.0	3.56	3.73	3.60	-4.6	-3.5	1.84	1.97	1.89	-6.6	-4.1
29	0.87	L	8.97	9.14	8.91	-1.9	-2.5	4.51	4.75	4.48	-5.1	-5.7	2.20	2.32	2.20	-5.2	-5.2
29*	0.87	L	8.60	8.59	8.53	+0.1	-0.7	4.50	4.45	4.47	+1.1	+0.4	2.21	2.17	2.21	+1.8	+1.8
30	0.87	L	8.52	8.54	8.45	-0.2	-1.1	4.47	4.52	4.44	-1.1	-1.8	2.20	2.29	2.20	-3.9	-3.9
23	0.87	L	8.49	8.77	8.40	-3.2	-4.2	4.50	4.55	4.46	-1.1	-2.0	2.22	2.21	2.20	+0.5	-0.5
21	0.88	L	8.90	9.14	8.70	-2.6	-4.8	4.69	4.73	4.59	-0.8	-3.0	2.28	2.29	2.23	-0.4	-2.6
22	0.86	L	7.82	8.02	7.81	-2.5	-2.6	4.22	4.27	4.22	-1.2	-1.2	2.13	2.20	2.13	-3.2	-3.2
24	0.87	S	2.32	2.44	2.30	-4.9	-5.7	1.19	1.28	1.18	-7.0	-7.8	0.58	0.64	0.58	-9.4	-9.4

note: * repeated run

Table 7.10 Predicted and measured chilling times to reach certain centre temperatures which corresponded to $Y_{c,exp} = 0.10, 0.35,$ and 0.70 for runs using saturated salt potassium chloride as the wetting agent. (continued)

Run	a_w	size	time (hrs.) to $Y_{c,exp} = 0.10$					time (hrs.) to $Y_{c,exp} = 0.35$					time (hrs.) to $Y_{c,exp} = 0.70$				
			simple model	exp.	finite diff.	Δ (%)		simple model	exp.	finite diff.	Δ (%)		simple model	exp.	finite diff.	Δ (%)	
						simple model	finite diff.				simple model	finite diff.				simple model	finite diff.
19	0.87	S	2.32	2.40	2.29	-3.3	-4.6	1.21	1.25	1.20	-3.2	-4.0	0.59	0.62	0.59	-4.8	-4.8
20	0.87	S	2.22	2.19	2.22	+1.4	+1.4	1.16	1.17	1.15	-0.9	-1.7	0.56	0.61	0.56	-8.2	-8.2
27	0.87	S	2.30	2.53	2.28	-9.1	-9.9	1.20	1.33	1.19	-9.8	-10.5	0.58	0.67	0.58	-13.4	-13.4
27*	0.87	S	2.31	2.27	2.29	+1.8	+0.9	1.20	1.17	1.19	+2.6	+1.7	0.58	0.56	0.58	+3.6	+3.6
28	0.87	S	2.26	2.32	2.23	-2.6	-3.9	1.18	1.22	1.17	-3.3	-4.1	0.58	0.61	0.57	-4.9	-6.6
25	0.87	S	2.83	2.75	2.81	+2.9	+2.2	1.43	1.39	1.41	+2.9	+1.4	0.65	0.64	0.65	+1.6	+1.6

note: * repeated run

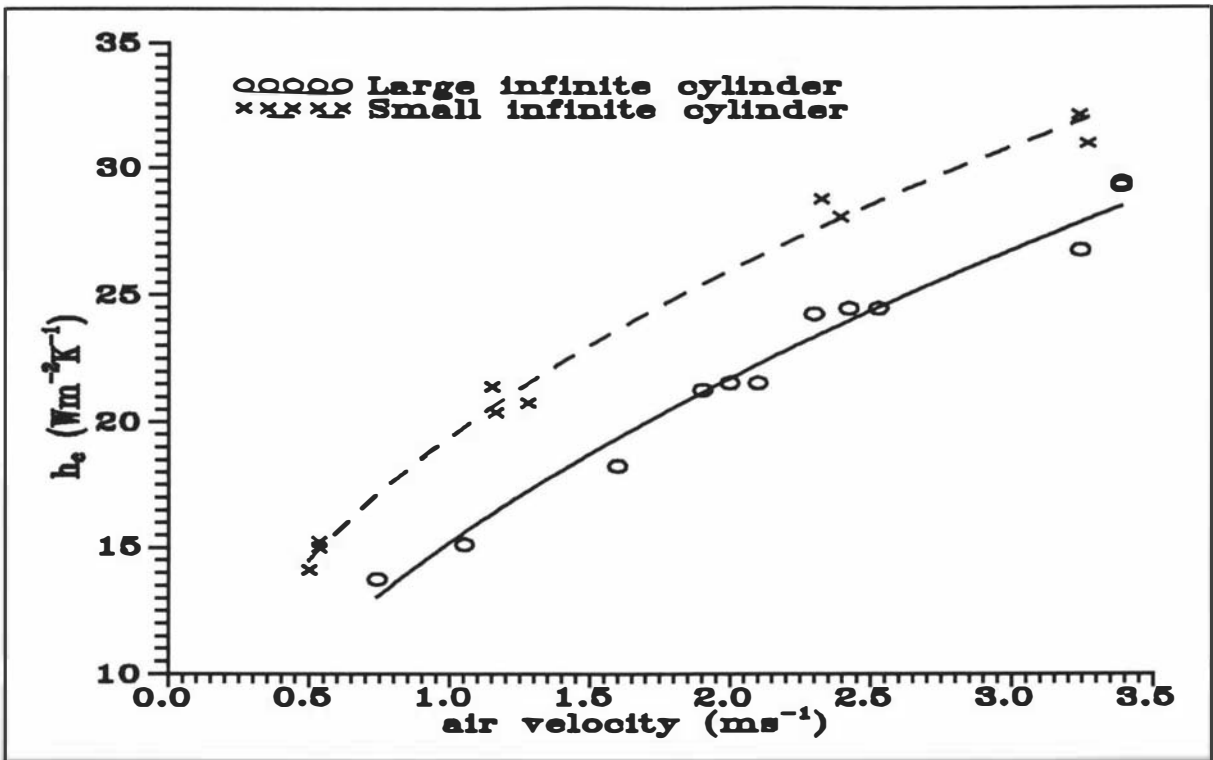


Figure 7.1 Plots of h_c vs air velocity for heat transfer coefficient measurement runs in which the wetting fluid was water.

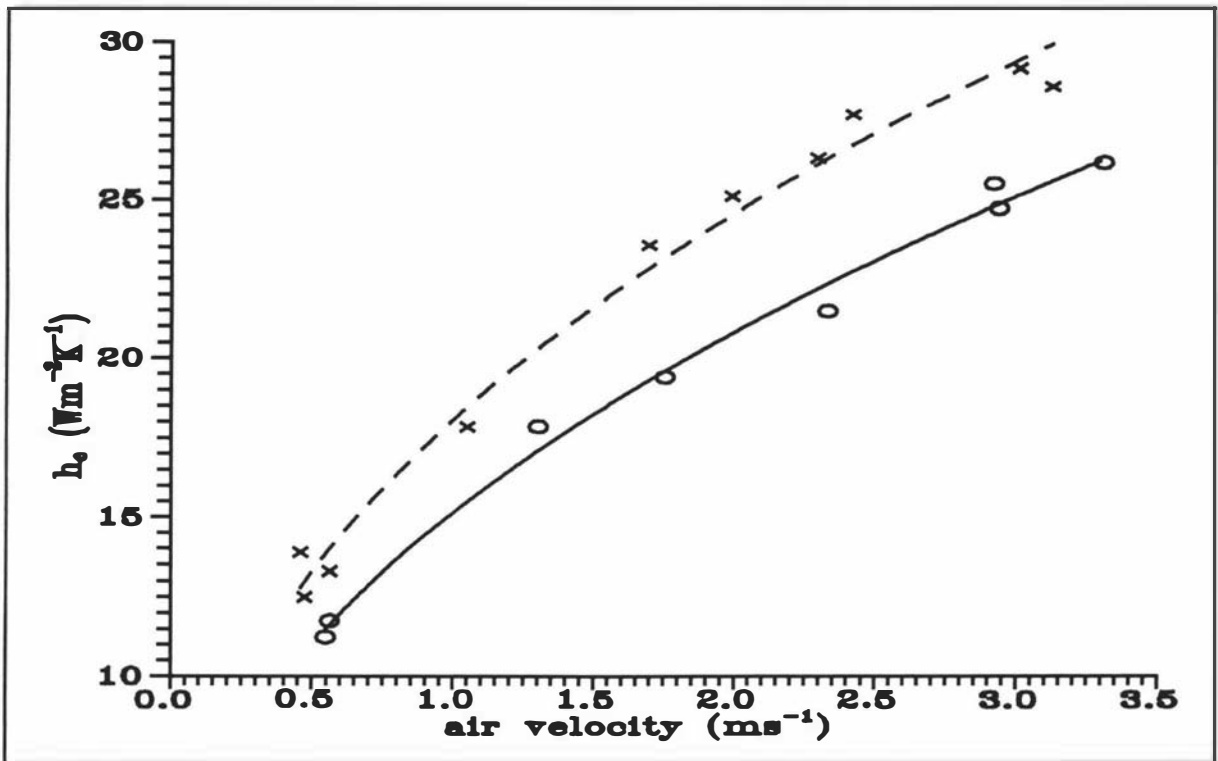


Figure 7.2 Plots of h_c vs air velocity for heat transfer coefficient measurement runs in which the wetting fluid was a saturated solution of NaCl. Key as in Figure 7.1.

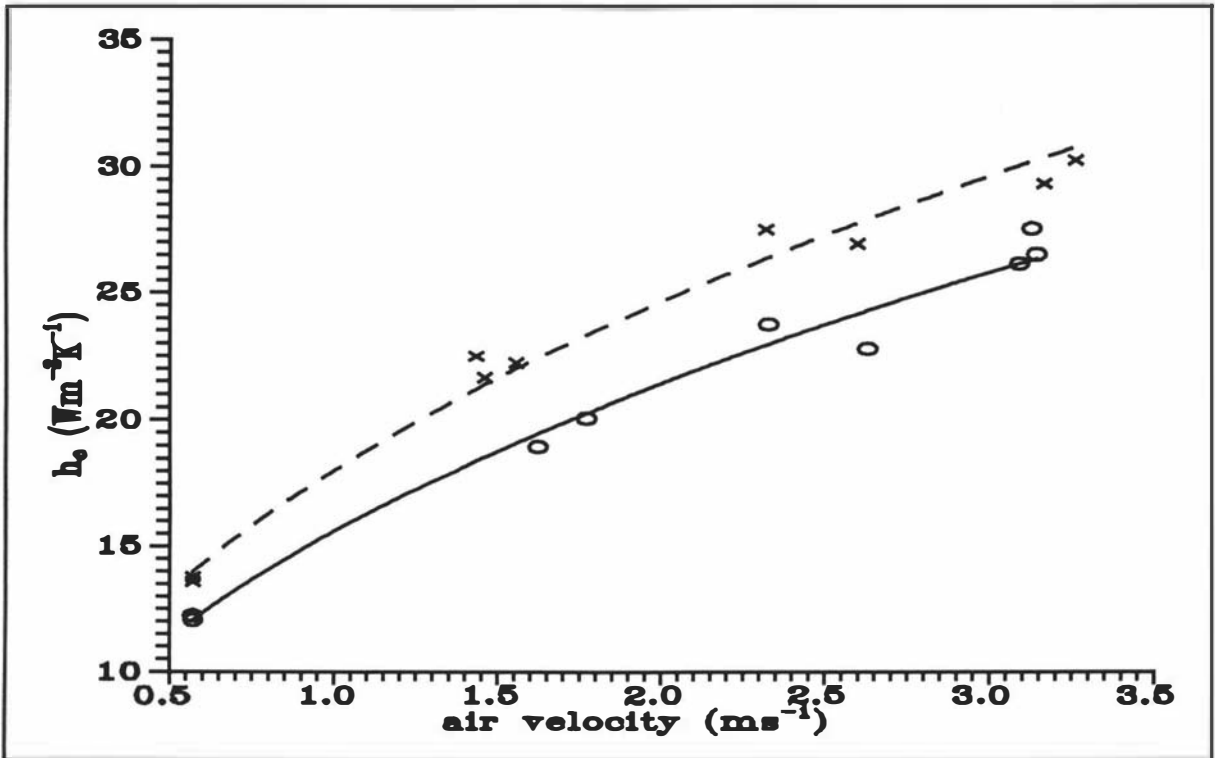


Figure 7.3 Plots of h_c vs air velocity for heat transfer coefficient measurement runs in which the wetting fluid was a saturated solution of KCl. Key as in Figure 7.1.

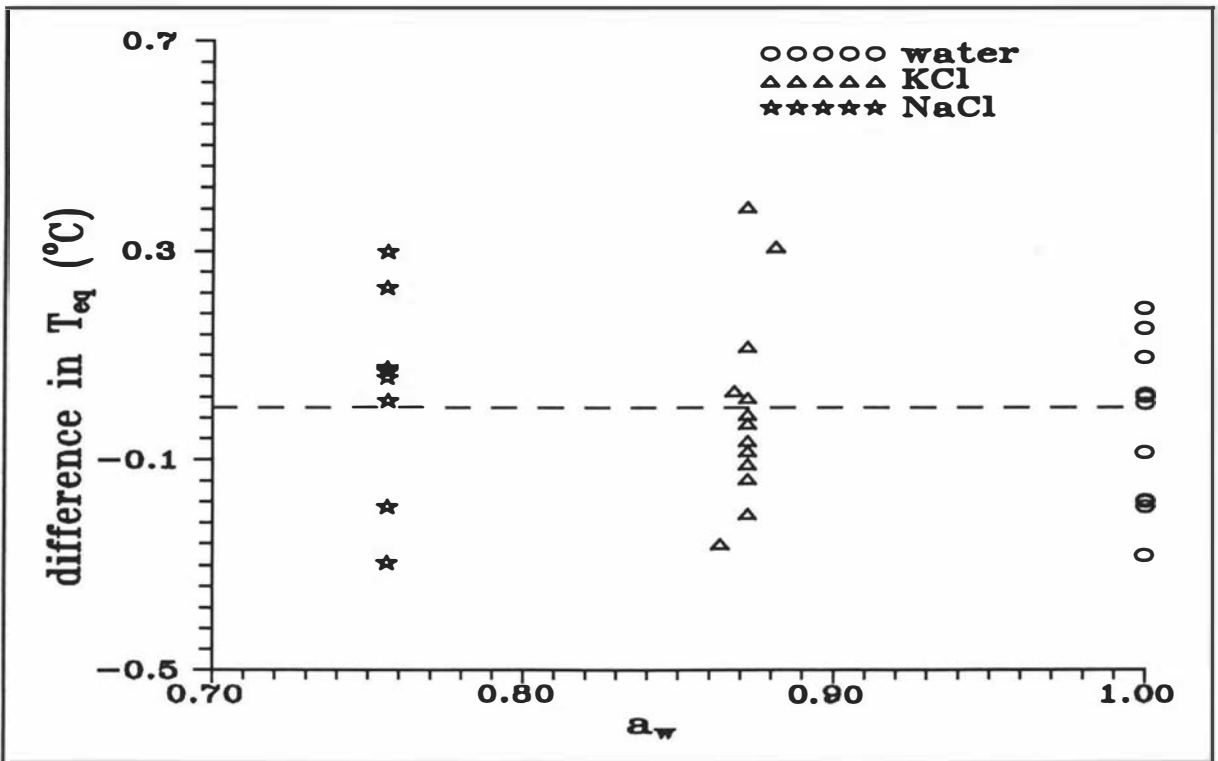


Figure 7.4 Plots of difference between $T_{eq,pred}$ and $T_{eq,exp}$ vs a_w for all experimental runs.

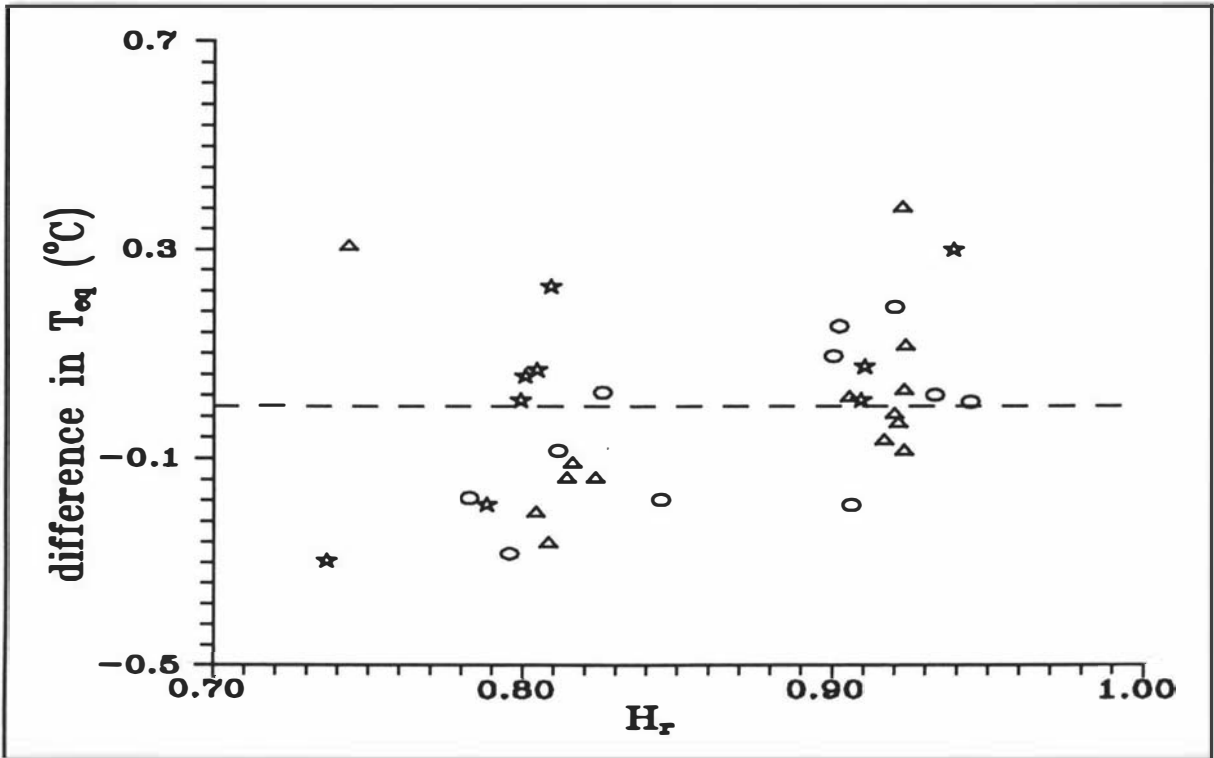


Figure 7.5 Plots of difference between $T_{eq,pred}$ and $T_{eq,exp}$ vs H_r for all experimental runs. Key as in Figure 7.4.

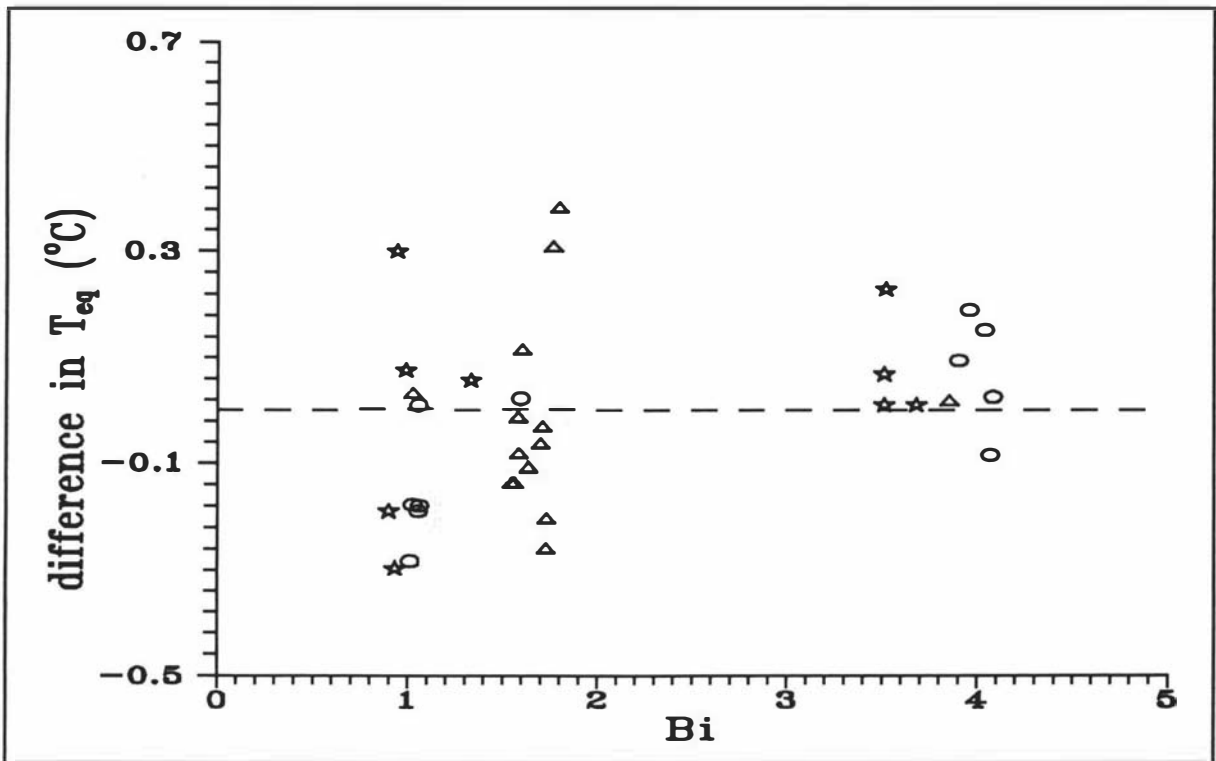


Figure 7.6 Plots of difference between $T_{eq,pred}$ and $T_{eq,exp}$ vs Bi for all experimental runs. Key as in Figure 7.4.

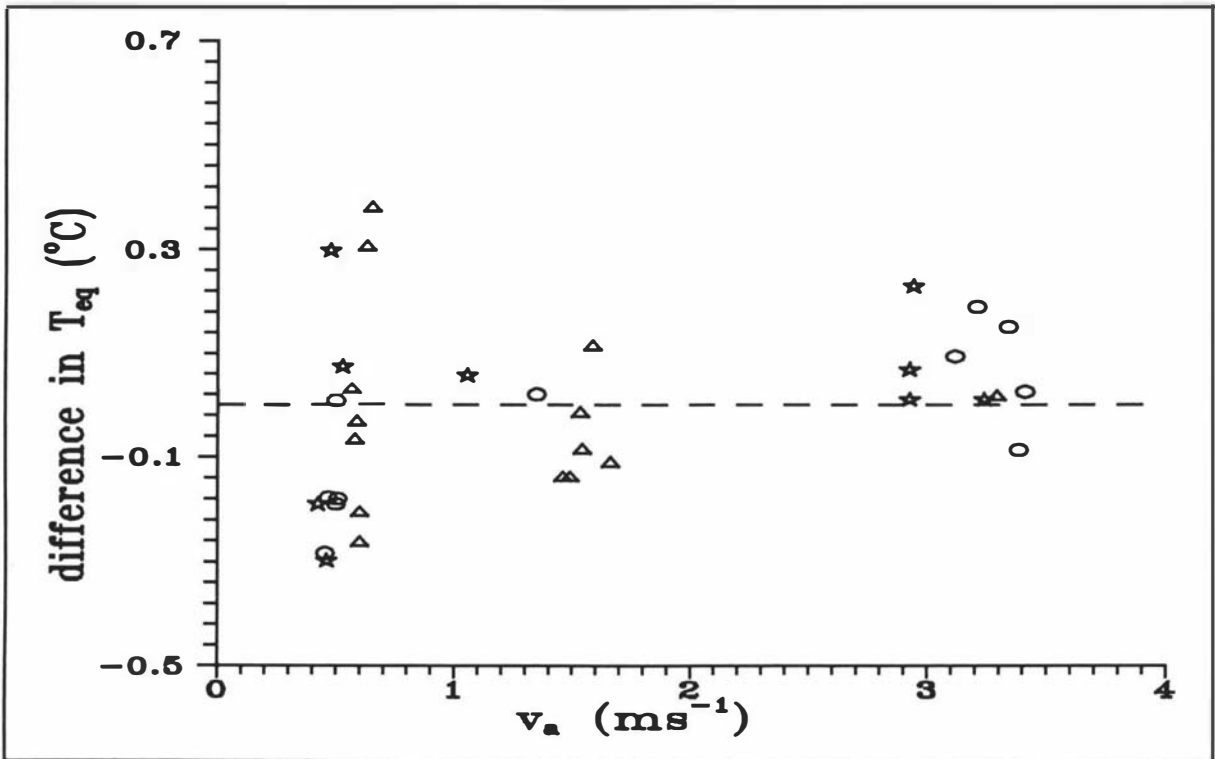


Figure 7.7 Plots of difference between $T_{eq,pred}$ and $T_{eq,exp}$ vs v_a for all experimental runs. Key as in Figure 7.4.

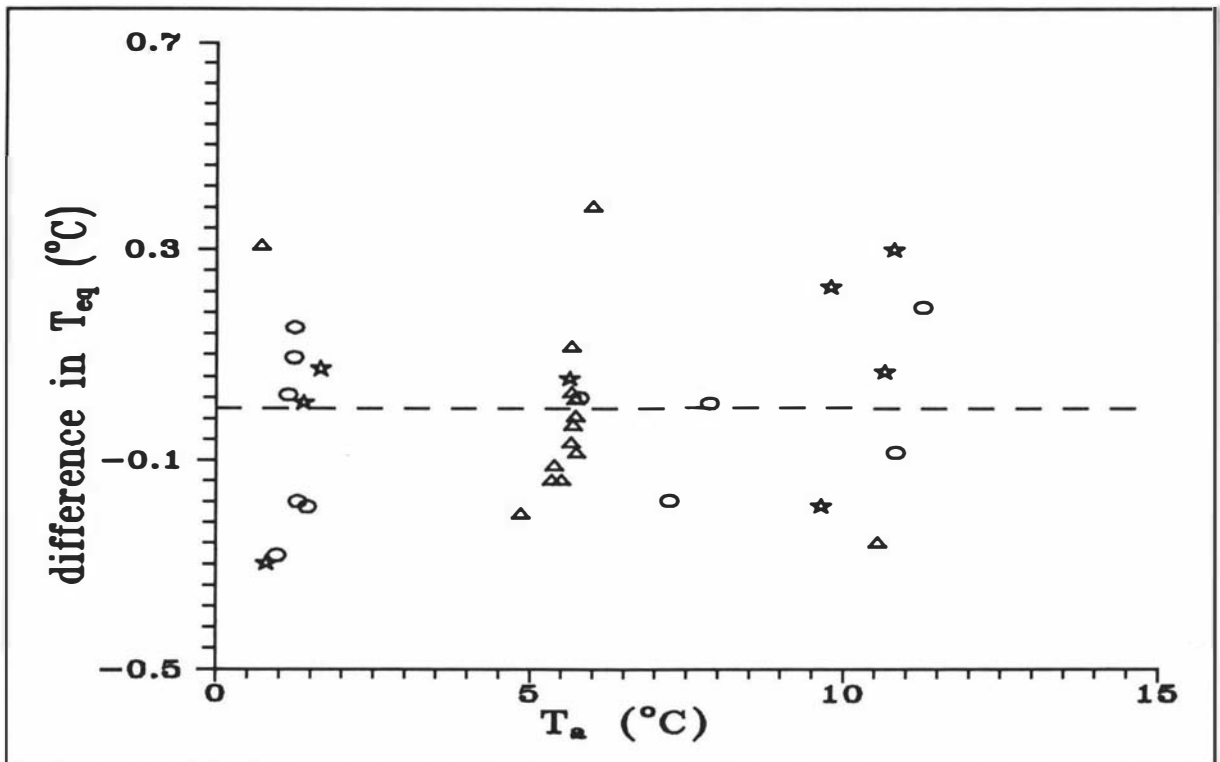


Figure 7.8 Plots of difference between $T_{eq,pred}$ and $T_{eq,exp}$ vs T_a for all experimental runs. Key as in Figure 7.4.

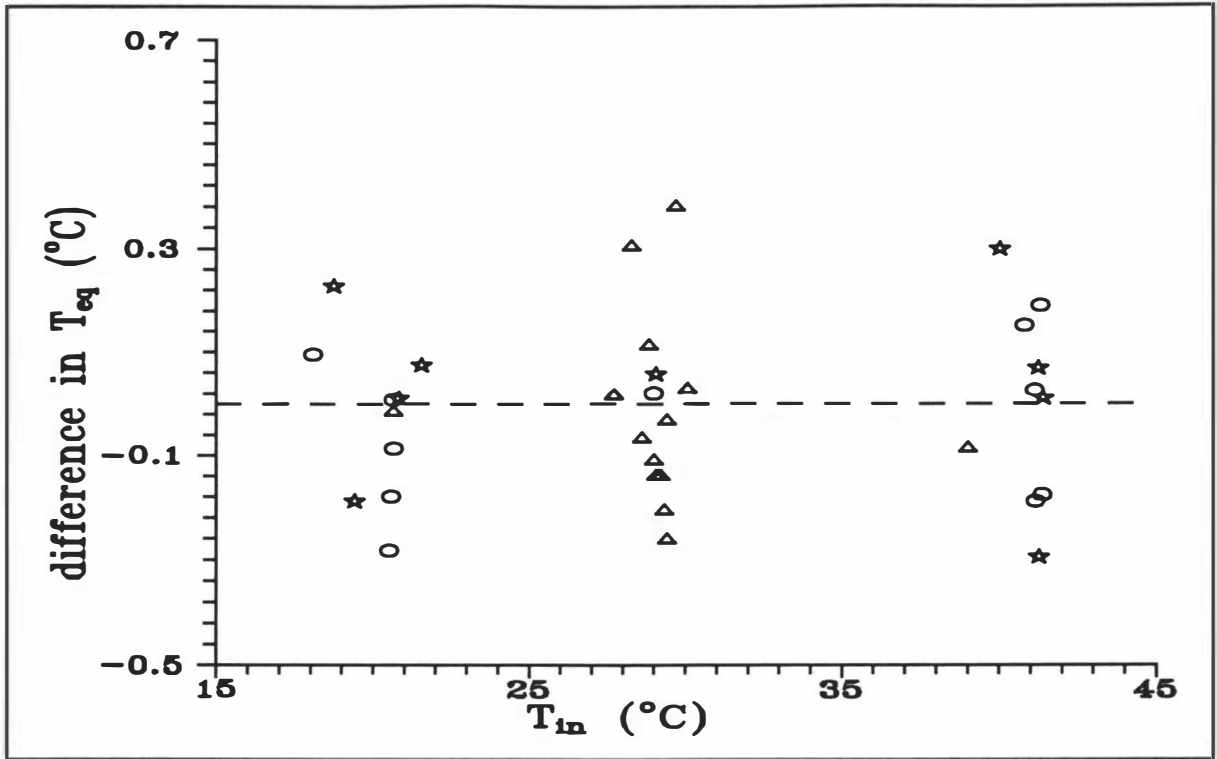


Figure 7.9 Plots of difference between $T_{eq,pred}$ and $T_{eq,exp}$ vs T_{in} for all experimental runs. Key as in Figure 7.4.

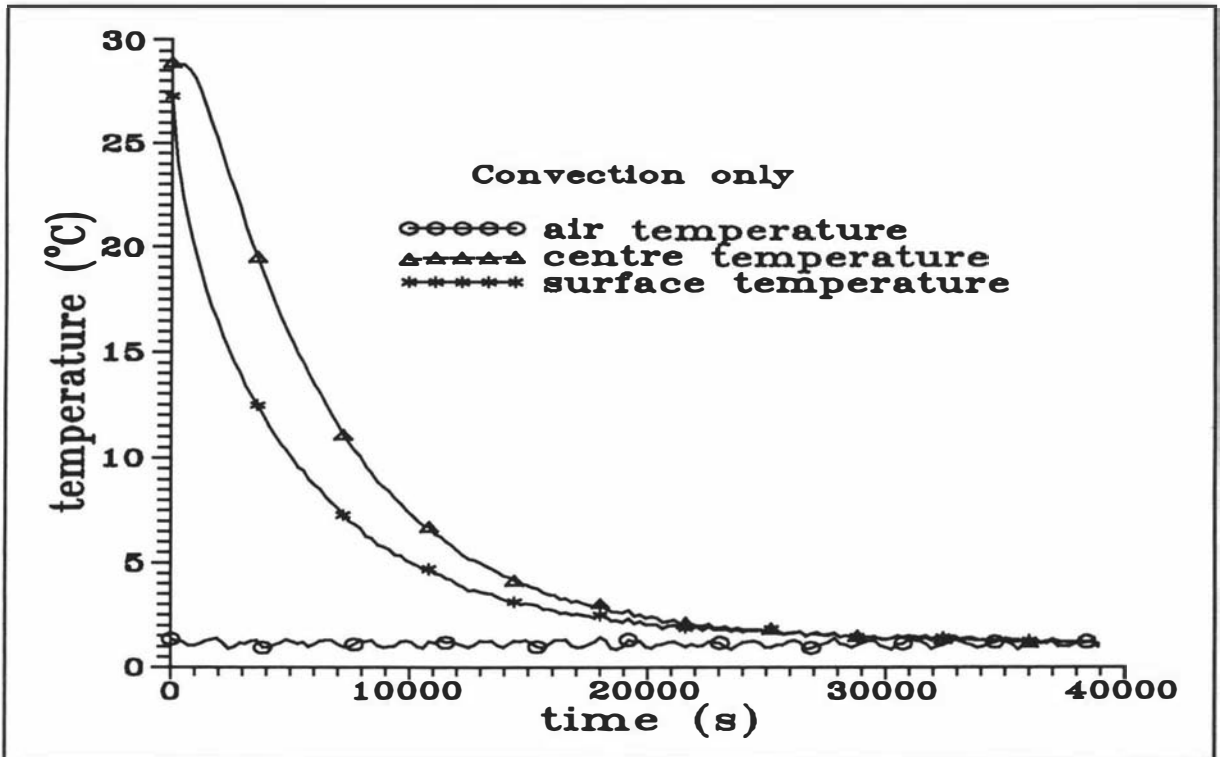


Figure 7.10 Typical plot of temperature vs time for cooling without evaporation ($T_{eq,exp} = T_a$).

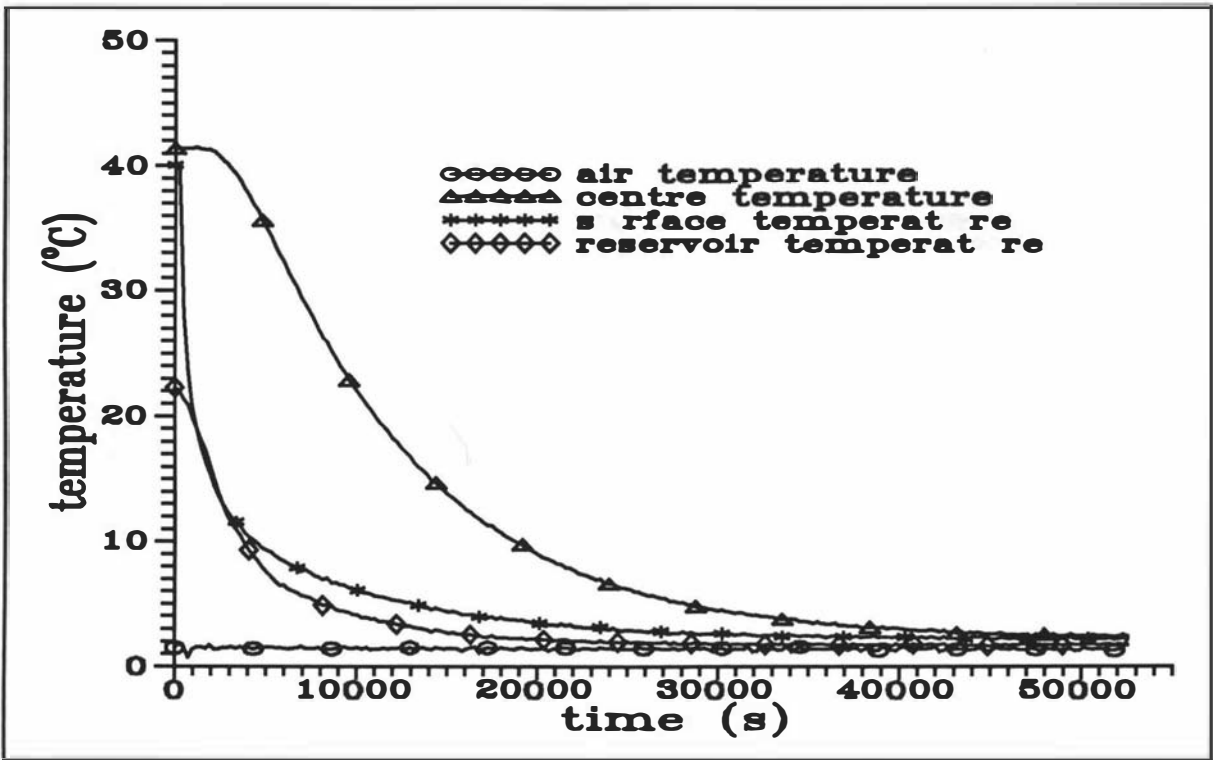


Figure 7.11 Typical plot of temperature vs time for cooling with evaporation ($T_{eq,exp} > T_a$ and $a_w < H_r$).

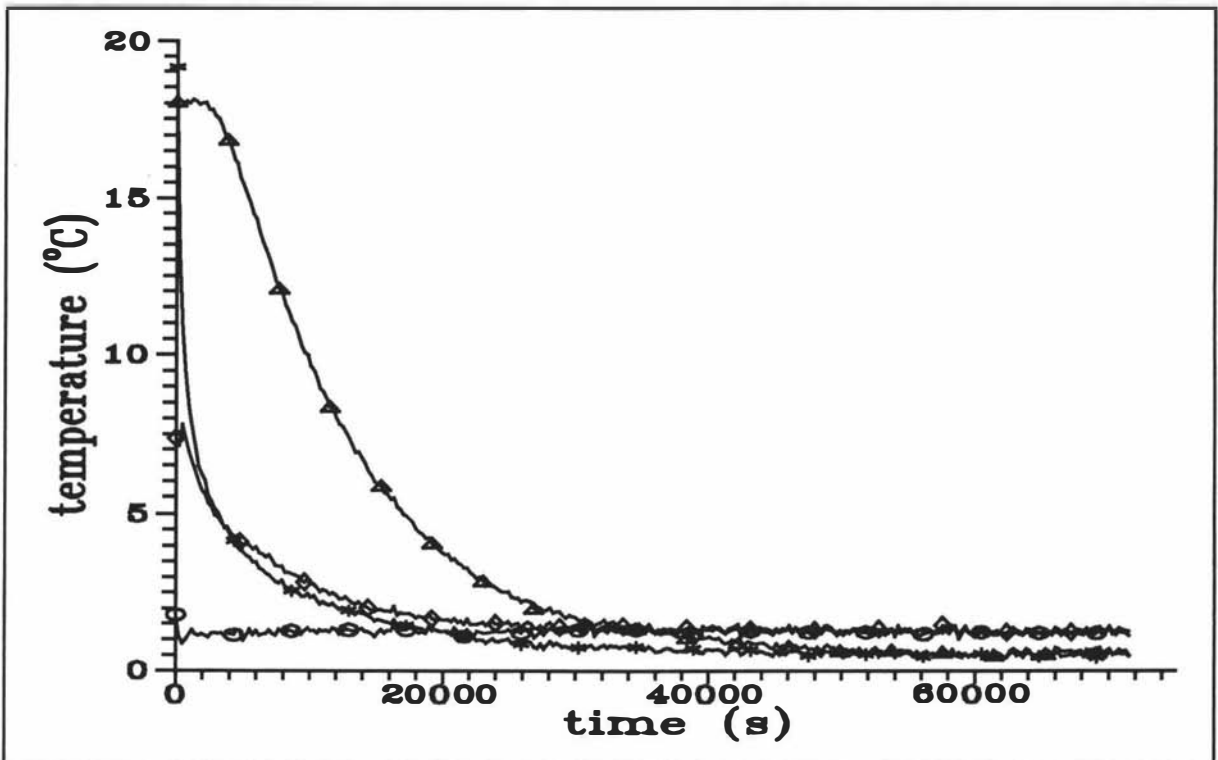


Figure 7.12 Typical plot of temperature vs time for cooling with evaporation ($T_{eq,exp} < T_a$ and $a_w > H_r$). Key as in Figure 7.11.

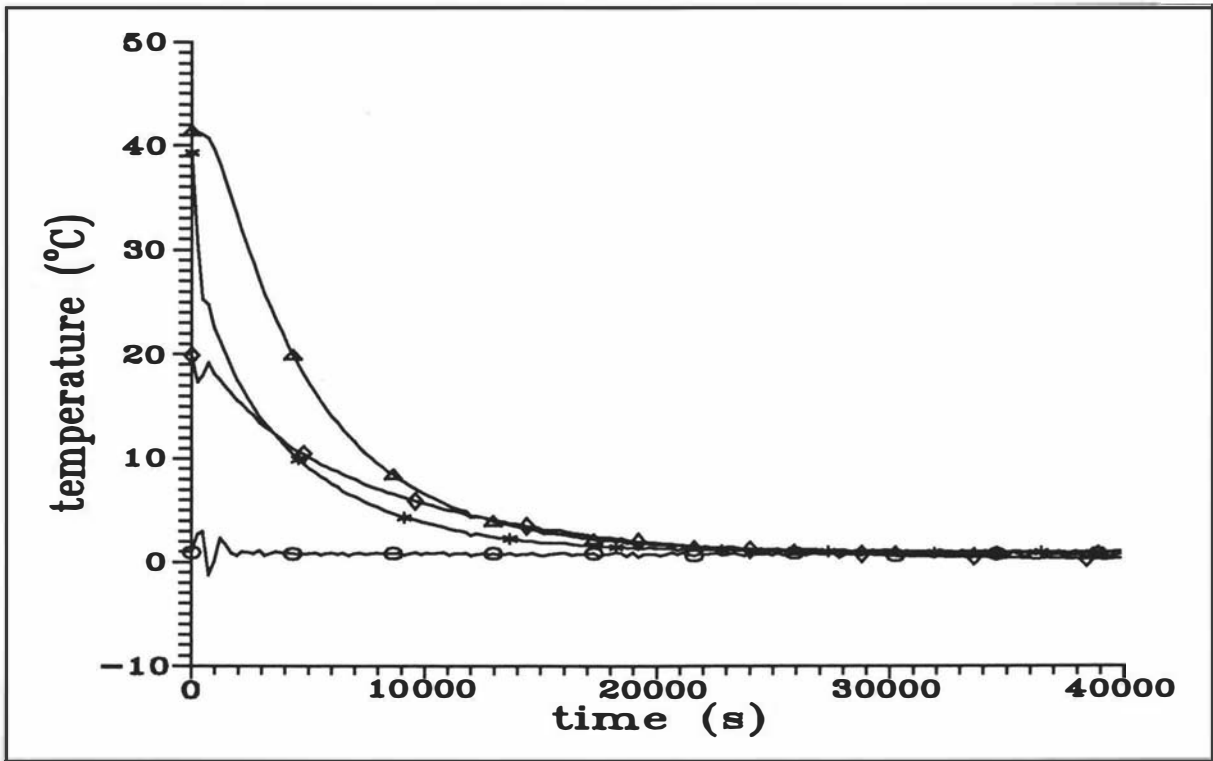


Figure 7.13 Typical plot of temperature vs time for cooling with evaporation ($T_{eq,exp} = T_a$ and $a_w = H_r$). Key as in Figure 7.11.

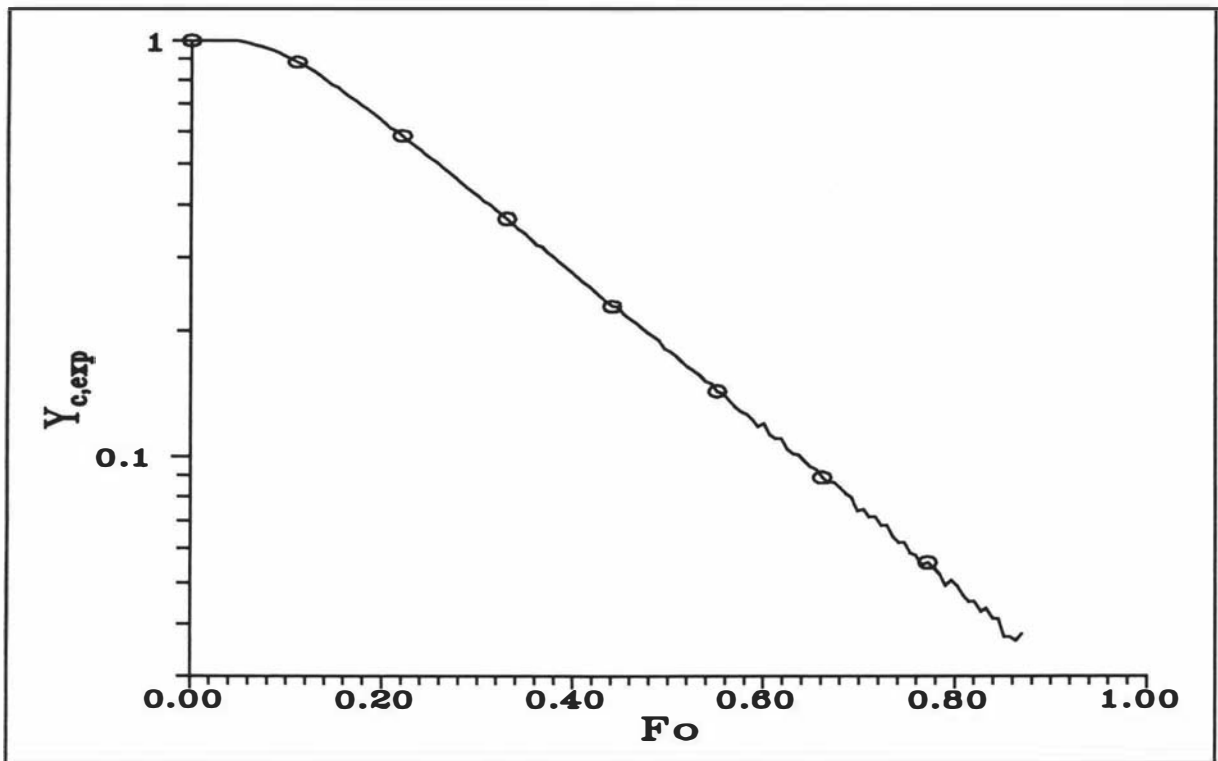


Figure 7.14 Plot of $\ln Y_{c,exp}$ vs Fo using $T_{eq,exp}$ as the reference temperature for the conditions in Fig. 7.11.

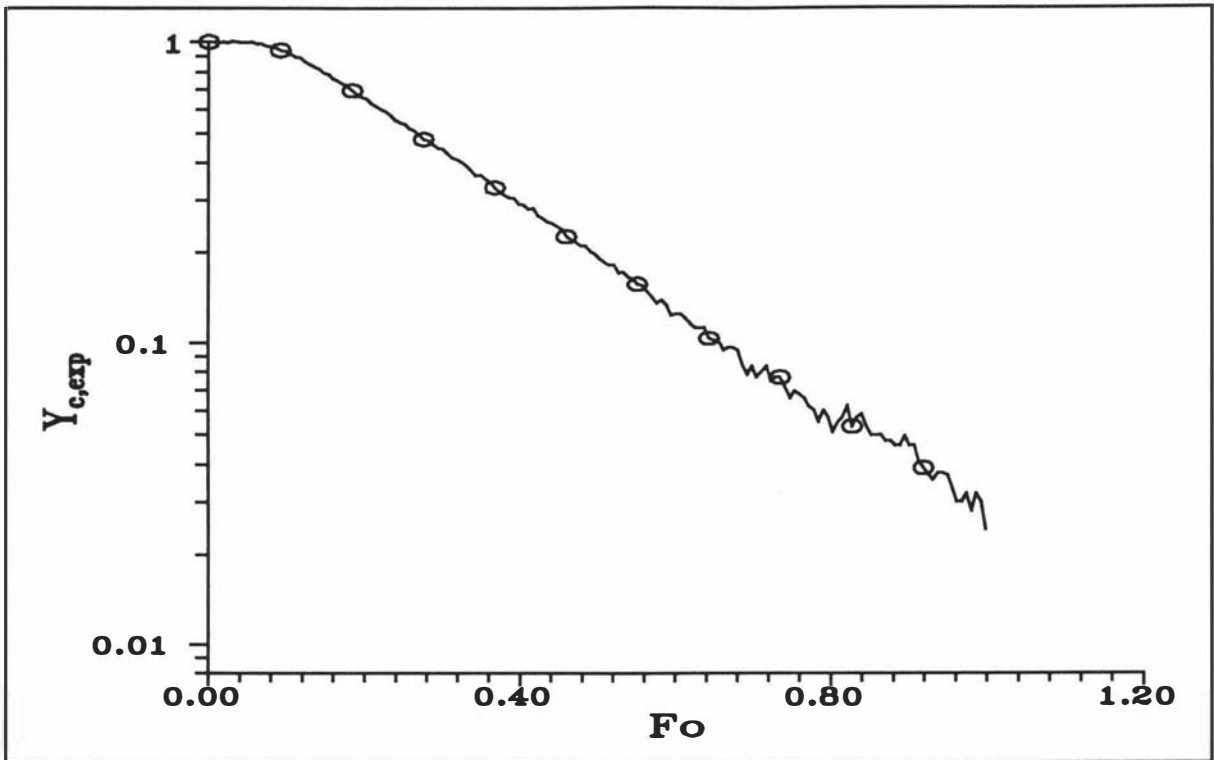


Figure 7.15 Plot of $\ln Y_{c,exp}$ vs Fo using $T_{eq,exp}$ as the reference temperature for the conditions in Fig. 7.12.

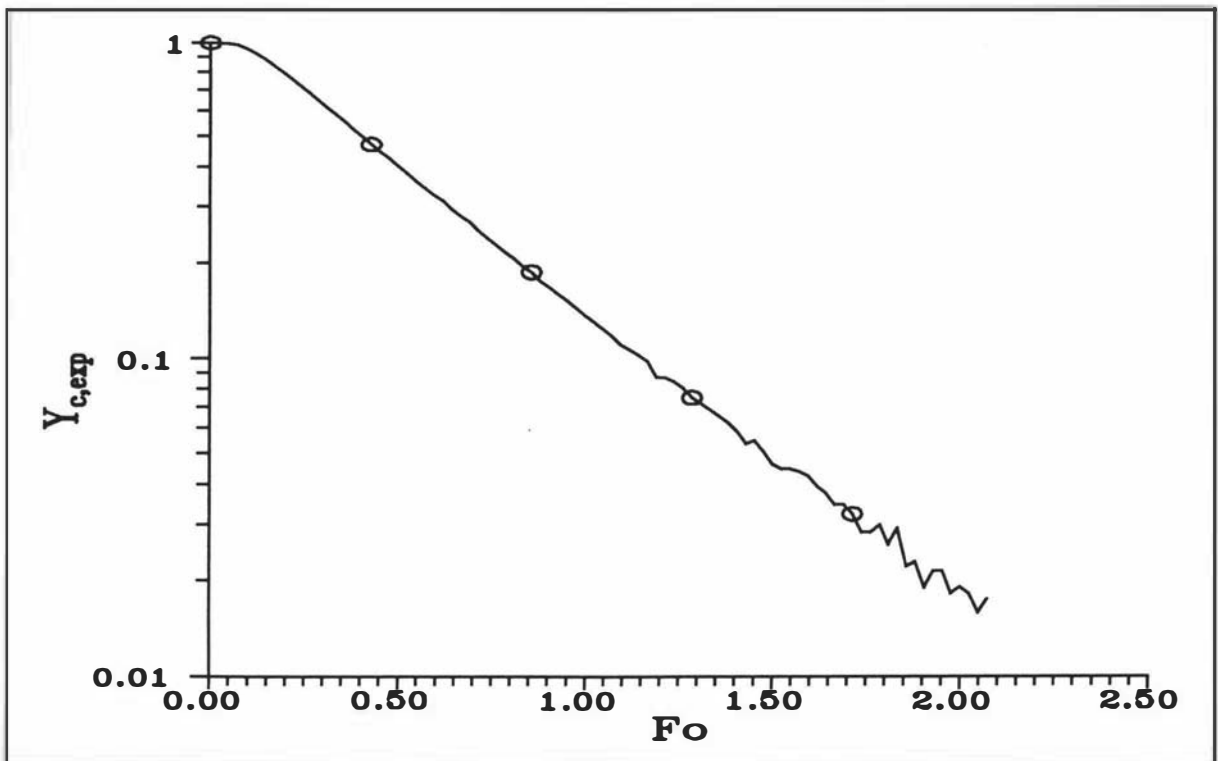


Figure 7.16 Plot of $\ln Y_{c,exp}$ vs Fo using $T_{eq,exp}$ as the reference temperature for the conditions in Fig. 7.13.

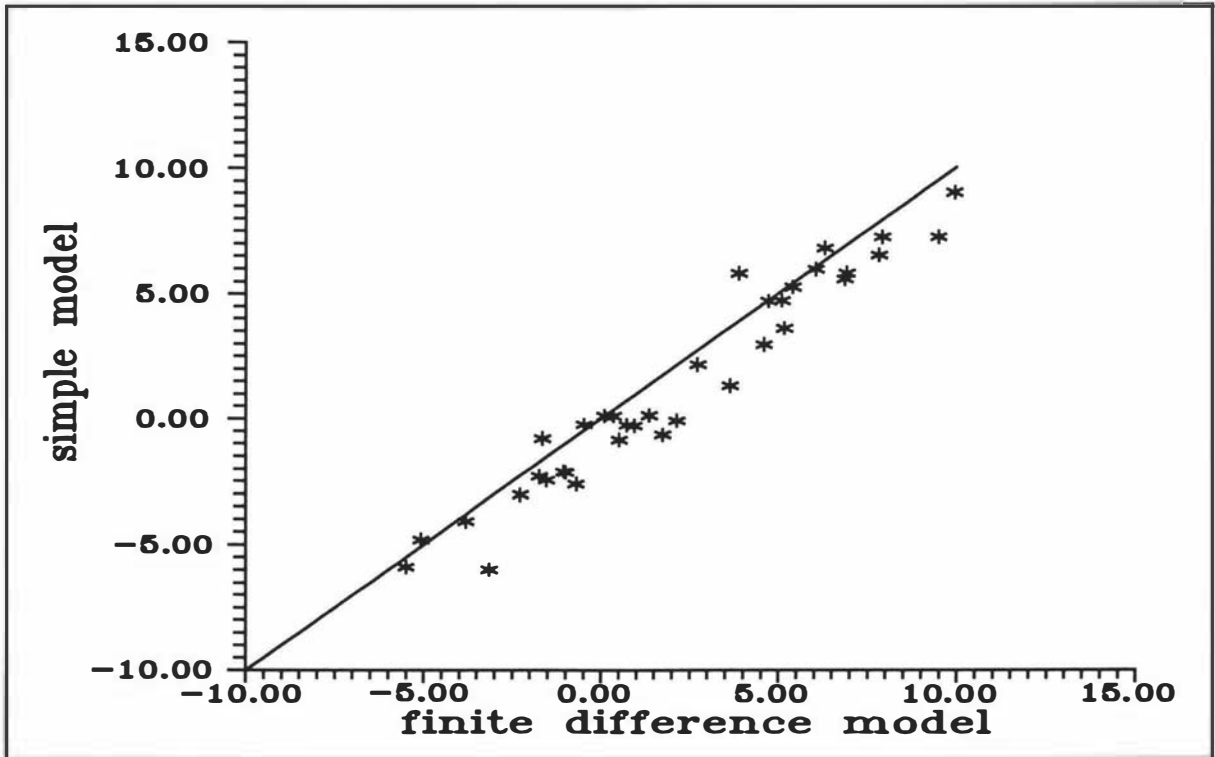


Figure 7.17 Comparisons of the % differences in f_{cEvap}/f_{cConv} between the simple model and the finite difference model.

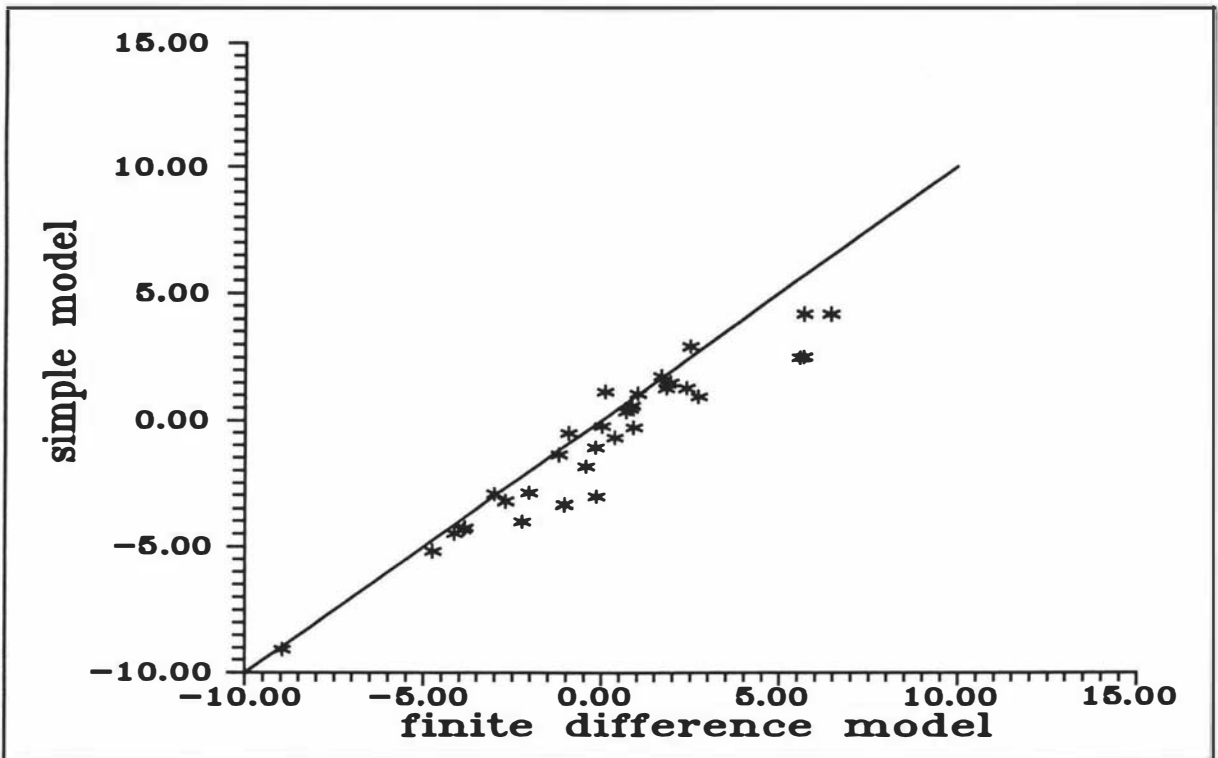


Figure 7.18 Comparisons of the % differences in j_{cEvap}/j_{cConv} between the simple model and the finite difference model.

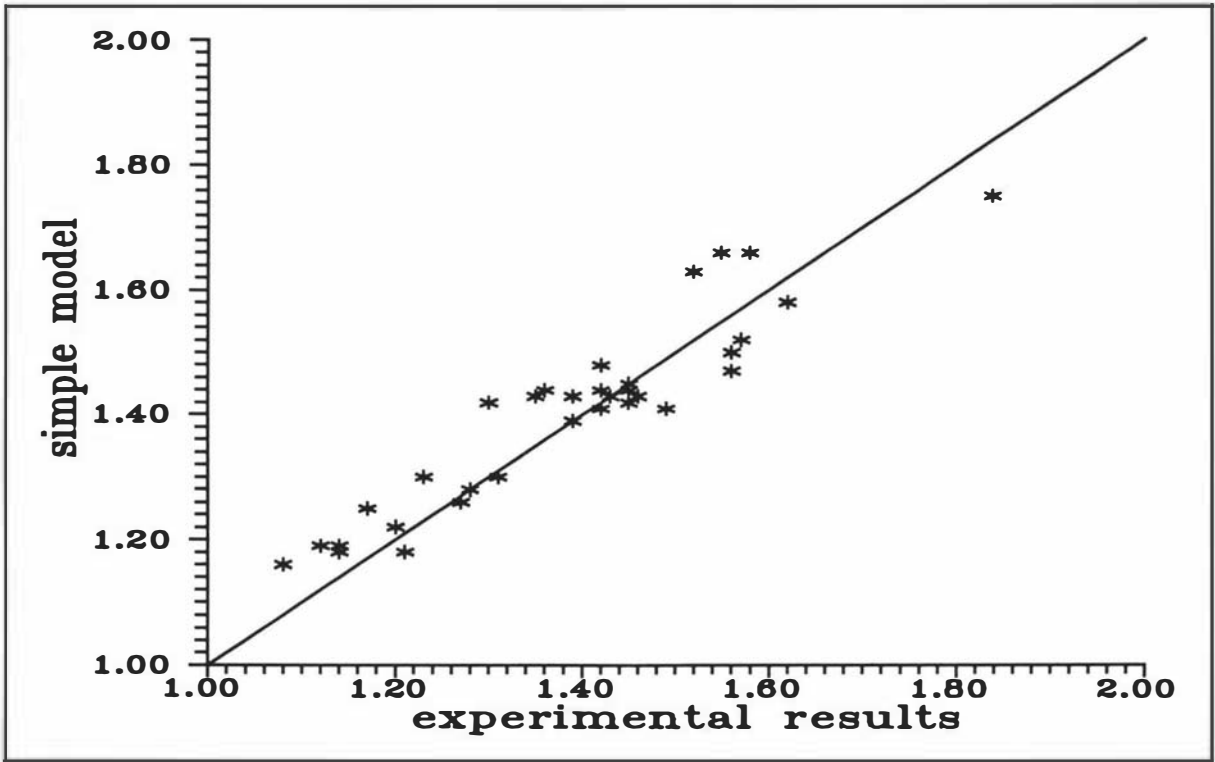


Figure 7.19 Comparisons of the values of f_{cEvap}/f_{cConv} between the simple model and the experimental results.

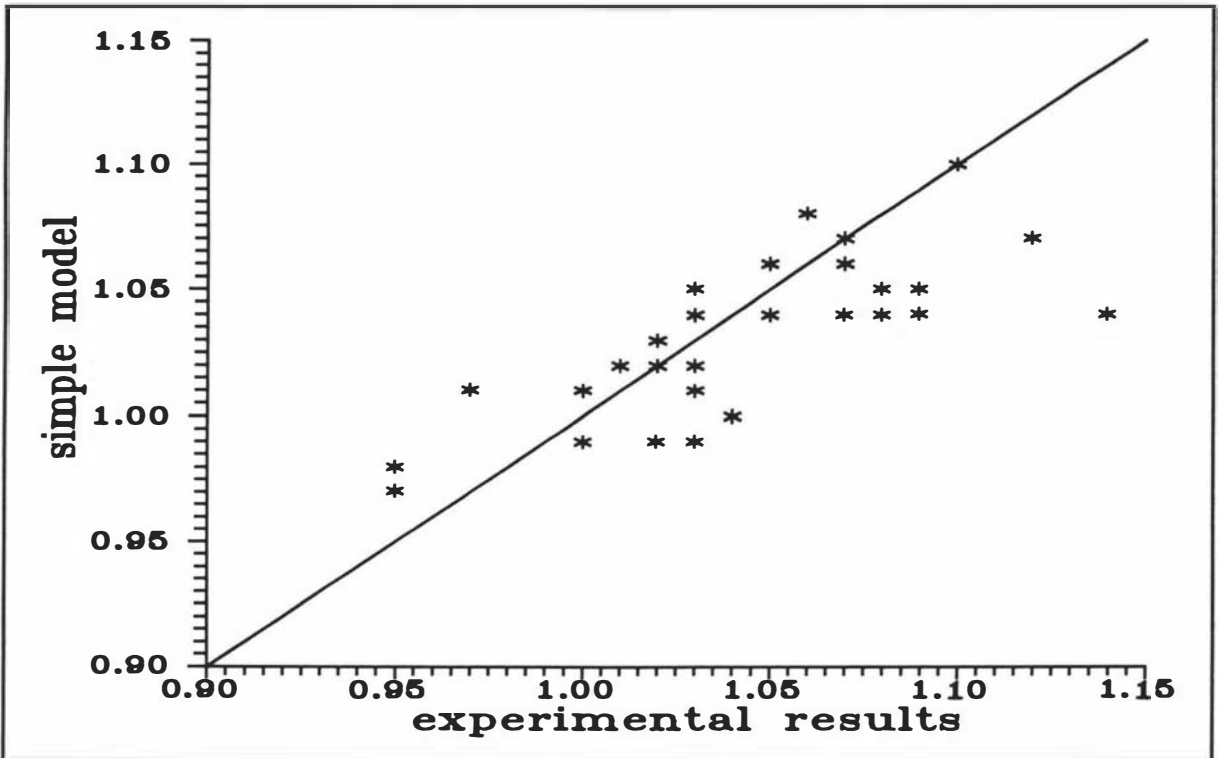


Figure 7.20 Comparisons of the values of j_{cEvap}/j_{cConv} between the simple model and the experimental results.

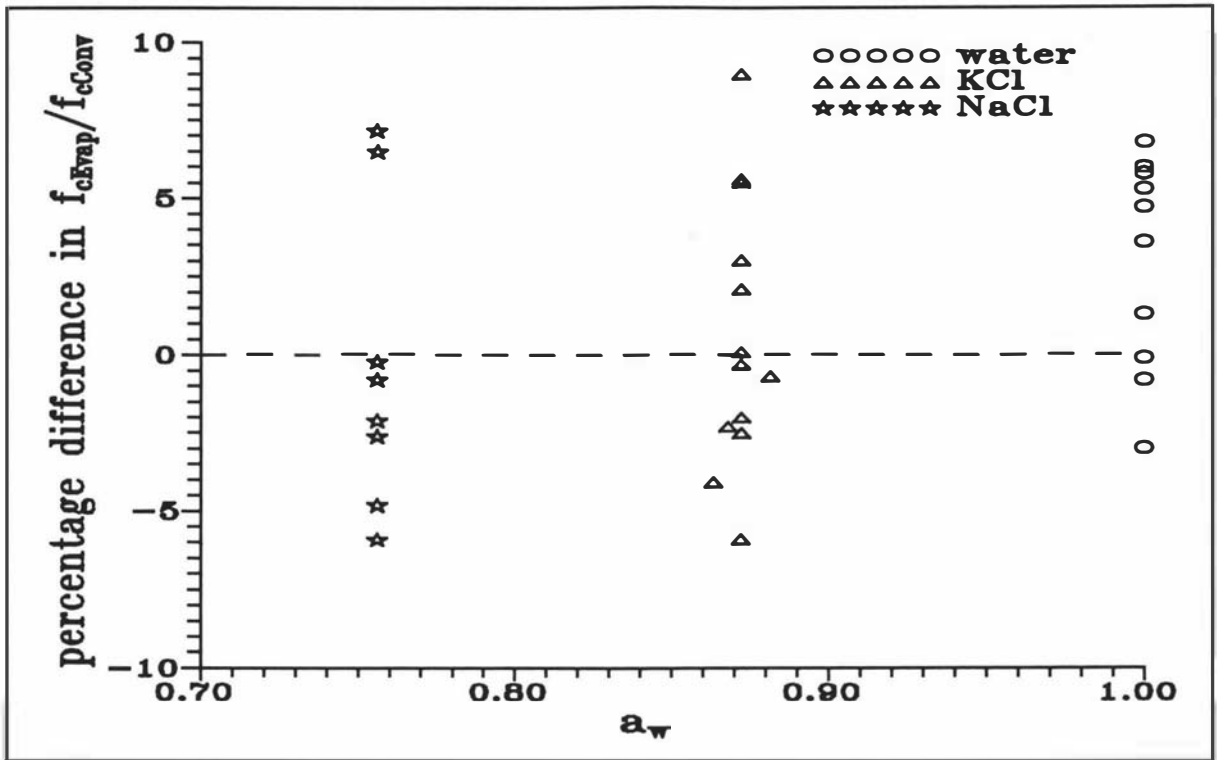


Figure 7.21 Plots of % difference in f_{cEvap}/f_{cConv} values calculated by the simple model compared to experimental values at different a_w .

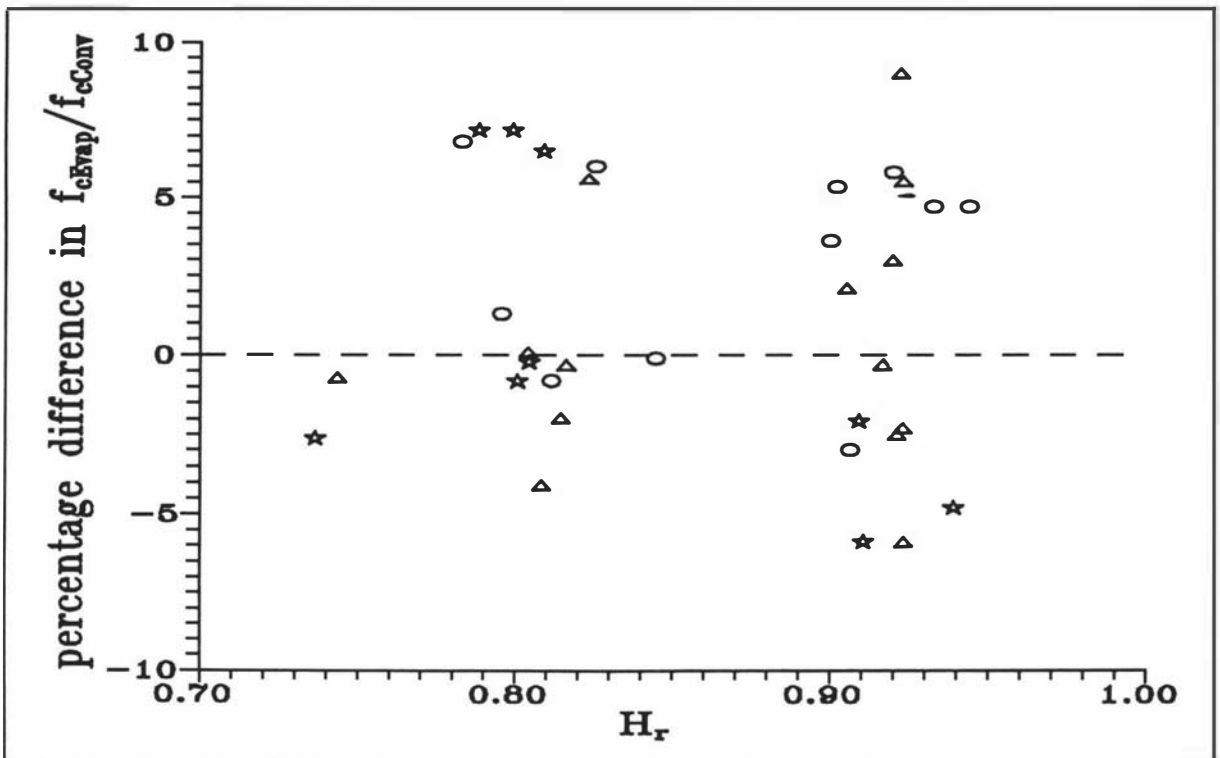


Figure 7.22 Plots of % difference in f_{cEvap}/f_{cConv} values calculated by the simple model compared to experimental values at different H_r . Key as in Figure 7.21.

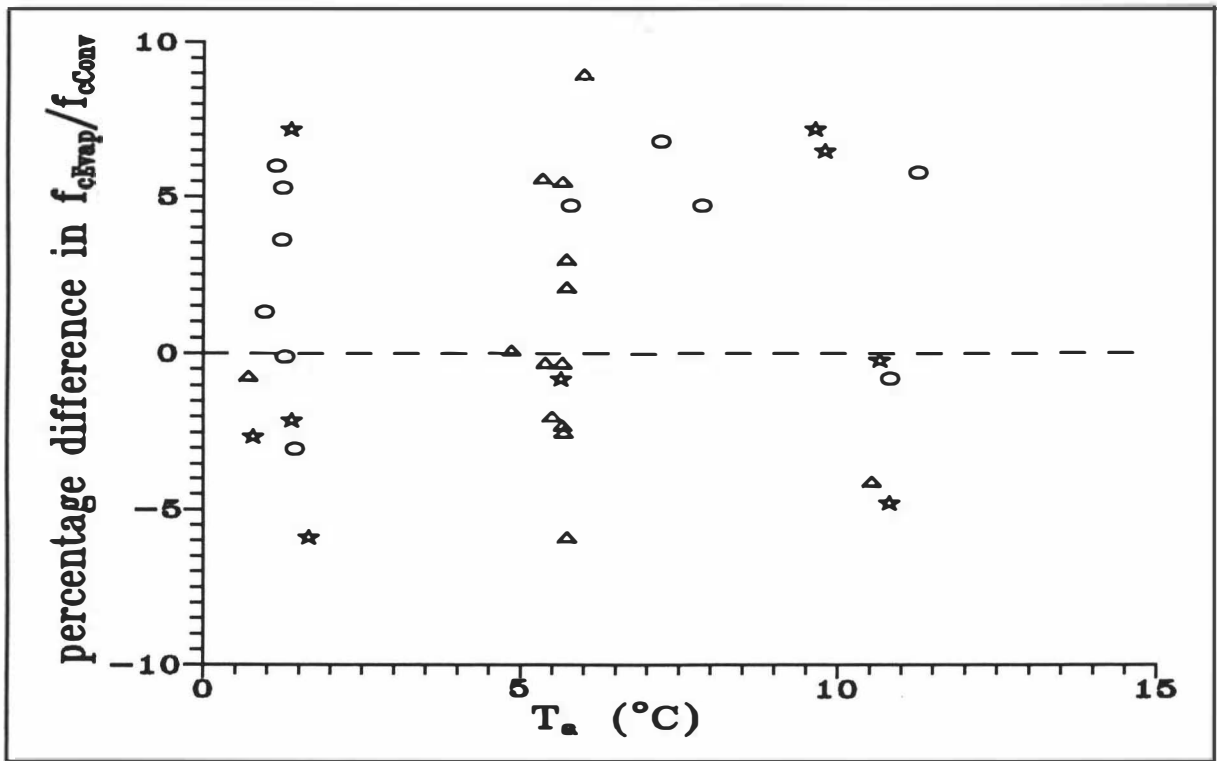


Figure 7.23 Plots of % difference in f_{cEvap}/f_{cConv} values calculated by the simple model compared to experimental values at different T_a . Key as in Figure 7.21.

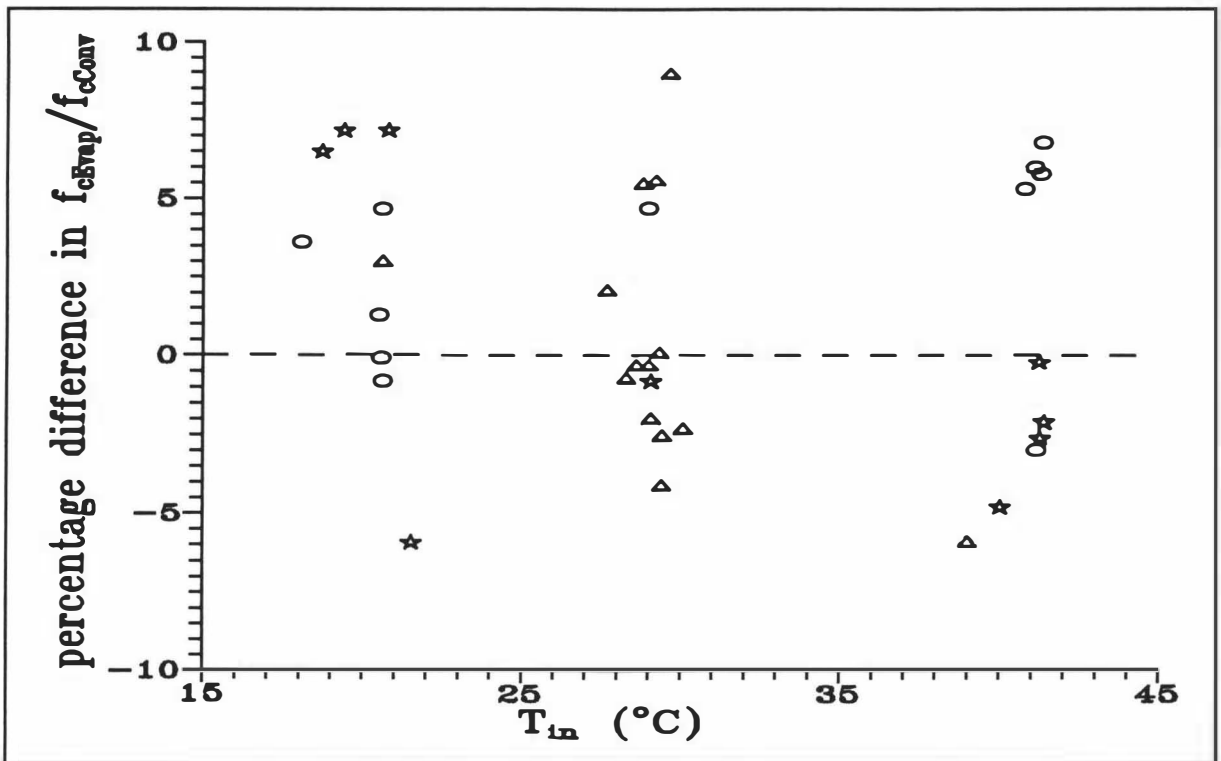


Figure 7.24 Plots of % difference in f_{cEvap}/f_{cConv} values calculated by the simple model compared to experimental values at different T_{in} . Key as in Figure 7.21.

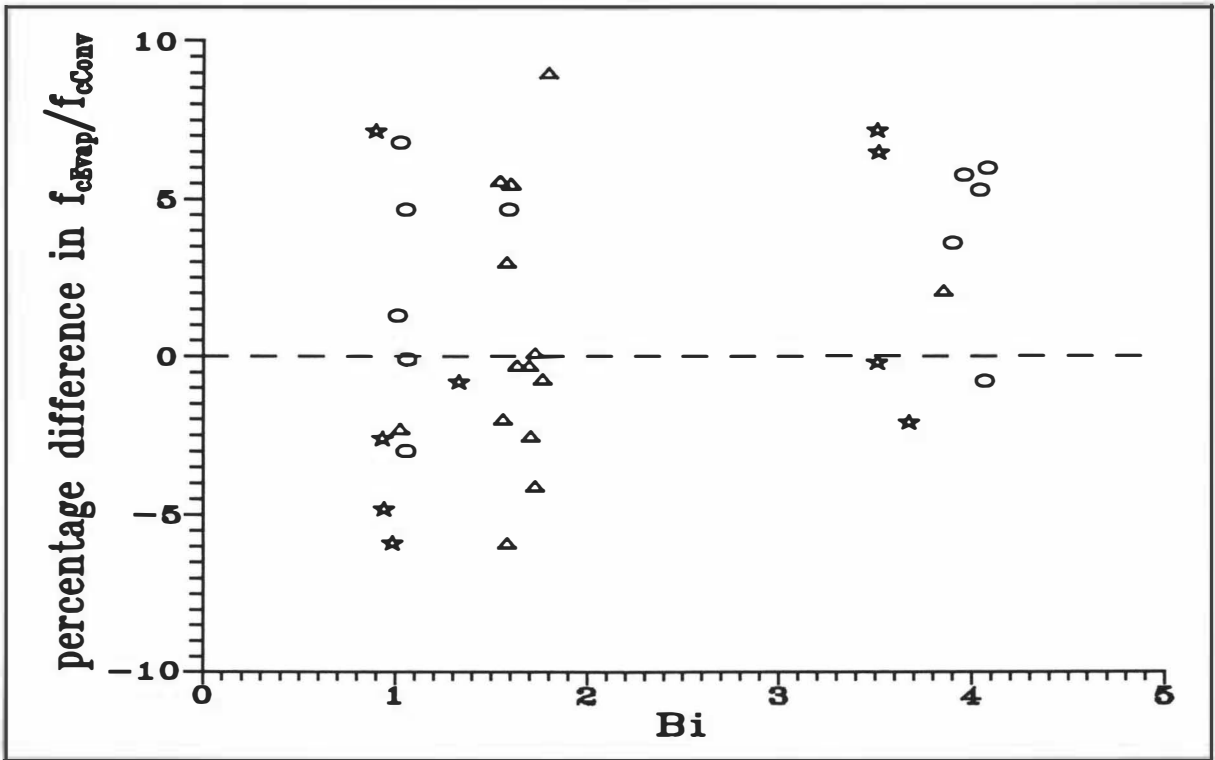


Figure 7.25 Plots of % difference in f_{cEvap}/f_{cConv} values calculated by the simple model compared to experimental values at different Bi . Key as in Figure 7.21.

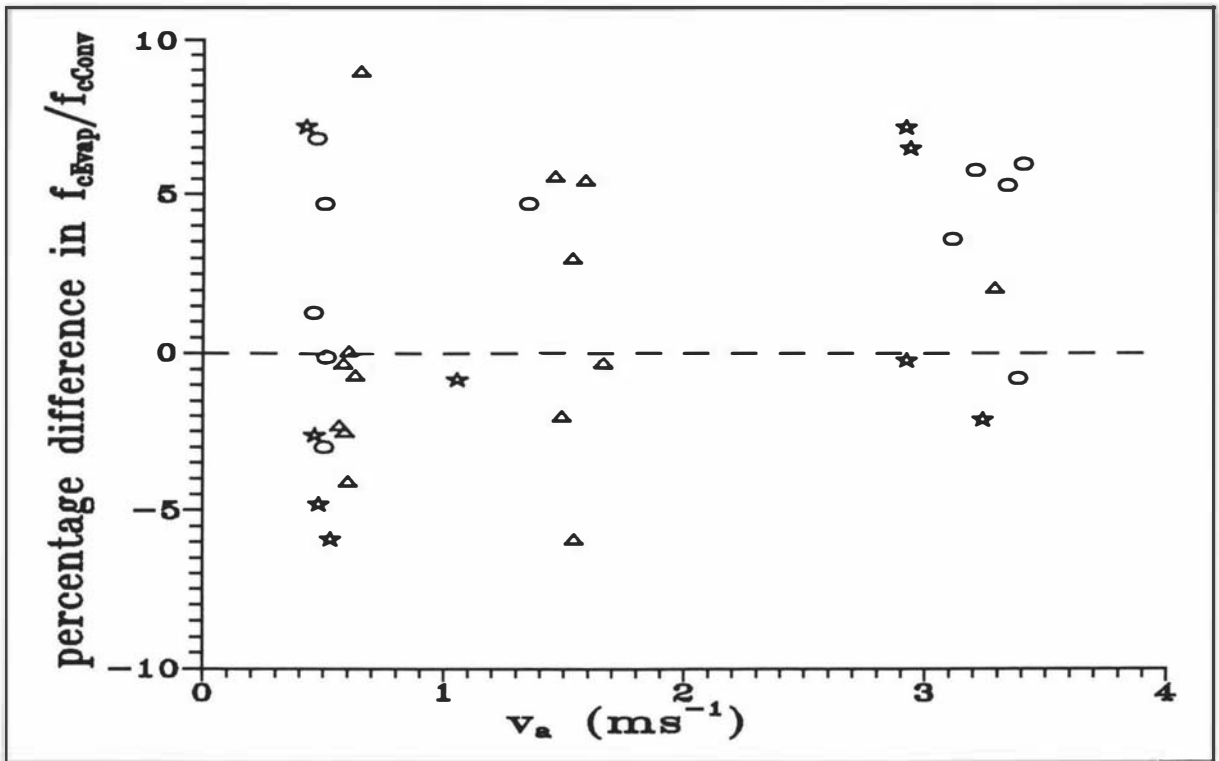


Figure 7.26 Plots of % difference in f_{cEvap}/f_{cConv} values calculated by the simple model compared to experimental values at different v_a . Key as in Figure 7.21.

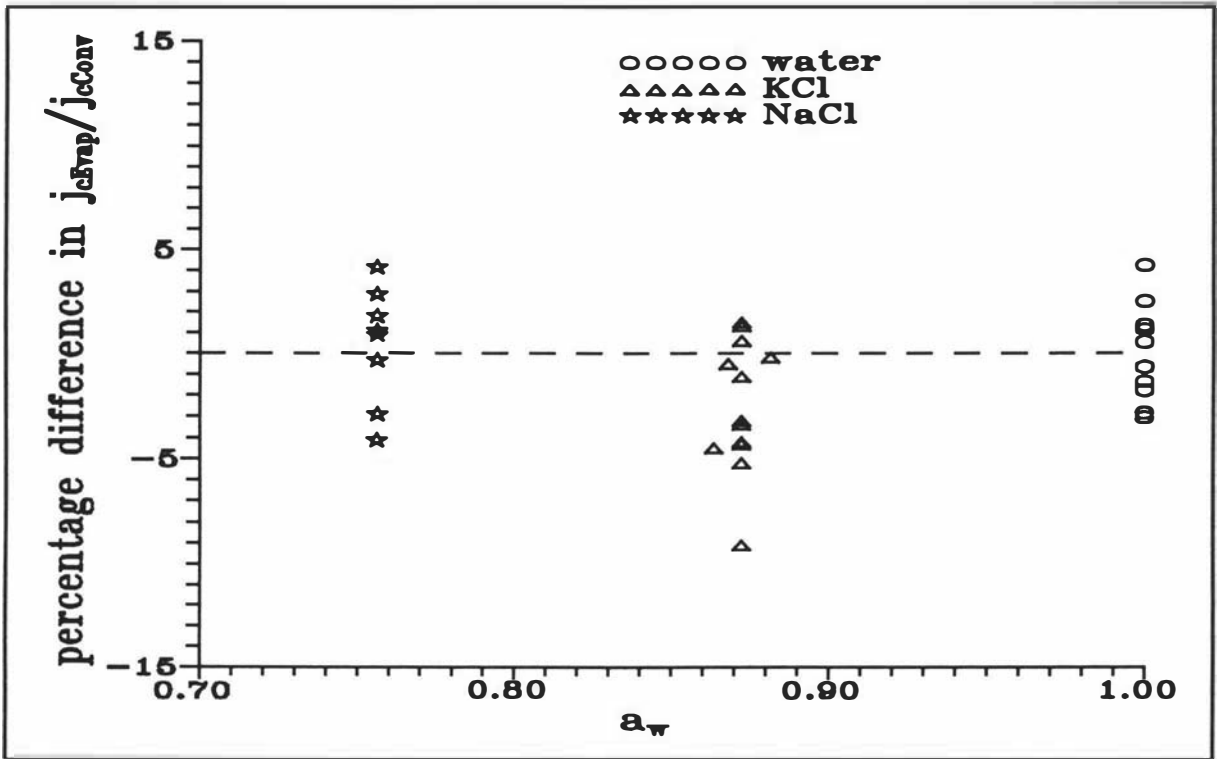


Figure 7.27 Plots of % difference in j_{cEvap}/j_{cConv} values calculated by the simple model compared to experimental values at different a_w .

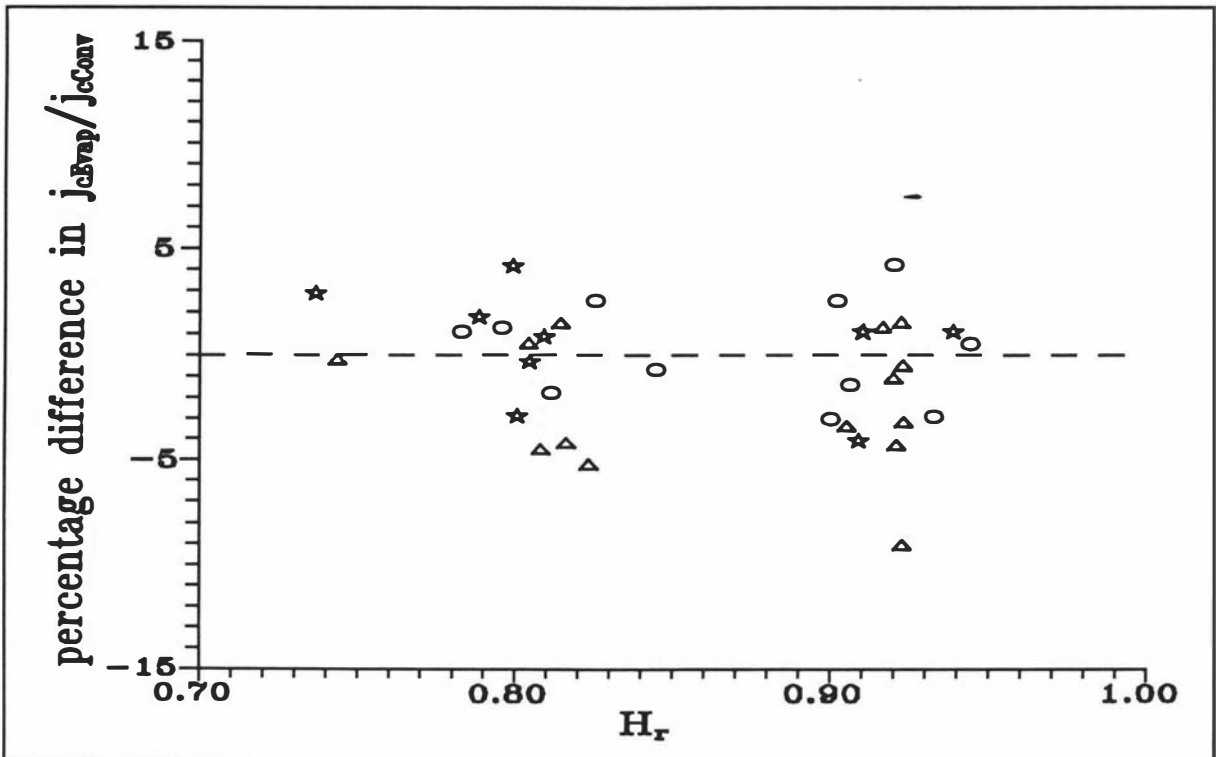


Figure 7.28 Plots of % difference in j_{cEvap}/j_{cConv} values calculated by the simple model compared to experimental values at different H_r . Key as in Figure 7.27.

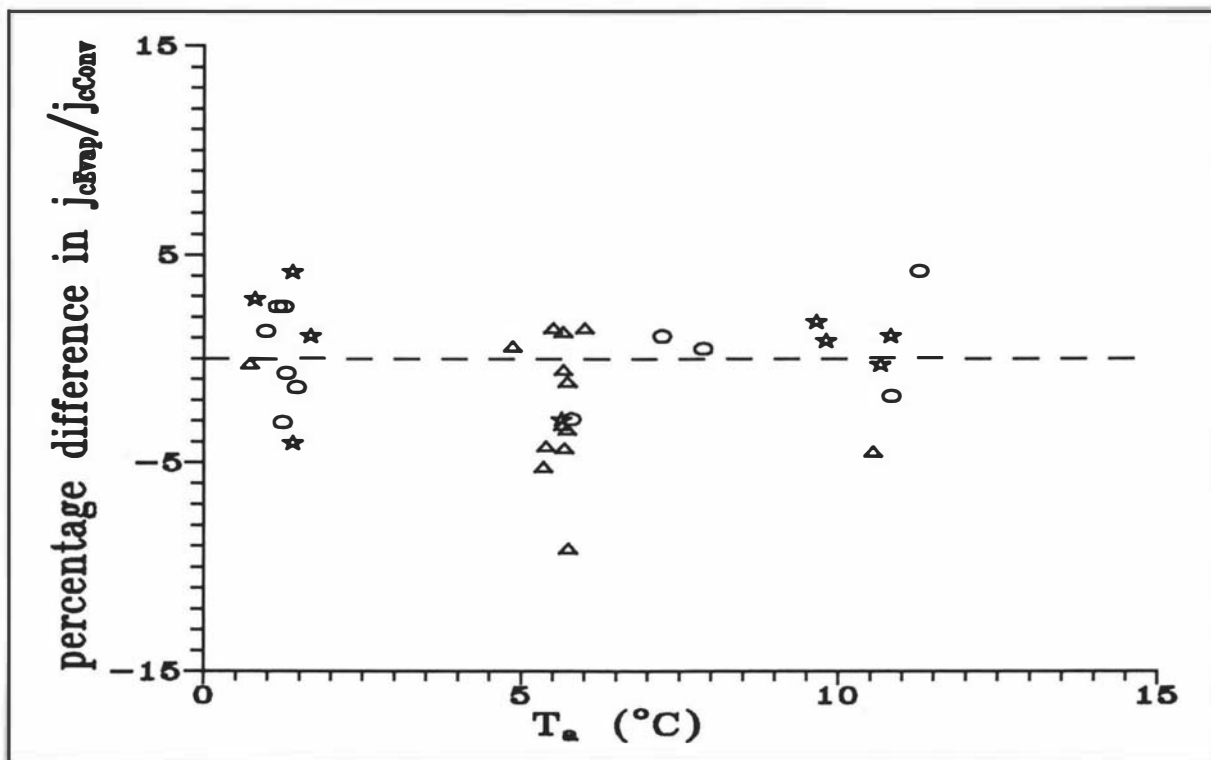


Figure 7.29 Plots of % difference in j_{cEvap}/j_{cConv} values calculated by the simple model compared to experimental values at different T_a . Key as in Figure 7.27.

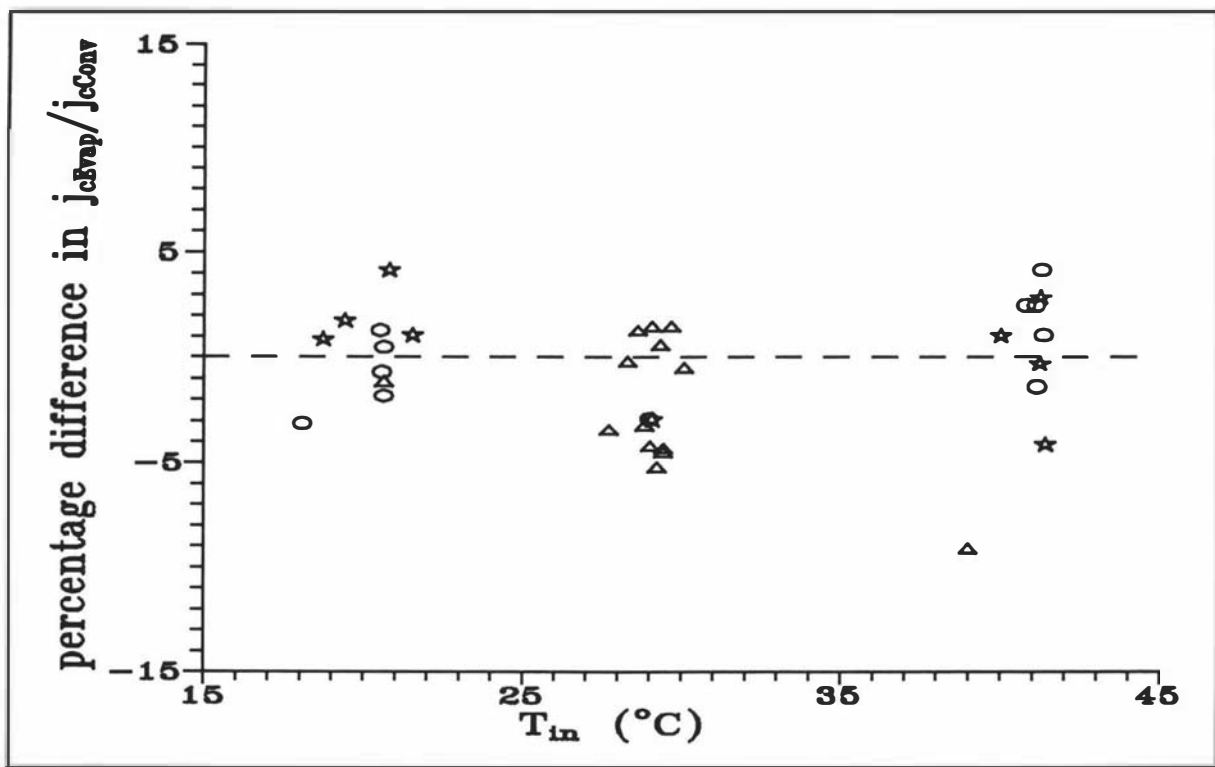


Figure 7.30 Plots of % difference in j_{cEvap}/j_{cConv} values calculated by the simple model compared to experimental values at different T_{in} . Key as in Figure 7.27.

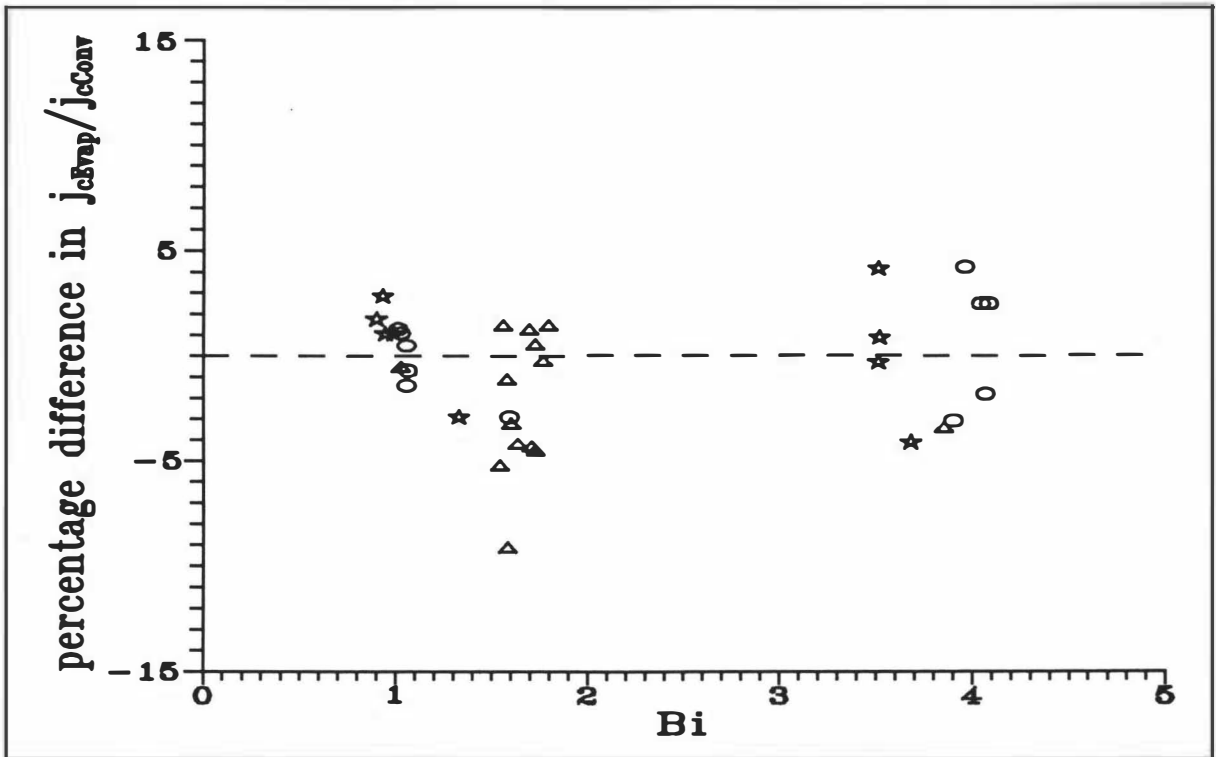


Figure 7.31 Plots of % difference in j_{cEvap}/j_{cConv} values calculated by the simple model compared to experimental values at different Bi . Key as in Figure 7.27.

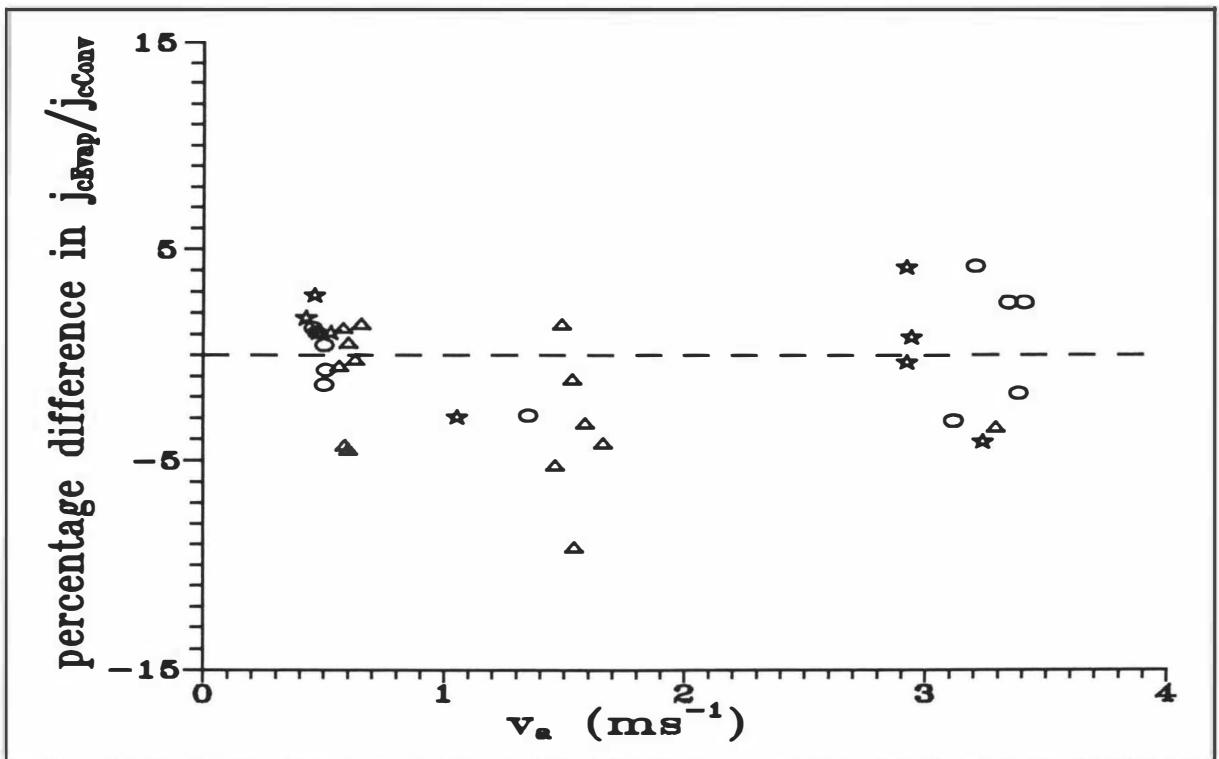


Figure 7.32 Plots of % difference in j_{cEvap}/j_{cConv} values calculated by the simple model compared to experimental values at different v_a . Key as in Figure 7.27.

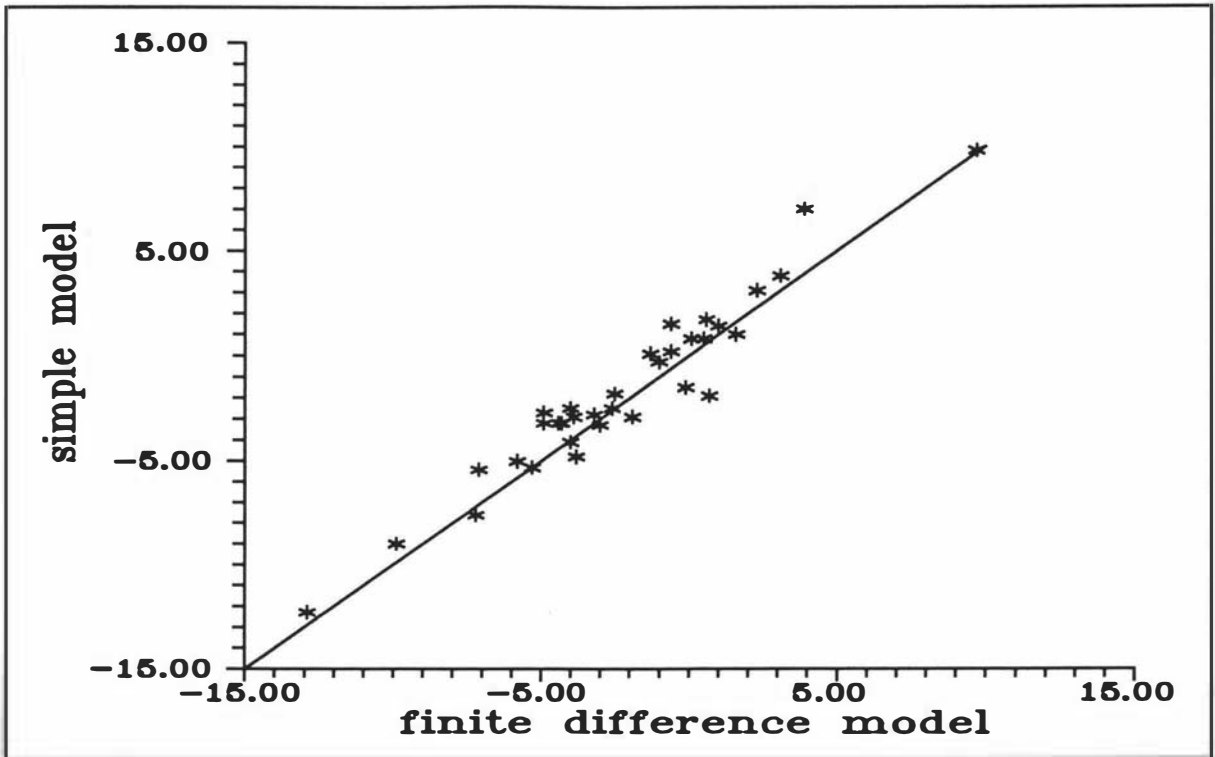


Figure 7.33 Comparisons of % differences in time to reach the temperature corresponding to $Y_{c,exp} = 0.10$ between the simple model and the finite difference model.

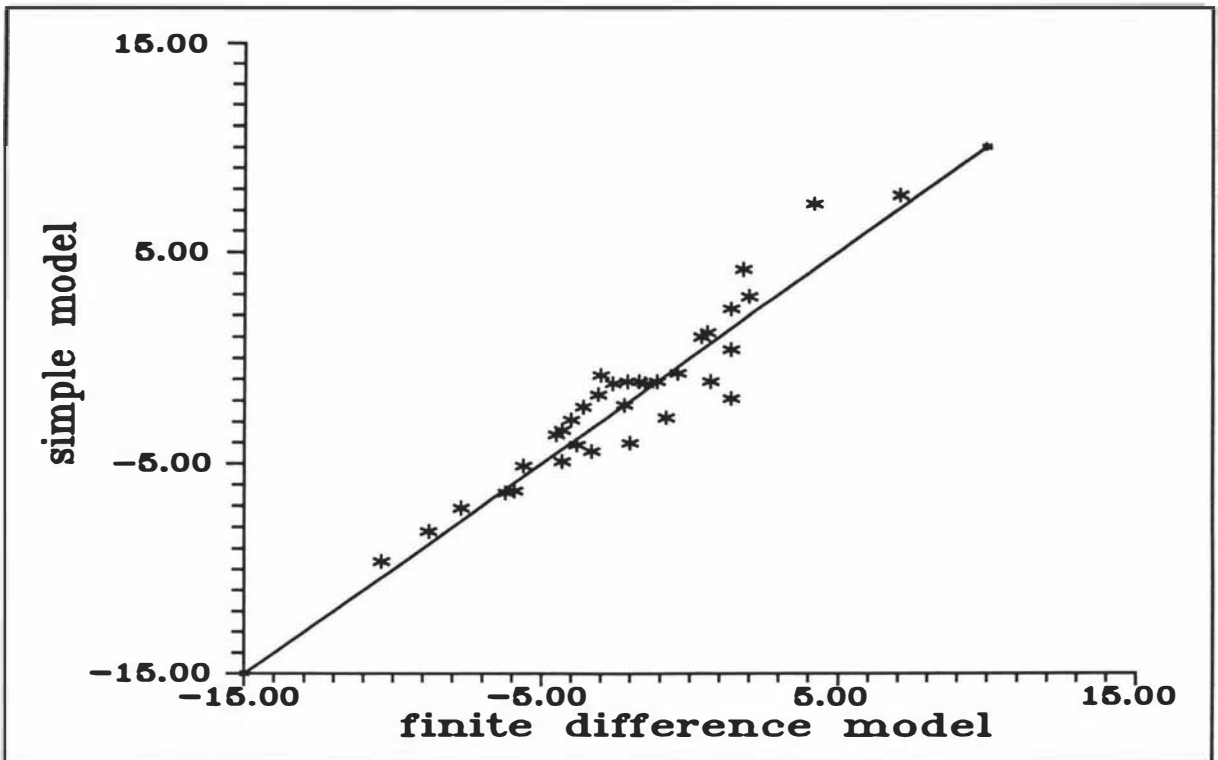


Figure 7.34 Comparisons of % differences in time to reach the temperature corresponding to $Y_{c,exp} = 0.35$ between the simple model and the finite difference model.

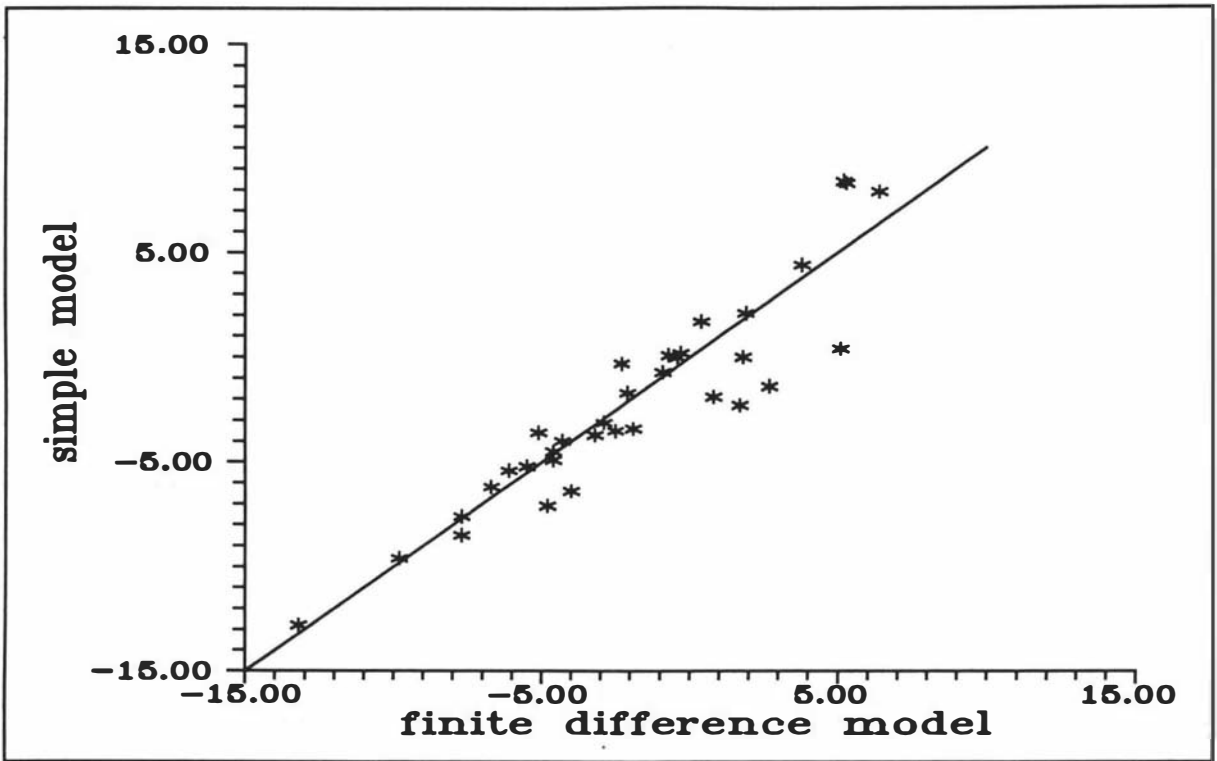


Figure 7.35 Comparisons of % differences in time to reach the temperature corresponding to $Y_{c,exp} = 0.70$ between the simple model and the finite difference model.

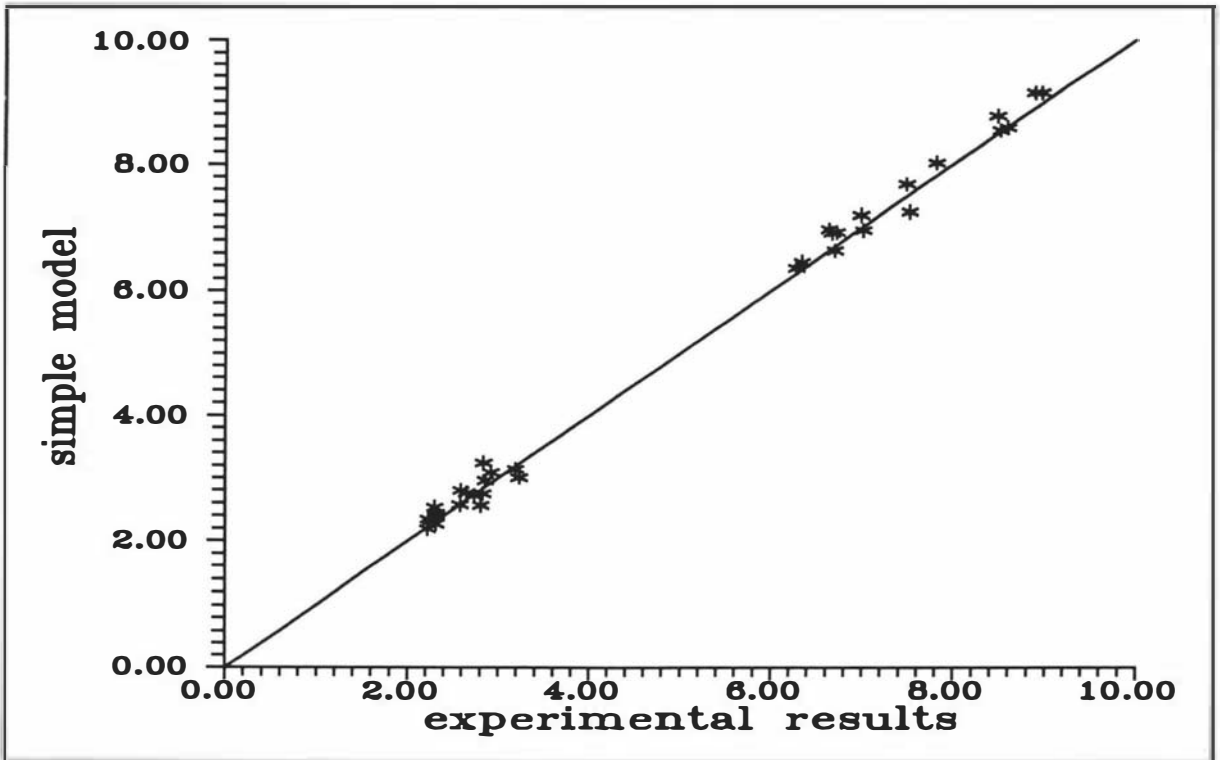


Figure 7.36 Comparisons of time (hrs.) to reach the temperature corresponding to $Y_{c,exp} = 0.10$ between the simple model and the experimental results.

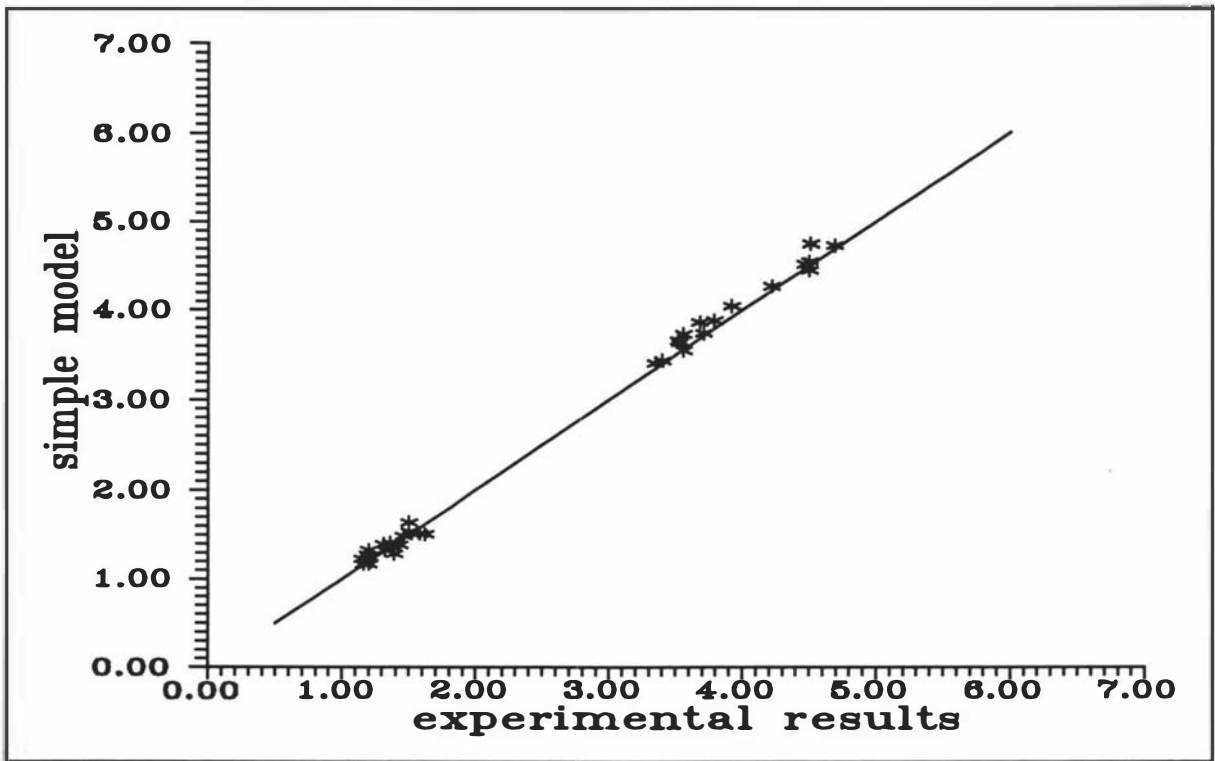


Figure 7.37 Comparisons of time (hrs.) to reach the temperature corresponding to $Y_{c,exp} = 0.35$ between the simple model and the experimental results.

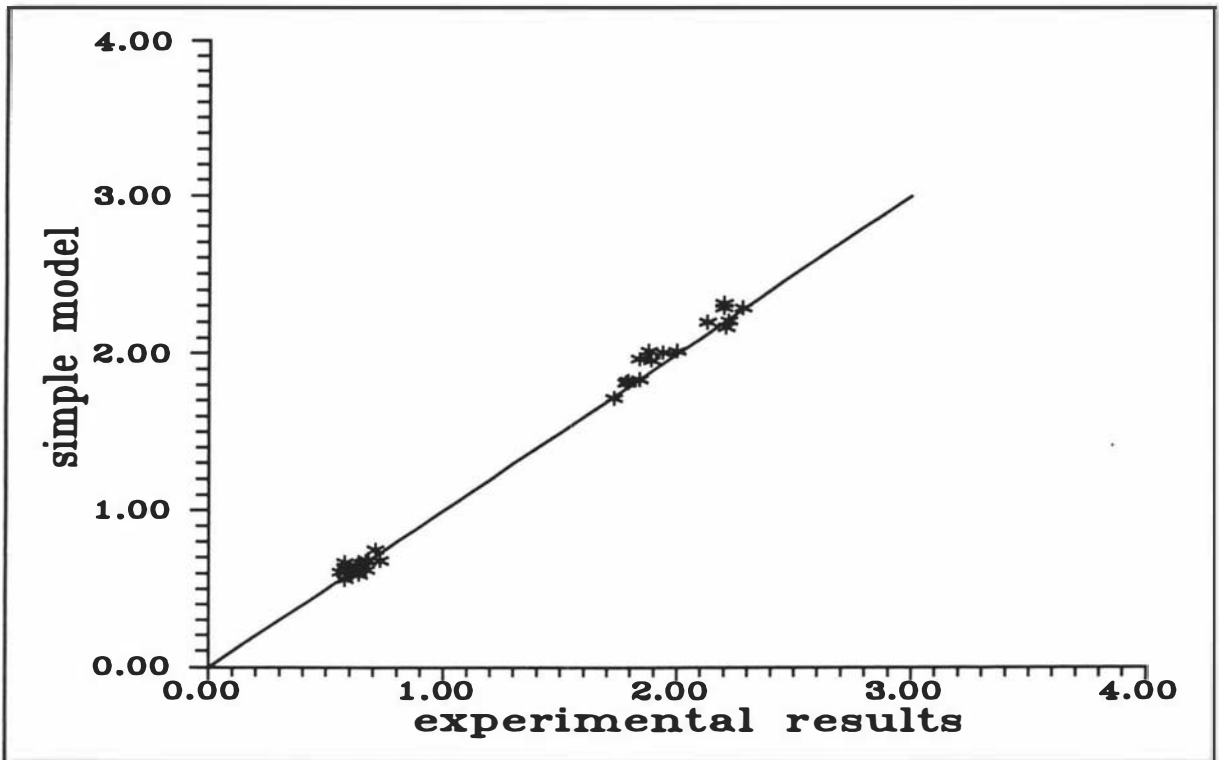


Figure 7.38 Comparisons of time (hrs.) to reach the temperature corresponding to $Y_{c,exp} = 0.70$ between the simple model and the experimental results.

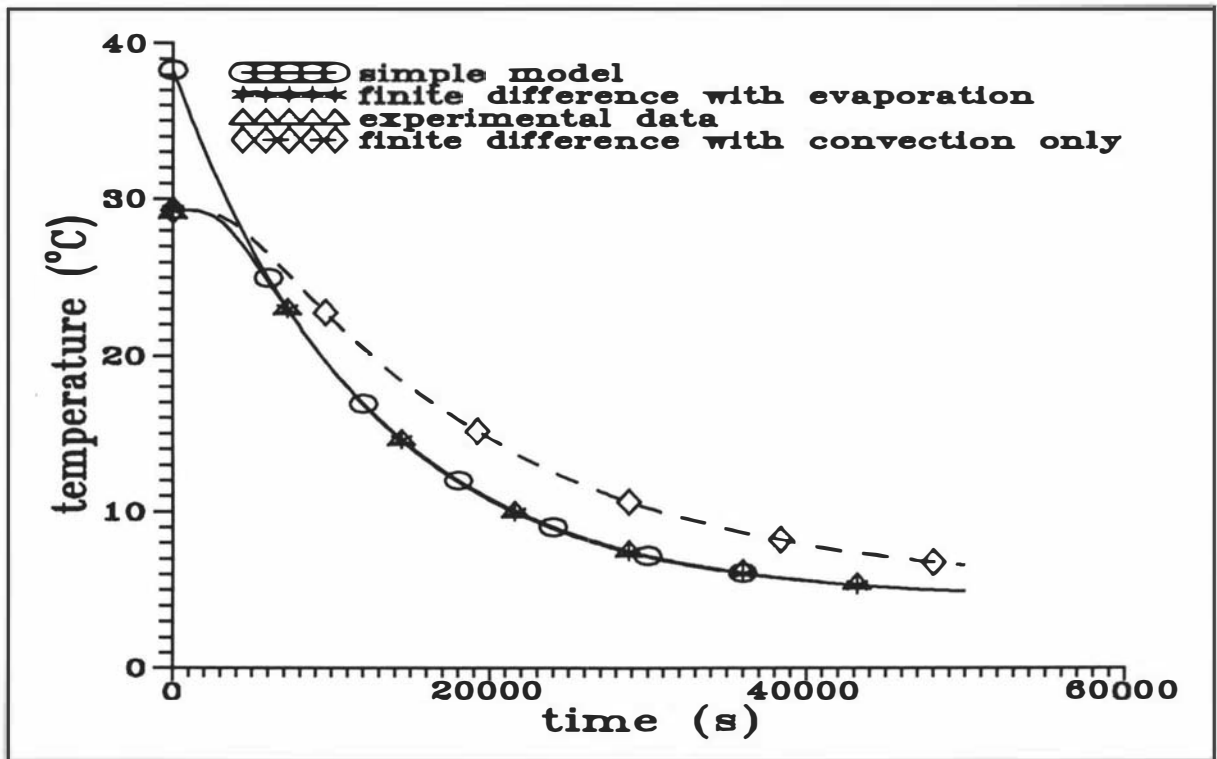


Figure 7.39 The best result of comparisons between the simple model, the finite difference with evaporation and without evaporation, and the experimental data.

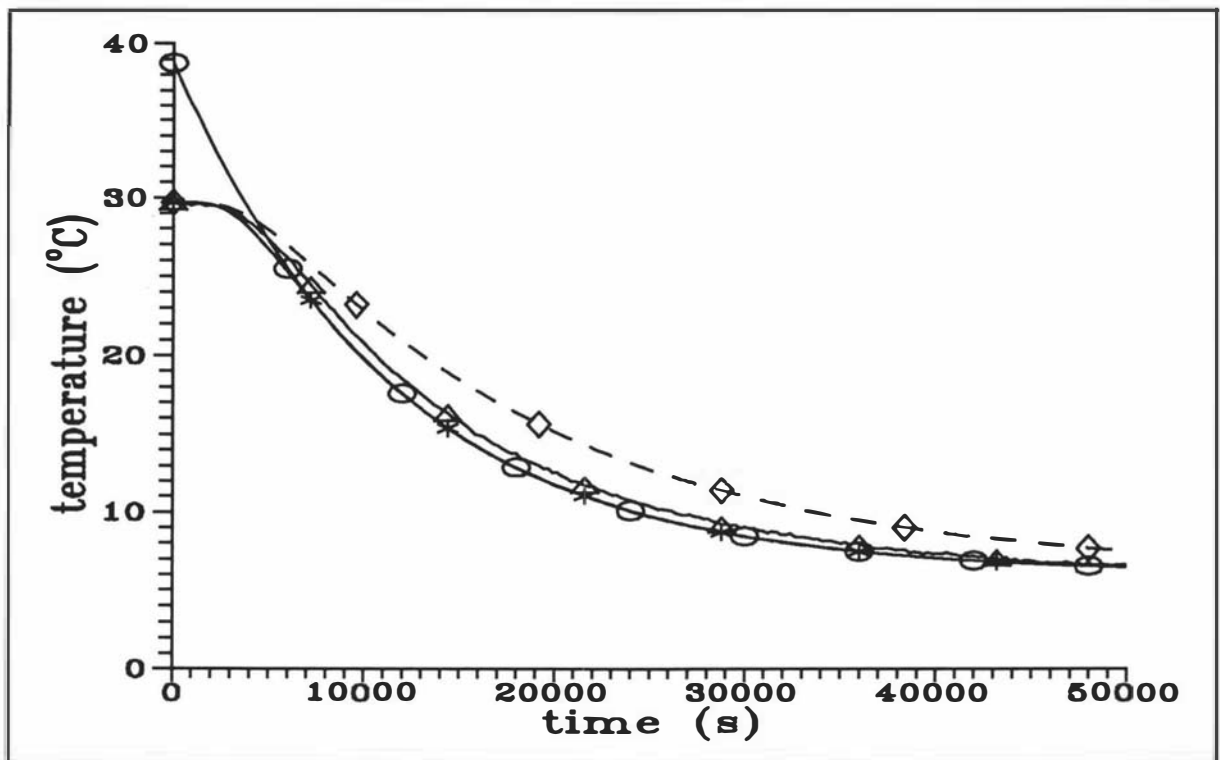


Figure 7.40 The worst result of comparisons between the simple model, the finite difference with evaporation and without evaporation, and the experimental data. Key as in Figure 7.39.

8. EXPERIMENTAL DESIGN AND METHODS FOR EXPERIMENTS WITH A REAL PRODUCT

8.1 INTRODUCTION

The proposed empirical method described in Chapter 5 was developed for situations in which the following assumptions are valid:

- (1) uniform initial product temperature
- (2) constant ambient conditions
- (3) constant product thermal properties and surface water activity
- (4) no skin resistance
- (5) one dimensional heat transfer

When tested in circumstances where these assumptions apply the model was shown to be accurate (Chapters 6 and 7).

In Chapters 8 to 11 extension of the model to less restrictive circumstances is considered. Two major areas of study seemed likely to yield most useful information - extension to multi-dimensional heat transfer, or extension to real food products in which there might be skin resistance and/or variable surface water activity. The decision made was to investigate the latter on the premise that if the model could not be successfully extended to real foods its extension to multi-dimensional shapes would offer little more than purely academic value.

8.2 EVAPORATIVE COOLING OF REAL FOOD PRODUCTS

One of the basic considerations in chilling of food products is the role of water in the product. The surface water activity is a measure of the degree of water vapour saturation or availability at the product surface and can be used to describe the variation of surface dryness throughout the cooling process.

8.2.1. Products without Skin Resistance

Products without a skin might be represented as a free water surface because they tend to lose moisture rapidly (Patel & Sastry 1988). However, as has been outlined, whilst the initial rate of evaporation may be the same as that from a fully wetted surface the surface will dry out if internal water movement is slow, resulting in a lower surface water activity (thus resulting in a difference between the surface water activity and the water activity inside the product), and decreasing rate of evaporation. The rate of evaporation at the surface can decline progressively as both surface temperature and a_w fall until equalisation is reached between evaporation rate and the rate of movement of water to the surface by diffusion or capillary action from the underlying tissues. As cooling proceeds still further, the partial pressure driving force for evaporation diminishes until the internal water transport rate exceeds the evaporation rate. The surface then progressively re-wets and the evaporation rate approaches that for a wetted surface again (Radford *et al.*, 1976). Thus, drying and rewetting phenomena commonly occur during evaporative cooling in the absence of skin resistance and have been reported by several groups of researchers (Hodgson, 1970; Lovett *et al.*, 1976; Daudin, 1986; James *et al.*, 1988b). For drying and rewetting not to occur internal water movement through the product must be rapid at all times.

8.2.2 Product with Skin Resistance

A model often used is to assume that the evaporating surface lies immediately beneath the product skin. The transport of water through the skin can then be considered only in terms of resistance (Fockens & Meffert, 1972). The diffusional resistance of the skin is often the controlling factor, especially at higher air velocities. Since it is assumed that there is no direct surface moisture, the transport of water through the skin might be in the form of vapour (Fockens & Meffert, 1972). Alternatively, it might be assumed that evaporation occurs primarily through small openings in the skin so that evaporative cooling is localized in small regions. Woods (1990) concluded that the rate of moisture loss observed experimentally were not sufficient to cause significant moisture gradients within most internal plant tissues because the major resistance to moisture movement was in the surface layer.

8.3 SELECTION OF TEST MATERIAL

It was decided to restrict further experimental investigation to the cylinder shape, thus matching the study for idealised products. It was desirable to use a product for which skin resistance could be included or excluded by choice, but which was also homogeneous and readily available. It was decided to use carrots - if chosen carefully they are close to cylindrical, they can have an appropriate length to diameter ratio, low respiration rate, and the skin can be easily peeled. Disadvantages were that they are not perfectly homogeneous or cylindrical, and they are relatively small so that accurate thermocouple placement is difficult.

It was decided to conduct two sets of experiments, one with skins peeled and other with skins present, each covering a wide range of chilling conditions. The results of these experiments would be used to assess possible methodologies or heuristics (rules of thumb) that might allow the extension of the model of Chapter 5 to less idealised conditions.

8.4 EXPERIMENTAL METHODS - PEELED CARROT

Only differences to equipment and methods reported in Chapter 6 are stated here.

8.4.1 Sample Preparation

The carrots available locally were 2 to 4 cm. in diameter with a ratio of length to diameter of 4 - 5 (i.e. about 13 to 20 cm. in length). To represent the infinite cylindrical shape, each sample was prepared as followed:

- (1) The carrot selected was as close to the infinite cylindrical shape as was practically possible. Since it was not perfectly homogeneous or cylindrical, it was peeled and then rounded (using a razor) until the size and shape were uniform. The diameter and length were measured using vernier calipers. The weight and volume (using a water displacement technique) were recorded.
- (3) Two copper-constanan thermocouples (28-30SWG) were inserted from each end to the desired depth (about 4 - 8 cm. from the end) in the central axis of the carrot as

indicated in Figure 8.1. Another thermocouple was inserted along the radius to the central axis at the mid point of the carrot. The diameter of each carrot was measured at the same level as each of these three thermocouples using vernier calipers. Since the carrots were not perfectly uniform, even after peeling, the mean of two diameters measured at right angles to each other was calculated for each measurement point.

- (4) Polystyrene end caps were applied to both ends of the carrot to minimise end effects.

8.4.2 Weight Loss, Water Content, and Surface Water Activity Measurement

The water content of a thin slice of peeled carrot was measured at the end of each cooling experiment by oven drying. The weight of the whole carrot was measured both immediately before chilling (in the incubator, because it was still necessary to maintain uniform initial temperature), and after cooling in the air tunnel, by weighing the total assembly of thermocouple wire, polystyrene end caps etc. However, when a sample was weighed in the incubator, an accurate reading of the true weight was difficult to obtain because of interference of the incubator air circulation with the weight measurement system. Further, because only small weight changes were occurring, and due to the awkward shape of the sample, the uncertainty in percentage weight loss data recorded in this manner was significant. Another difficulty was that because weight loss does not stop when steady state is achieved a single percentage weight loss value is much less valuable than a continuing weight change versus time history. Therefore although data are reported in Chapter 9, their usefulness was limited.

Before chilling (in the incubator) and at the conclusion of the cooling trial, thin slices of peeled carrot were taken and a_w measured using a Water Activity System model CX-2. The CX-2 uses the cooled mirror (dewpoint) technique for measuring water activity. Because this is a primary measurement of relative humidity based on dew point, no calibration needs to be performed. The temperature of the sample should be within 2-3 degrees of the CX-2 temperature so cold samples were rewarmed before measurements were taken. After adjusting for temperature, the error in the CX-2 reading should be within $\pm 0.3\%$ of a_w .

8.4.3 Temperature and Relative Humidity Measurement

Temperature and air velocity measurement were described in Section 6.4. The methods used for relative humidity measurement were different from those in Chapter 6.

A Squirrel Series 1206 data logger was used. The humidity probes were Capacitive Humidity Probes in which the sensor is a small plastic capacitor inside a ptfе membrane filter, with a protective guard. Circuits inside the probe handle provide a voltage output proportional to relative humidity. After calibration against saturated salt solution measurement accuracy was $\pm 2\%$ below 80 % relative humidity and $\pm 3\%$ above 80 %.

8.4.4 Cooling Trials

- (1) The carrot sample was wrapped with a plastic film which had a very low permeability to water vapour.
- (2) This sample was placed in a thermostatically controlled incubator for 8 - 10 hours to equilibrate to the required initial temperature.
- (3) The refrigeration system and fans in the air tunnel were started and operation stabilised at the desired conditions.
- (4) The relative humidity was stabilised at the desired value.
- (5) The air velocity in the air tunnel was measured after the conditions in the air tunnel are stable.
- (6) Sample was weighed.
- (7) The test sample was transferred from the incubator in an insulated container.
- (8) Thermocouples from the product were connected to the data logger.
- (9) The plastic film was removed immediately before placement of the product in the air tunnel.
- (10) Sample rotation by a sample oscillator (to minimise position variation of heat transfer conditions) was commenced.
- (11) Chilling was continued for 3.5 hours to achieve apparent equilibration.
- (12) The air velocity in the air tunnel was measured prior to sample removal.
- (13) Samples was reweighed.

- (14) Although there were three temperature readings, temperature-time data obtained from the thermocouple which gave the slowest rate of temperature change were used, irrespective of whether this thermocouple was at the position where the largest diameter measurement was made. This selection was made on the basis that the slowest cooling thermocouple was most central in the carrot, and positioning error was more significant than diameter measurement uncertainty.

8.4.5 Heat Transfer Coefficient Measurement

Heat transfer coefficients were determined by cooling every sample in a separate trial which preceded the evaporative cooling trial. All steps described in Section 8.4.4 were applied other than sample weighing and removal of the plastic film.

8.4.6 Experimental Design

Ideally, the conditions used should cover wide ranges likely to occur in practice. However due to the small sample size two difficulties were encountered. Firstly, due to the low thermal mass it was difficult to maintain the sample at a uniform initial temperature if this was well above ambient. A top limit of about 10°C above ambient (30°C) was therefore imposed. Secondly, the total cooling time was short (<3.5 hours) and for very rapid cooling conditions (high air velocity) the time for sample set up became an unacceptably large part of the total experimental time. Therefore the velocity was restricted a maximum of about 3 ms⁻¹. The ranges sought were set at:

air velocity (m s ⁻¹)	=	0.5 - 3.0
relative humidity	=	0.75 - 0.95
air temperature (°C)	=	0 - 10
initial temperature (°C)	=	20 - 30

Using a normal factorial design, for four variables the number of runs was 16 to which two additional runs at the centre point were added (Table 8.1). Thus, in total 18 runs were planned. The time required to move from one set of experimental conditions to another was considerable, and when runs for heat transfer coefficient measurement were included 36 trials

were required. Further, each pair of trials (with and without a plastic film present) required preparation of a new sample. Therefore to avoid excessive time requirements, the experimental plan of Table 8.1 was slightly modified in the interests of expediency. Nevertheless, the runs carried out covered a wide range of conditions as intended.

8.5 EXPERIMENTAL METHODS - UNPEELED CARROT

In this Section only differences to Chapter 6 and Section 8.4 are reported.

8.5.1 Sample Preparation

Each unpeeled carrot was about 2 to 4 cm. in diameter with the ratio of length to diameter of 4 - 5 (or about 13 to 20 cm. in length). In spite of not being perfectly homogeneous or cylindrical it must be used as it was. To avoid the influence of end effects, two copper-constantan thermocouples (28-30SWG) were placed about 2 - 3 cm. away from the mid point through the ends and another thermocouple was inserted along the radius to the center position at the mid point of the carrot (Figure 8.1). The diameter of the carrot was measured at the same level as these three thermocouples using vernier calipers. Since the carrot was not perfectly round, the mean diameter of 2 measurements at right angles to each other was calculated. The largest of the three values thus derived was used in all further analysis. Only the thermocouple which gave the slowest temperature change was used in further calculations, irrespective of whether it was the one located at the thickest diameter position. This was justified on the basis that data from a very central thermocouple in a slightly thinner region would more accurately represent the true centre temperature at the thickest position than a badly placed thermocouple in the thickest region.

8.5.2 Weight Loss, Water Content, and Surface Water Activity Measurement

The diffusional resistance of the skin makes determination of surface water activity and internal surface water activity difficult (Roth & Loncin, 1985). A sufficiently small sample could not be collected in which the skin was not cut, so the surface water activity was not measured. As was the case with peeled carrots, weight loss measurements were affected by

data errors.

8.5.3 Experimental Design

The experimental design of Table 8.1 was applied, but again varied slightly in the interests of expediency.

8.6 THERMOPHYSICAL PROPERTIES OF CARROTS

The mean measured water content of the peeled carrots was 86 % and the range of measured values 84 - 88 %. The mean measured density was 1050 kg m⁻³ and the range of measured values 1010 - 1090 kg m⁻³.

Thermal properties of carrot were not experimentally measured. It was thus necessary to use thermal properties from other resources. A thermal conductivity of 0.5192 W m⁻¹ K⁻¹ is reported by Hayakawa (1978) and the mean specific heat capacity from Heldman & Singh (1981) and Hayes (1987) is 3.8725 kJ kg⁻¹ K⁻¹. The accuracy of these data is unknown, but they are consistent with expectations for a product of about 86 % water content. Further, because these data were used for heat transfer coefficient determination and cooling trial analysis any error in thermal properties would be expected to largely cancel itself.

8.7 HEAT TRANSFER COEFFICIENTS FOR PEELED AND UNPEELED CARROTS

In the trial runs for heat transfer coefficient measurement the resistance to heat transfer could be modelled as follows:

$$\frac{1}{h_c} = \frac{1}{h_a} + \frac{x_1}{k_1} \quad (8.1)$$

where h_c = surface heat transfer coefficient (W m⁻² K⁻¹)
 h_a = air convection heat transfer coefficient (W m⁻² K⁻¹)
 k_1 = thermal conductivity of plastic film (W m⁻¹ K⁻¹)
 x_1 = thickness of plastic film (m)

Because the plastic film was very thin (<0.1 mm.) and fitted tightly it was assumed that it did not change the overall heat transfer coefficient significantly. Variations in heat transfer coefficients could be caused by any pockets of air trapped between the carrot and the plastic film, the difference between the diameter used in calculation and the true diameter as described in Sections 8.4.1 and 8.5.1, and to a lesser extent by deviation of thermocouples from the central axis of the cylinder.

Experimental data for h_c were found by using the same theory and technique as already described in the Chapter 6. Based on these experimental data, a dimensional analysis approach was used to form an empirical equation for h_c or Nu by using the standard form of correlation (equation 8.2). This approach rather than the simpler h_c versus v_a approach was justified by the diameter varying between carrots. Similar diameter deviation between samples did not occur for the model samples used in earlier work on model systems.

$$Nu = aRe^bPr^e \quad (8.2)$$

- where Nu = Nusselt Number ($h_c D / k_a$)
 Re = Reynolds Number ($D v_a / \nu_a$)
 Pr = Prandtl Number ($C_a \mu_a / k_a$)
 D = carrot diameter (m)
 k_a = air thermal conductivity ($W\ m^{-1}\ K^{-1}$)
 v_a = air velocity ($m\ s^{-1}$)
 ν_a = air kinetic viscosity ($m^2\ s^{-1}$)
 μ_a = air viscosity ($kg\ m^{-1}\ s^{-1}$)
 C_a = air heat capacity ($J\ kg^{-1}\ K^{-1}$)
 a, b, e = fitted constants

The value of Pr for air between 0 and 10°C is virtually constant (0.705 - 0.707) so the Pr term can be neglected. Therefore:

$$Nu = a(Re)^b \quad (8.3)$$

Nonlinear regression analysis of the data for peeled carrots (Figure 8.2) gave:

$$Nu = 0.267 Re^{0.597} \quad (R^2 = 0.913) \quad (8.4)$$

Percentage differences between h_c obtained from equation (8.4) and experimental values of h_c were plotted against Re (Figure 8.3). It was found that data points were scattered in a random manner.

For unpeeled carrots, the non-homogeneous cylindrical shape may result in extra error in back-calculation of h_c values from the temperature-time data, but this effect cannot be avoided. Nonlinear regression analysis for unpeeled carrots (Figure 8.4) yielded:

$$Nu = 0.704Re^{0.466} \quad (R^2 = 0.870) \quad (8.5)$$

Figure 8.5 shows there are randomly distributed percentage differences between h_c obtained from equation (8.5) and experimental results.

Other than surface roughness there was no reason to expect different surface heat transfer coefficients for peeled and unpeeled carrots. All data were plotted together in Figure 8.6 where it can be observed that the experimental values of Nu and hence h_c for unpeeled carrots were lower than those for peeled carrots especially at high Re . Nonlinear regression analysis was used to fit a unified equation:

$$Nu = 0.462Re^{0.522} \quad (R^2 = 0.840) \quad (8.6)$$

It was found that the values of a and b were between those in equation (8.4) and (8.5). Equation 8.6 underpredicts measured h_c for peeled carrots and overpredicts h_c for unpeeled carrot. Because there was a sensible physical reason to explain the differences that occurred it was decided to use equations (8.4) and (8.5) rather than equation (8.6) in further analysis.

8.8 FINISHING REMARKS

The methods described above have allowed sufficient data to be collected to allow an initial investigation of the applicability of the model developed in Chapter 5 to chilling of one real food product. Chapters 9 and 10 describe this investigation.

Table 8.1 Experimental plan for cooling trials with carrots.

Run	T_{in} (°C)	T_a (°C)	H_r	v_a (m s ⁻¹)
1	20	0	0.75	0.5
2	30	0	0.75	0.5
3	20	10	0.75	0.5
4	30	10	0.75	0.5
5	20	0	0.95	0.5
6	30	0	0.95	0.5
7	20	10	0.95	0.5
8	30	10	0.95	3.0
9	20	0	0.75	3.0
10	30	0	0.75	3.0
11	20	10	0.75	3.0
12	30	10	0.75	3.0
13	20	0	0.95	3.0
14	30	0	0.95	3.0
15	20	10	0.95	3.0
16	30	10	0.95	3.0
17	25	5	0.87	1.8
18	25	5	0.87	1.8

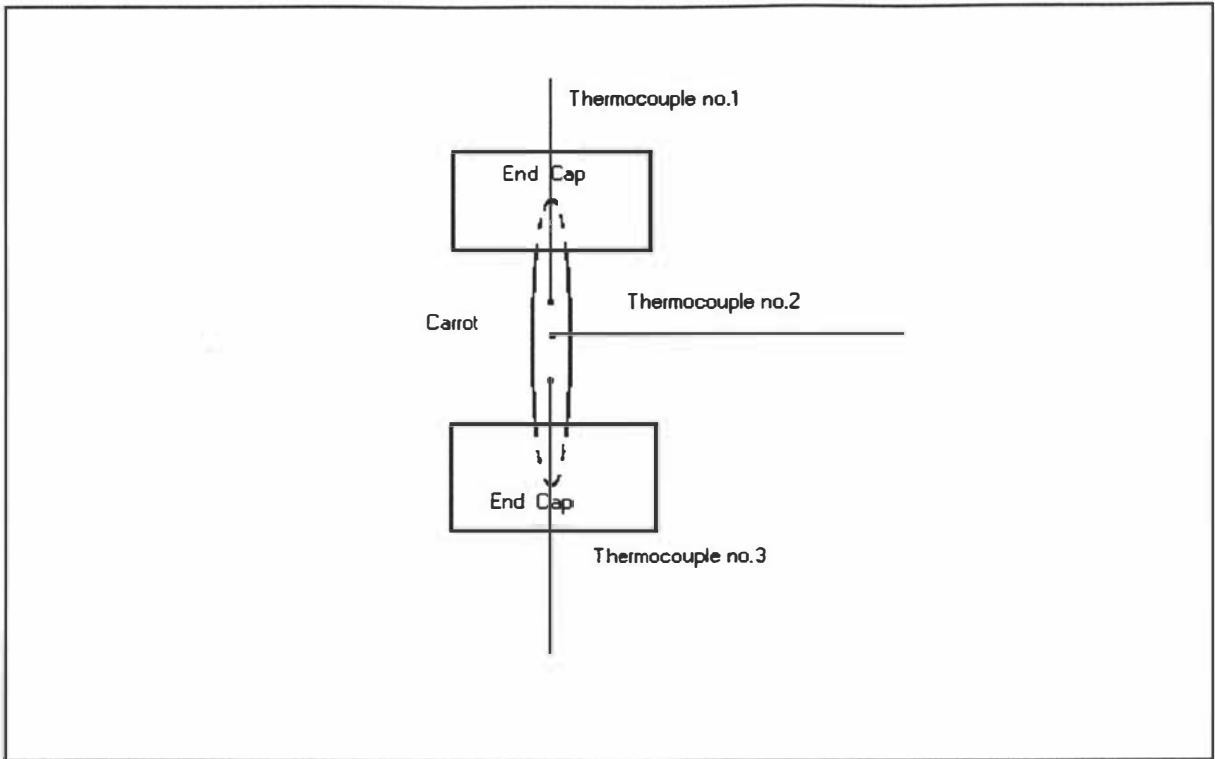


Figure 8.1 A typical infinite cylindrical carrot sample used in experimental work.

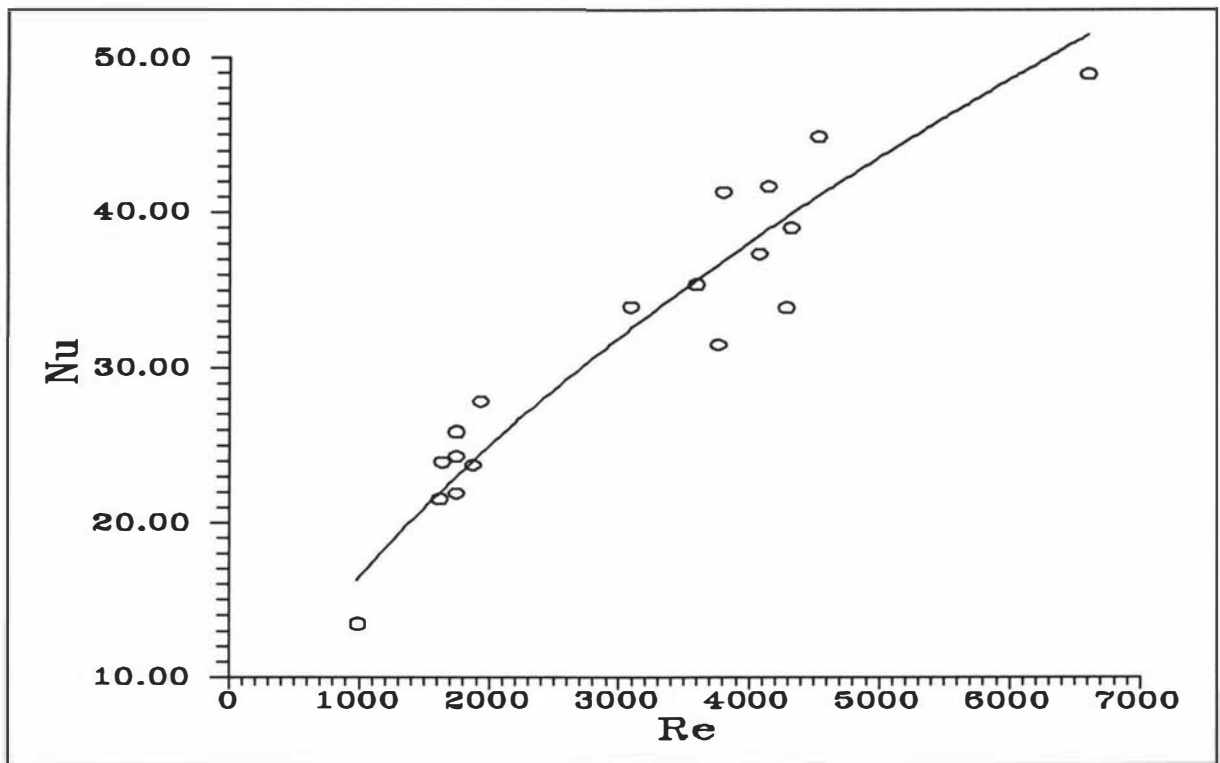


Figure 8.2 Plot of Nu vs Re for runs with peeled carrots.

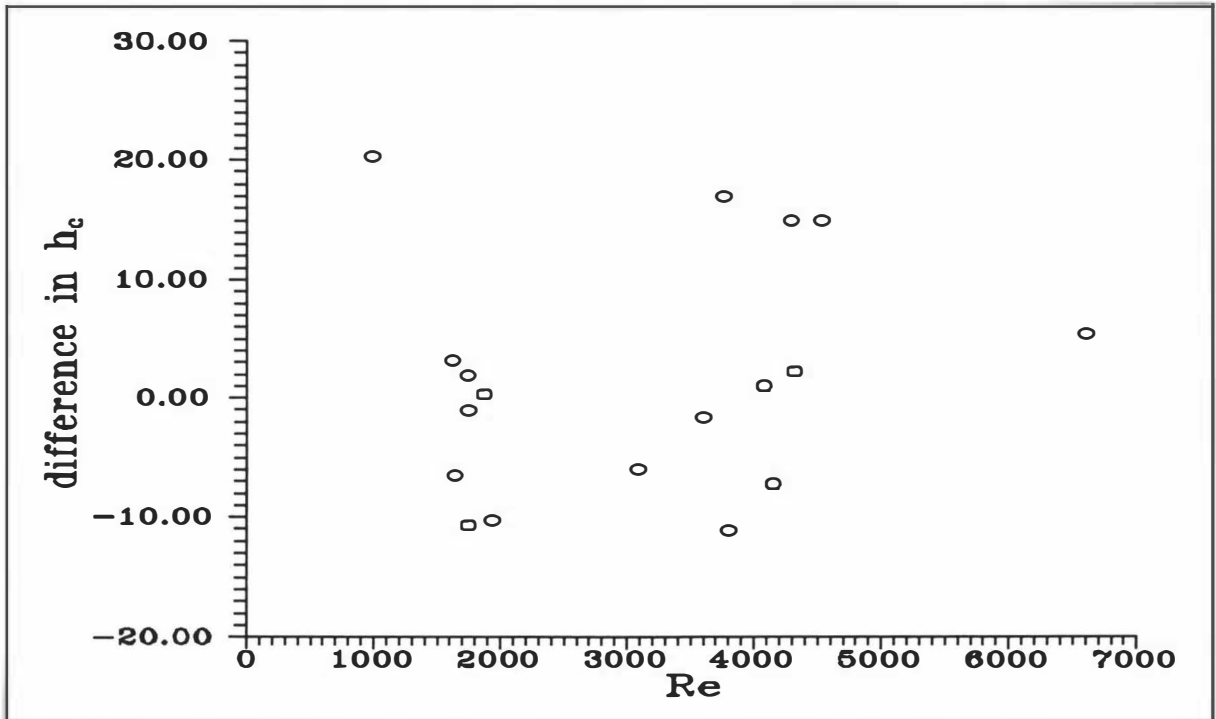


Figure 8.3 Plot of percentage difference in h_c (between calculated results using equation 8.4 and experimental results) for peeled carrots vs Re .

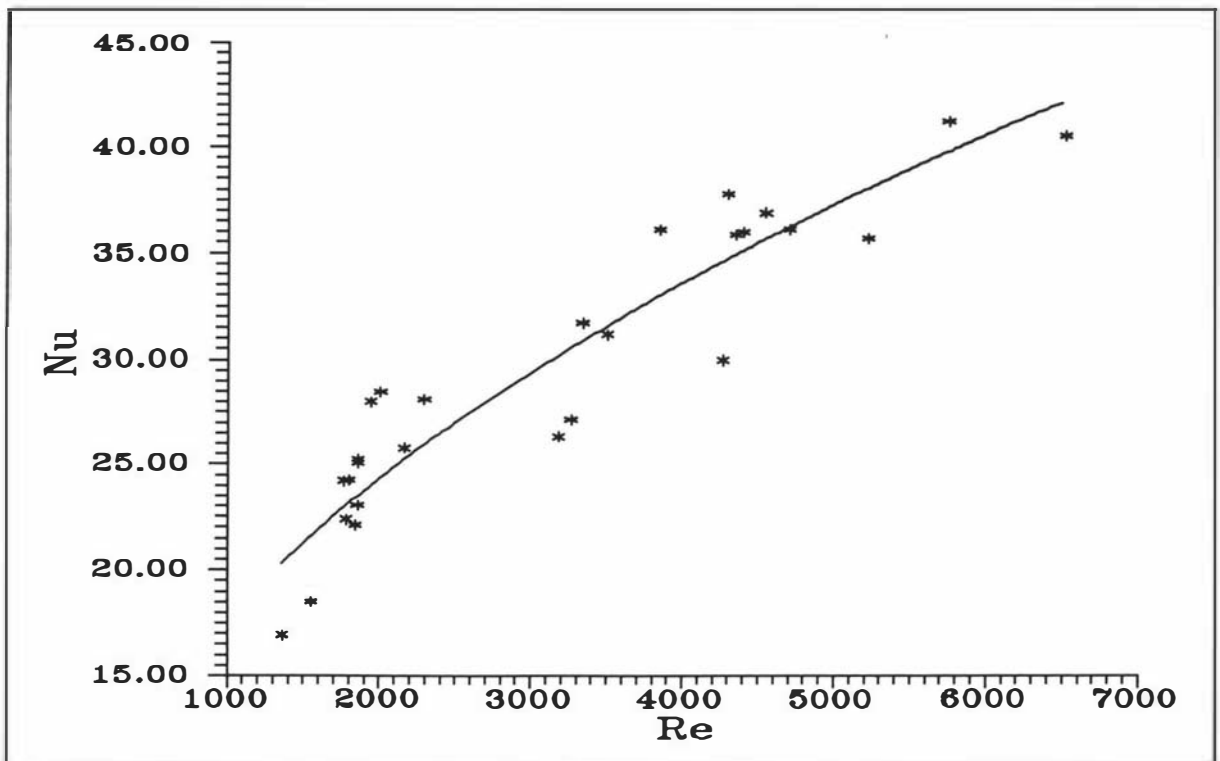


Figure 8.4 Plot of Nu vs Re for runs with unpeeled carrots.

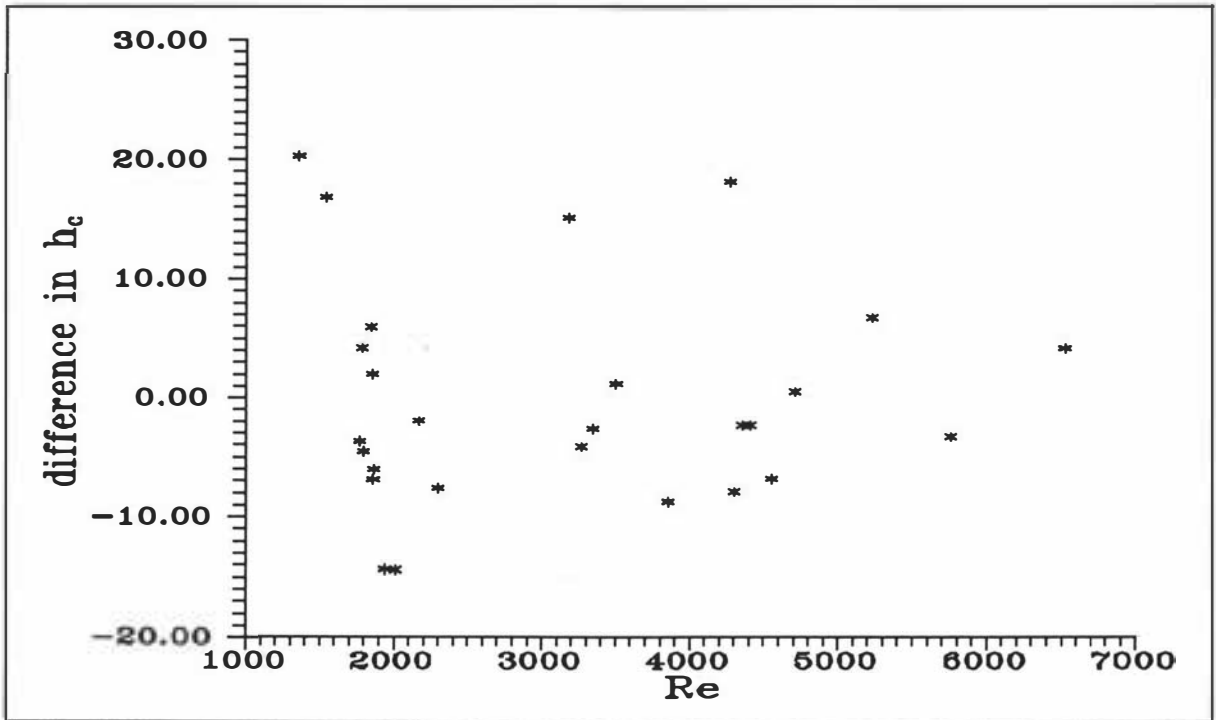


Figure 8.5 Plots of percentage difference in h_c (between calculated results using equation 8.5 and experimental results) for unpeeled carrots vs Re .

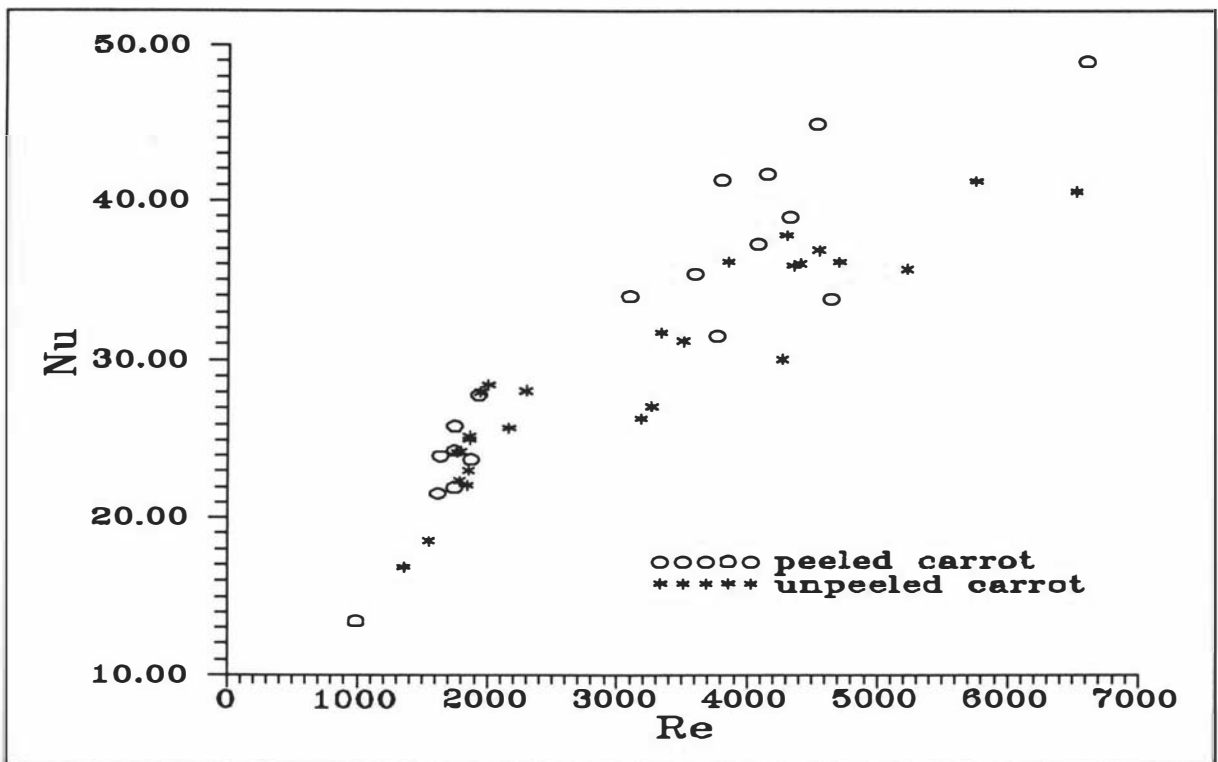


Figure 8.6 Plot of Nu vs Re for runs with peeled & unpeeled carrots.

9. TESTING OF THE PROPOSED MODEL AGAINST EXPERIMENTAL DATA FOR A REAL PRODUCT WITHOUT SKIN RESISTANCE

9.1 INTRODUCTION

This chapter describes the use of the experimental chilling data for peeled carrots to assess the accuracy of the simple prediction method described in Chapter 5. In total, there were 18 experimental trials which are summarised in Table 9.1.

9.2 SURFACE WATER ACTIVITY AND EQUILIBRIUM TEMPERATURE ANALYSIS

The prediction accuracy of the model for the equilibrium temperature was tested. The apparent steady state condition at 3.5 hours was used as an approximation to equilibrium as all runs had reached steady state within the sensitivity of the measurement system in less than 3.5 hours. The mean of a_w measured prior to the commencement of chilling was 0.981 and after chilling was completed was 0.972. The overall mean measured a_w for all samples was 0.977 and the range of measured values was 0.954 -1.0.

Since the equilibrium temperature depends on T_a , H_r , and a_w , the experimental equilibrium temperature ($T_{eq,exp}$) can be used to back calculate a_w or vice versa (using equation 5.11). Figure 9.1 compares predicted values of a_w (when $T_{eq,exp}$ was used in back calculation of this parameter) and measured values of a_w versus H_r for all 18 runs. The measured and back-predicted a_w values were effectively independent of H_r , although two runs at low relative humidity had low back-calculated a_w values. Figures 9.2 - 9.6 use the same data to plot the differences between the predicted value of the equilibrium temperature ($T_{eq,pred}$) at $a_w = 0.977$ and the experimental steady state temperature ($T_{eq,exp}$) against different parameters. These figures do not show evidence of any significant trend although the mean difference is not exactly zero. The experimental steady state temperature closely matched the predicted value of the equilibrium temperature at $a_w = 0.977$ (Tables 9.1 and 9.2). Therefore, any effect of product respiration was probably negligible, and use of the average a_w of 0.977 for the rest

of the analysis was justified. The 95% confidence bounds were $-0.3\text{ }^{\circ}\text{C}$ to $+0.6\text{ }^{\circ}\text{C}$ (Tables 9.3 and 9.4) which is of the same magnitude as the estimated uncertainty. This suggested that within the limits of the methods used the model adequately predicted the experimental data for the steady state condition. The two points on Figure 9.1 that lie away from the others may be caused entirely by experimental error.

9.3 LINEARIZATION OF SEMI-LOG PLOTS

As expected, when the product was wrapped with the plastic film (no evaporation), it was found that at steady state condition, $T_{eq,exp}$ equalled to T_a (e.g. Figure 9.7). Figure 9.8 shows a typically cooling curve with evaporation. As described in Chapter 4, the difference between H_r and a_w was the important factor that indicated the final state of the equilibrium condition relative to the air temperature. In the experiment, since a_w ($= 0.977$) is always higher than H_r ($\approx 0.73 - 0.93$), the equilibrium temperature is always less than ambient air temperature. When modified $Y_{c,exp}$ values were predicted using $T_{eq,exp}$ to replace T_a as discussed in Chapter 5 it was observed that the modified $Y_{c,exp}$ and $T_{eq,exp}$ linearized the plots of $\ln Y_{c,exp}$ versus FO successfully. For example Figure 9.9 is the result of linearization of data in Figure 9.8 using $T_{eq,exp}$. The jagged appearance of the lines at lower $Y_{c,exp}$ arises from analogue to digital conversion accuracy in the data logging system. The portion of the line below modified $Y_{c,exp} = 0.70$ could be best-fitted by a straight line with $R^2 > 0.980$ for all runs. This verified that $T_{eq,exp}$ satisfactorily linearised the cooling curves.

9.4 COOLING WITH EVAPORATIVE EFFECTS

The experimental results and comparisons to model predictions are shown in Tables 9.1 - 9.4. The relative rate of cooling with evaporation to convection only ranges between 1.4 and 2.1. Experimental values of f_{cEvap} and j_{cEvap} were derived from plots of $\ln Y_{c,exp}$ versus FO using equation (7.7). Predicted values of f_{cEvap} and j_{cEvap} were obtained from the simple algebraic equations (equation 5.19 and 5.20 respectively) using the mean measured surface water activity of 0.977. In Tables 9.1 and 9.2 comparisons are also made with the finite difference model of Chapter 4. Tables 9.3 and 9.4 summarise the results in Tables 9.1 and 9.2. It was found that the results from two methods (finite difference method and that from the proposed

curve-fit equation) were similar. The predicted values of f_{cEvap} and j_{cEvap} from the finite difference method or the proposed curve-fit equation, generally agreed within $\pm 13\%$ of the experimental data. The mean offset for the f values was close to 0% , whereas for the j values the mean difference was about $+3.0\%$ (Tables 9.3 and 9.4).

Figures 9.10 - 9.19 show the differences between the predicted results (simple model) and the experimental results plotted versus various experimental parameters. It was concluded that there were no major systematic trends leading to lack of agreement of prediction and experiment. One run, Run 16, appears to sit away from the rest of the data. However there was also a run in which the absolute value of the lack of fit was similar (Run 3), so the Run 16 result was attributed to experimental error.

Plots of f_{cEvap}/f_{cConv} and j_{cEvap}/j_{cConv} values predicted by the simple model against the experimental results are shown in Figures 9.20 and 9.21 respectively. Most data are clustered around the diagonal line, although the j data are less well correlated. Overall the agreement between the simple model and the experimental results was considered acceptable taking into consideration likely data uncertainties, especially in heat transfer coefficients, deviation of thermocouples from the central position inside the products, possible nonuniformity of product diameter, and differences in both composition and maturity between different carrots (Gan & Woods, 1989).

Table 9.2 shows chilling times to reach certain temperatures ($T_{c,exp}$) which corresponded to $Y_{c,exp} = 0.10, 0.35,$ and 0.70 (using equation 7.7, equation 7.8 where $T_{eq,pred}$ was predicted by using $a_w = 0.977$ in equation 5.11, and equation 7.9). The finite difference and simple model failed to predict experimental data in similar ways (the correlation coefficients between $\%$ difference of the two models were close to 1). Tables 9.3 and 9.4 summarise the results. The mean offset for chilling time of both models at $Y_{c,exp} = 0.10$ and $Y_{c,exp} = 0.35$ was close to zero whereas at $Y_{c,exp} = 0.70$ the mean offset was about 6% . The reason for the poorer agreement at the higher Y value is that the exponential cooling regime is not always well established before this $Y_{c,exp}$ is reached. This was discussed in Chapter 7, and is a well-known weakness of any model based on exponential behaviour. As $Y_{c,exp}$ came close to zero, error in T_{eq} is much more significant in its effect on the relationship between $T_{c,exp}$ and $Y_{c,exp}$ than at higher

$Y_{c,exp}$ values. Thus the standard deviation is greater at $Y_{c,exp} = 0.10$ than at 0.35. When chilling times predicted by the simple model were plotted against those from the experiments (Figures 9.22 - 9.24), it was found that the agreement was generally good.

9.5 WEIGHT LOSS

Measured weight loss during the 3.5 hour cooling process ranged between 1.5 % and 5 % (Table 9.1). Weight loss tended to increase at higher air velocity (Figure 9.25). However the uncertainty in these data (as described in Chapter 8) was significant. The weight loss data are not necessary to test the ability of the model to predict cooling rate, but are reported here to help others who may wish to use the experimental data in the future.

9.6 DISCUSSION AND CONCLUSIONS

The model of Chapter 5 using the equilibrium temperature and the modified unaccomplished temperature change successfully linearised the experimental cooling curves. The finite difference method, the simple model, and the experimental results were generally similar and disagreement could be effectively explained by experimental uncertainty, thus indicating that the simple model can be used with confidence for peeled carrots without skin resistance across the range of conditions covered.

An implication of the observed success with which the model was applied was that for the conditions studied internal water movement in the carrots (probably more by capillary action than diffusion) was always sufficiently fast to keep the surface at virtually constant a_w . This was in spite of total moisture losses of 1.5 to 5 %. Whilst the results reported in this Chapter suggest that the model of Chapter 5 will probably apply to any product with rapid internal moisture transfer cooled under typical chilling conditions they do not help define means for establishing whether full surface wetting can be assumed for any particular product. This is an area in which future research is justified.

Table 9.1 Experimental data and predicted results for runs using peeled carrot as the product with $a_w = 0.977$.

Run	2R (m)	T_{in} (°C)	T_a (°C)	H_r (%)	v_a (ms ⁻¹)	h_c (Wm ⁻² K ⁻¹)	Bi	f_{cSnap} (exp.)	f_{cConv} (anal. soln.)	j_{cSnap} (exp.)	j_{cConv} (anal. soln.)	type	f_{cSnap}/f_{cConv}	j_{cSnap}/j_{cConv}	$\Delta f_{cSnap}/f_{cConv}$ (%)		$\Delta j_{cSnap}/j_{cConv}$ (%)		T_{eq} (°C)			weight loss (%)
															simple model	finite diff.	simple model	finite diff.	exp.	model	ΔT_{eq} (°C)	
1	0.025	21.4	1.4	73	0.9	21.7	0.52	-1.34	-0.91	1.06	1.12	simple model	1.57	0.98	+7.5	+8.2	+3.2	+3.2	0.4	-0.1	-0.5	3.2
												experiment	1.46	0.95								
												finite diff.	1.58	0.98								
2	0.027	26.9	1.4	73	0.9	20.9	0.55	-1.56	-0.95	1.11	1.12	simple model	1.58	0.97	-4.2	-3.6	-2.0	-2.0	0.3	-0.1	-0.4	3.2
												experiment	1.65	0.99								
												finite diff.	1.59	0.97								
3	0.026	19.9	11.4	81	0.6	16.2	0.40	-1.31	-0.72	1.04	1.09	simple model	2.01	1.04	+9.8	+8.7	+9.5	+8.4	10.2	9.8	-0.4	2.8
												experiment	1.83	0.95								
												finite diff.	1.99	1.03								
4	0.027	27.8	11.3	81	0.9	20.8	0.54	-1.77	-0.94	1.07	1.12	simple model	1.96	1.03	+4.3	+3.7	+7.3	+7.3	10.0	9.8	-0.2	3.3
												experiment	1.88	0.96								
												finite diff.	1.95	1.03								
5	0.024	19.4	1.7	86	1.0	24.5	0.55	-1.54	-0.97	1.04	1.13	simple model	1.55	1.00	-0.6	+0.6	+8.7	+8.7	1.2	0.9	-0.3	1.7
												experiment	1.59	0.92								
												finite diff.	1.60	1.00								
6	0.023	26.6	1.7	86	1.0	23.7	0.54	-1.60	-0.95	1.12	1.12	simple model	1.64	0.98	-2.4	-3.0	-1.0	-1.0	0.9	0.9	+0.0	2.6
												experiment	1.68	0.99								
												finite diff.	1.63	0.98								
7	0.026	19.9	11.5	92	1.0	23.0	0.58	-1.85	-1.01	1.10	1.13	simple model	1.97	1.07	+7.1	+6.5	+10.3	+11.3	11.3	11.1	-0.2	2.9
												experiment	1.84	0.97								
												finite diff.	1.96	1.08								

Table 9.1 Experimental data and predicted results for runs using peeled carrot as the product with $a_w = 0.977$. (continued)

Run	2R (m)	T_{in} (°C)	T_a (°C)	H_r (%)	v_a (ms ⁻¹)	h_c (Wm ⁻² K ⁻¹)	Bi	f_{cbvap} (exp.)	f_{cCom} (anal. soln.)	j_{cbvap} (exp.)	j_{cCom} (anal. soln.)	type	f_{cbvap}/f_{cCom}	j_{cbvap}/j_{cCom}	$\Delta f_{cbvap}/f_{cCom}$ (%)		$\Delta j_{cbvap}/j_{cCom}$ (%)		T_{eq} (°C)			weight loss (%)
															simple model	finite diff.	simple model	finite diff.	exp.	model	ΔT_{eq} (°C)	
8	0.027	27.3	11.5	92	1.0	23.2	0.59	-2.16	-1.03	1.23	1.13	simple model	1.99	1.06	-5.2	-5.7	-2.8	-3.7	11.0	11.0	+0.0	3.0
												experiment	2.10	1.09								
												finite diff.	1.98	1.05								
9	0.025	20.1	1.8	81	2.0	36.0	0.86	-2.05	-1.39	1.20	1.18	simple model	1.49	1.02	+1.4	+3.4	+1.0	+1.0	0.9	0.8	-0.1	4.0
												experiment	1.47	1.01								
												finite diff.	1.52	1.02								
10	0.024	27.7	1.8	81	2.4	40.5	0.93	-2.34	-1.49	1.19	1.20	simple model	1.50	1.00	-4.5	-3.2	+0.0	+1.0	0.9	0.8	-0.1	4.6
												experiment	1.57	1.00								
												finite diff.	1.52	1.01								
11	0.023	19.5	10.6	81	2.2	44.7	0.98	-2.54	-1.56	1.22	1.20	simple model	1.70	1.08	+4.3	+4.3	+6.9	+6.9	9.5	9.1	-0.4	4.9
												experiment	1.63	1.01								
												finite diff.	1.70	1.08								
12	0.024	22.8	10.6	81	2.2	38.1	0.86	-2.43	-1.40	1.20	1.18	simple model	1.77	1.07	+1.7	+1.1	+4.9	+4.9	9.2	9.1	-0.1	5.1
												experiment	1.74	1.02								
												finite diff.	1.76	1.07								
13	0.033	18.3	0.8	88	2.7	38.1	1.2	-2.49	-1.81	1.20	1.24	simple model	1.40	1.03	+1.4	+4.3	+6.2	+7.7	0.4	0.3	-0.1	2.5
												experiment	1.38	0.97								
												finite diff.	1.44	1.04								
14	0.031	26.3	0.8	88	2.0	30.4	0.90	-2.11	-1.47	1.14	1.19	simple model	1.49	1.00	+4.2	+6.3	+4.2	+4.2	0.4	0.3	-0.1	2.5
												experiment	1.43	0.96								
												finite diff.	1.52	1.00								

Table 9.1 Experimental data and predicted results for runs using peeled carrot as the product with $a_w = 0.977$. (continued)

Run	2R (m)	T_{in} (°C)	T_a (°C)	H_r (%)	v_a (ms ⁻¹)	h_c (Wm ⁻² K ⁻¹)	Bi	f_{cEvap} (exp.)	f_{cCom} (anal. soln.)	j_{cEvap} (exp.)	j_{cCom} (anal. soln.)	type	f_{cEvap}/f_{cCom}	j_{cEvap}/j_{cCom}	$\Delta f_{cEvap}/f_{cCom}$ (%)		$\Delta j_{cEvap}/j_{cCom}$ (%)		T_{eq} (°C)			weight loss (%)
															simple model	finite diff.	simple model	finite diff.	exp.	model	ΔT_{eq} (°C)	
15	0.021	19.3	10.9	88	2.5	42.5	0.86	-2.53	-1.40	1.32	1.18	simple model	1.79	1.09	-1.1	-1.1	-2.7	-2.7	10.1	10.1	+0.0	4.1
												experiment	1.81	1.12								
												finite diff.	1.79	1.09								
16	0.021	27.8	10.9	88	2.6	44.2	0.89	-2.97	-1.44	1.32	1.19	simple model	1.80	1.07	-12.6	-12.6	-3.6	-3.6	10.0	10.1	+0.1	4.8
												experiment	2.06	1.11								
												finite diff.	1.80	1.07								
17	0.028	23.9	5.6	86	2.0	33.3	0.91	-2.40	-1.47	1.20	1.19	simple model	1.60	1.04	-2.4	-1.8	+3.0	+3.0	4.9	4.3	-0.6	3.6
												experiment	1.64	1.01								
												finite diff.	1.61	1.04								
18	0.027	24.1	5.6	86	1.57	29.2	0.77	-2.20	-1.28	1.21	1.17	simple model	1.66	1.03	-3.5	-3.5	-1.0	-1.0	4.8	4.8	+0.0	5.6
												experiment	1.72	1.04								
												finite diff.	1.66	1.03								

Table 9.2 Predicted and measured chilling times to reach certain centre temperatures which corresponded to $Y_{c,exp} = 0.10, 0.35, \text{ and } 0.70$ for runs using peeled carrot as the product.

Run	time (min.) to $Y_{c,exp} = 0.10$					time (min.) to $Y_{c,exp} = 0.35$					time (min.) to $Y_{c,exp} = 0.70$				
	simple model	exp.	finite diff.	Δ (%)		simple model	exp.	finite diff.	Δ (%)		simple model	exp.	finite diff.	Δ (%)	
				simple model	finite diff.				simple model	finite diff.				simple model	finite diff.
	1	30.9	36.3	30.8	-14.8	-15.1	15.4	17.1	15.4	-9.5	-9.7	6.2	6.4	6.2	-3.7
2	35.0	36.4	34.5	-4.0	-5.3	17.2	17.4	17.0	-1.5	-2.8	6.9	6.9	6.7	-2.3	-3.6
3	31.3	37.4	31.5	-16.4	-15.8	15.9	17.4	16.0	-8.6	-8.1	6.7	6.3	6.7	+5.7	+6.1
4	29.0	31.2	29.2	-7.1	-6.5	14.6	14.8	14.7	-1.0	-0.4	6.2	5.6	6.3	+10.8	+11.4
5	27.5	28.3	27.1	-2.8	-4.1	13.7	13.1	13.5	+4.0	+2.8	5.6	4.7	5.6	+19.2	+18.0
6	27.5	26.8	27.1	+2.6	+1.0	13.1	12.9	12.9	+1.9	+0.2	5.2	5.2	5.1	+0.6	-1.5
7	25.3	28.9	25.7	-12.5	-11.3	13.3	13.8	13.5	-3.8	-2.5	6.0	5.5	6.1	+10.5	+12.1
8	27.7	26.8	28.1	+3.6	+5.0	13.7	13.4	13.9	+2.2	+3.4	6.0	6.0	6.1	-0.5	+0.5
9	22.2	22.9	21.8	-2.9	-4.7	11.2	11.3	11.0	-1.3	-3.0	4.9	4.9	4.8	-0.4	-1.8

Table 9.2 Predicted and measured chilling times to reach certain centre temperatures which corresponded to $Y_{c,exp} = 0.10, 0.35, \text{ and } 0.70$ for runs using peeled carrot as the product. (continued)

Run	time (min.) to $Y_{c,exp} = 0.10$					time (min.) to $Y_{c,exp} = 0.35$					time (min.) to $Y_{c,exp} = 0.70$				
	simple model	exp.	finite diff.	Δ (%)		simple model	exp.	finite diff.	Δ (%)		simple model	exp.	finite diff.	Δ (%)	
				simple model	finite diff.				simple model	finite diff.				simple model	finite diff.
10	20.5	19.6	20.3	+4.8	+3.8	10.3	9.7	10.2	+5.8	+5.0	4.5	4.2	4.5	+6.7	+5.9
11	15.6	16.6	15.6	-5.6	-5.6	8.5	8.3	8.5	+2.7	+2.5	4.0	3.7	4.0	+9.8	+9.3
12	18.2	18.6	18.3	-2.2	-1.6	9.5	9.2	9.5	+2.6	+2.1	4.4	4.0	4.4	+8.4	+8.7
13	34.0	34.0	33.3	+0.0	-2.0	17.5	16.9	17.2	+3.9	+2.1	8.1	7.3	8.0	+10.2	+9.4
14	35.8	36.4	35.0	-1.6	-3.7	17.9	17.7	17.4	+1.1	-1.3	7.8	7.3	7.6	+6.7	+3.8
15	19.9	16.9	20.1	+17.8	+18.7	10.1	8.8	10.2	+14.0	+14.8	4.7	4.4	4.3	+7.3	+8.0
16	16.5	13.9	16.6	+18.9	+19.3	8.2	7.1	8.3	+15.3	+15.7	3.8	3.4	3.8	+11.5	+11.8
17	26.5	26.4	26.5	+0.3	+0.3	13.6	13.1	13.6	+4.1	+3.7	6.2	5.7	6.2	+8.9	+7.7
18	28.1	26.8	28.0	+4.8	+4.7	13.8	13.3	13.8	+3.6	+3.4	6.1	5.9	6.0	+2.7	+2.4

Table 9.3 Differences between results calculated by the finite difference method (assuming $a_w = 0.977$) and results from the experiments (for peeled carrots).

	% difference in f_{cEvap}/f_{cConv}	% difference in j_{cEvap}/j_{cConv}	% difference in time to $Y_{c,exp} =$			difference in T_{eq} (°C)
			0.10	0.35	0.70	
mean	+0.7	+3.0	-1.3	+1.5	+5.8	-0.1
std.	5.4	4.6	9.2	6.2	5.9	0.2
95% conf. interval	-10.6 to +12.0	-6.6 to +12.6	-20.6 to +18.1	-11.5 to +14.6	-6.6 to +18.2	-0.6 to +0.3

Table 9.4 Differences between results calculated by the proposed curve-fit equations (simple model) and results from the experiments (for peeled carrots).(*Correlation coefficient between (a) % difference between simple method prediction and experiment, and (b) % difference between finite difference predictions and experiments)

	% difference in f_{cEvap}/f_{cConv}	% difference in j_{cEvap}/j_{cConv}	% difference in time to $Y_{c,exp} =$			difference in T_{eq} (°C)
			0.10	0.35	0.70	
mean	+0.3	+2.9	-0.9	+2.0	+6.2	-0.1
std.	5.3	4.4	9.1	6.1	5.7	0.2
95% conf. interval	-10.9 to +11.5	-6.4 to +12.2	-20.1 to +18.2	-10.8 to +14.7	-5.7 to +18.2	-0.6 to +0.3
*R ²	0.959	0.995	0.986	0.969	0.967	-

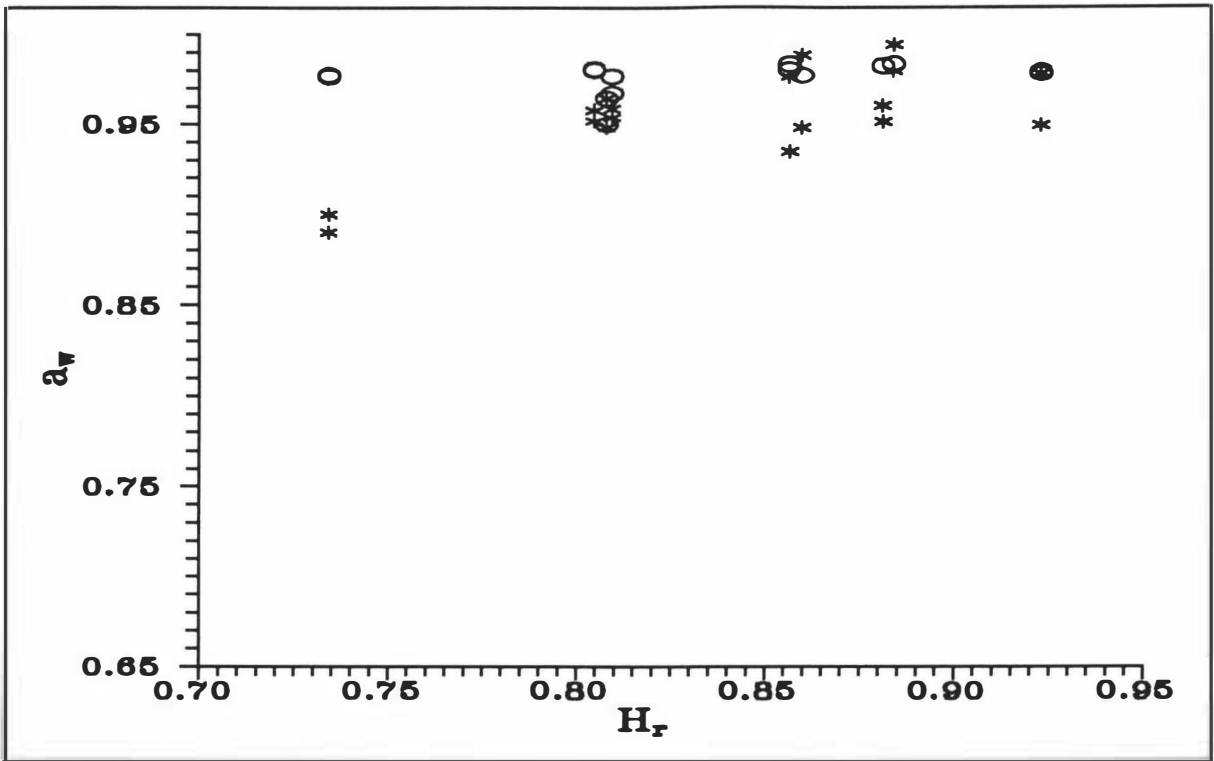


Figure 9.1 Plot of measured a_w (o) and back-calculated a_w (*) vs H_r .

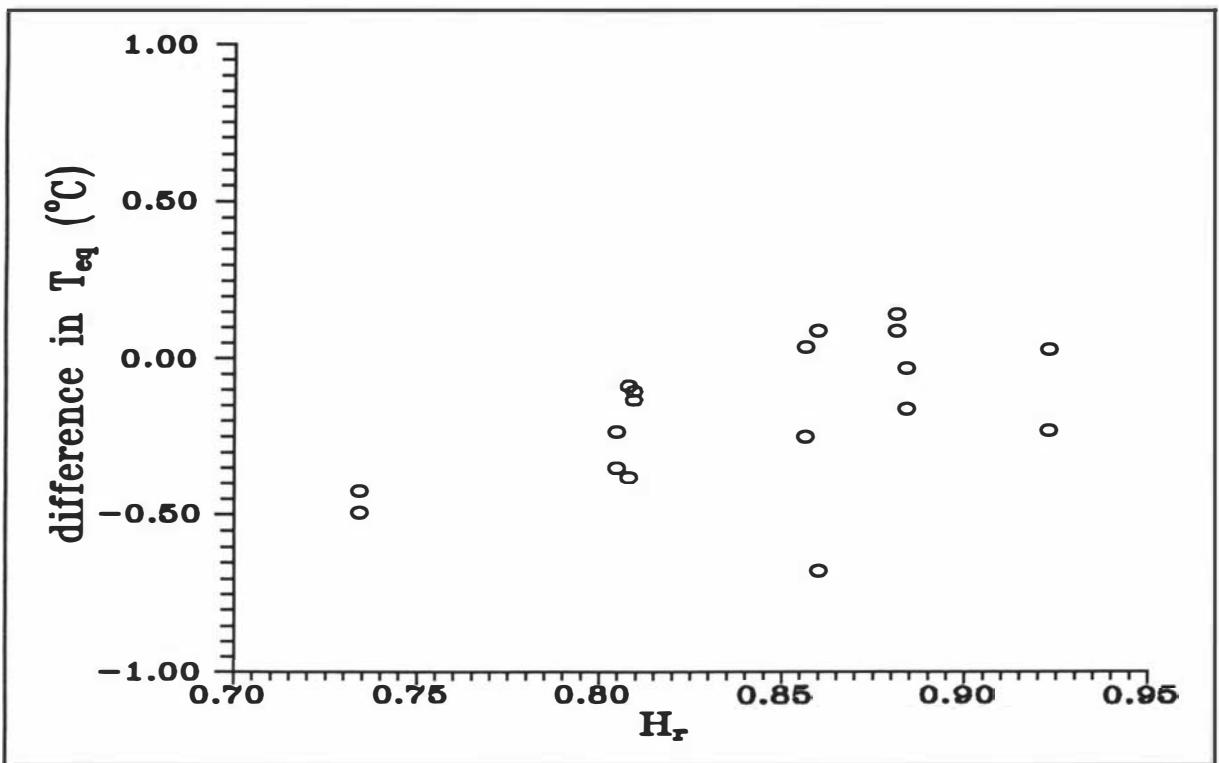


Figure 9.2 Plot of difference between $T_{eq,pred}$ and $T_{eq,exp}$ vs H_r for all experimental runs.

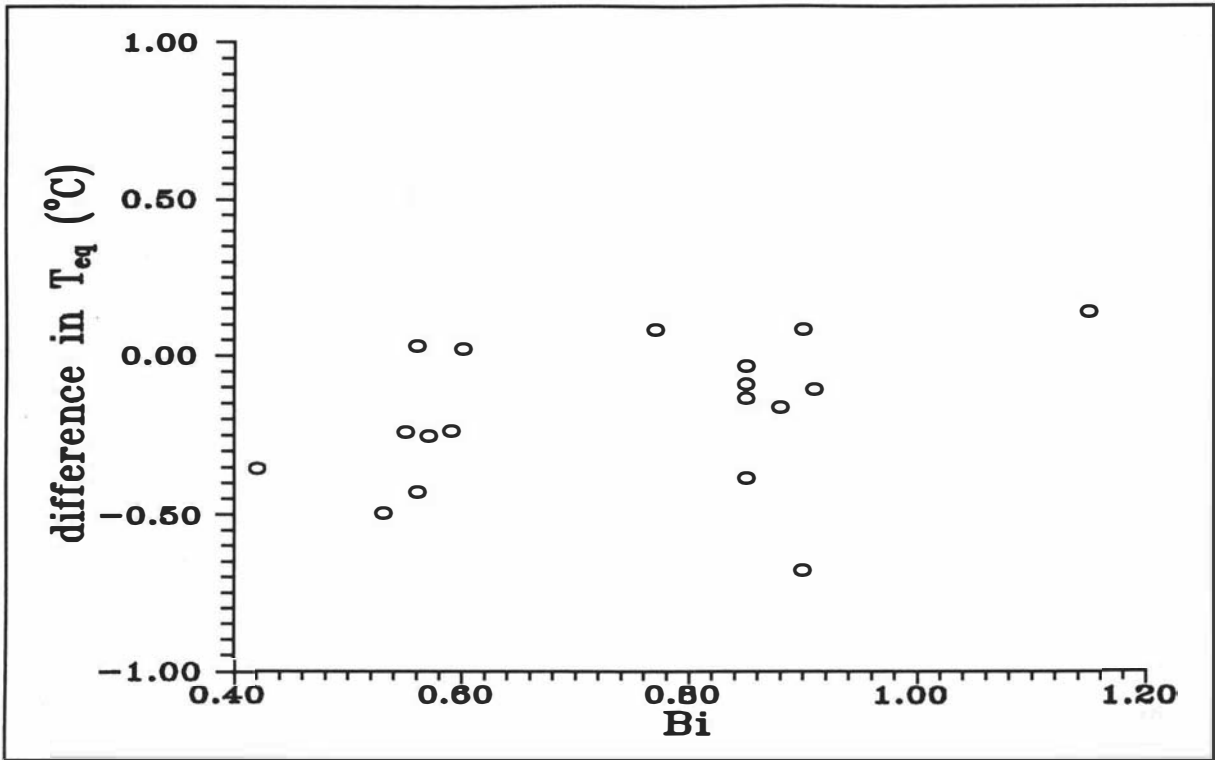


Figure 9.3 Plot of difference between $T_{eq,pred}$ and $T_{eq,exp}$ vs Bi for all experimental runs.

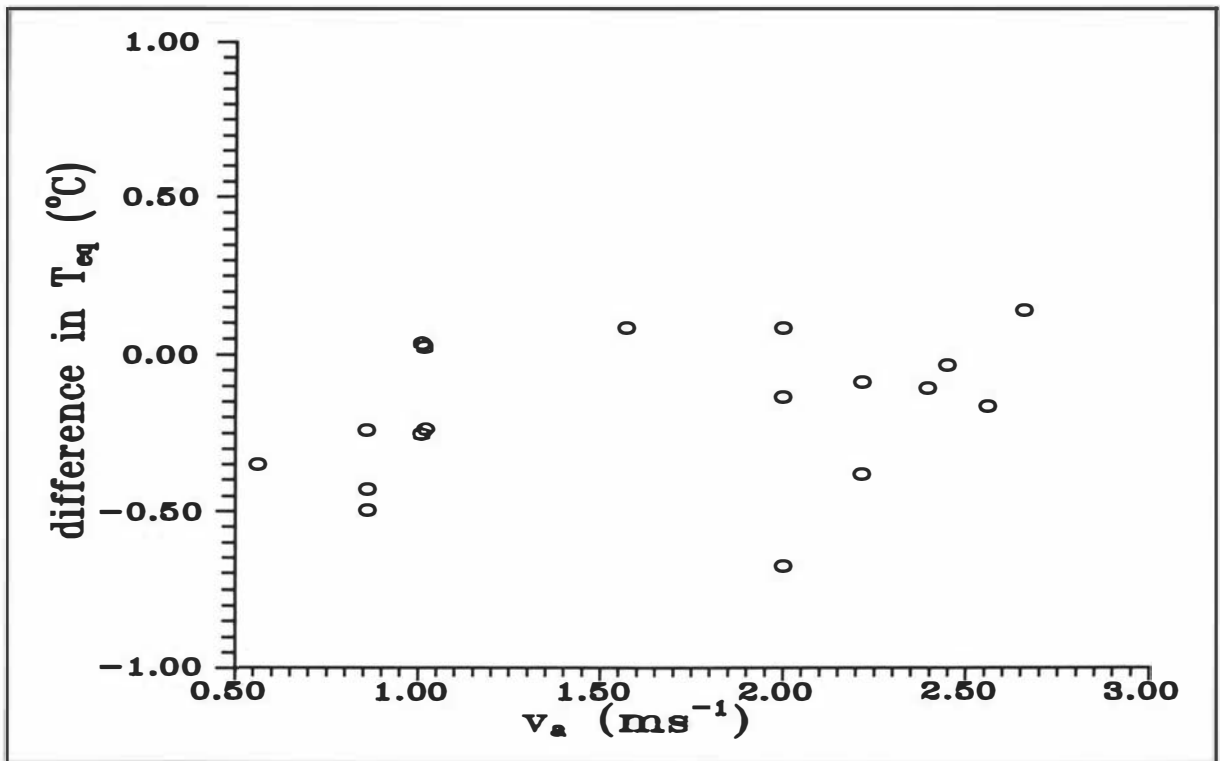


Figure 9.4 Plot of difference between $T_{eq,pred}$ and $T_{eq,exp}$ vs v_a for all experimental runs.

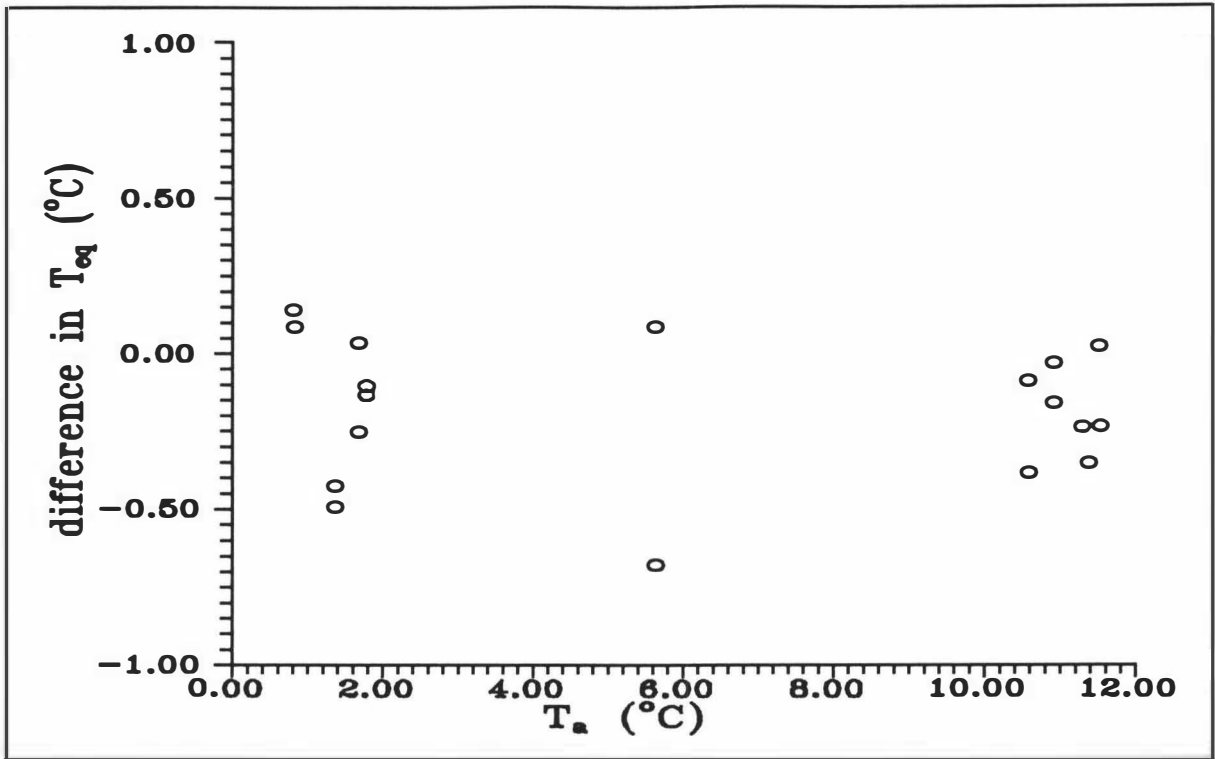


Figure 9.5 Plot of difference between $T_{eq,pred}$ and $T_{eq,exp}$ vs T_a for all experimental runs.

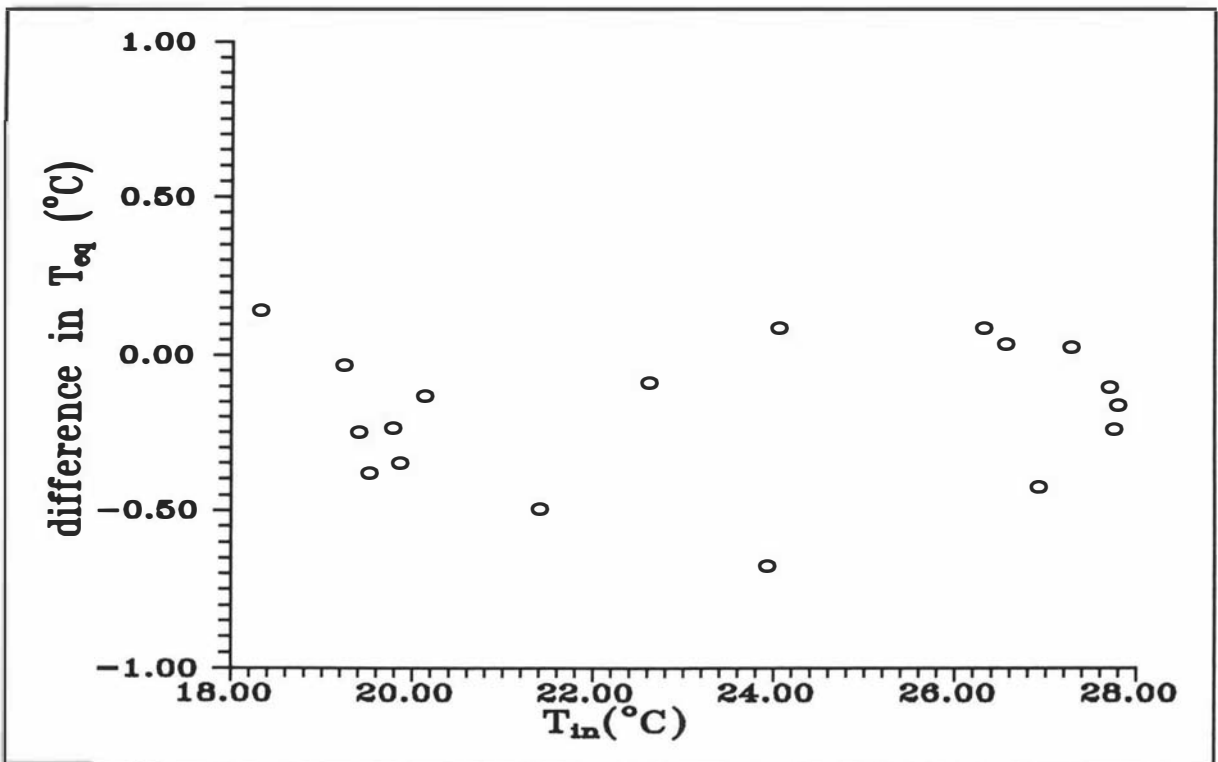


Figure 9.6 Plot of difference between $T_{eq,pred}$ and $T_{eq,exp}$ vs T_{in} for all experimental runs.

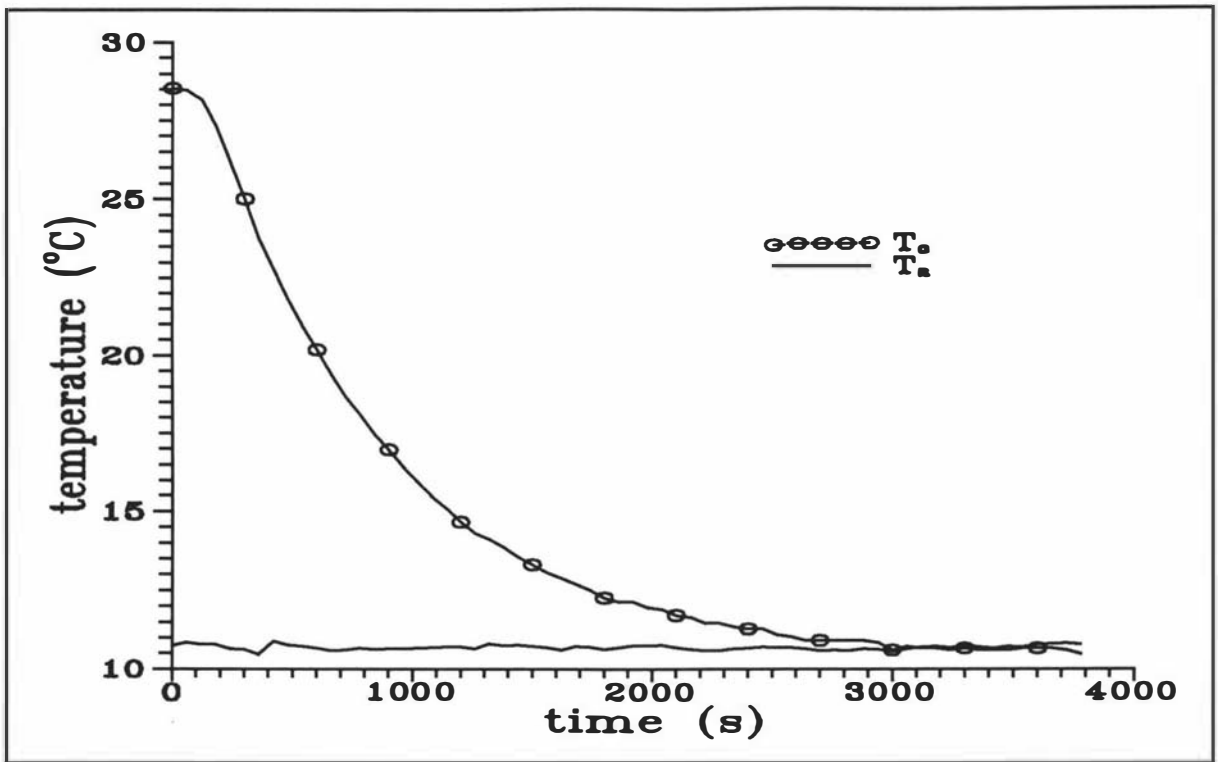


Figure 9.7 Typical plot of temperature vs time for cooling of a peeled carrot without evaporation ($T_{eq,exp} = T_a$).

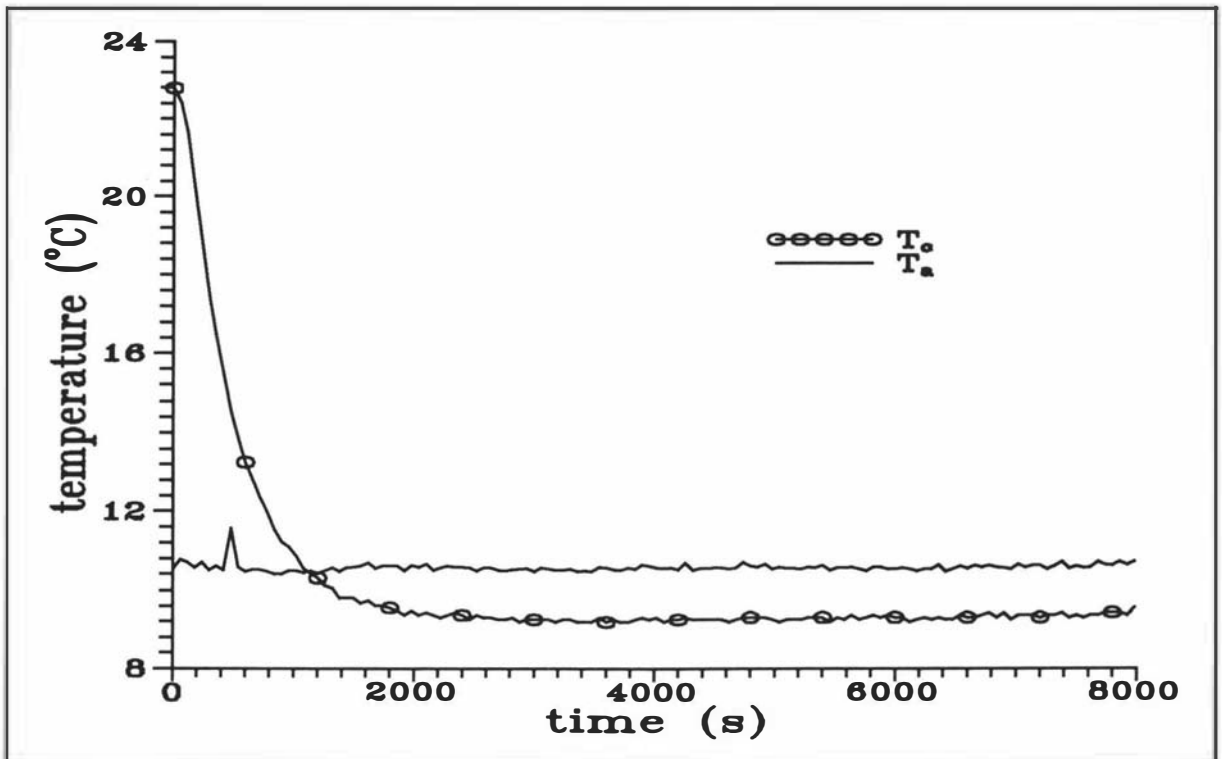


Figure 9.8 Typical plot of temperature vs time for cooling of a peeled carrot with evaporation at the product surface.

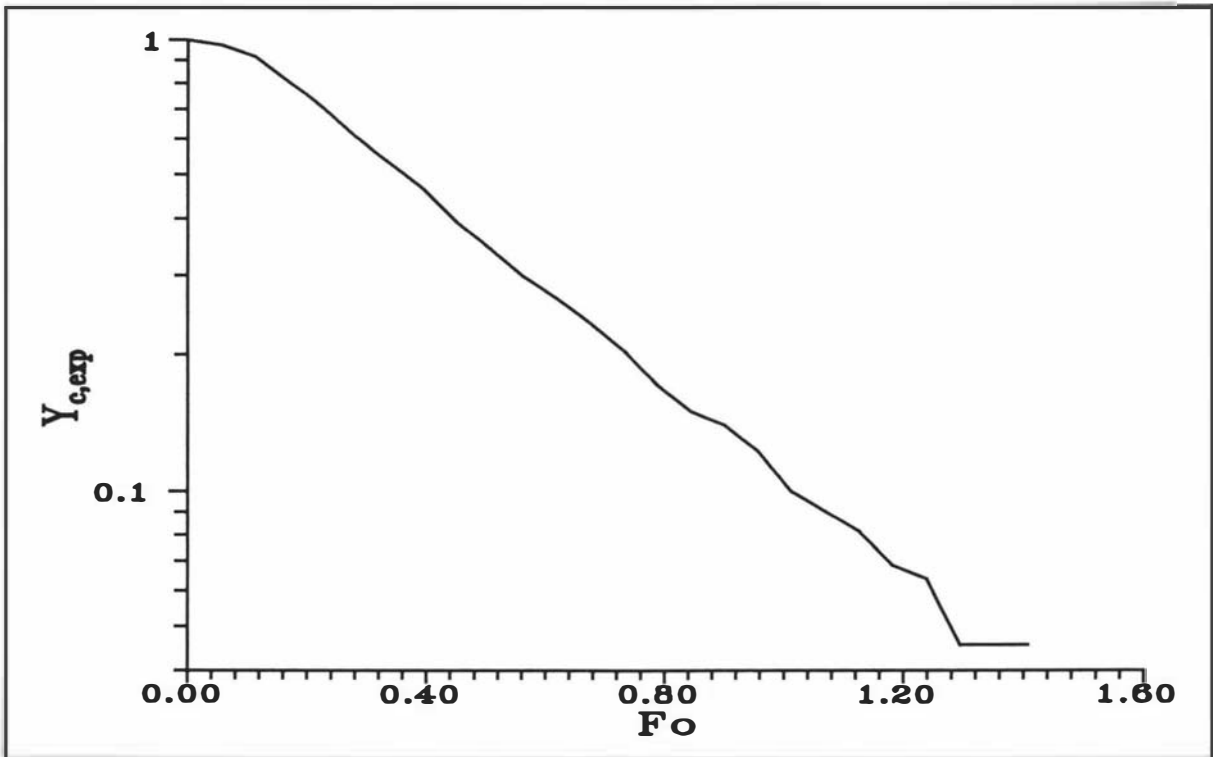


Figure 9.9 Plot of $\ln Y_{c,exp}$ vs FO using $T_{eq,exp}$ as the reference temperature for the conditions in Fig. 9.7.

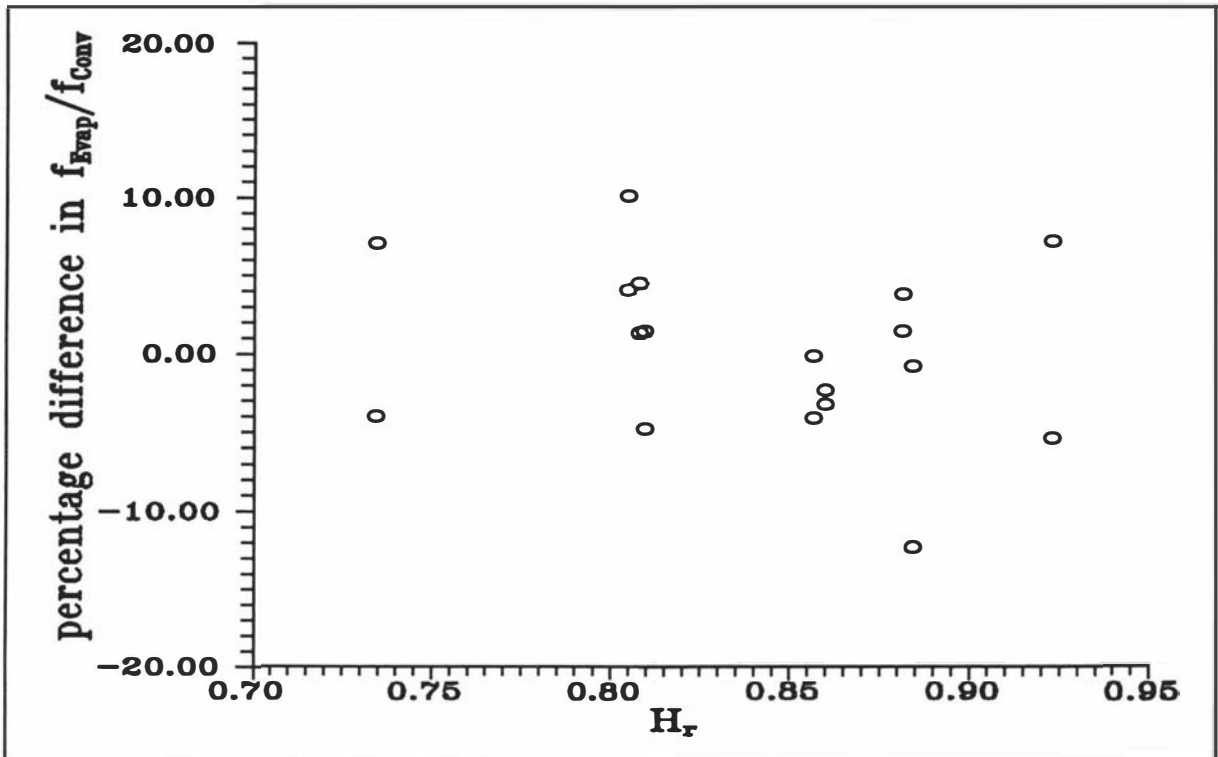


Figure 9.10 Plot of % difference in f_{cEvap}/f_{cConv} values calculated by the simple model compared to experimental values vs H_r .

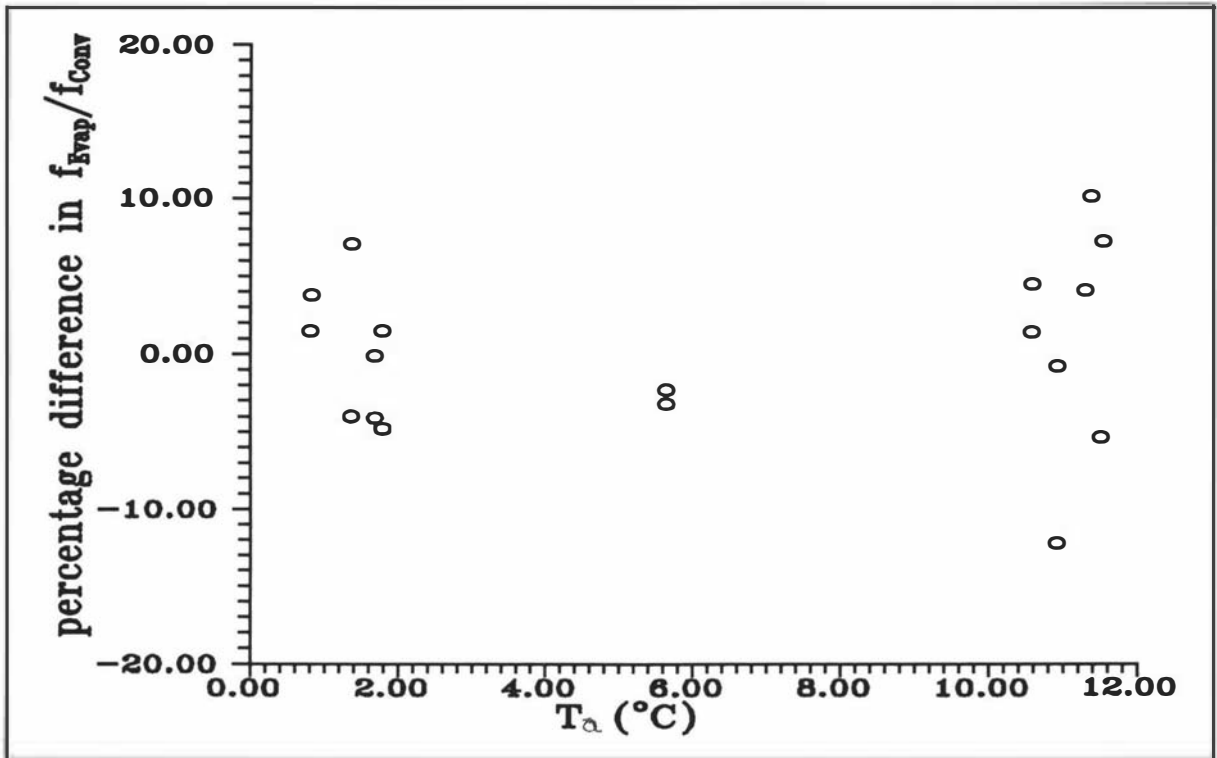


Figure 9.11 Plot of % difference in f_{cEvap}/f_{cConv} values calculated by the simple model compared to experimental values vs T_a .

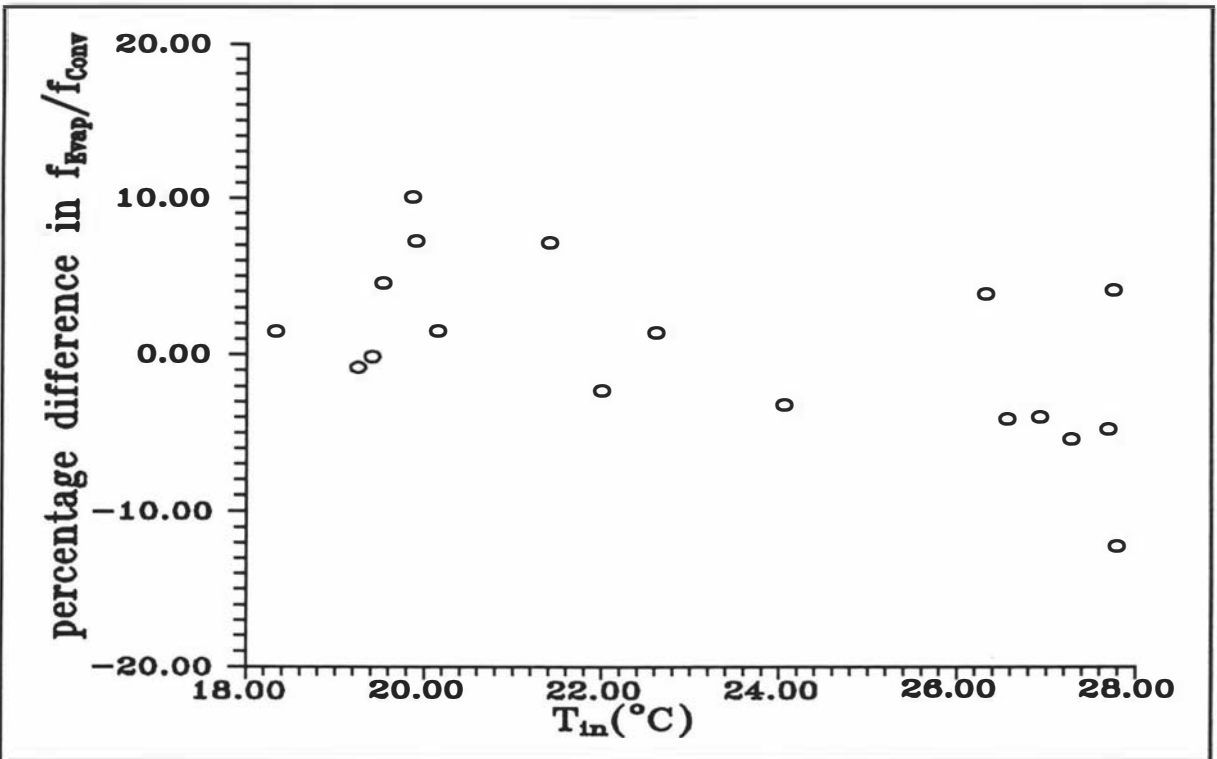


Figure 9.12 Plot of % difference in f_{cEvap}/f_{cConv} values calculated by the simple model compared to experimental values vs T_{in} .

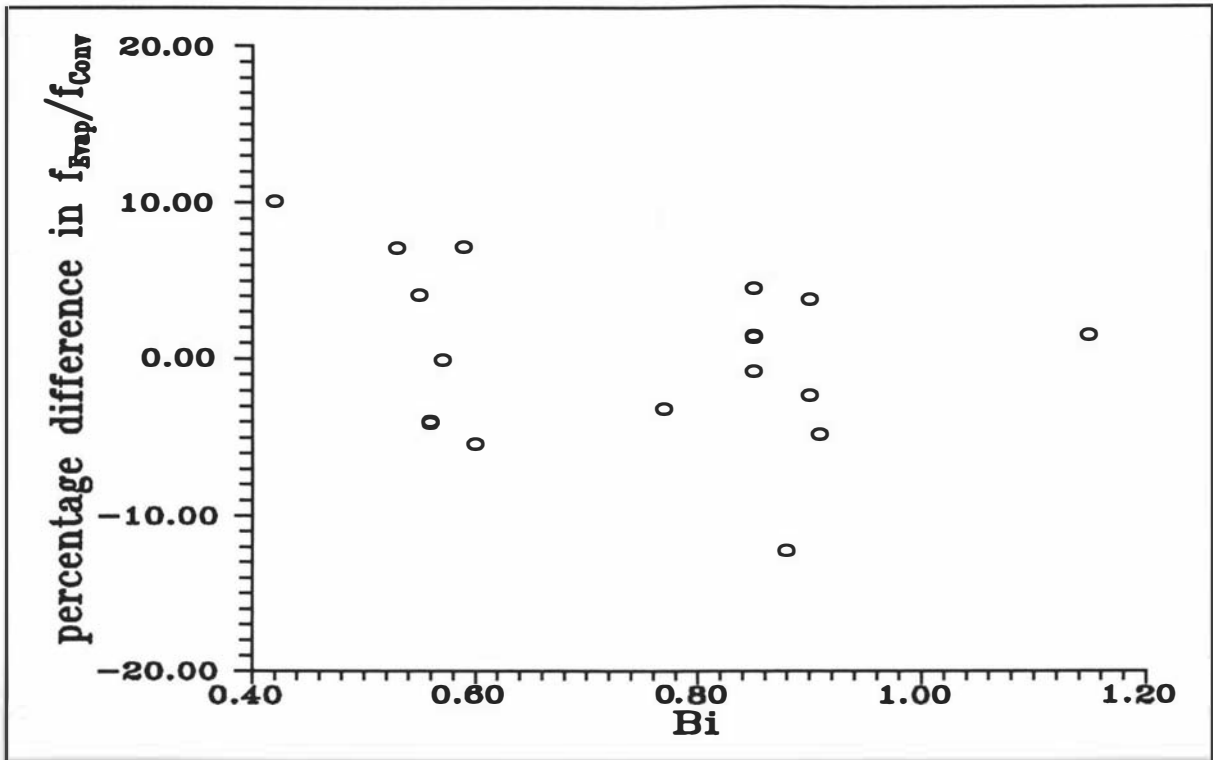


Figure 9.13 Plot of % difference in f_{cEvap}/f_{cConv} values calculated by the simple model compared to experimental values vs Bi .

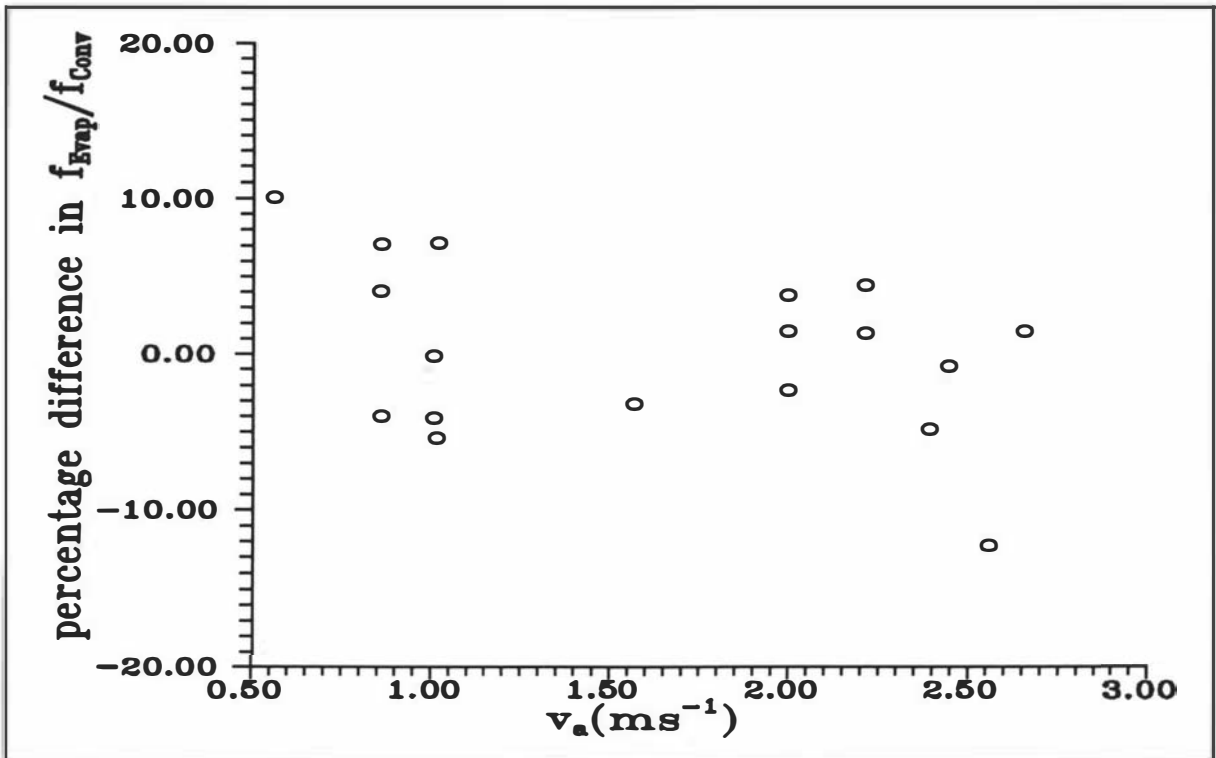


Figure 9.14 Plot of % difference in f_{cEvap}/f_{cConv} values calculated by the simple model compared to experimental values vs v_a .

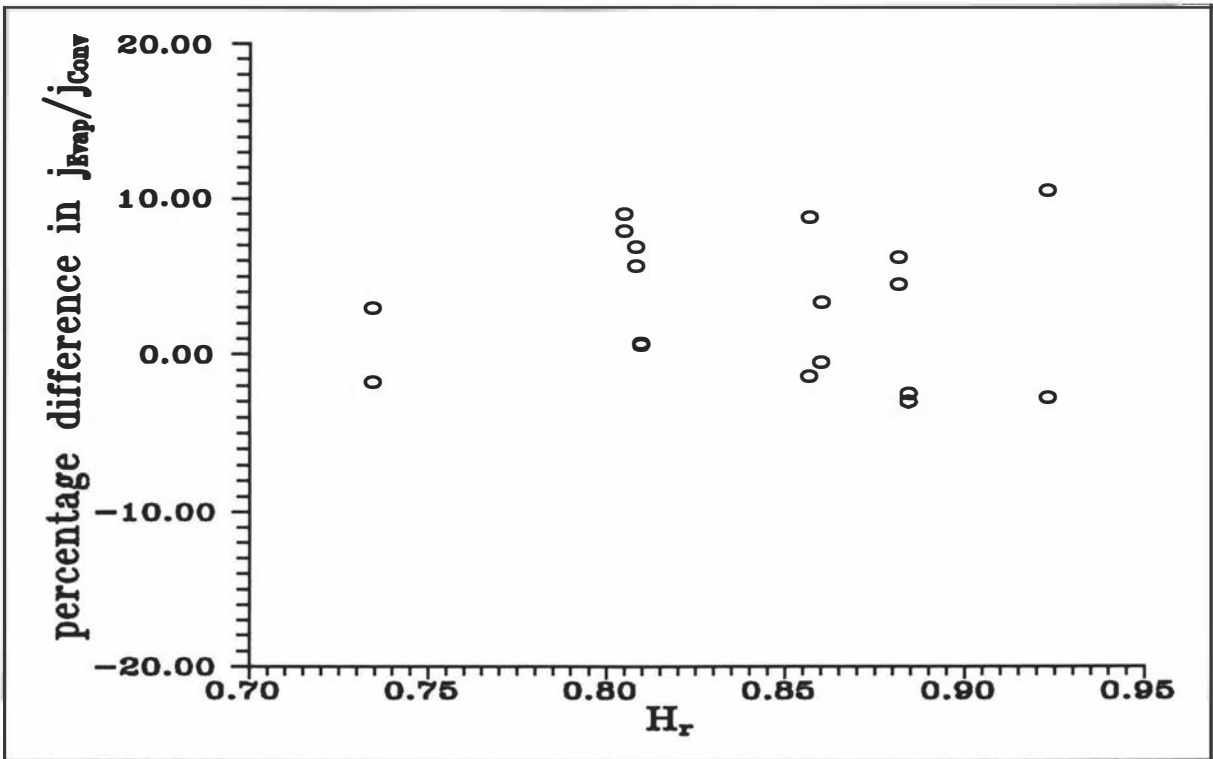


Figure 9.15 Plot of % difference in j_{cEvap}/j_{cConv} values calculated by the simple model compared to experimental values vs H_r .

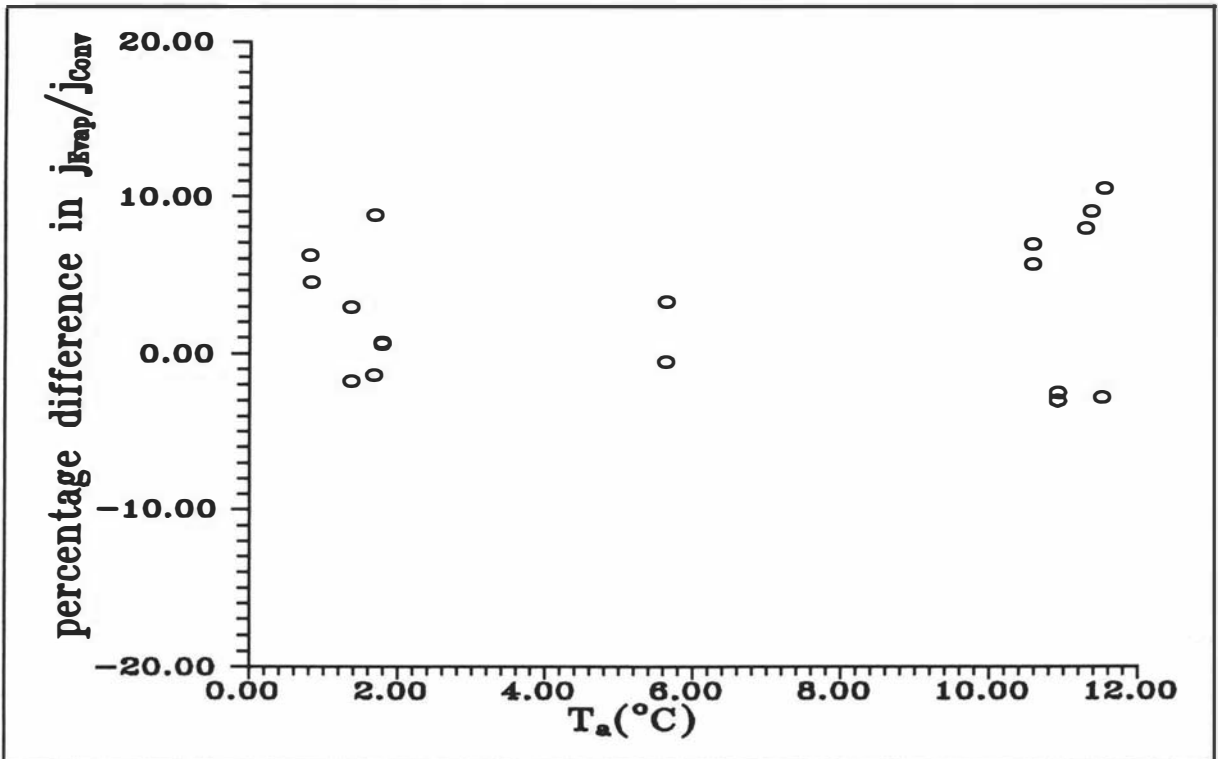


Figure 9.16 Plot of % difference in j_{cEvap}/j_{cConv} values calculated by the simple model compared to experimental values vs T_a .

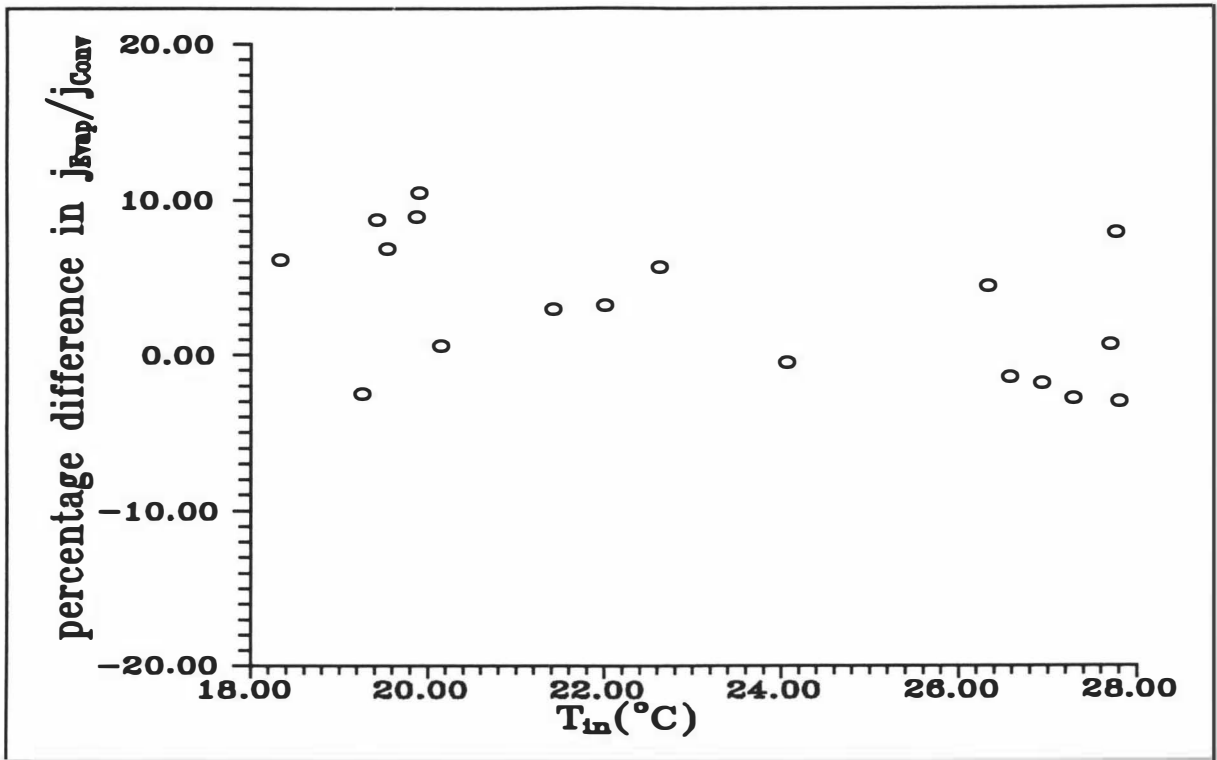


Figure 9.17 Plot of % difference in j_{cEvap}/j_{cConv} values calculated by the simple model compared to experimental values vs T_{in} .

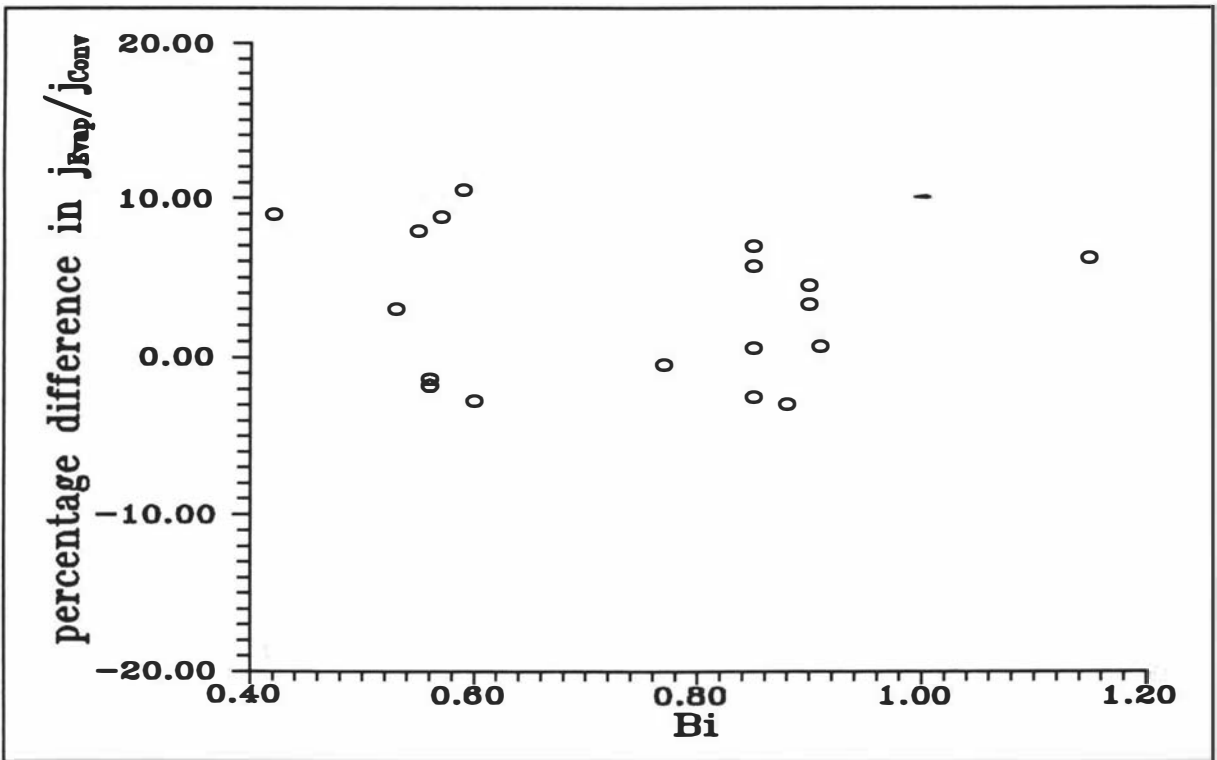


Figure 9.18 Plot of % difference in j_{cEvap}/j_{cConv} values calculated by the simple model compared to experimental values vs Bi .

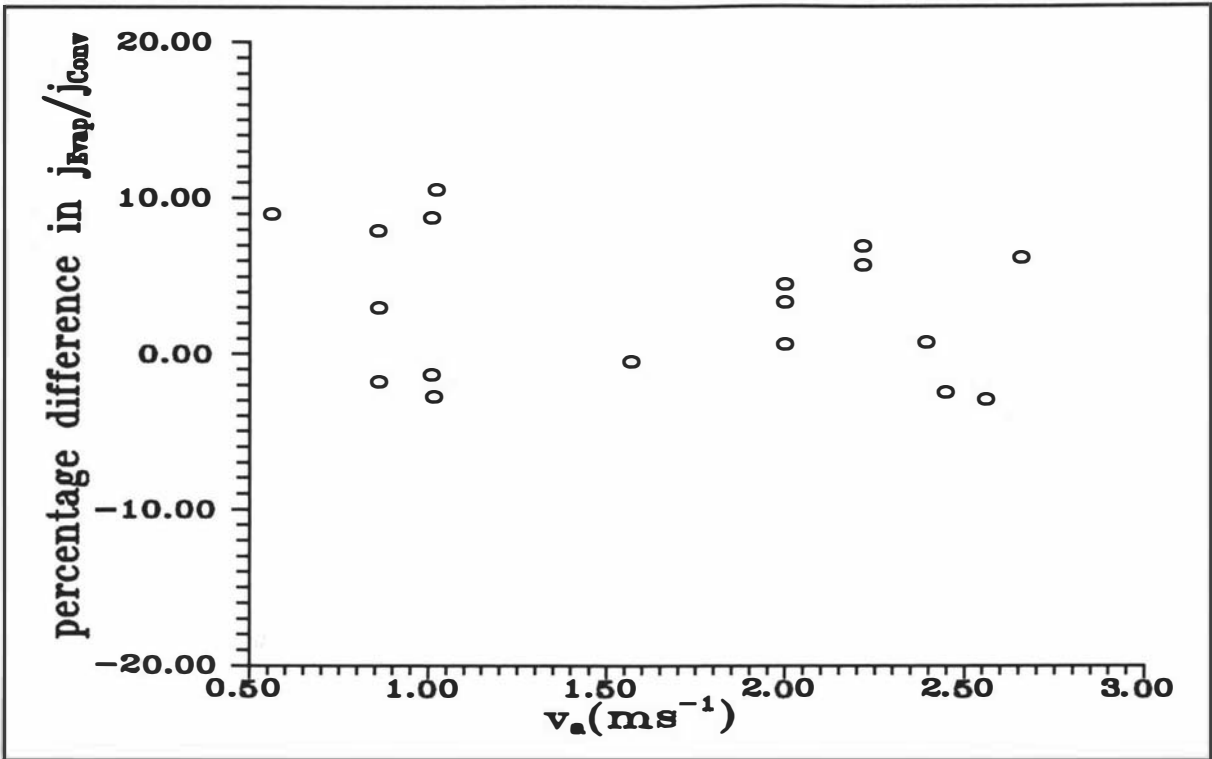


Figure 9.19 Plot of % difference in j_{cEvap}/j_{cConv} values calculated by the simple model compared to experimental values vs v_a .

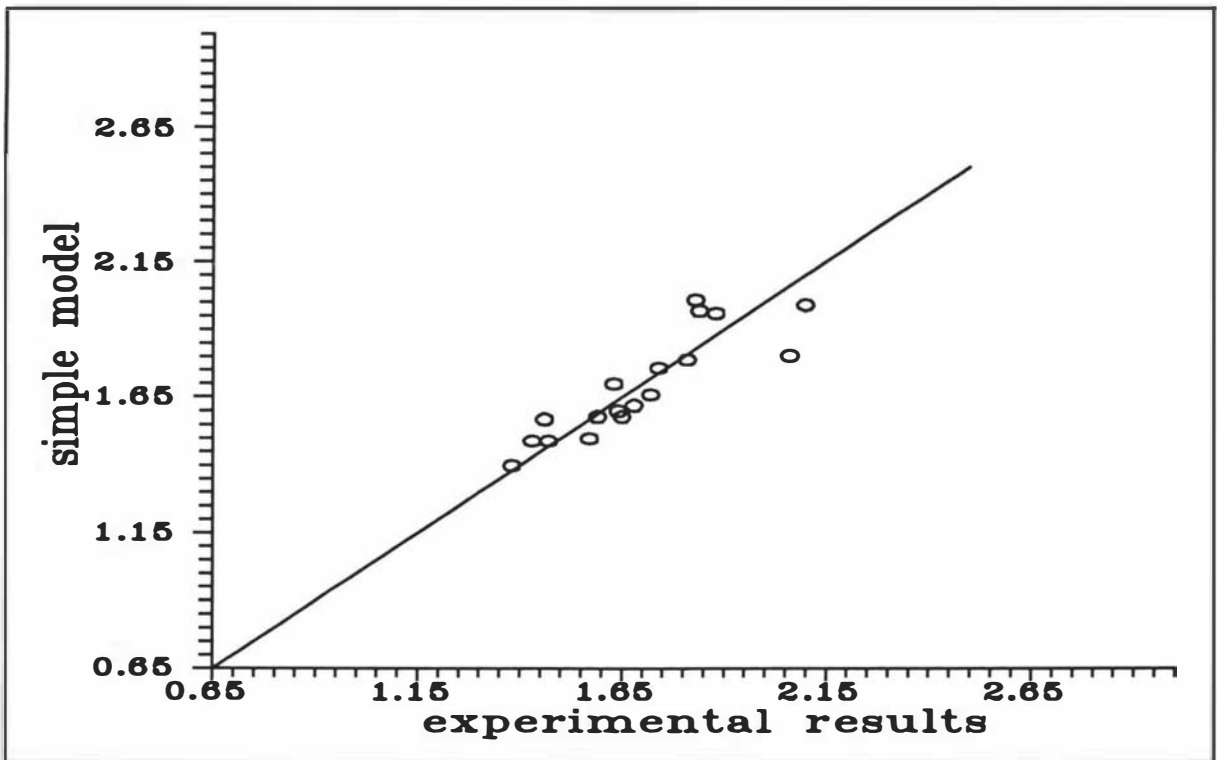


Figure 9.20 Comparisons of the values of f_{cEvap}/f_{cConv} between the simple model and the experimental results.

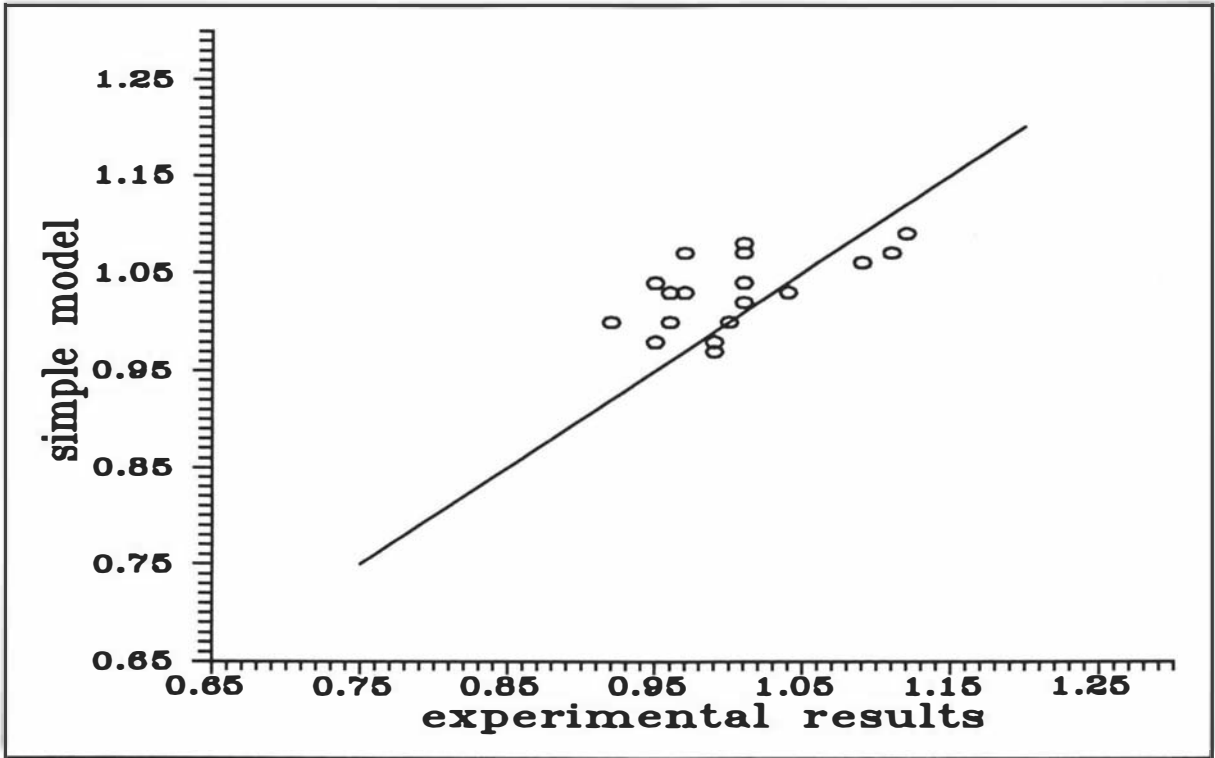


Figure 9.21 Comparisons of the values of j_{cEvap}/j_{cConv} between the simple model and the experimental results.

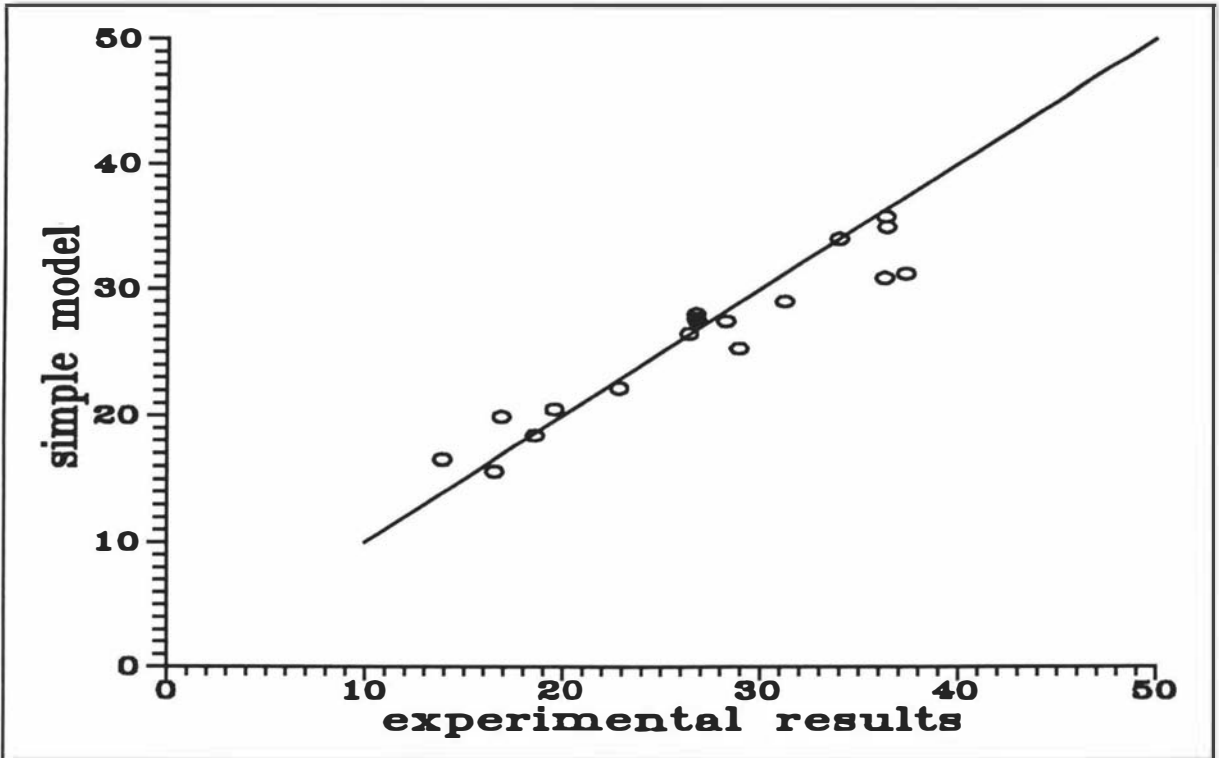


Figure 9.22 Comparisons of time (min.) to reach the centre temperature corresponding to $Y_{c,exp} = 0.10$ between the simple model and the experimental results.

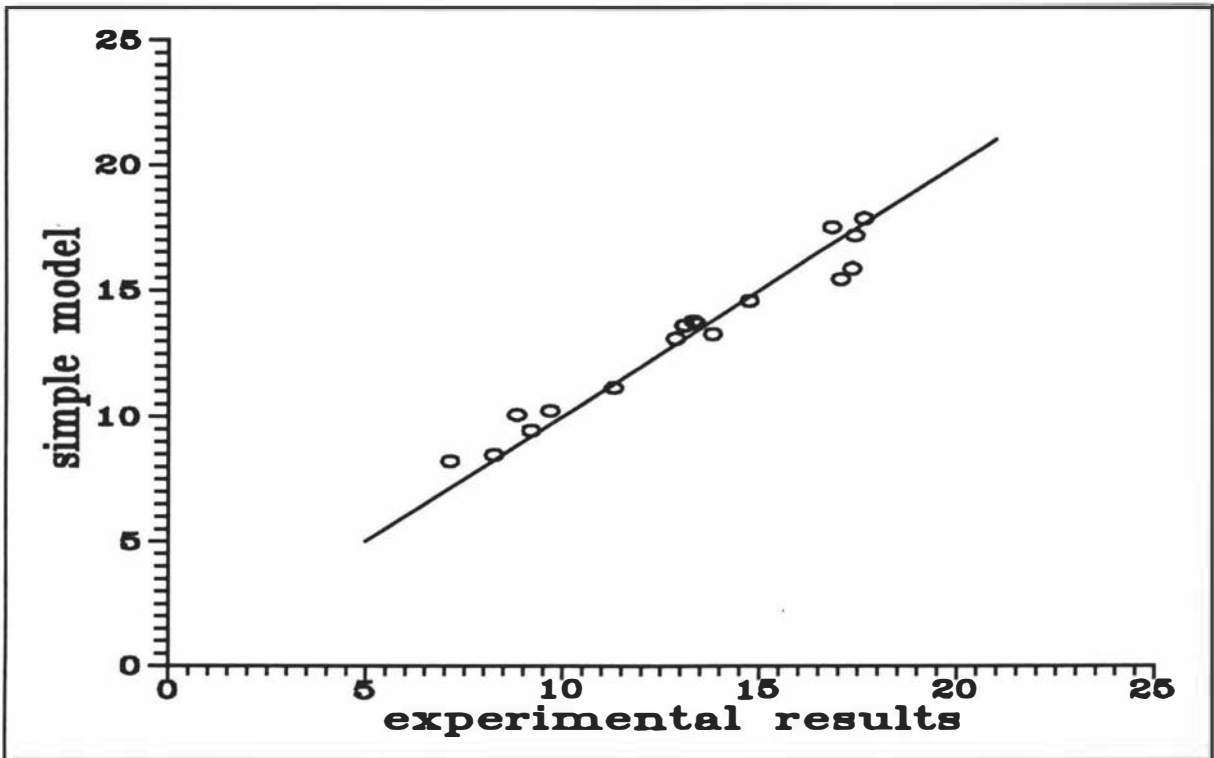


Figure 9.23 Comparisons of time (min.) to reach the centre temperature corresponding to $Y_{c,exp} = 0.35$ between the simple model and the experimental results.

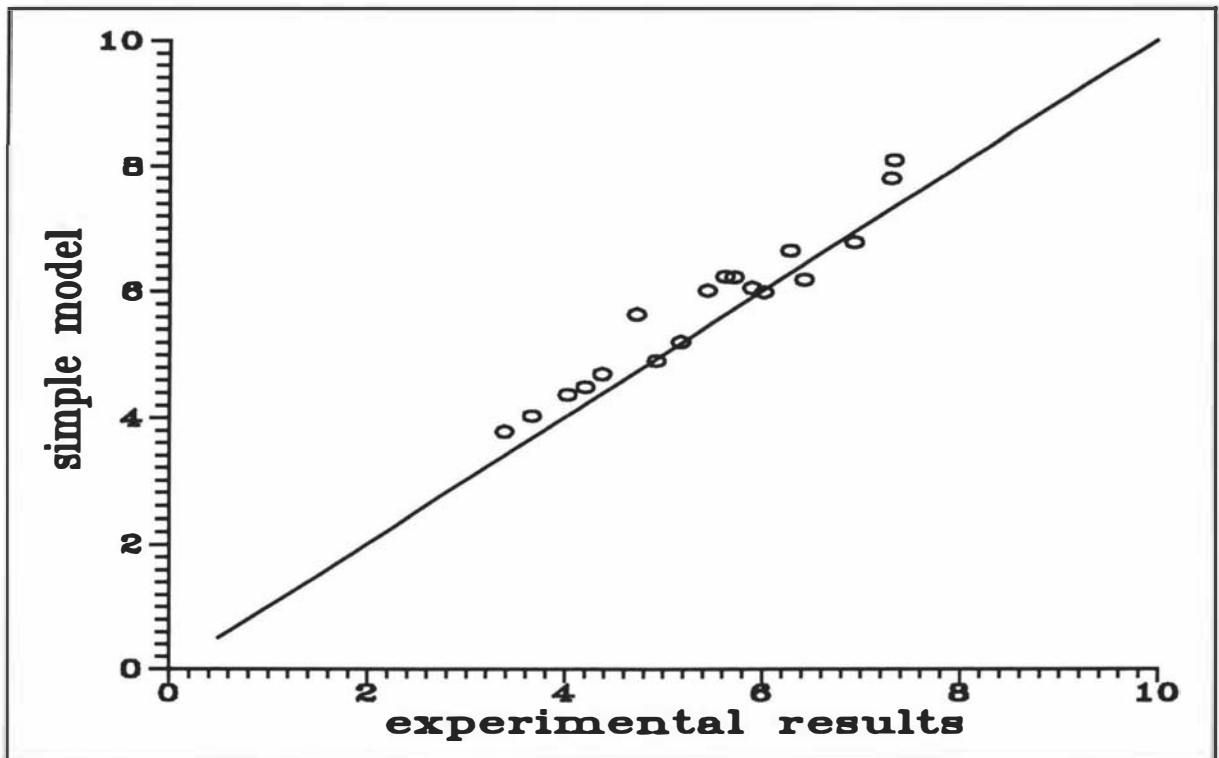


Figure 9.24 Comparisons of time (min.) to reach the centre temperature corresponding to $Y_{c,exp} = 0.70$ between the simple model and the experimental results.

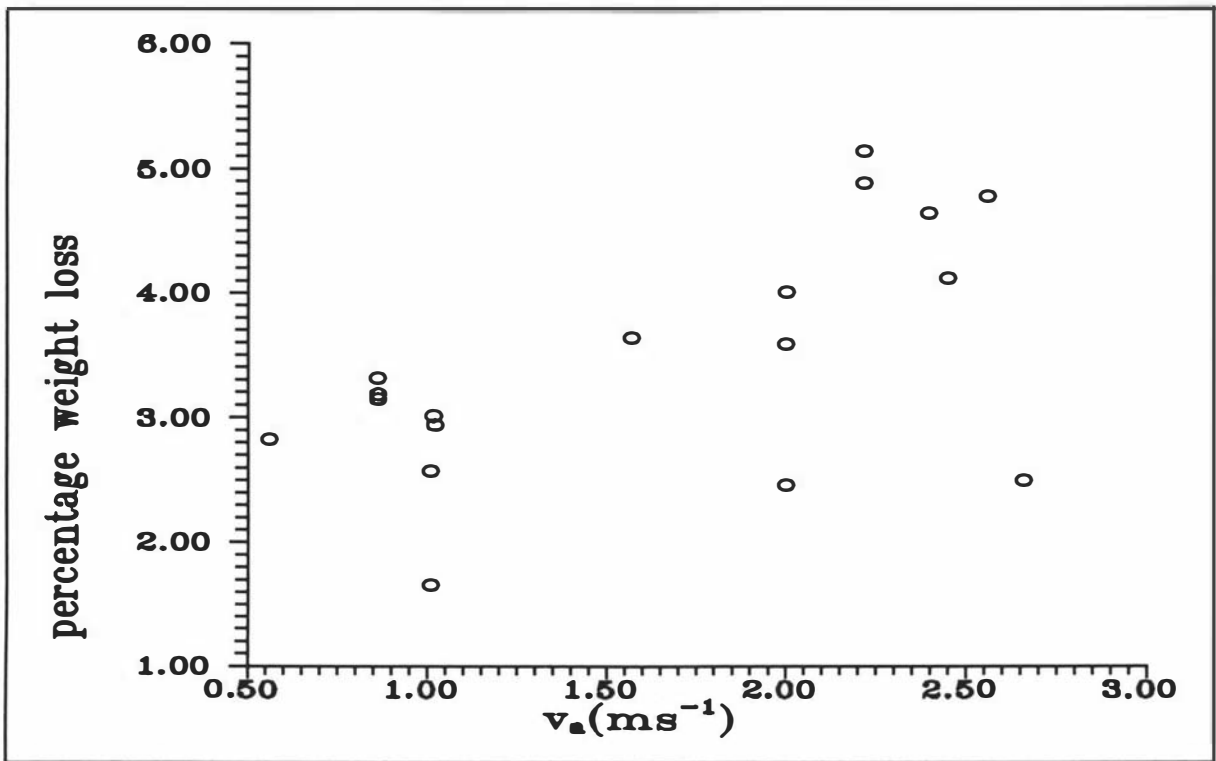


Figure 9.25 Weight loss of peeled carrots vs air velocity.

10. TESTING OF THE PROPOSED MODEL AGAINST EXPERIMENTAL DATA FOR A REAL PRODUCT WITH SKIN RESISTANCE

10.1 INTRODUCTION

This chapter describes the use of the experimental chilling data for unpeeled carrots to assess the accuracy of the simple prediction method described in Chapter 5 for a product with significant skin resistance, and as appropriate, to develop rules of thumb for adapting the method for non-constant surface water activity. In total, there were 28 experimental trials which are summarised in Table 10.1.

As expected, under the same environmental conditions, the cooling curves of peeled and unpeeled carrot were different (e.g. Figure 10.1). For an unpeeled carrot, there is an additional major resistance to moisture movement in the surface layer which lowers evaporation rate and thus rate of cooling. One can visualise two water activities, that immediately below the skin which Chapter 9 suggests is approximately 0.977 (because water movement through the underlying tissue was proven to be rapid), and that of the skin surface in contact with the air. If water movement through the skin is relatively slow, and the product surface temperature high there will be rapid surface water loss, thus lowering a_w . These circumstances arise at the start of chilling as Figure 10.2 shows. As cooling proceeds and the surface temperature drops a_w goes through a minimum value at which the water movement through the skin equals the evaporation rate. Thereafter, evaporation continues to be retarded as the surface temperature drops, and as a result a_w rises. Eventually a quasi-equilibrium state is reached (no further temperature change, constant evaporation rate). This is only a quasi-steady state because such a state can only exist while total water depletion does not significantly affect the values of a_w immediately below the skin. Such a quasi-equilibrium state will arise in most food chilling processes similar to those used in the present work. For simplicity the terms "active chilling" and "quasi-equilibrium" will be used to refer to the two stages of the process.

10.2 SURFACE WATER ACTIVITY IN THE QUASI-EQUILIBRIUM STAGE

As discussed in Chapter 8, the apparent steady state condition at 3.5 hours was used as an approximation to the true equilibrium state as all runs had reached steady state within the sensitivity of the measurement system in less than this time. As was the case in Chapter 9. The value of temperature reached was designated $T_{eq,exp}$.

In Chapter 9, for peeled carrots it was found that the model based on the Lewis relationship (equation 5.11) accurately predicted measured steady state temperature, $T_{eq,exp}$, when $a_w = 0.977$ (mean measured initial value) was used to represent the surface condition reached.

For an unpeeled carrot, a_w cannot be experimentally measured (as described in Chapter 8). However, the experimental equilibrium temperatures can be used to back-calculate a_w using equation (5.11). Figure 10.3 plots values of a_w calculated in this manner versus H_r for all 28 runs. The relationship between the back-calculated a_w value and H_r could be best-fitted by:

$$a_w = 0.792H_r + 0.215 \quad (R^2 = 0.853) \quad (10.1)$$

These results are in contrast to Figure 9.1 in which an equivalent plot is shown for peeled carrots. The effect of skin resistance is very significant in determining the quasi-equilibrium condition. In Figure 10.3 a line in which $a_w = H_r$ is also shown. This line represents the equilibrium that would be expected if skin resistance is very large in which case equation (5.11) suggests that $T_{eq} = T_a$ and thus at equilibrium $a_w = H_r$ (so there is no evaporation). The skin resistance of the carrots is sufficient to make the carrots behave more like this than a fully wetted carrot surface ($a_w = 0.977$).

In theory, the quasi-equilibrium a_w might also depend on Bi (rising Bi reduces external resistance to evaporation), and T_a (higher T_a lifts water vapour pressure and thus potential for evaporation). Plots of back-calculated a_w versus these variables showed no trends distinguishable from experimental error, indicating that the effects of these variables are much smaller than the effect of H_r .

In summary, the relationship between a_w and H_r in the quasi-equilibrium state can be

represented as follows:

- (A) $a_w = \text{constant}$, (peeled carrot, no skin resistance, rapid internal water movement)
- (B) $a_w = H_r$, (large skin resistance or slow internal water movement)
- (C) a_w represented by equation (10.1), (unpeeled carrots under the conditions studied in the present work).

Table 10.1 includes comparisons of predicted values of T_{eq} ($T_{eq,pred}$) with $T_{eq,exp}$ for each of these three models. Only equation (10.1) achieves the quality of fit reported in Chapter 9 for peeled carrots, but $a_w = H_r$ introduces only a modest extra error.

10.3 LINEARIZATION OF SEMI-LOG PLOTS

As expected, in the runs when the product was wrapped with the plastic film (no evaporation), it was found that at the steady state condition, $T_{eq,exp}$ equalled T_a (e.g. Figure 10.4). Figure 10.5 shows a typically cooling curve with evaporation. Using $T_{eq,exp}$ (the measured quasi-equilibrium temperature) in calculation of $Y_{c,exp}$, the plots of $\ln Y_{c,exp}$ versus FO were linearised within a tolerance for experimental uncertainty; for example Figure 10.6 is the result of linearisation of the data in Figure 10.5. This does not imply that the true relationship is exactly linear, but does suggest that in spite of a variable a_w the linearised semi-log plot is an adequate model for practical purposes.

10.4 f AND j VALUES FOR ACTIVE CHILLING PHASE

To gain some insight into what a_w leads to correct f and j values in active chilling, a_w values were back-calculated from the experimental values of f_{cEvap}/f_{cConv} (in Table 10.1) using equation (5.19) and from j_{cEvap}/j_{cConv} (in Table 10.1) using equation (5.20). This process was expected to lead to significant scatter because the equations had only weak dependence on a_w , and hence experimental error would lead to large shifts in apparent a_w . The a_w obtained from f_{cEvap}/f_{cConv} was designated a_{wf} and a_w obtained from j_{cEvap}/j_{cConv} was designated a_{wj} .

10.4.1 a_{wf}

Figure 10.7 and 10.8 show plots of a_{wf} versus Bi and H_r . A very wide spread of a_{wf} values is seen. Some of the calculated values were negative, but these have been shown as zero on the graphs. Such anomalous results arise solely from the use of experimental data with significant uncertainty in an equation with weak a_w dependence to back-calculate a_w .

For comparison, similar calculations were carried out using the peeled carrot data of Chapter 9. These showed less spread than Figures 10.7 and 10.8, and led to a mean back-calculated a_{wf} value of 1.0. This is very close to the measured a_w value ($a_w = 0.977$) which led to accurate prediction of f_{cEvap}/f_{cConv} . This confirmed that in spite of the effect of experimental error the back-calculation procedure could be useful.

Returning to the unpeeled carrot data, the mean calculated value of a_{wf} was 0.16 (with a standard deviation of 0.21). There were no trends evident in Figures 10.7 and 10.8, nor in similar plots of a_{wf} versus T_a and T_{in} .

These results suggest that to accurately predict f_{cEvap}/f_{cConv} the value of a_{wf} should be low (this implies significant drying out of the product surface in active chilling). Use of $a_{wf} = 0.16$ would be expected to best-fit the experimental data. Table 10.2 shows predictions of f_{cEvap}/f_{cConv} at this a_{wf} value. Also shown are results at $a_{wf} = 0.30$. These are included to show the sensitivity of the predictions to selection of a_{wf} . The standard deviation (about 9 %) is higher than for peeled carrots (about 5.5 %), presumably due to higher experimental error arising from the less defined surface of an unpeeled carrot. Changing between $a_{wf} = 0.16$ and $a_{wf} = 0.30$ moved the mean error from 2.6 % to 8.1 % without changing standard deviation significantly.

10.4.1 a_{wj}

Figure 10.9 and 10.10 show plots of a_{wj} versus Bi and H_r . Again, two negative values arose, but the tendency was for a_{wj} to be high, even greater than 1.0. This relates to the effect of experimental error being amplified by the back-calculation. The mean calculated value of a_{wj}

was 1.23 (with a standard deviation of 0.72) which was higher than the measured initial value of 0.977.

Physically, there is no justification for $a_w > 0.977$, but because j represents the starting point of the process at which a_w is probably at its highest value, $a_{wj} = 0.977$ can be justified as a model. Table 10.2 shows its performance. Neither of Figures 10.9 or 10.10 showed any trends between a_{wj} and Bi or H_r , and similar plots of a_{wj} versus T_a and T_{in} also showed only random scatter.

10.5 COOLING WITH EVAPORATIVE EFFECTS AND CHILLING TIME PREDICTION

The analyses of Sections 10.3 and 10.4 led to the concept that for products in which a constant surface water activity cannot be assumed, different a_w might be required for estimating T_{eq} , f , and j :

T_{eq}	:	a_w in quasi-equilibrium state
j	:	initial a_w (a_{wj})
f	:	mean a_w in active chilling phase (a_{wf})

For unpeeled carrots, greatest accuracy would be expected using:

T_{eq}	:	a_w represented by equation (10.1) (best-fits data)
j	:	$a_{wj} = 0.977$ (initial value)
f	:	$a_{wf} = 0.16$ (best-fits data)

From comparison, other possibilities were also tested:

T_{eq}	:	$a_w = 0.977, a_w = H_r$
j	:	-
f	:	$a_{wf} = 0.30$

Chilling times to reach certain centre temperatures ($T_{c,exp}$) which corresponded to $Y_{c,exp} = 0.10, 0.35, \text{ and } 0.70$ were calculated. The value of $Y_{c,exp}$ was substituted in equation (7.7) to find $T_{c,exp}$ for each run. The corresponding $Y_{c,pred}$ value at which to make the prediction was calculated from equation (7.8), where $T_{eq,pred}$ was the temperature at the quasi-equilibrium state calculated from equation (5.11) using each of the three possible models:

$$(A) a_w = 0.977$$

$$(B) a_w = H_r$$

$$(C) a_w = 0.792H_r + 0.215 \text{ (equation 10.1)}$$

The predicted chilling time, t_{pred} , was then:

$$t_{pred} = \left(\frac{\ln Y_{c, pred} - \ln j_{cEvap, pred \text{ at } a_w}}{k f_{cEvap, pred \text{ at } a_w}} \right) \rho C R^2 \quad (10.2)$$

where $f_{cEvap, pred \text{ at } a_w} =$ predicted value of f_{cEvap} using a_{wf} in equation (5.19)

$j_{cEvap, pred \text{ at } a_w} =$ predicted value of j_{cEvap} using a_{wj} in equation (5.20)

Note that the a_w used to find j and f are not necessarily the same.

Table 10.3 show the summary of comparisons of time (min.) between the experimental results (at $Y_{c,exp} = 0.10, 0.35,$ and 0.70) and the model prediction using different a_{wf} (0.16 or 0.30), a_{wj} (0.977), and a_w for finding $T_{eq, pred}$ (Cases A, B, and C). The error in mean difference was as low as 0 % and as high as -19 %. It can be seen that there was poorer agreement in cases (A) and (B) than in case (C).

Table 10.4 shows more detailed comparisons between the experimental results (at $Y_{c,exp} = 0.10, 0.35,$ and 0.70) and the model predictions using $a_{wf} = 0.30, a_{wj} = 0.977,$ and a_w for $T_{eq, pred}$ from equation (10.1).

Table 10.5 shows more detailed comparisons between the experimental results (at $Y_{c,exp} = 0.10, 0.35,$ and 0.70) and the model prediction using $a_{wf} = 0.16, a_{wj} = 0.977,$ and a_w for $T_{eq, pred}$ from equation (10.1).

As expected $a_{wj} = 0.977, a_{wf} = 0.16,$ and use of equation (10.1) to evaluate a_w for estimating $T_{eq, pred}$ gave best predictions overall. Generally, predictions at $Y_{c,exp} = 0.70$ were poor due to non-linearity of the $\ln Y_{c,exp}$ versus FO plot. During experiments in which a_w was changing the time at which linearity was established was larger than a_w was constant. Those sets of predictions for which the $T_{eq, pred}$ predictions were poor were worse at temperature corresponding to $Y_{c,exp} = 0.10$ than for higher Y values. When $Y_{c,exp}$ is close to zero, any error

in $T_{eq,pred}$ is much more significant in its effect on chilling time prediction than at higher Y values.

In comparison to $a_{wf} = 0.16$, $a_{wj} = 0.977$, and use of equation (10.1) the effect of using less product - specific models can be assessed (Table 10.3):

- (1) Use of $a_w = H_r$ in finding $T_{eq,pred}$. The mean difference was increased by about 10 %, standard deviation barely altered.
- (2) Use of $a_w = 0.977$ in finding $T_{eq,pred}$. Results adequately predicted except at low $Y_{c,exp}$.
- (3) Use of $a_{wf} = 0.30$. Mean difference drops by about 5 %.
- (4) Use of both $a_w = H_r$ for $T_{eq,pred}$ and $a_{wf} = 0.30$. The errors introduced roughly cancel.
- (5) Use of both $a_w = 0.977$ for $T_{eq,pred}$ and $a_{wf} = 0.30$. Worst predictions.

Purely chance, if the situation - specific formula (equation 10.1) had not been available and $a_w = H_r$ had been used in finding $T_{eq,pred}$, and if $a_{wf} = 0.30$ had been arbitrarily chosen, predictions of almost equal accuracy to the best situation - specific formulae would have resulted.

10.8 WEIGHT LOSS

Measured weight loss during the 3.5 hour cooling process ranged between -0.1 % and 1.5 % (Table 10.1). It was found that weight loss tended to reduce at higher relative humidity and air velocity. However the uncertainty in these data (as described in Chapter 8) was significant. The weight loss data are not necessary to test the ability of the model to predict cooling rate, but are reported here to help others who may wish to use the experimental data in the future.

Table 10.1 Experimental data for experiments with unpeeled carrot and comparisons of measured quasi-equilibrium temperature ($T_{eq,exp}$) to predictions of T_{eq} calculated using (A) $a_w = 0.977$, (B) $a_w = H_r$, (C) a_w calculated from equation (10.1).

Run	2R (m)	T_{in} (°C)	T_a (°C)	$T_{eq,exp}$ (°C)	H_r (%)	v_a (ms ⁻¹)	h_c (Wm ⁻² K ⁻¹)	Bi	f_{cEvap} (exp.)	j_{cEvap} (exp.)	f_{cEvap}/f_{cCom} (exp)	j_{cEvap}/j_{cCom} (exp)	ΔT_{eq} (°C)			weight loss (%)
													A	B	C	
1	0.031	19.2	1.9	1.3	69	0.9	19.25	0.58	-1.42	1.19	1.42	1.05	-1.2	0.5	0.1	1.9
2	0.029	27.8	1.9	1.3	70	0.9	20.05	0.56	-1.26	1.08	1.30	0.96	-1.1	0.6	0.2	2.0
3	0.024	18.5	10.0	9.5	76	0.9	20.92	0.49	-1.19	1.07	1.37	0.97	-1.4	0.6	0.0	1.5
3*	0.028	20.0	10.0	9.7	75	0.9	19.51	0.52	-1.21	1.09	1.31	0.98	-1.6	0.3	-0.3	1.0
4	0.035	28.2	10.1	9.3	75	0.9	18.21	0.61	-1.43	1.04	1.36	0.91	-1.2	0.7	0.2	2.0
4*	0.030	27.7	10.1	9.6	77	0.9	19.77	0.57	-1.26	1.07	1.28	0.95	-1.3	0.5	-0.0	0.9
5	0.029	19.7	2.2	1.7	85	0.9	20.11	0.55	-1.26	1.10	1.30	0.97	-0.2	0.5	0.3	0.8
6	0.033	28.1	2.2	1.7	86	0.9	19.22	0.61	-1.60	1.10	1.51	0.97	-0.2	0.5	0.3	1.2
7	0.029	19.7	10.5	10.1	85	0.9	19.95	0.56	-1.36	1.04	1.40	0.93	-0.8	0.4	0.0	0.5
7*	0.030	19.3	10.7	10.4	91	0.9	19.58	0.57	-1.33	1.01	1.34	0.90	-0.3	0.2	0.1	0.2
7*	0.029	19.2	10.7	10.5	90	0.9	20.20	0.56	-1.42	1.00	1.46	0.88	-0.5	0.2	-0.1	0.9
8	0.031	26.6	10.2	10.1	89	0.9	19.37	0.57	-1.51	1.19	1.52	1.05	-0.6	0.2	-0.1	0.5
8*	0.032	27.7	10.8	10.5	90	0.9	19.11	0.58	-1.48	1.04	1.47	0.92	-0.5	0.2	-0.0	0.3
8*	0.028	28.0	10.4	10.2	90	0.9	20.49	0.56	-1.39	1.12	1.48	1.00	-0.5	0.1	-0.1	0.3

* replicated run

Table 10.1 Experimental data for experiments with unpeeled carrot and comparisons of measured quasi-equilibrium temperature ($T_{eq,exp}$) to predictions of T_{eq} calculated using (A) $a_w = 0.977$, (B) $a_w = H_r$, (C) a_w calculated from equation (10.1). (continued)

Run	2R (m)	T_{in} (°C)	T_a (°C)	$T_{eq,exp}$ (°C)	H_r (%)	v_a (ms ⁻¹)	h_c (Wm ⁻² K ⁻¹)	Bi	$f_{cb,exp}$ (exp.)	$j_{cb,exp}$ (exp.)	$f_{cb,exp}/f_{c,com}$ (exp)	$j_{cb,exp}/j_{c,com}$ (exp)	ΔT_{eq} (°C)			weight loss (%)
													A	B	C	
9	0.022	19.4	0.9	0.5	79	2.1	34.89	0.74	-1.31	1.08	1.06	0.93	-0.7	0.4	0.1	0.0
10	0.025	27.6	1.0	10.7	80	2.8	37.26	0.89	-1.52	1.09	1.06	0.91	-0.4	0.5	0.2	-0.1
11	0.028	20.1	11.1	10.9	75	2.2	31.41	0.85	-2.14	1.22	1.54	1.03	-1.9	0.1	-0.4	1.5
11*	0.028	20.1	10.7	10.4	81	2.2	31.41	0.85	-1.84	1.11	1.33	0.94	-1.2	0.3	-0.1	1.1
12	0.030	27.8	11.0	10.4	75	2.2	29.91	0.89	-2.16	1.15	1.51	0.97	-1.4	0.7	0.2	1.7
12*	0.029	27.8	10.7	10.4	81	2.2	30.87	0.86	-2.03	1.21	1.45	1.02	-1.1	0.3	-0.1	1.4
13	0.032	19.6	1.1	0.9	89	2.7	31.53	0.99	-1.83	1.28	1.17	1.06	-0.3	0.2	0.0	-0.1
14	0.031	28.1	1.1	0.9	89	2.4	31.06	0.94	-1.67	1.22	1.12	1.02	-0.3	0.2	0.0	0.0
15	0.024	19.5	10.9	10.8	89	2.5	35.72	0.84	-1.84	1.04	1.34	0.88	-0.6	0.1	-0.1	0.3
16	0.030	28.3	11.1	10.7	89	2.2	29.92	0.88	-2.35	1.29	1.65	1.09	-0.4	0.4	0.1	0.4
17	0.026	23.9	4.8	4.2	79	1.7	29.10	0.72	-1.37	1.05	1.13	0.91	-0.7	0.5	0.2	0.7
17*	0.027	23.7	5.1	4.6	79	1.7	28.22	0.74	-1.62	1.11	1.31	0.95	-0.8	0.2	0.1	0.5
18	0.026	24.3	5.1	4.9	79	1.7	28.59	0.73	-1.50	1.20	1.23	1.04	-1.3	0.3	-0.2	0.1
18*	0.028	24.2	4.9	4.5	79	1.7	27.63	0.75	-1.65	1.18	1.31	1.01	-1.0	0.6	-0.0	0.5
												mean	-0.9	0.4	0.0	
												std.	0.5	0.2	0.2	

note:* repeated run

Table 10.2 Comparisons between experimental results and model predictions of f_{cEvap}/f_{cConv} (at $a_{wf} = 0.30$ and 0.16) and j_{cEvap}/j_{cConv} (at $a_{wj} = 0.977$).

Run	T_{in} (°C)	T_a (°C)	H_r (%)	Bi	f_{cEvap}/f_{cConv} (exp)	j_{cEvap}/j_{cConv} (exp)	Model Prediction of					
							f_{cEvap}/f_{cConv} to $a_{wf} = 0.30$		f_{cEvap}/f_{cConv} to $a_{wf} = 0.16$		j_{cEvap}/j_{cConv} to $a_{wj} = 0.977$	
							value	Δ (%)	value	Δ (%)	value	Δ (%)
1	19.2	1.9	69	0.58	1.42	1.05	1.26	-11.2	1.19	-16.3	0.99	-5.5
2	27.8	1.9	70	0.56	1.30	0.96	1.28	-1.7	1.20	-7.7	0.97	0.8
3	18.5	10.0	76	0.49	1.37	0.97	1.57	14.6	1.49	8.9	1.04	7.2
3*	20.0	10.0	75	0.52	1.31	0.98	1.56	19.1	1.48	13.3	1.04	6.0
4	28.2	10.1	75	0.61	1.36	0.91	1.55	13.7	1.47	8.0	1.03	13.0
4*	27.7	10.1	77	0.57	1.28	0.95	1.57	22.3	1.49	16.1	1.03	8.0
5	19.7	2.2	85	0.55	1.30	0.97	1.30	-0.3	1.22	-6.2	1.00	3.4
6	28.1	2.2	86	0.61	1.51	0.97	1.30	-14.0	1.22	-19.2	0.99	1.7
7	19.7	10.5	85	0.56	1.40	0.93	1.60	14.4	1.52	8.9	1.06	13.7
7*	19.3	10.7	91	0.57	1.34	0.90	1.63	21.5	1.55	15.7	1.07	18.7
7*	19.2	10.7	90	0.56	1.46	0.88	1.63	11.6	1.55	6.2	1.07	21.1
8	26.6	10.2	89	0.57	1.52	1.05	1.61	5.9	1.53	0.6	1.04	-0.7
8*	27.7	10.8	90	0.58	1.47	0.92	1.63	11.2	1.55	5.6	1.05	13.7
8*	28.0	10.4	90	0.56	1.48	1.00	1.63	14.0	1.55	8.2	1.04	3.9

note: * repeated run

Table 10.2 Comparisons between experimental results and model predictions of f_{cEvap}/f_{cConv} (at $a_{wf} = 0.30$ and 0.16) and j_{cEvap}/j_{cConv} (at $a_{wj} = 0.977$). (continued)

Run	T_{in} (°C)	T_a (°C)	H , (%)	Bi	f_{cEvap}/f_{cConv} (exp)	j_{cEvap}/j_{cConv} (exp)	Model Prediction of					
							f_{cEvap}/f_{cConv} to $a_{wf} = 0.30$		f_{cEvap}/f_{cConv} to $a_{wf} = 0.16$		j_{cEvap}/j_{cConv} to $a_{wj} = 0.977$	
							value	Δ (%)	value	Δ (%)	value	Δ (%)
9	19.4	0.9	79	0.74	1.06	0.93	1.22	15.4	1.16	9.0	1.01	8.1
10	27.6	1.0	80	0.89	1.06	0.91	1.22	15.2	1.16	8.9	1.00	9.6
11	20.1	11.1	75	0.85	1.54	1.03	1.50	-2.8	1.43	-6.9	1.07	4.2
11*	20.1	10.7	81	0.85	1.33	0.94	1.51	13.4	1.44	8.6	1.08	14.7
12	27.8	11.0	75	0.89	1.51	0.97	1.50	-0.6	1.44	-4.9	1.06	9.3
12*	27.8	10.7	81	0.86	1.45	1.02	1.51	4.4	1.45	-0.2	1.06	4.2
13	19.6	1.1	89	0.99	1.17	1.06	1.21	3.6	1.15	-1.6	1.02	-3.5
14	28.1	1.1	89	0.94	1.12	1.02	1.23	9.6	1.16	3.7	1.01	-1.4
15	19.5	10.9	89	0.84	1.34	0.88	1.54	15.2	1.48	10.3	1.09	3.2
16	28.3	11.1	89	0.88	1.65	1.09	1.55	-6.2	1.48	-10.3	1.07	-1.5
17	23.9	4.8	79	0.72	1.13	0.91	1.35	19.8	1.28	13.6	1.02	12.0
17*	23.7	5.1	79	0.74	1.31	0.95	1.36	3.9	1.29	-1.4	1.02	7.7
18	24.3	5.1	79	0.73	1.23	1.04	1.36	10.7	1.29	4.9	1.02	-1.8
18*	24.2	4.9	79	0.75	1.31	1.01	1.35	3.1	1.28	-2.2	1.02	1.2
						mean		8.1		2.6		6.1
						std.		9.4		9.1		6.6

note:* repeated run

Table 10.3 Comparisons of time (to the temperature that corresponds to $Y_{c,exp} = 0.10, 0.35, \text{ and } 0.70$) between the experimental results and simple model using $a_{wf} = 0.16$ & $a_{wj} = 0.977$, and $a_{wf} = 0.30$ & $a_{wj} = 0.977$, and $T_{eq,pred}$ at (A) $a_w = 0.977$, (B) $a_w = H_r$, and (C) $a_w = 0.792H_r + 0.215$.

simple model		% difference in time								
		(A) $T_{eq,pred}$ at $a_w = 0.977$			(B) $T_{eq,pred}$ at $a_w = H_r$			(C) $T_{eq,pred}$ at $a_w = 0.792H_r + 0.215$		
		$Y_{c,exp}$ [0.10]	$Y_{c,exp}$ [0.35]	$Y_{c,exp}$ [0.70]	$Y_{c,exp}$ [0.10]	$Y_{c,exp}$ [0.35]	$Y_{c,exp}$ [0.70]	$Y_{c,exp}$ [0.10]	$Y_{c,exp}$ [0.35]	$Y_{c,exp}$ [0.70]
$a_{wf} = 0.30$ & $a_{wj} = 0.977$	mean	-19.0	-10	-0.2	5.7	1.3	6.5	-5.3	-2.8	4.1
	std.	11.4	8.7	10.0	10.6	7.9	10.6	9.3	7.7	10.2
$a_{wf} = 0.16$ & $a_{wj} = 0.977$	mean	-14.7	-5.2	5.1	11.3	6.7	12.1	-0.2	2.4	9.6
	std.	12.3	9.4	10.6	11.3	6.7	12.1	10.1	8.3	10.7

Table 10.4 Predicted (using $a_{wf} = 0.30$, $a_{wj} = 0.977$, and a_w from equation 10.1 in equation 10.2) and measured chilling time to the time that corresponds to $Y_{c,exp} = 0.10$, 0.35, and 0.70 for an unpeeled carrot.

Run	time (min.) to $Y_{c,exp} = 0.10$			time (min.) to $Y_{c,exp} = 0.35$			time (min.) to $Y_{c,exp} = 0.70$		
	simple model	exp.	Δ (%)	simple model	exp.	Δ (%)	simple model	exp.	Δ (%)
1	61.0	54.4	12.1	29.0	26.9	7.9	11.7	11.7	0.2
2	55.4	53.2	4.3	26.1	25.1	3.6	10.1	9.6	5.0
3	34.7	38.8	-10.7	17.0	18.4	-7.7	7.1	7.1	0.8
3*	38.7	49.1	-21.2	20.0	23.4	-14.7	8.6	9.1	-6.0
4	58.8	61.8	-5.0	28.4	28.7	-1.2	12.0	10.4	15.5
4*	45.6	54.6	-16.4	22.4	25.8	-13.0	9.4	9.9	-4.1
5	54.9	51.0	7.7	25.6	24.3	5.4	10.4	9.6	8.3
6	63.9	52.5	21.9	30.1	25.0	20.4	12.1	9.9	23.1
7	44.0	47.6	-7.5	21.7	22.2	-2.1	9.4	8.1	16.0
7*	49.1	54.5	-10	24.2	25.0	-3.3	10.6	8.6	22.5
7*	39.6	44.2	-10.5	19.9	21.4	-6.8	8.8	8.7	0.2
8	47.0	51.3	-8.4	23.4	25.4	-7.6	10.1	11.0	-8.3
8*	54.0	57.5	-6.1	26.8	26.8	-0.1	11.5	9.8	17.7
8*	37.5	42.8	-12.5	18.6	20.6	-9.7	8.0	8.4	-4.6

note:* repeated run

Table 10.4 Predicted (using $a_{wf} = 0.30$, $a_{wj} = 0.977$, and a_w from equation 10.1 in equation 10.2) and measured chilling time to the time that corresponds to $Y_{c,exp} = 0.10, 0.35$, and 0.70 for an unpeeled carrot. (continued)

Run	time (min.) to $Y_{c,exp} = 0.10$			time (min.) to $Y_{c,exp} = 0.35$			time (min.) to $Y_{c,exp} = 0.70$		
	simple model	exp.	Δ (%)	simple model	exp.	Δ (%)	simple model	exp.	Δ (%)
9	26.3	29.0	-9.4	12.8	13.7	-7.1	5.4	5.3	2.1
10	29.9	32.5	-8.0	14.5	15.4	-5.8	6.3	6.0	4.3
11	26.3	28.8	-8.9	14.4	14.4	0.0	6.9	6.4	7.4
11*	28.5	32.2	-11.5	14.9	15.4	-3.4	7.0	6.1	13.7
12	35.7	34.1	4.6	18.0	16.6	8.3	8.2	7.0	18.4
12*	29.8	31.3	-4.9	15.3	15.6	-2.0	7.0	6.9	2.3
13	45.3	47.5	-4.5	22.7	24.2	-6.1	10.2	11.3	-9.4
14	42.8	47.1	-9.1	21.2	23.5	-9.7	9.3	10.4	-10.8
15	22.9	27.2	-16.0	12.0	13.7	-12.6	5.6	6.2	-9.1
16	35.5	32.7	8.5	17.8	16.7	6.5	8.2	7.8	4.7
17	33.9	37.4	-9.4	16.4	17.5	-6.3	7.0	6.5	8.1
17*	35.6	35.3	0.9	17.4	16.9	2.8	7.5	6.7	11.3
18	33.4	38.7	-13.6	16.9	19.2	-12.2	7.3	8.4	-12.8
18*	38.5	39.7	-3.4	19.1	19.6	-2.4	8.3	8.4	-1.2
mean			-5.3			-2.8			4.1
std.			9.3			7.7			10.2

note: * repeated run

Table 10.5 Predicted (using $a_{wf} = 0.16$, $a_{wj} = 0.977$, and a_w from equation 10.1 in equation 10.2) and measured chilling time to the time that corresponds to $Y_{c,exp} = 0.10, 0.35$, and 0.70 for an unpeeled carrot.

Run	time (min.) to $Y_{c,exp} = 0.10$			time (min.) to $Y_{c,exp} = 0.35$			time (min.) to $Y_{c,exp} = 0.70$		
	simple model	exp.	Δ (%)	simple model	exp.	Δ (%)	simple model	exp.	Δ (%)
1	64.7	54.4	18.9	30.8	26.9	14.5	12.4	11.7	6.3
2	59.0	53.2	11.1	27.7	25.1	10.4	10.8	9.6	11.9
3	36.5	38.8	-6.1	17.8	18.4	-2.9	7.5	7.1	6.1
3*	40.7	49.1	-17.1	21.0	23.4	-10.3	9.0	9.1	-1.2
4	61.8	61.8	0.0	29.8	28.7	4.0	12.6	10.4	21.5
4*	48.1	54.6	-11.9	23.6	25.8	-8.4	10.1	9.9	1.0
5	58.4	51.0	14.5	27.3	24.3	12.1	11.0	9.6	15.2
6	68.1	52.5	29.8	32.1	25.0	28.2	12.9	9.9	31.1
7	46.3	47.6	-2.8	22.8	22.2	2.9	9.9	8.1	21.8
7*	51.6	54.5	-5.5	25.4	25.0	1.6	11.1	8.6	28.6
7*	41.6	44.2	-6.0	20.9	21.4	-2.1	9.2	8.7	5.3
8	49.5	51.3	-3.6	24.7	25.4	-2.7	10.6	11.0	-3.4
8*	56.9	57.5	-1.2	28.2	26.8	5.1	12.2	9.8	23.9
8*	39.5	42.8	-7.8	19.6	20.6	-4.8	8.4	8.4	0.5

note: * repeated run

Table 10.5 Predicted (using $a_{wf} = 0.16$, $a_{wj} = 0.977$, and a_w from equation 10.1 in equation 10.2) and measured chilling time to the time that corresponds to $Y_{c,exp} = 0.10, 0.35$, and 0.70 for an unpeeled carrot. (continued)

Run	time (min.) to $Y_{c,exp} = 0.10$			time (min.) to $Y_{c,exp} = 0.35$			time (min.) to $Y_{c,exp} = 0.70$		
	simple model	exp.	Δ (%)	simple model	exp.	Δ (%)	simple model	exp.	Δ (%)
9	27.8	29.0	-4.1	13.5	13.7	-1.7	5.7	5.3	8.1
10	31.6	32.5	-2.8	15.4	15.4	-0.4	6.6	6.0	10.2
11	27.4	28.8	-4.9	15.0	14.4	4.4	7.2	6.4	12.1
11*	29.8	32.2	-7.6	15.6	15.4	0.9	7.3	6.1	18.7
12	37.3	34.1	9.4	18.8	16.6	13.2	8.6	7.0	23.8
12*	31.2	31.3	-0.5	16.0	15.6	2.6	7.4	6.9	7.1
13	47.7	47.5	0.5	23.9	24.2	-1.2	10.7	11.3	-4.7
14	45.2	47.1	-3.9	22.4	23.5	-4.6	9.8	10.4	-5.7
15	23.9	27.2	-12.2	12.5	13.7	-8.7	5.9	6.2	-5.1
16	37.1	32.7	13.5	18.6	16.7	11.4	8.6	7.8	9.6
17	35.7	37.4	-4.4	17.3	17.5	-1.1	7.4	6.5	14.1
17*	37.5	35.3	6.3	18.3	16.9	8.3	7.9	6.7	17.3
18	35.3	38.7	-8.8	17.8	19.2	-7.4	7.7	8.4	-8.1
18*	40.5	39.7	1.8	20.1	19.6	2.9	8.7	8.4	4.1
mean			-0.2			2.4			9.6
std.			10.1			8.3			10.7

note:* repeated run

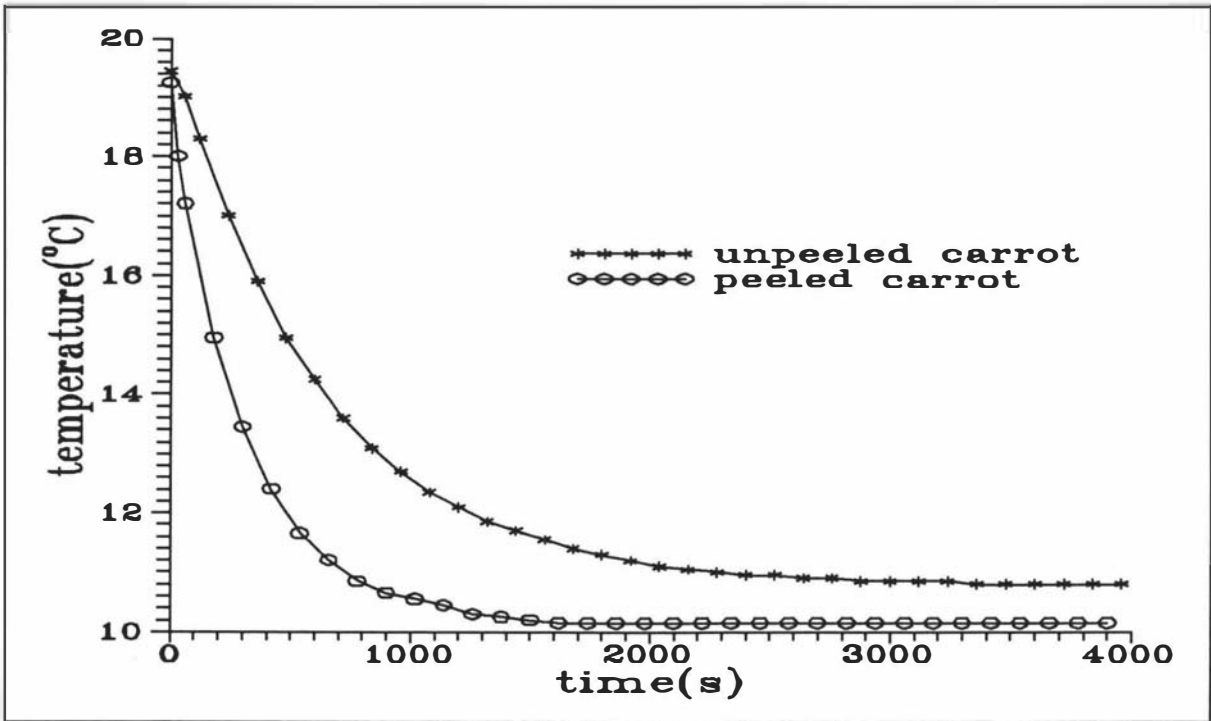


Figure 10.1 Comparison of the cooling curves of peeled and unpeeled carrot under the same environmental conditions (Runs 15 of Table 9.1 and 10.1).

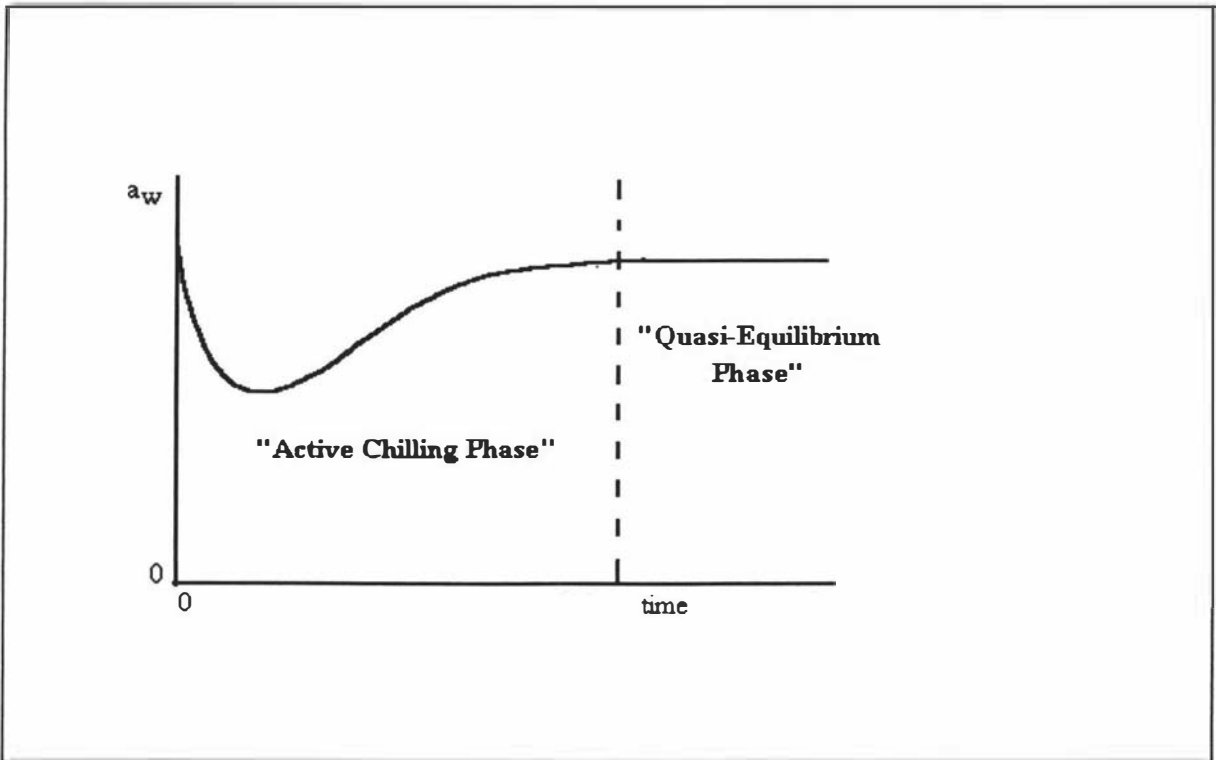


Figure 10.2 Plot of a_w vs time during a typical chilling experiment in which internal water movement rate to the product cannot always exceed evaporation rate.

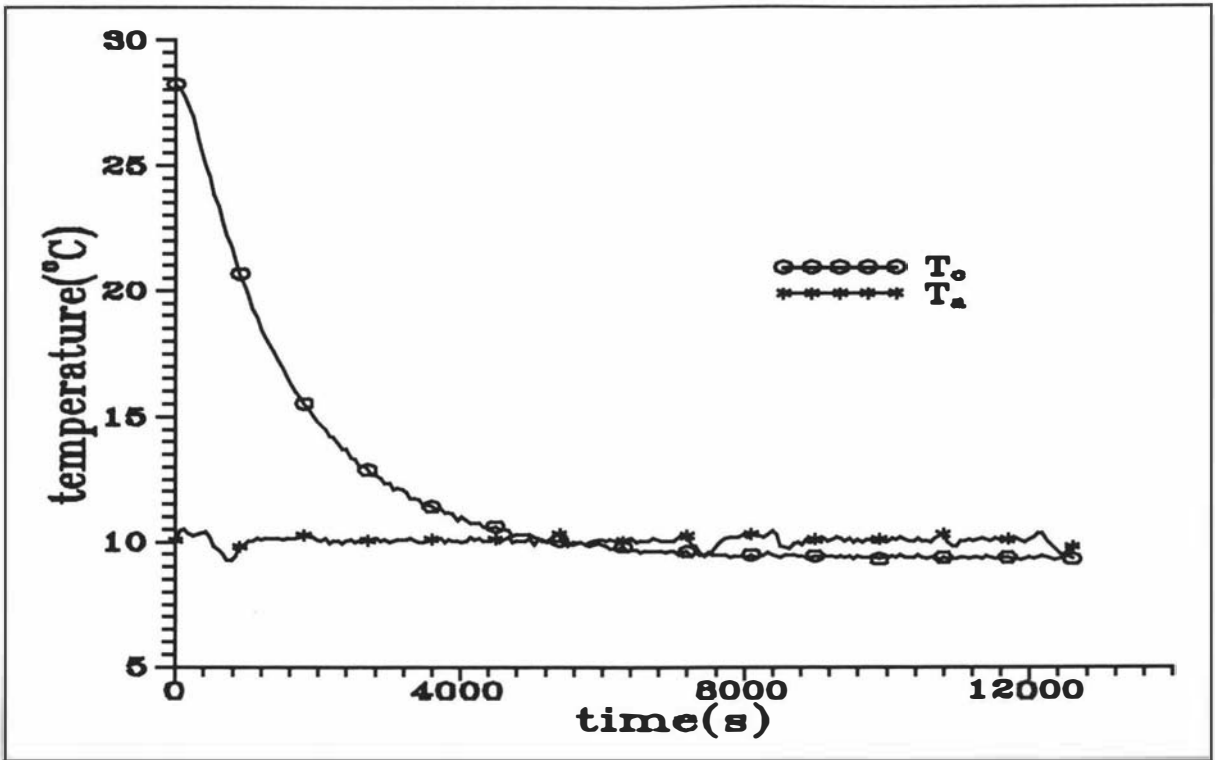


Figure 10.5 Typical plot of temperature vs time for cooling of an unpeeled carrot with evaporation at the product surface.

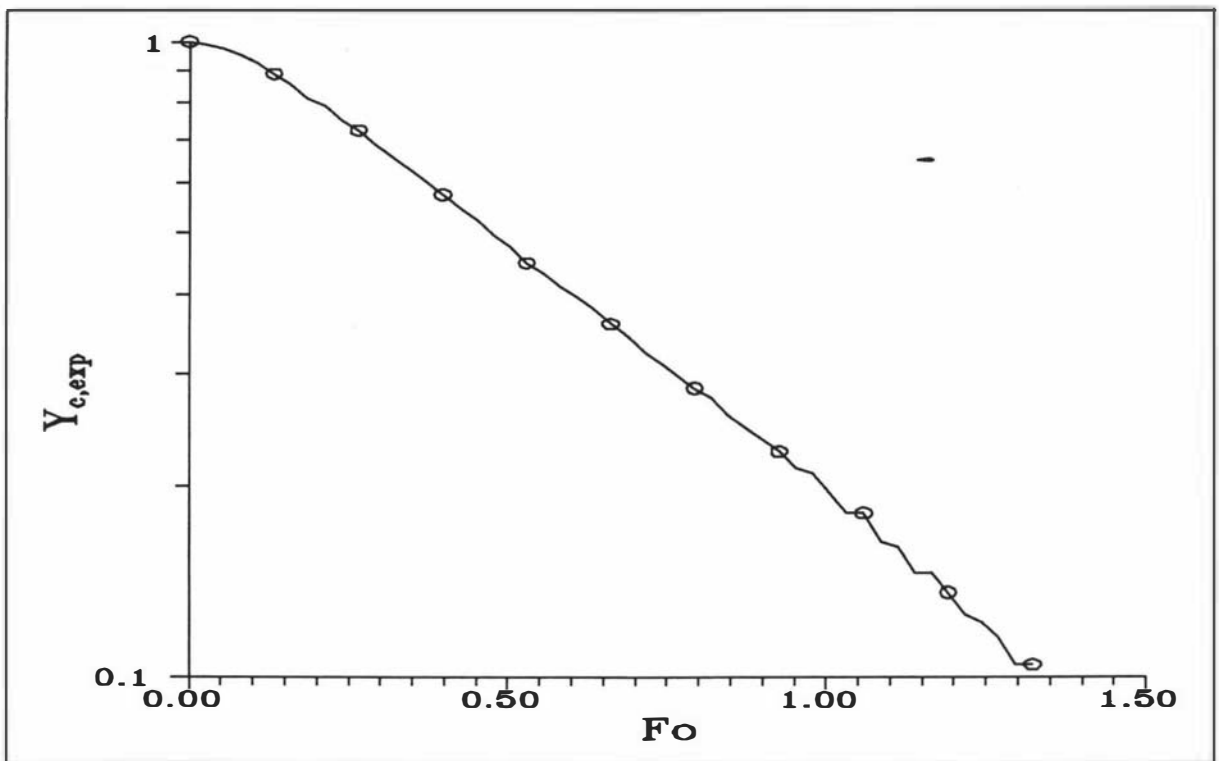


Figure 10.6 Plot of $\ln Y_{c,exp}$ (using $T_{eq,exp}$ as the reference temperature) vs Fo for the conditions in Figure 10.5.

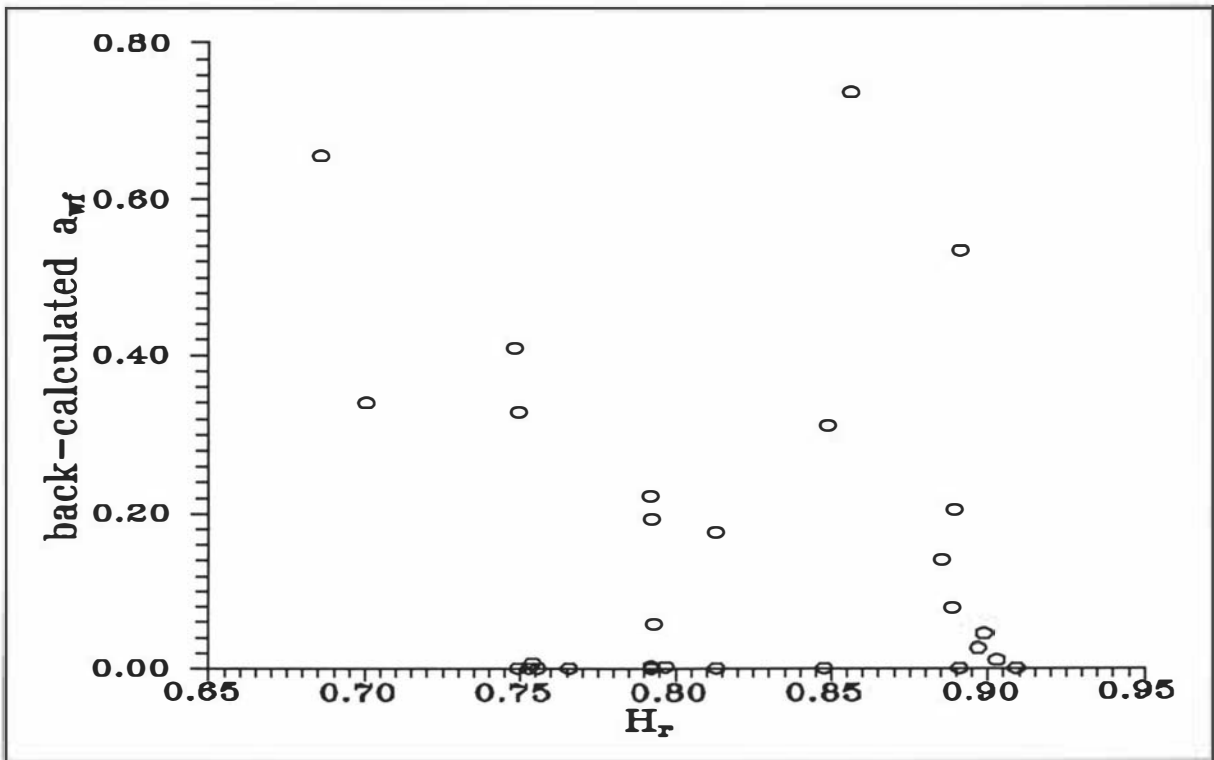


Figure 10.7 Plot of a_{wf} vs H_r during the active chilling phase.

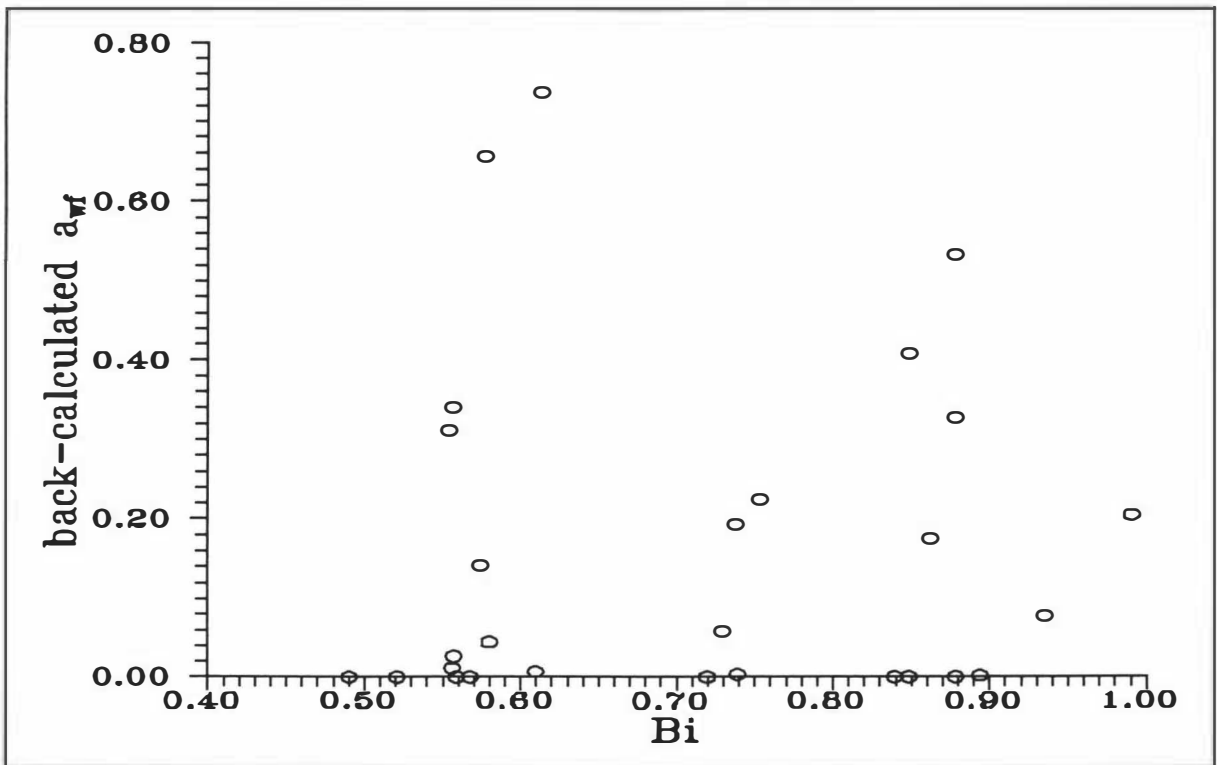


Figure 10.8 Plot of a_{wf} vs Bi during the active chilling phase.

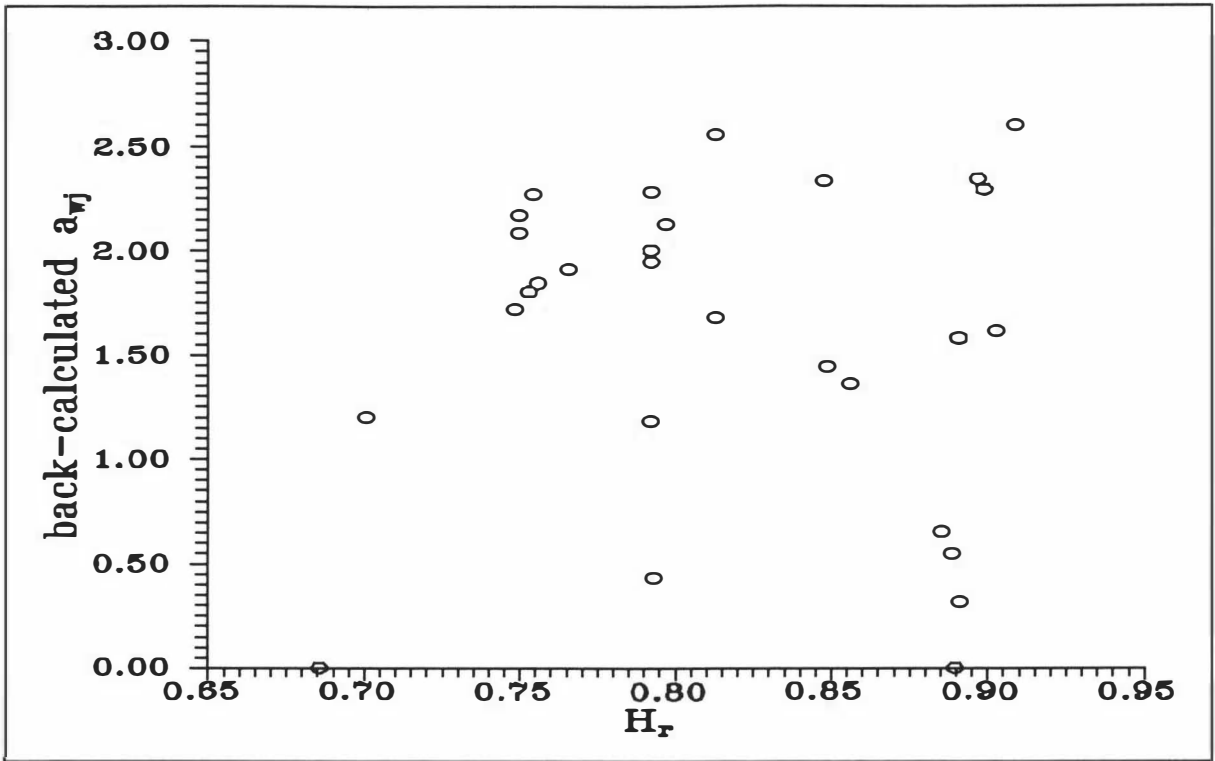


Figure 10.9 Plot of a_{wj} vs H_r during the active chilling phase.

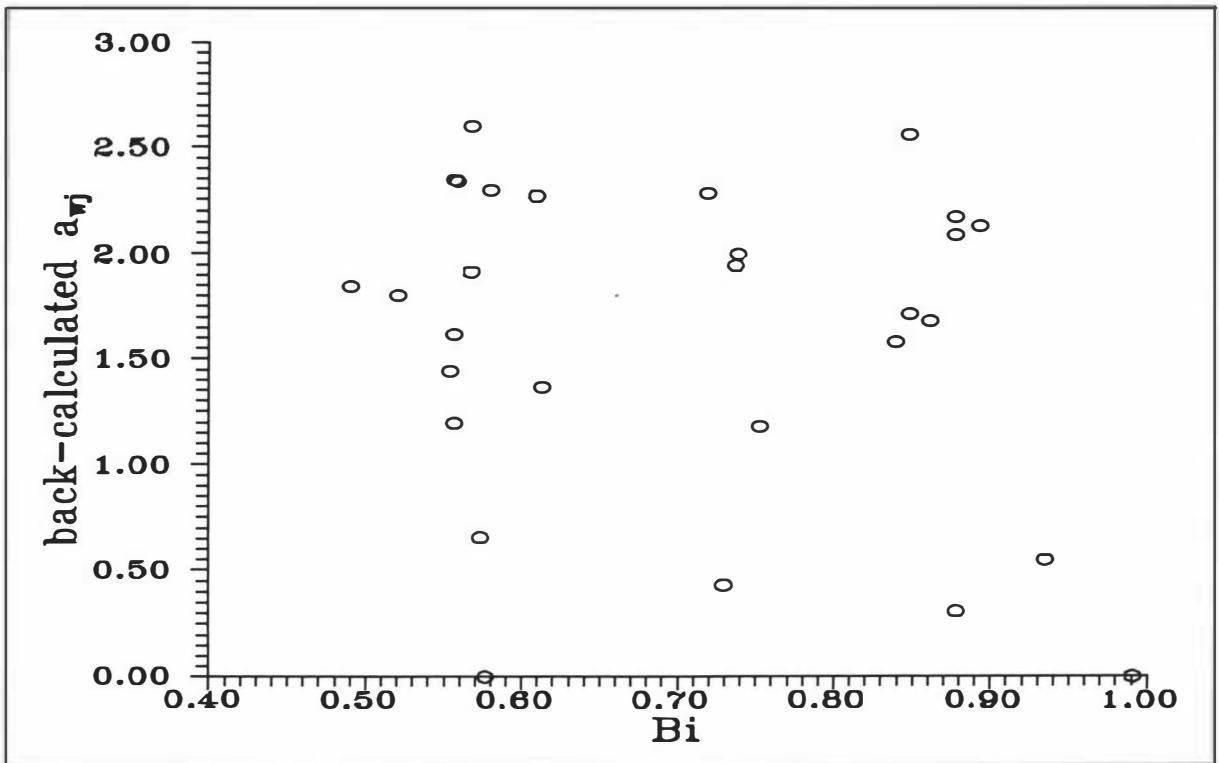


Figure 10.10 Plot of a_{wj} vs Bi during the active chilling phase.

11. DISCUSSION AND CONCLUSION

11.1 DISCUSSION

The philosophy used in this research was to first generate, on a theoretical basis, an algebraic model for predicting chilling times of foods subject to evaporative cooling at the product surface. Initially this model was restricted to simple geometric shapes, constant surface water activity, and to situations where the Lewis relationship applies. Experimental testing using an idealised product was restricted to just the infinite cylinder shape. The observed behaviour matched the predicted chilling profiles within a range of differences which could almost totally be explained by data uncertainties.

Two possibilities for further work were then considered. One was to investigate a greater range of shapes, the other to consider application to real food products in which constant surface water activity may not occur during chilling. The latter was considered to be of higher priority because if the methodology did not apply to real food products its extension to further shapes would have little practical value.

The chilling behaviour of peeled carrots across a range of conditions likely to occur in industrial practice could be adequately represented by the model assuming constant surface water activity. However, the behaviour of unpeeled carrots could not, largely because of the influence of skin resistance on mass transfer. Instead, it was found that three different a_w values were needed in the simple model, an initial (time zero) value used to determine j , a mean value during active chilling used to determine f , and a quasi-equilibrium a_w used to determine T_{eq} . Product-specific values were determined for carrots. Heat generation by respiration did not appear to exert any significant influence.

Two possibilities for further method development were considered. One was to return to Chapters 4 and 5, include the effect of skin resistance in finite difference simulations and derive new curve-fitted algebraic equations including the extra variable. In this approach a_w would be assumed to be constant under the skin.

The other approach was to consider skin resistance only in that it leads to a lower, and possibly time-variable, surface water activity on the product outer surface and then to seek empirical means to define the effect of the time varying surface water activity on cooling rate. In seeking generality, a weakness of the former approach is that there are products without skins whose surface activity varies with time because internal water movement cannot maintain a constant surface concentration during cooling. The second approach allows such products to be treated in the same way as those with skins. There was not time to consider both approaches so only the latter was selected for study.

In an attempt to generalise the carrot results the concept of bounds was introduced. This can be illustrated by Figure 10.3.

For estimating $T_{eq,pred}$ for unpeeled carrots the possible bounds are:

upper bound : $a_w = 0.977$

lower bound : $a_w = H_r$

For other products where a best-fit equation such as equation (10.1) is not available it would be useful to provide advice to users of the proposed method. Based on the results for peeled and unpeeled carrots that advice might be to determine $T_{eq,pred}$ using a_w estimated as follows:

- (A) No skin resistance, rapid water movement internal to product:
 $a_w = \text{constant} = a_w$ for the material prior to the commencement of chilling;
- (B) Significant product skin resistance and/or slow internal water movement internal to product:
 use $a_w = H_r$;
- (C) Intermediary product characteristics:
 a product-specific equation should be used if available, or the user must use judgement to estimate where between the upper and lower bounds a_w might lie.

It is worth noting that even the skin of the carrots led to behaviour much closer to the lower bound than the upper bound.

For estimating j the carrot results suggest that upper and lower bounds are not needed and a_{wj}

= a_w for the material prior to the commencement of chilling is recommended.

For estimating f the possible bounds are

upper bound : $a_{wf} = a_w$ for the material prior to the commencement of chilling ($a_w = 0.977$ for unpeeled carrots)

lower bound : $a_{wf} = 0$

It is probable that for other products a_{wf} should be low. It might be expected that if skin resistance is high or internal water movement slow $a_{wf} \rightarrow 0$ will give the best fit. The thin skin of the carrots led to $a_{wf} \rightarrow 0$.

If bounds of this nature are used the method might have wider industrial application. Appendix B illustrates the use of the proposed method, and shows that the arithmetic calculation required can be carried out with a hand calculator. The other approach discussed earlier, that of including skin resistance directly, may yield an equally simple and accurate prediction method if implemented.

11.2 CONCLUSIONS AND RECOMMENDATIONS FOR FUTURE WORK

A chilling time prediction method has been successively developed by curve-fitting algebraic equations for three parameters representing the relative rate of chilling with evaporation at the product surface and chilling with only convection at the surface, to easily measurable parameters such as relative humidity, air temperature, product initial temperature, and (constant) surface water activity. The curve-fit equations predicted chilling times for infinite slabs, infinite cylinders, and spheres, undergoing cooling subject to constant chilling conditions and with constant surface water activity, that agree within $\pm 5\%$ of times predicted by simulations using the finite difference numerical method. Measured centre temperature data collected under idealised experimental conditions in which the surface water activity of infinite cylinders was held constant agreed sufficiently well (within $\pm 10\%$) with both the simple method predictions and the finite difference simulations for the lack of fit to be explainable by experimental uncertainty.

Although not tested experimentally, there is no reason to expect that the simple method would not predict the behaviour of spheres and infinite slabs with sufficient accuracy for the method to be used in industrial situations. Similarly, the ability to predict mass-average temperature has not been tested, but there is no reason in theory to expect poor predictions for the three shapes studied. The accuracy that would arise if the method was applied to other shapes with constant surface water activity is unknown, and this is an area in which further research is justified. The ranges of conditions for which the method is recommended for industrial application are:

Bi	:	0.1 to 10.0
a_w	:	0.6 to 1.0
H_r	:	0.5 to 1.0
T_a	:	0 to 20 °C
T_{in}	:	20 to 50 °C
shape	:	infinite slab, infinite cylinder, sphere
product thermal properties	:	$\rho C = 2 \times 10^6$ to 4×10^6 J m ⁻³ K ⁻¹ $k = 0.3$ to 0.6 W m ⁻¹ K ⁻¹ .
position	:	centre and mass-average temperature

Application of the method to centre temperature prediction for products with non-constant surface water activity may be possible if three different a_w values are used, one to represent the starting condition, one to represent the a_w value during the active chilling phase, and the third to represent the quasi-equilibrium phase. Lower and upper bounds, defined on a theoretical basis, may be useful for defining the three a_w values. The presence or absence of skin resistance, and the ease of water movement internal to the product define how closely the behaviour of a particular product will match one or other bound. The skin resistance of unpeeled carrots forced the behaviour of this product close to the lower bounds. However peeled carrots behaved very close to the upper bounds because water movement within the carrot maintained an almost constant surface water activity. For both peeled and unpeeled carrots the quality of fit between experiment and prediction (within about ± 20 %) was poorer than for the experiments with the idealised test conditions, but the experimental uncertainty was significantly greater. Further research is required to establish whether the concept of

bounds is more generally applicable than to just carrots, and to establish whether the error introduced by representing the constantly changing a_w that occurs in practice by three constant values in calculations is significant, both for other food products, and for wider ranges of conditions than investigated here. Comparison of the bounds approach to the alternative where by skin resistance would be added to the empirical equations as an extra variable is also justified. Experimental measurement of a_w during chilling may be required in further work, and measurement of mass-average temperature should also be attempted.

Overall, the work reported here represents a significant step towards development of an accurate simple algebraic chilling time prediction method for situations where evaporative cooling of the product surface is important.

NOTATION

a	fitted constant
a_w	surface water activity
a_{wf}	mean surface water activity in active chilling phase
a_{wj}	initial surface water activity
A	surface area of solid (m^2)
b	fitted constant
Bi	Biot number = $h_c R/k$
Bi_l	Biot number of small sample at low air velocity
Bi_{m1}	Biot number of small sample at mid range air velocity
Bi_{m2}	Biot number of large sample at low air velocity
Bi_h	Biot number of large sample at high air velocity
c	water concentration (kg m^{-3})
c_0	water concentration at node 0 (kg m^{-3})
c_1	water concentration at node 1 (kg m^{-3})
c_{av}	mass-average water concentration (kg m^{-3})
c_{in}	initial water concentration (kg m^{-3})
c_j	water concentration at node j (kg m^{-3})
c_J	water concentration at node J (kg m^{-3})
C	specific heat of solid ($\text{J kg}^{-1} \text{K}^{-1}$)
C_a	air humid heat capacity on a dry air mass basis ($\text{J kg}^{-1} \text{K}^{-1}$)
C_{air}	specific heat capacity of dry air ($\text{J kg}^{-1} \text{K}^{-1}$)
C_v	specific heat capacity of water vapour ($\text{J kg}^{-1} \text{K}^{-1}$)
D	carrot diameter (m)
D	mass diffusivity ($\text{m}^2 \text{s}^{-1}$) (Chapter 4 only)
D_a	mass diffusivity of air ($\text{m}^2 \text{s}^{-1}$)
e	fitted constant
E	shape factor
E_o	1 for infinite slab; 2 for infinite cylinder; 3 for sphere
E_∞	0.75 for infinite slab; 1.76 for infinite cylinder; 3.0 for sphere
f	slope of a plot of $\ln Y$ versus Fo
f_{av}	f at mass-average position

f_{avConv}	f at mass-average position for convection-only cooling
f_{avEvap}	f at mass-average position for cooling with evaporation as well as convection
f_c	f at centre position
f_{cConv}	f at centre position for convection-only cooling
f_{cEvap}	f at centre position for cooling with evaporation as well as convection
$f_{cEvap,exp}$	slope of a plot of $\ln Y_{c,exp}$ versus FO
$f_{cEvap,pred}$	predicted value of f_{cEvap}
$f_{cEvap,pred}$ at a_{wj}	predicted value of f_{cEvap} using a_{wj} in equation (5.19)
$f_{cEvap,pred(finite\ diff.)}$	predicted value of f_{cEvap} using finite difference method
$f_{cEvap,pred(model)}$	predicted value of f_{cEvap} using simple model (equation 5.19)
f_{Conv}	f for convection-only cooling
f_{Evap}	f for cooling with evaporation as well as convection
F	functional relationship
FO	Fourier number = $\alpha t/R^2$
g	time for a 90 % reduction in $Y = 3.3222 t_{0.5}$ (s)
G	geometry index
h_a	air convection heat transfer coefficient ($W\ m^{-2}\ K^{-1}$)
h_c	surface heat transfer coefficient ($W\ m^{-2}\ K^{-1}$)
H_{air}	absolute humidity of the ambient air ($kg\ water\ kg^{-1}\ dry\ air$)
H_r	air relative humidity
H_j	absolute humidity in the boundary layer over the product surface ($kg\ water\ kg\ dry\ air^{-1}$)
i	number of time step or time level in numerical calculations
j	space position in r direction in numerical calculations (Chapter 4 only)
j	lag factor or intercept of a plot of $\ln Y$ versus FO
j_{av}	j at mass-average position
j_{avConv}	j at mass-average position for convection-only cooling
j_{avEvap}	j at mass-average position for cooling with evaporation as well as convection
j_c	j at centre position
j_{cConv}	j at centre position for convection-only cooling
j_{cEvap}	j at centre position for cooling with evaporation as well as convection
$j_{cEvap,exp}$	intercept of a plot of $\ln Y_{c,exp}$ versus FO
$j_{cEvap,pred}$	predicted value of j_{cEvap}
$j_{cEvap,pred}$ at a_{wj}	predicted value of j_{cEvap} using a_{wj} in equation (5.20)

$j_{cEvap,pred(finite\ diff.)}$	predicted value of j_{cEvap} using finite difference method
$j_{cEvap,pred(model)}$	predicted value of j_{cEvap} using simple model (equation 5.20)
$j_m(\Delta V)$	j at mass-average position calculated by analytical solution (convection-only cooling)
$j_m(r)$	j at position r , calculated by analytical solution (convection-only cooling)
j_{Conv}	j for convection-only cooling
j_{Evap}	j for cooling with evaporation as well as convection
J	number of nodes = $R/(\Delta r)$
J_1	first order Bessel function of first kind
J_0	zero order Bessel function of first kind
k	thermal conductivity of solid ($W\ m^{-1}\ K^{-1}$)
k_1, k_2, k_3, k_4	thermal conductivities of plastic film, aluminium, cloth, and liquid ($W\ m^{-1}\ K^{-1}$)
k_a	air thermal conductivity ($W\ m^{-1}\ K^{-1}$)
K	overall mass transfer coefficient ($kg\ s^{-1}\ m^{-2}\ Pa^{-1}$)
K_a	air film mass transfer coefficient ($kg\ s^{-1}\ m^{-2}\ Pa^{-1}$)
K_p	packaging mass transfer coefficient ($kg\ s^{-1}\ m^{-2}\ Pa^{-1}$)
K_s	skin mass transfer coefficient ($kg\ s^{-1}\ m^{-2}\ Pa^{-1}$)
K_x	equivalent transpiration coefficient ($kg\ s^{-1}\ m^{-2}\ Pa^{-1}$)
K_y	mass transfer coefficient in humidity units ($kg\ m^{-2}\ s^{-1}$)
Le	Lewis number = $h_c/K_y C_a$
L_x, L_y, L_z	axis lengths of elliptical shapes
m	evaporation rate ($kg\ s^{-1}\ m^{-2}$)
m_p	rate of moisture loss per unit pore area ($kg\ s^{-1}\ m^{-2}$)
Nu	Nusselt Number = $h_c D/k_a$
p_a	partial pressure of water vapour in the surrounding air (Pa)
p_{bm}	mean partial pressure of dry air (Pa)
$p_{r=R}$	partial pressure of water vapour in the boundary layer at the product surface (Pa)
p_{wa}	(saturation) vapour pressure of pure water at surrounding air temperature T_a (Pa)
$p_{w(r=R)}$	(saturation) vapour pressure of pure water at product surface temperature $T_{r=R}$ (Pa)
p_{wJ}	(saturation) vapour pressure of pure water at the evaporating surface

	temperature T_j (Pa)
P_j	partial pressure of water vapour at evaporating surface (Pa)
Pr	Prandtl Number = $C_a \mu_a / k_a$
P_t	total air pressure (Pa)
Q	respiration rate ($W m^{-3}$)
r	space position within solid relative to centre position (m)
R	characteristic length for solid (radius of sphere or cylinder and half-thickness of slab) (m)
Re	Reynolds Number = Dv_a / ν_a
Sc	Schmidt number = $\mu_a / \rho_a D_a$
t	time (s)
$t_{0.5}$	half life time (s)
t_{exp}	chilling time measured experimentally (s)
t_{pred}	predicted chilling time (s)
$t_{pred(finite\ diff.)}$	predicted chilling time using finite difference method (s)
$t_{pred(model)}$	predicted chilling time using simple model (s)
T	temperature of solid (K or °C)
T_0	temperature of solid at node 0 (K or °C)
T_1	temperature of solid at node 1 (K or °C)
T_a	surrounding cooling medium temperature (K or °C)
T_{av}	mass-average temperature of solid (K or °C)
T_c	centre temperature of the product (K or °C)
$T_{c,exp}$	centre temperature measured experimentally (K or °C)
T_{eq}	equilibrium or steady state temperature (°C)
$T_{eq,exp}$	equilibrium temperature measured experimentally (°C)
$T_{eq,pred}$	equilibrium temperature calculated from equation (5.11) (°C)
T_{in}	uniform initial temperature of the product (K or °C)
T_j	temperature of solid at node j (K or °C)
T_r	temperature within the solid at position r (K or °C)
$T_{r=R}, T_j$	surface temperature of solid (K or °C)
v_a	air velocity ($m s^{-1}$)
V	volume of solid (m^3)
x	space position within solid (m) (Chapter 1-4 only)

x_1, x_2, x_3, x_4	thickness of plastic film, aluminium, cloth, and liquid respectively (m)
y	space position within solid (m)
Y	fractional unaccomplished temperature change
Y_{av}	fractional unaccomplished temperature change at mass-average position
Y_c	fractional unaccomplished temperature change at centre position
$Y_{c,exp}$	measured value of Y_c
$Y_{c,pred}$	predicted value of Y_c corresponding to $T_{c,exp}$ and $T_{eq,pred}$
Y_r	dimensionless temperature ratio as a function of time and position within the solid (fractional unaccomplished temperature change)
z	space position within solid (m)

GREEK SYMBOLS

α	thermal diffusivity (m^2s^{-1})
β_l	1st root of the appropriate transcendental equation
β_m	m^{th} root of the appropriate transcendental equation
Δr	thickness of slices (m)
Δt	time step (s)
ρ	density of solid (kg m^{-3})
ρ_a	density of air (kg m^{-3})
ρC	volumetric specific heat capacity ($\text{J m}^{-3} \text{K}^{-1}$)
Φ	the fraction of fruit surface area covered by pores
ϕ	surface heat flow (W)
ν_a	air kinetic viscosity ($\text{m}^2 \text{s}^{-1}$)
μ_a	air viscosity ($\text{kg m}^{-1} \text{s}^{-1}$)
τ	skin thickness (m)
δ	diffusion coefficient of water vapour in air ($\text{m}^2 \text{s}^{-1}$)
ϵ_a	enthalpy of cooling air (J kg^{-1})
ϵ_{fg}	latent heat of vapourisation of water (J kg^{-1})
ϵ_s	enthalpy of saturated air evaluated at the product surface temperature (J kg^{-1})

REFERENCES

- Abdul Majeed, P. M. (1982). Prediction of cooling characteristics during air cooling of cylindrical food products with a flowing film of cold water at the surface (air-film cooling). *Trans. Amer. Soc. Agric. Eng.*, **25**, 508-514.
- Abdul Majeed, P. M., Srinivasa Murthy, S. & Krishna Murthy, M. V. (1980). Prediction of aircooling characteristics of moist food products. *Trans. Amer. Soc. Agric. Eng.*, **23**, 778-792.
- Akimoto, K. (1975). Heat transfer characteristics of rectangular products. *Res. Bull., Fac. Agr. Gifu Univ.*, **38**, 75-82.
- Alyamovski, I. G. (1974). Heat exchange during cooling fruit and/ or vegetables in stacks or in bulk. *Refrig. Sci. & Technol.*, **1974-3**, 75-81.
- Anon. (1981). *ASHRAE Handbook Fundamentals*. The American Society of Heating, Refrigerating and Air-Conditioning Engineers., Atlanta, GA., Chapter 13.
- Anon. (1977). *ASHRAE Handbook & Product Directory*. American Society of Heating, Refrigerating, and Air-Conditioning Engineers., New York, NY, 29.1.
- Anon. (1985). Influence of air flow rate, respiration, evaporative cooling, and other factors affecting weight loss calculation for fruits and vegetables. *ASHRAE Trans.*, **91(1B)**, 690-707.
- Ansari, F. A. & Afag, A. (1986). New method of measuring thermal diffusivity of spherical produce. *Int. J. Refrig.*, **9**, 158-160.
- Ansari, F. A. & Afaq, A. (1986). Precooling of cylindrical food products. *Int. J. Refrig.*, **9**, 161-163.

- Apeland, J. & Baugerod, H. (1971). Factors affecting weight loss in carrots. *Acta Hort.*, **20**, 90-97.
- Arce, J. A., Potluri, P.L., Schneider, K.C., Sweat, V. E. & Dutson, T.R. (1983). Modeling beef carcass cooling using finite element techniques. *Trans. Amer. Soc. Agric. Eng.*, **26**, 950-954, 960.
- Awberry, J. H. (1927). The flow of heat in a body generating heat. *Phil Mag.*, **4**(7), 629.
- Badari Narayana, K. & Krishna Murthy, M. V. (1981). Heat and mass transfer characteristics and the evaluation of thermal properties of moist food material. *Trans. Amer. Soc. Agric. Eng.*, **24**, 789-793.
- Baehr, H. D. (1953). Die berechnung der kuhldauer bei ein-und mehr-dimensionalen warmefluss. *Kalotechnik*, **5**, 255-259.
- Balaban, M. (1989). Effect of volume change in foods on the temperature and moisture content predictions of simultaneous heat and moisture transfer models. *J. Food Process Engng.*, **12**, 67-88.
- Boelter, L. M. K., Cherry, V. H., Johnson, H. A. & Martinelli, R. C. (1948). *Heat transfer notes*. University of California Press, U.S.A.
- Bonacina, C. & Comini, G. (1971). Mass and heat transfer during cooling, freezing and cold storage of foodstuffs. *Int. J. Refrig.*, **51**(6), 1539-1557.
- Brown, T. & James, S. J. (1992). Process design data for pork chilling. *Int. J. Refrig.*, **15**(5), 281-288.
- Buescher, R. W. (1979). Influence of high temperature on physiological and compositional characteristics of tomato fruits. *Lebensm.-Wiss, U.-Technol.*, **12**, 162.

- Carslaw, H. S. & Jaeger, J. C. (1959). *Conduction of Heat in Solids*, 2nd ed. Clarendon Press, Oxford.
- Chau, K. V. & Gaffney, J. J. (1990). A finite-difference model for heat and mass transfer in products with internal heat generation and transpiration. *J. Food Sci.*, **55**(2), 484-487.
- Chau, K. V. & Gaffney, J. J. (1985). A mathematical model for the transpiration of fruits and vegetables. Paper No. 85-6002, *Amer. Soc. Agric. Eng.*
- Chau, K. V., Gaffney, J. J. & Romero, R. A. (1988). A mathematical model for the transpiration from fruits and vegetables. *ASHRAE Trans.*, **94**(1), 1541-1552.
- Chau, K. V., Gaffney, J. J. & Baird, C. D. (1985). Transient heat and mass transfer for oranges in closed containers. *Refrig. Sci. & Technol.*, **1985-5**, 283-290.
- Chau, K. V., Romero, R. A., Baird, C. D. & Gaffney, J. J. (1988). Transpiration coefficients for certain fruits and vegetables. *ASHRAE Trans.*, **94**(1), 1553-1562.
- Chirife, J. & Fontan, C. F. (1982). Water activity of fresh foods. *J. Food Sci.*, **47**, 661-663.
- Clary, B. L., Nelson, G. L. & Smith, R. E. (1968). Heat transfer from hams during freezing by low temperature air. *Trans. Amer. Soc. Agric. Eng.*, **11**, 496-499.
- Cleland, A. C. (1989). *Food Refrigeration Processes Analysis, Design and Simulation*. Elsevier Science Publishers Ltd., England.
- Cleland, A. C. & Earle, R. L. (1982). A simple method for prediction of heating and cooling rates in solids of various shapes. *Int. J. Refrig.*, **5**(2), 98-106.
- Cleland, A. C. & Earle, R. L. (1977). The Third kind of boundary condition in numerical freezing calculations. *Int. J. Heat Mass Transfer*, **20**, 1029-1034.

- Cleland, D. J., Cleland, A. C. & Jones, R. S. (1994). Collection of accurate experimental data for testing the performance of simple methods for food freezing time prediction. *J. Food Proc. Eng.*, **17**, 93-119.
- Comini, G. & Lewis, R. W. (1976). A numerical solution of two-dimensional problems involving heat and mass transfer. *Int. J. Heat Mass Transfer*, **19**, 1387-1392.
- Daudin, J. D. (1986). Calculation of water activity on the surface of hot bonded muscles during chilling. *Refrig. Sci. & Technol.*, **1986-3**, 389-395.
- De Baerdemaeker, J., Singh, R. P. & Segerlind, L. J. (1977). Modelling heat transfer in foods using the finite-element method. *J. Food Proc. Eng.*, **1**, 37-50.
- Devres, Y. O. (1989). Temperature and weight loss analyses of some fruit and vegetables in cold storage. Research memorandum 113, Institute of Environmental Engineering, South Bank Polytechnic, London, 1-18.
- Drumm, B. M., Joseph, R. L. & McKenna, B. M. (1992). Line chilling of beef. 1. The prediction of temperature. *J. Food Engng.*, **16**, 251-265.
- Earle, R. L. & Fleming, A. K. (1967). Cooling and freezing of lamb and mutton carcasses. I. Cooling and freezing rates in legs. *Food Technol.*, **21**, 79.
- Feldman, C. (1976). Transfer de chaleur et de masse entre une sphere et de l'air a basse temperature. *CTGREF No 6 Memoire (March)*.
- Fikiin, A. & Fikiina, I. (1971). Calculating the cooling time for foodstuffs and solids. *Proc. 13th Int. Congr. Refrig.*, **2**, 411-414.
- Fockens, F. H. & Meffert, H. F. T. (1972). Biophysical properties of horticultural products as related to loss of moisture during cooling down. *J. Sci. Food Agric.*, **23**, 285-298.

- Fukushima, T., Yarimizu, K., Kitamura, T. & Iwata, T. (1980). The relation between water stress and the climacteric in respiration of some fruits. *Scientia Horticulturae*, **12**, 259.
- Fulton, G. S., Burfoot, D., Bailey, C. & James, S. J. (1987). Predicting weight loss from unwrapped chilled meat in retail display. *Proc. 17th Int. Congr. Refrig.*, 555-562.
- Gaffney, J. J. & Baird, C. D. (1977). Forced-air cooling of bell peppers in bulk. *Trans. Amer. Soc. Agric. Eng.*, **20**, 1174.
- Gaffney, J. J. & Baird, C. D. (1975). Forced-air cooling of bell peppers in bulk. Paper No. 75-6525, *Amer. Soc. Agric. Eng.*
- Gaffney, J. J., Baird, C. C. & Chau, K. V. (1985a). Methods for calculating heat and mass transfer in fruits and vegetables, individually and in bulk. *ASHRAE Trans.*, **91**(1B), 333-352.
- Gaffney, J. J., Baird, C. G. & Chau, K. V. (1985b). Influence of airflow rate, respiration, evaporative cooling, and other factors affecting weight loss calculations for fruit and vegetables. *ASHRAE Trans.*, **91**(2B), 690-707.
- Gan, G. & Woods, J. L. (1989). A deep bed simulation of vegetable cooling. *Proc. 11th Int. Congr. Agric. Engng.*, 2301-2308.
- Gigiel, A. J., Collett, P. & James, S. J. (1989). Fast and slow beef chilling in a commercial chiller and the effect of operational factors on weight loss. *Int. J. Refrig.*, **12**, 338-349.
- Gigiel, A. & Creed, P. G. (1987). Effect of air speed, temperature and carcass weight on cooling rates and weight losses of goat carcasses. *Int. J. Refrig.*, **10**, 305-306.
- Goodman, T. R. (1964). Application of integral methods to transient non-linear heat transfer. *Adv. Heat Transfer*, **1**, 51-121.

- Greenspan, L. (1977). Humidity Fixed Points of Binary Saturated Aqueous Solutions. *Journal of Research of the National Bureau of Standards - A. Physics and Chemistry*, **81A**(1), 89-96.
- Gupta, C. P. & Prakash, R. (1979). *Engineering Heat Transfer*. Nem Chand and Bros, Roorkee, India, pp. 265, 518.
- Gurney, H. P. & Lurie, J. (1923). Charts for estimating temperatures distributions in heating or cooling of solid shapes. *Ind. Eng. Chem.*, **15**(11), 1170- 1172.
- Haas, E. & Felsenstein, G. (1985). Factors affecting the cooling rate of avocados packed in corrugated cartons. *Refriger. Sci. & Technol.*, **1985-5**, 291-300.
- Hayakawa, K. (1978). Computerised simulation for heat transfer and moisture loss from an idealised fresh produce. *Trans. Amer. Soc. Agric. Eng.*, **21**, 1015-1024.
- Hayakawa, K. (1971). Estimating food temperatures during various processing or handling treatments. *J. Food Sci.*, **36**, 374- 385.
- Hayakawa, K. (1970). Experimental formulas for accurate estimation of transient temperature of food and their application to thermal process evaluation. *Food Technol.*, **24**(12), 1407.
- Hayakawa, K. & Succar, J. (1982). Heat transfer and moisture loss of spherical fresh produce. *J. Food Sci.*, **47**, 596-605.
- Hayes, G. D. (1987). *Food Engineering Data Handbook*. Wiley, New York.
- Heisler, M. P. (1947). Temperature charts for induction and constant temperature heating. *ASME Trans.*, **69**(4), 227-236.
- Heldman, D. R. (1975). *Food Process Engineering*, AVI Publishing Co., Westport, CT.

- Heldman, D. R. & Singh, R. P. (1981). *Food Process Engineering*, 2nd ed. AVI Publishing Co., Westport, CT.
- Hicks, E. W. (1955). Precooling of fruit and vegetables - Some theoretical considerations. *Proc. 9th Int. Congr. Refrig.*, 0078-0085.
- Hodgson, T. (1966). The effect of environmental conditions on chilling rates of meat. *Refrig. Sci. & Technol.*, **1966-1**, 636.
- Hodgson, T. (1970). The effect of air velocity and evaporator size on product weight losses in carcasses chilling rooms. *Refrig. Sci. & Technol.*, **1970-3**, 161-167.
- Hood, C. F. (1964). *Temperature progression during cooling of pickling cucumbers*. Ph.D. Dissertation, Agricultural Engineering Department, North Carolina State University, Raleigh, NC, U.S.A.
- James, S. (1990). Cooling of cooked products. *Refrig. Sci. & Technol.*, **1990-4**, 551-557.
- James, S. J. & Bailey, C. (1986). Temperature changes, weight loss and product loads during beef chilling. *Refrig. Sci. & Technol.*, **1986-3**, 105-114.
- James, S. J., Fulton, G. S., Swain, M. V. L. & Burfoot, D. (1988a). Modelling the effect of temperature and relative humidity fluctuations on weight loss in retail display. *Refrig. Sci. & Technol.*, **1988-1**, 187- 194
- James, S. J., Swain, M. V. L. & Daudin, J. D. (1988b). Mass transfer under retail display conditions. *Proc. 34th Int. Congr. Meat Sci. Tech.*, 652-654.
- Jiang, H., David, R., Thompson, R. & Vance, M. (1987). Finite element model of temperature distribution in broccoli stalks during forced-air precooling. *Trans. Amer. Soc. Agric. Eng.*, **30(5)**, 1473-1477.

- King, C. J. (1968). Rates of moisture sorption and desorption in porous, dried foodstuffs. *Food Technol.*, **22**, 509.
- Krischer, O. & Mahler, K. (1959). Über die Bestimmung des Diffusionswiderstands und der kapillaren Flüssigkeitsleitfähigkeit aus stationären und instationären Vorgängen. *V.D.I.-Forsch. Heft.*, 473.
- Kusunose, H. & Sawamura, M. (1980). Ethylene production and respiration of post harvest and citrus fruits and Wase Satsuma Mandarin fruit. *Agric. Biol. Chem.*, **44**, 1917.
- Levy, F. L. (1986). Measuring the convective heat transfer coefficient while chilling carcasses. *Int. J. Refrig.*, **9**, 84-88.
- Lin, Z. (1994). *Prediction of chilling times of foods*. PhD Thesis, Massey University, N.Z.
- Lovett, D. A. (1988). Performance of a simple mathematical model for predicting thermal changes in meat. *Proc. 34th Int. Congr. Meat Sci. Tech.*, 655-659.
- Lovett, D. A., Herbert, L. S. & Radford, R. D. (1976). Chilling of meat - experimental investigations of weight loss., *Refrig. Sci. & Technol.*, **1976-1**, 307-314.
- Luikov, A. V. (1968) *Analytical heat diffusion theory*. Academic Press, New York.
- Luikov, A. V. (1966). *Heat and mass transfer in capillary-porous bodies*. Pergamon Press, Oxford-London.
- Lutz, J. M. & Hardenburg, R. E. (1968). *The commercial storage of fruits, vegetables, and florist and nursery stocks*. Agricultural Handbook No. 66. U.S. Government Printing Office, Washington DC.
- Mallikarjunan, L. & Mittal, G.S. (1995). Prediction of beef carcass chilling time and mass loss. *J. Food Proc. Eng.*, **18**, 1-15.

- Mannapperuma, J. D. & Singh, R. P. (1988). Prediction of freezing and thawing times of foods using a numerical method based on enthalpy formation. *J. Food. Sci.*, **53**(2), 626-630.
- McAdams, W. H. (1954). *Heat transmission*. McGraw-Hill, New York.
- Meffert, H. F. T., Rudolphij, J. W. & Eelkman Rooda, J. (1971). Heat transfer during the cooling process of heat generation produce. *Proc. 13th Int. Congr. Refrig.*, **2**, 379-338.
- Mohsenin, N. N. (1980). *Thermal properties of foods and agricultural materials*. Gordon and Breach Science Publishers, New York.
- Morley, M. N. (1972). *Thermal properties of meat. Tabulated data*. Special report no. 1, Agricultural Research Council, Meat Research Institute, Langford, Bristol BS187DY, U.K.
- Narasimha Rao, K. V., Narasimham, G. S. V. L. & Krishna Murthy, M. V. (1993). Analysis of heat and mass transfer during bulk hydraircooling of spherical food products. *Int. J. Heat Mass Trasfer*, **36**(3), 809-822.
- Newman, A. B. (1936). Heating and cooling rectangular and cylindrical solids. *Ind. Engng. Chem.*, **28**(5), 545-548.
- Nicholas, R. C., Motawi, K. E. H. & Blaisdell, J. L. (1964). Cooling rates of individual fruit in air and in water. *Mich. Ag. Exp. Sta. Quarterly Bull.*, **47**(1), 51-64.
- Ozisik, M. N. (1968). *Boundary value problems in heat conduction*. Int Text Book Co., pp. 301.
- Pasternak, I. S. & Gauvin, W. H. (1960). Turbulent heat and mass transfer from stationary particles. *Can. J. Chem. Eng.*, **38**, 34.

- Patel, L. N., Pai, T. K. & Sastry, S. K. (1988). Effects of temperature, relative humidity and storage time on the transpiration coefficients of selected perishables. *ASHRAE Trans.*, **94**(1), 1563-1587.
- Patel, P. N. & Sastry, S. K. (1988). Effects of temperature fluctuation on transpiration of selected perishables: mathematical models and experimental studies. *ASHRAE Trans.*, **94**(1), 1588-1600.
- Pflug, I. J. & Kopelman, I. J. (1966). Correlating and predicting transient heat transfer rates in food products. *Refrig. Sci. & Technol.*, **1966-2**, 89-100.
- Pham, Q. T. (1987). Moisture transfer due to temperature changes or fluctuations. *J. Food Engng.*, **6**, 33-49.
- Pham, Q. T. & Willix, J. (1984). A model for food desiccation in frozen storage. *J. Food Sci.*, **49**, 1275-1282.
- Pham, Q. T. & Willix, J. (1985). Weight loss from lamb carcasses in frozen storage: influence of environmental factors. *Int. J. Refrig.*, **8**(4), 231-235.
- Poulsen, K.P. (1982). Thermal diffusivity of foods measured by simple equipment. *J. Food Engng.*, **1**, 115-122.
- Radford, R. D., Herbert, L. S. & Lovett, D. A. (1976). Chilling of meat - a mathematical model for heat and mass transfer. *Refrig. Sci. & Technol.*, **1976-1**, 323-330.
- Riedel, L. (1960). Eine Prufsubstanz für gefrierersuche. *Kaltetechnik*, **12**, 222-226.
- Rockland, L. B. (1960). Saturated salt solutions for static control of relative humidity between 5 and 40 °C. *Anal. Chem.*, **32**, 1375.

- Romero, R. A. & Chau, K. V. (1987). A mathematical simulation for transpiration from fruits and vegetables in bulk storage. Paper No. 87-6007, *Amer. Soc. Agric. Eng.*
- Roth, T. & Loncin, M. (1985). *Properties of Water in Foods*. Martinus Nijhoff Publishers, Dordrecht, Netherlands, pp 331- 342.
- Rutov, D. G. (1958). Calculation of the time of cooling of food products. *Refrig. Sci. & Technol.*, **1958-2**, 415-421.
- Sainsbury, G. F. (1985). Practical application of cooling performance data for perishable commodities. *Refrig. Sci. & Technol.*, **1985-5**, 275-282.
- Sastry, S. K. (1985). Factors Affecting Shrinkage of Foods in Refrigerated Storage. *ASHRAE Trans.*, **91(1B)**, 683-689.
- Sastry, S. K. (1985). Moisture losses from perishable commodities: recent research and developments. *Int. J. Refrig.*, **8**, 343-346.
- Sastry, S. K., Baird, C. D. & Buffington, D. E. (1978). Transpiration rates of certain fruits and vegetables. *ASHRAE Trans.*, **84(2)**, 237-255.
- Sastry, S. K. & Buffington, D. E. (1982). Transpiration rates of stored perishable commodities: a mathematical model and experiments on tomatoes. *ASHRAE Trans.*, **88**, 159-184.
- Sastry, S. K. & Buffington, D. E. (1983). Transpiration rates of stored perishable commodities: a mathematical model and experiments on tomatoes. *Int. J. Refrig.*, **6(2)**, 84-96.
- Sastry, S. K., Uritz, C. A. & Anantheswaran, R. C. (1985). Interaction between heat and mass transfer in foods. *ASHRAE Trans.*, **91(2B)**, 353-370.

- Schneider, K. C., Sweat, V. E., Arce, J. A., Dutson, T. R. & Dahm, P. F. (1982). Factors affecting beef carcass chilling rates. *Trans. Amer. Soc. Agric. Eng.*, **25**, 498-501.
- Schneider, P. J. (1963). *Temperature response charts.*, John Wiley & Sons, Inc., New York.
- Self, K. & Burfoot, D. (1986). Predicting the effect of air distribution on cooling time. *Refrig. Sci. & Technol.*, **1986-3**, 381-387.
- Skelland, A. H. P. & Cornish, A. R. H. (1963). Mass transfer from spheroids to an air stream. *A.I.Ch.E.J.*, **9**, 73.
- Smith, R. E., Nelson, G. L. & Hendrickson, R. L. (1967). Analysis of transient heat transfer from anomalous shapes. *Trans. Amer. Soc. Agric. Eng.*, **10**, 236-245.
- Smith, R. E., Nelson, G. L. & Henrickson, R. L. (1968). Applications of geometry analysis of anomalous shape to problems in transient heat transfer. *Trans. Amer. Soc. Agric. Eng.*, **11**, 296-302.
- Smith, R. E. & Nelson, G. L. (1969). Transient heat transfer in solids:theory versus experimental. *Trans. Amer. Soc. Agric. Eng.*, **12**, 833-836, 844.
- Srinivasa Murthy, S., Krishna Murthy, M. V. & Ramachandran, A. (1974). Heat transfer during air cooling and storing of moist food products. *Trans. Amer. Soc. Agric. Eng.*, **17**, 769-773.
- Srinivasa Murthy, S., Krishna Murthy, M. V. & Ramachandran, A. (1976). Heat transfer during aircooling and storing of moist food products - II. spherical and cylindrical shapes. *Trans. Amer. Soc. Agric. Eng.*, **19**, 577-583.
- Stermer, R. A., Brasington, C. F., Camp, T. H. & Vanderzant, C. (1986). Hydro-chilling - a rapid method for cooling meats. *Trans. Amer. Soc. Agric. Eng.*, **29**, 306-311.

- Stermer, R. A., Camp, T. H. & Brasington, F. (1984). A liquid chill system for rapid cooling of meats. *J. Food Protect.*, **47**, 871-875.
- Stoecker, W. F. (1977). *Refrigeration and airconditioning*. Tata- McGraw-Hill Pub. Co., New Delhi, pp 252.
- Troller, J. A. & Christian, J. H. B. (1978). *Water Activity and Food*. Academic Press, New York.
- Van Arsdel, W. B. (1963). *Food Dehydration-I. Principles.*, Avi Publishing Co., Westport, Connecticut.
- Van Beek, G. (1985). Practical applications of transpiration coefficients of horticultural produce. *ASHRAE Trans*, **91**, 708-725.
- Van Beek, G. (1983). Weight Loss of Hard Fruit During Storage as Influenced by Cold Room Climate and Transpiration Coefficient. *Proc. 16th Int. Congr. Refrig.*, **4**, 225-230.
- Villa, L. G. (1973). *Single particle convective moisture loss from horticultural products in storage*. Ph.D. Thesis, Michigan State University, East Lansing.
- Von Rosenberg, D. U. (1969). *Methods for the numerical solution of partial differential equations*. American Elsevier Publ. Co. Inc., New York.
- Wade, N.L. (1984). Estimation of the refrigeration capacity required to cool horticultural produce. *Int. J. Refrig.*, **7**(6), 358-366.
- Williamson, E. D. & Adams, L. H. (1919). Temperature distributions of solids during heating or cooling. *Physical Review*, **14**(2), 99-114.
- Willis, R. B. H. & McGlasson, W. B. (1971). Effect of storage temperatures on apple volatiles associated with low temperature breakdown. *J. Hort. Sci.*, **46**, 115.

Woods, J. L. (1990). Moisture loss from fruits and vegetables. *Postharvest News and Information*, 1(3), 195-199.

Wu, M. T. & Salunke, D. K. (1975). Effect of alternating storage temperatures on ripening of tomato fruits. *Lebensm.-Wiss. U.- Technol.*, 8, 119.

APPENDIX A
COMPUTER PROGRAM USED FOR CHILLING
PROCESS SIMULATION AND ANALYSIS

1 INTRODUCTION

Essentially, a single computer program was used for all finite difference simulations, for simulations by the proposed method, and for processing experimental results.

2 PROGRAM LISTING

In the listing below explanatory comments in italics have been added on the right hand side. The program is suitable for programming in the PASCAL programming language.

```

{Prediction of temperature and chilling time at centre position of a peeled carrot}
{Finite Difference Model & Simple Model & Experimental Result}
PROGRAM PEELED_CARROT(input,output);
{$N+}

const
J=11;
k=0.5192;
d=1.08E-10;
CCp=3.8725;
Pt=101.3*1000;
Ca=1010.0;

type

arrayofreal1=array[0..137] of real;
arrayofreal11=array[0..15] of real;
arrayofreal0=array[0..400] of real;
arrayofreal2=array[1..3] of extended;

var
Ta, Tequ, Ti, Tav, rH, Hc, Kg, Pwj, Pwa, PJ, Pa, Pw, PP, B, Hfg, time, telaps, BB, C1, Ts, Tc, Cs, Cc, Cav,
tprint, Dr, Dt, R, C, M, O, Q, W, MM, WW, CO1, CO2, CO3, CO4, CO5, CO6, CO7, sum1, sum2, Bi, Fo,
Yc, Ys, Yav, aw, Va, Eo, Einf, E, DD,
Hini, Hend, Hflow, HFlux, Hend1, Htotal_flow, Hwsurf, Hwair, AA1, AA2,
Mini, Mend, Mflow, MFlux, Mtotal_flow, Mend1, FcRef, JcRef, Fcfinite,
Jcfinite, coefC, ff, Fcexp, Jcexp, Diff1, Diff2, deltaFcA, deltaFcB, deltaJcA, deltaJcB,
RatioFcfinite, RatioJcfinite, RatioFcexp, RatioJcexp, RatioFcmodel, RatioJcmodel,
Fcmodel, Jcmodel, TeqExp, TeqCal,
timeExp, timeModel, timeFinite, den, Cp: real;
Rt, S: extended;
fig, I, L, IJ, II, count, X, shape, n, n1, n2, n3, n4, nn: integer;
cccl, ccc2: char;
Result: text;
Cnow, Cnew, Tnew, Tnow, Tas, Tins, Times, Hrs: arrayofreal1;
Foo, Ycc, Yavv, Fu, Yccc: arrayofreal0;
lim, fun, diff, Ycx: arrayofreal2;
filename: string;

```

```

PROCEDURE askprop;                                     {Read Properties}
BEGIN
  Writeln;Writeln;
  Write('write result in file named '); Readln(filename);
  Assign(Result,filename);Rewrite(Result);
  Write('Shape,{shape:1:infinite slab,2:infinite cyl,3:sphere} =');Readln(shape);
  Write('density (kg m-3) = ');      Read(den);                {Density}
  Write('Bi = ');                    Read(Bi);                {Biot number}
  Write('Tin (°C) = ');            Read(Ti);                {Initial Temperature}
  Write('Ta (°C) = ');            Read(Ta);                {Ambient Air Temperature}
  Write('Hr (ratio) = ');        Read(rH);                {Relative Humidity}
  Write('Teq,exp (°C) = ');        Read(TeqExp);{Experimental Equilibrium Temperature}
  Write('Teq,pred (°C) = ');        Read(TeqCal); {Calculated Equilibrium Temperature}
  Write('av = ');                Read(aw);                {Surface Water Activity}
  Write('Diameter (m.) = ');        Read(DD);                {Solid Diameter}
  write('fc,exp : ');              Read(FcExp);            {f-value}
  write('jc,exp : ');              Read(JcExp);            {j-value}
  write('time to print out (s) = '); Readln(tprint);          {Time to Print Out}
END;

```

```

FUNCTION Dtt (shape : integer; Bi:real) : real;       {Find Delta Time}
var i:integer;
BEGIN
  if abs(Bi - 0.1) < 0.00001 then i := 1
  else if abs(Bi - 0.3162)<0.00001 then i := 2
  else if abs(Bi - 1.0) < 0.00001 then i := 3
  else if abs(Bi - 3.162) <0.00001 then i := 4
  else i := 5;

  case shape of
  1 :
    begin case i of
      1: dtt:=0.04;
      2: dtt:=0.05;
      3: dtt:=0.01;
      4: dtt:=0.9;
      5: dtt:=0.2;
    end;
  end;

  2 :
    begin case i of
      1: dtt:=1;
      2: dtt:=1;
      3: dtt:=1;
      4: dtt:=1;
      5: dtt:=1;
    end;
  end;

  3 :
    begin case i of
      1: dtt:=0.05;
      2: dtt:=0.1;
      3: dtt:=0.2;
      4: dtt:=0.3;
      5: dtt:=0.1;
    end;
  end;
end;
END;

```

```

PROCEDURE writeshape(shape:integer; var Eo,Einf:real); {Choose Shape}
BEGIN
case shape of
  1:begin
    Eo:=1.0;
    Einf:=0.75;
    writeln('////////// This shape:infinite slab //////////');
    writeln(result,'          ////////// This shape:infinite slab //////////');
  end;
  2:begin

```

```

    Eo:=2.0;
    Einf:=1.76;
    writeln('@@@@@@@@ This shape:infinite cylinder @@@@@@@@@');
    writeln(result,' @@@@@@@@@ This shape:infinite cylinder@@@@@@@@');
end;
3:begin
    Eo:=3.0;
    Einf:=3;
    writeln('00000000# This shape:sphere #00000000');
    writeln(result,' 00000000# This shape:sphere #00000000');
end;
end;
END;

```

```

FUNCTION factorial(number:longint):extended; {Factorial Term for Infinite Cylinder}
var i:longint;dummy:extended;

```

```

BEGIN
    dummy:=1;
    if number>0 then for i:=1 to number do dummy:=dummy*i;
    factorial:=dummy;
END;

```

```

FUNCTION power(num,expt:extended):extended; {Power Term for Infinite Cylinder}
var dummy:extended;i,n:longint;

```

```

BEGIN
    dummy:=1;
    if ((num=0) and (expt=0)) then {undefined values}
    begin
        { Write(' ');}
        Halt;
    end;
    if expt=0 then dummy:=1; {special cases}
    if num=0 then dummy:=0;
    if num>0 then if (expt>0) {no restrictions}
        then dummy:=exp(expt*ln(Abs(num)))
        else dummy:=1/exp(expt*ln(Abs(num)));
    if num<0 then if abs(Trunc(expt))=abs(expt) {exponent must be an integer}
    then
    begin
        dummy:=1;
        for n:=1 to Trunc(abs(expt)) do dummy:=dummy*num;
        if expt<0 then dummy:=1/dummy;
    end else
    begin
        Halt;
    end;
    power:=dummy;
END;

```

```

FUNCTION J1(s:extended):extended; {J1 for Infinite Cylinder}
var term,sum:extended;n:longint;

```

```

BEGIN
    sum:=s/2;
    n:=0;
    repeat
        n:=n+1;
        term:=power(-1,n)*power(s,n*2+1)/(power(2,n*2+1)*factorial(n)*factorial(n+1));
        sum:=sum+term;
    until Abs(term)<0.000001;
    J1:=sum;
END; {J1}

```

```

FUNCTION J0(s:extended):extended; {J0 for Infinite Cylinder}
var sum,term:extended;n:integer;

```

```

BEGIN
    sum:=1;
    n:=0;
    repeat

```

```

n:=n+1;
term:=power(-1,n)*power(s,n*2)/power(2,n*2)/Sqr(factorial(n));
sum:=sum+term;
until abs(term)<0.000001;
J0:=sum;
END;

```

```

FUNCTION root(Shape:integer;Bi:real):extended;           {roots for every shape}
var smid,diff:real;lim,fun:arrayofreal2;

```

```

procedure TransEquation(shape:integer;Bi:extended;lim:arrayofreal2;var
fun:arrayofreal2);                                     {Transcendental Equation}
var s:byte;
begin
for s:=1 to 3 do
case shape of
1:if (cos(lim[s])=0)                                   {Infinite Slab}
then fun[s]:=1.1E4931
else fun[s]:=lim[s]*sin(lim[s])/cos(lim[s])-Bi;
2:fun[s]:=lim[s]*J1(lim[s]) - Bi*J0(lim[s]);          {Infinite Cylinder}

3:if (sin(lim[s])=0)                                   {Sphere}
then fun[s]:=1.1E4931
else fun[s]:=lim[s]*cos(lim[s])/sin(lim[s])+(Bi-1);

end;
end;

```

```

procedure ZbrentPause;                                 {Iteration Method to Find Roots}
begin
lim[2]:=(lim[1]+lim[3])/2;
end;

```

```

BEGIN
case shape of
1:begin
lim[1]:=1.5708;                                       {Infinite Slab}
lim[3]:=0.000001;
lim[2]:=0;
end;
2:begin
lim[1]:=2.4048;                                       {Infinite Cylinder}
lim[3]:=0.000001;
lim[2]:=0;
end;
3:begin
lim[1]:=3.1416;                                       {Sphere}
lim[3]:=0.000001;
lim[2]:=0;
end;
end;
repeat
smid:=lim[2];
lim[2]:=(lim[1]+lim[3])/2;
TransEquation(Shape,Bi,lim,fun);
if ((fun[1]*fun[3]) >= 0)
then ZbrentPause;
if (fun[3]<0) then if fun[2]<=0 then lim[3]:=lim[2] else lim[1]:=lim[2];
if (fun[3]>=0) then if fun[2]<=0 then lim[1]:=lim[2] else lim[3]:=lim[2];
diff:=abs(lim[2])-smid;
until abs(diff)<0.000001;
root:=lim[2];
END;

```

```

PROCEDURE Ref_shape(Shape:integer;Bi:real;Rt:extended;var FcRef,JcRef:real);
{Find Slope & Intercept of Basic Shape from Analytical Solution}
var ln_intecetC0,ln_intecetAV0:extended;
BEGIN
case shape of
1:begin
{Infinite Slab}

```

```

Rt:=root(shape,Bi);
ln_intecetC0:=ln(2*Bi/(cos(Rt)*(Bi*(Bi+1)+Sqr(Rt))));
JcRef:=exp(ln_intecetC0);
FcRef:=-Sqr(Rt);
end;

2:begin
Rt:=root(shape,Bi);
ln_intecetC0:=ln(2*Bi/(Sqr(Rt)+Sqr(Bi))/JO(Rt));
JcRef:=exp(ln_intecetC0);
FcRef:=-Sqr(Rt);
end;

3:begin
Rt:=root(shape,Bi);
ln_intecetC0:=ln(2*Bi*sin(Rt)*(Sqr(Rt)+Sqr(Bi-1))/(Rt*(Sqr(Rt)+(Bi-1)*Bi)));
JcRef:=exp(ln_intecetC0);
FcRef:=-Sqr(Rt);
end;
end;
END;

```

(##### END OF ANALYTICAL PART #####)

```

PROCEDURE writeprop;
BEGIN
Writeshape(shape,Eo,Einf);
Writeln(Result,'R = ',R:4:3,' m');
Writeln(Result,'k = ',k:8:7,' Wm-1K-1');
Writeln(Result,'Ka = ',Kg:15:14,' sm-1');
Writeln(Result,'Bi = ',Bi:7:4);
Writeln(Result,'hc = ',Hc:8:3,' Wm-1K-1');
writeln(result,'aw = ',aw:4:3);
writeln(result,'Hr = ',rH:4:3);
writeln(Result);
Writeln('R = ',R:4:3,' m');
Writeln('k = ',k:8:7,' Wm-1K-1');
Writeln('Ka = ',Kg:15:14,' sm-1');
Writeln('hc = ',Hc:8:3,' W/m2K-1');
writeln('aw = ',aw:4:2);
writeln('Hr = ',rH:4:2);
writeln(Result);
writeln(Result,' ++++++');

Ref_shape(shape,Bi,Rt,FcRef,JcRef);
Writeln(Result);
Writeln(Result,'reference slope = ',FcRef:5:2,' reference intercept = ',JcRef:5:2);
Writeln(Result);
END;

```

(***** START NUMERICAL PARTS *****)

```

PROCEDURE Tequi(Ca,aw,rH,Ta:real;var Tequ:real);
var Tequ1:real;
BEGIN
Tequ:=Ta;
Pwj:=exp(23.4795-3990.56/(Tequ+233.833));
Pwa:=exp(23.4795-3990.56/(Ta+233.833));
PJ:=aw*Pwj;
Pa:=rH*Pwa;
Hfg:=2.50E6-2.5E3*Tequ;

Hwsurf:=18*PJ/29/(Pt-PJ);
Hwair:=18*Pa/29/(Pt-Pa);
Tequ1:=Ta-(Hwsurf-Hwair)/Ca*Hfg;

while abs(Tequ1-Tequ)>0.000001 do
begin
Tequ:=(Tequ1+Tequ)/2;
Pwj:=exp(23.4795-3990.56/(Tequ+233.833));
Pwa:=exp(23.4795-3990.56/(Ta+233.833));
PJ:=aw*Pwj;
Pa:=rH*Pwa;

```

```

Hfg:=2.50E6-2.5E3*Tequ;

Hwsurf:=18*PJ/29/(Pt-PJ);
Hwair:=18*Pa/29/(Pt-Pa);
Tequ:=Ta-(Hwsurf-Hwair)/Ca*Hfg;
end;
Tequ:=Tequ;
END;

PROCEDURE coef1(K,Dt,Dr,Cp,Hc,Kg,Hfg,d:real;var M,Q,W,MM,WW:real);
      {Common Coefficients of Numerical Solutions for Every Shape}
BEGIN
      {heat balance}
      M:=K*Dt/Dr/Dr/Cp;
      Q:=Hc*Dt/Cp/Dr;
      W:=Kg*Dt*Hfg/Cp/Dr;

      {mass balance}
      MM:=d*Dt/Dr/Dr;
      WW:=Kg*Dt/Dr;
END;

PROCEDURE coef2(shape:integer;R,Dr:real;J:integer;var PP,BB,C1,CO1,CO2,CO3,CO4,CO6,
CO7:real);
      {Coefficients of Numerical Solutions for Each Shape}
      {shape:1:infinite slab,2:infinite cyl,3:sphere}
BEGIN
      if shape=1 then
      begin
      PP:=R;
      BB:=2;
      C1:=2;
      CO1:=1;
      CO2:=1;
      CO3:=1/2;
      CO4:=1/2;
      CO6:=J;
      CO7:=Dr;
      end
      else if shape=2 then
      begin
      PP:=R/2;
      BB:=4;
      C1:= 2;
      CO1:=(J-0.5)/(J-0.25);
      CO2:=(J/(J-0.25));
      CO3:=(J-0.25);
      CO4:=1/4;
      CO6:=J*J;
      CO7:=(Dr*Dr/2/R);
      end
      else
      begin
      PP:=R/3;
      BB:=6;
      C1:=3;
      CO1:=(J-0.5)*(J-0.5)/(J*J*J-(J-0.5)*(J-0.5)*(J-0.5));
      CO2:=J*J/(J*J*J-(J-0.5)*(J-0.5)*(J-0.5));
      CO3:=J*J*J-(J-0.5)*(J-0.5)*(J-0.5);
      CO4:=1/8;
      CO6:=J*J*J;
      CO7:=Dr*Dr*Dr/3/R/R;
      end;
END;

PROCEDURE coef3(shape:integer;L:real;var AA1,AA2:real);
      {Coefficients of Numerical Solutions for Each Shape}
BEGIN
case shape of
1:begin
      AA1:=1;
      AA2:=1;
end;

```

```

2:begin
  AA1:=(1+0.5/L);
  AA2:=(1-0.5/L);
end;
3:begin
  AA1:=(1+1/L);
  AA2:=(1-1/L);
end;
end;
END;

FUNCTION CO55(shape,L:integer):real;
                                     {Coefficients of Numerical Solutions for Each Shape}
BEGIN
case shape of
  1:CO55:=1;
  2:CO55:=2*L;
  3:CO55:=(L+0.5)*(L+0.5)*(L+0.5)-(L-0.5)*(L-0.5)*(L-0.5);
end;
END;

PROCEDURE check(J:integer;Tnow:arrayofreal;Ta,Hc,Dt,Hfg,Kg,PJ,Pa:real; var Hflux,
Hflow,Mflux,Mflow:real);
                                     {Check Heat and Mass Balance}
BEGIN
  Hflux:=Hc*(Tnow[J]-Ta)+Kg*Hfg*(PJ-Pa);
                                     {Js-1m-2}
  Hflow:=Hflow+Dt*Hflux;
                                     {Jm-2}
  Mflux:=Kg*(PJ-Pa);
                                     {kgs-1m-2}
  Mflow:=Mflow+Dt*Mflux;
                                     {kgm-2}
END;

PROCEDURE Y(Tc,Tav,Ts,Tequ:real;var Yc,Yav,Ys:real);
                                     {Dimensionless Temperature}
BEGIN
  Yc:=(Tc-Tequ)/(Ti-Tequ);
  Yav:=(Tav-Tequ)/(Ti-Tequ);
  Ys:=(Ts-Tequ)/(Ti-Tequ);
END;

PROCEDURE printout;
                                     {Print Result Out}
BEGIN
  Writeln(time:8:1,' ',Fo:5:3,' ',Yc:4:3,' ',Yav:4:3,' ',Ys:4:3,' ',Tc:7:2,'
  ',Tav:7:2,' ',Ts:7:2,' ',Tequ:7:2);
  Writeln(RESULT,time:8:1,' ',Fo:5:3,' ',Yc:4:3,' ',Yav:4:3,' ',Ys:4:3,' ',Tc:7:2,'
  ',Tav:7:2,' ',Ts:7:2,' ',Tequ:7:2);
  telaps:=0;
END;
{*****}

PROCEDURE fitcurve(count:integer;Foo,Ycc:arrayofreal0;var Fcfinite,Jcfinite,coef
:real);
                                     {Regression Analysis: Slope and Intercept}
var YY,XX,XY,X2,Y2,Yt,int1,int2,int3,int4,numFo,lnY,Y,Fo,int:real;
BEGIN
YY:=0;XX:=0;XY:=0;X2:=0;Y2:=0;Fo:=0;Y:=0;
for count:=1 to count do
begin
  Fo:=Foo[count];
  Y:=Ycc[count];
  lnY:=ln(abs(Y));
  XY:=XY+Fo*lnY;
  XX:=XX+Fo;
  YY:=YY+lnY;
  X2:=X2+Sqr(Fo);
  Y2:=Y2+Sqr(lnY);
end;
Yt:=YY/count;
numFo:=XX/count;
Fcfinite:=(XY-YY*XX/count)/(X2-Sqr(XX)/count);
                                     {Slope}

int:=Yt-Fcfinite*numFo;
                                     {Intercept}
Jcfinite:=exp(int);

```

```

int1:=count*XY-YY*XX;
int2:=count*Y2-Sqr(YY);
int3:=count*X2-Sqr(XX);
int4:=Sqrt(int2*int3);

```

```

coef:=int1/int4;
END;

```

```

PROCEDURE Findcurve_writersresult (var Fcfinite,Jcfinite,RatioFcfinite, RatioJcfinite
:real);

```

```

BEGIN
Fitcurve(count, Foo, Ycc, Fcfinite, Jcfinite, coefC);
(slope and intercept for reference shapes)

```

```

Rt:=root(Shape, Bi);
Ref_shape(shape, Bi, Rt, FcRef, JcRef);
RatioFcfinite:=Fcfinite/FcRef;
RatioJcfinite:=Jcfinite/JcRef;

```

```

writeln(Result, ' ', 'Bi    Tin    Ta    Hr', ' ');
WriteLn(result, Bi:4:2, ' ', Ti:3:1, ' ', Ta:4:1, ' ', rH:3:2);
writeln(' ', 'Bi    Tin    Ta    Hr', ' ');
WriteLn(Bi:4:2, ' ', Ti:3:1, ' ', Ta:4:1, ' ', rH:3:2);
writeln;

```

```

WriteLn(result, ' ', 'Teq = ', Tequ:6:3, ' hc = ', hc:8:3, ' ');
WriteLn(' ', 'Teq = ', Tequ:6:3, ' hc = ', hc:8:3, ' ');

```

```

WriteLn(result, ' ', 'fcRef = ', FcRef:6:3, ' ', 'jcRef = ', JcRef:6:3, ' ');
WriteLn(' ', 'fcRef = ', FcRef:6:3, ' ', 'jcRef = ', JcRef:6:3, ' ');

```

```

END;

```

```

PROCEDURE check_compare; (Check Heat and Mass Balance)

```

```

BEGIN
check(J, Tnow, Ta, Hc, Dt, Hfg, Kg, PJ, Pa, Hflux, Hflow, Mflux, Mflow);
(Heat and Mass Left in Solid)

```

```

Hend:=CO3*Tnew[J]+CO4*Tnew[0];
Mend:=CO3*Cnew[J]+CO4*Cnew[0];

```

```

For L:=1 to J-1 Do
begin
CO5:=CO55(shape, L);
Hend:=Hend+CO5*Tnow[L];
Mend:=Mend+CO5*Cnow[L];
end;

```

```

Hend:=Hend*Cp*CO7; (Jm-2)
Mend:=Mend*CO7; (kgm-2)
(Total Heat & Mass Flow, Htotal_flow should equal to Hflow)

```

```

Htotal_flow:=Hini-Hend;
Mtotal_flow:=Mini-Mend;
Diff1:= Htotal_flow - Hflow;
Diff2:= Mtotal_flow - Mflow;;

```

```

WriteLn;
WriteLn('check Ht. & mass balance');
WriteLn('Htotal_flow = (Hinitial) ', Hini:10:2, ' - (Hend) ', Hend:10:2, ' = ', Htotal_flow:10:2);
WriteLn('total diff. = (Htotal_flow) ', Htotal_flow:10:2, ' - (Hflow) ', Hflow:10:2, ' = ', Diff1:8:2);
WriteLn(' % diff. = ', Diff1/Htotal_flow*100:5:3);

```

```

WriteLn('Mtotal_flow = (Minitial) ', Mini:10:4, ' - (Mend) ', Mend:10:4, ' = ', Mtotal_flow:10:4);
WriteLn('total diff. = (Mtotal_flow) ', Mtotal_flow:10:4, ' - (Mflow) ', Mflow:10:4, ' = ', Diff2:8:4);
WriteLn(' % diff. = ', Diff2/Mtotal_flow*100:5:3);
END;

```

```

PROCEDURE FindSimpleModel (Ta, rH, Ti, aw, Bi, Einf, Eo, FcRef, JcRef:real;
var RatioFcmodel, RatioJcmodel, Fcmodel, Jcmodel:real); (Simple Model)

```

```

var coef1,coef2,coef3,coef4,coef5,coef6,A,E:real;

BEGIN
coef1:=Ta*(rH+0.34)+(5*rH+0.12*Ti+9.87)*exp(0.8*ln(aw));
RatioFcmodel:=1+Bi/15/(exp(1.5*ln(Bi))+1.5)+coef1/19/(exp(1.2*ln(Bi))+1.2);

A:=exp(4*ln(Bi)/3);
E:=(A+1.85)/(A/Einf+1.85/Eo);

coef2:=0.0335*E*exp(-(Bi-2.5)*(Bi-2.5));
coef3:=rH*(0.0725*exp(-(Bi-0.7)*(Bi-0.7)));
coef4:=Ta*(0.00338*rH+0.00413*exp(-(Bi-0.9)*(Bi-0.9)));
coef5:=Ti*(0.00447*exp(-1.3*Bi)+0.000599);
coef6:=0.0153*(exp(2.4*ln(aw)))/exp(0.4*ln(Bi));
RatioJcmodel:=1-coef6+coef3+coef4-coef5+coef2;

Fcmodel:=RatioFcmodel*FcRef;
Jcmodel:=RatioJcmodel*JcRef;
END;

PROCEDURE finalresult;
BEGIN
Writeln('','','fcModel = ',Fcmodel:5:2,' jcModel = ',Jcmodel:5:2,
' RatiofcModel = ',RatioFcmodel:5:2,' RatiojcModel = ',RatioJcmodel:5:2,'');
Writeln('','','fcExp = ',FcExp:5:2,' jcExp = ',JcExp:5:2,
' RatiofcExp = ',RatioFcExp:5:2,' RatiojcExp = ',RatioJcExp:5:2,'');
Writeln('','','fcFinite = ',FcFinite:5:2,' jcFinite = ',JcFinite:5:2,
' RatiofcFinite = ',RatioFcFinite:5:2,' RatiojcFinite = ',RatioJcFinite:5:2,'');
Writeln;

Writeln('% Different between Model-Exp');
Writeln('Ratiofc(Model-Exp.) = ',deltaFcA:6:1,' Ratiojc(Model-Exp.) = ',deltaJcA:6:1);
Writeln('% Different between Finite diff.-Exp. ');
Writeln('Ratiofc(Finite diff.-Exp.) = ',deltaFcB:6:1,' Ratiojc(Finite diff.-Exp.) = ',deltaJcB:6:1);

Writeln(Result,'','','fcModel = ',Fcmodel:5:2,' jcModel = ',Jcmodel:5:2,
' RatiofcModel = ',RatioFcmodel:5:2,' RatiojcModel = ',RatioJcmodel:5:2,'');
Writeln(Result,'','','fcExp = ',FcExp:5:2,' jcExp = ',JcExp:5:2,
' RatiofcExp = ',RatioFcExp:5:2,' RatiojcExp = ',RatioJcExp:5:2,'');
Writeln(Result,'','','fcFinite = ',FcFinite:5:2,' jcFinite = ',JcFinite:5:2,
' RatiofcFinite = ',RatioFcFinite:5:2,' RatiojcFinite = ',RatioJcFinite:5:2,'');
Writeln(Result);

Writeln(Result,'% Different between Model-Exp');
Writeln(Result,'Ratiofc(Model-Exp.) = ',deltaFcA:6:1,' Ratiojc(Model-Exp.) = ',deltaJcA:6:1);
Writeln(Result,'% Different between Finite diff.-Exp. ');
Writeln(Result,'Ratiofc(Finite diff.-Exp.) = ',deltaFcB:6:1,' Ratiojc(Finite diff.-Exp.) = ',deltaJcB:6:1);
END;

Procedure CompareTime (TeqExp, TeqCal, FcRef, JcRef, FcExp, JcExp, R:real; var
timeExp,timeModel,timeFinite:real);
(Compare Time of (Simple Model)-Exp. and (Finite Difference Model)-Exp.)
var FoExp,FoModel,FoFinite:real;n:integer;diffA,diffB,Ycx,Ycxx:arrayofreal2;

BEGIN

Findcurve_writeresult (Fcfinite, Jcfinite, RatioFcfinite, RatioJcfinite);
FindSimpleModel (Ta, rH, Ti, aw, Bi, Einf, Eo, FcRef, JcRef, RatioFcmodel, RatioJcmodel,
Fcmodel, Jcmodel);

RatioFcExp:=FcExp/FcRef;
RatioJcExp:=JcExp/JcRef;

deltaFcA:=(RatioFcmodel-RatioFcExp)/RatioFcExp*100; (Model-Exp.)
deltaJcA:=(RatioJcmodel-RatioJcExp)/RatioJcExp*100;

deltaFcB:=(RatioFcfinite-RatioFcExp)/RatioFcExp*100; (Finite Diff.-Exp.)
deltaJcB:=(RatioJcfinite-RatioJcExp)/RatioJcExp*100;

writeln;

```

```

writeln(result);

finalresult;

Ycxx[1]:=0.1;Ycxx[2]:=0.35;Ycxx[3]:=0.7;                                {Yc,exp at Teq,exp}

For n:=1 to 3 do
begin
  Ycx[n]:=(Ycxx[n]*(Ti-TeqExp)+TeqExp)-TeqCal)/(Ti-TeqCal);          {Yc,pred at Teq,exp}
  FoExp:=(ln(Ycxx[n])-ln(Jcexp))/(Fcexp);                            {Exp.}
  FoModel:=(ln(Ycx[n])-ln(Jcmodel))/(Fcmodel);                       {Model}
  FoFinite:=(ln(Ycx[n])-ln(Jcfinite))/(Fcfinite);                    {Finite Diff.}

  timeExp:=FoExp*R*R*Cp/k/60/60;                                     {Experimental Time to Reach Teq,exp}
  timeModel:=FoModel*R*R*Cp/k/60/60;                                {Predicted Time (Model) to Reach Teq,exp}
  timeFinite:=FoFinite*R*R*Cp/k/60/60;                             {Predicted Time (Finite Diff.) to Reach Teq,exp}

  diffA[n]:=(timeModel-timeExp)/timeExp*100;                        {Model-Exp.}
  diffB[n]:=(timeFinite-timeExp)/timeExp*100;                       {Finite Diff.=Exp.}
  writeln;
  writeln('n : ',n:1,' Yc['',n:1,'] = ',Ycx[n]:5:2);
  writeln('Time (min.) from Simple Model : ',timeModel:6:2,' Experimental Time
(min): ',timeExp:6:2,' Time (min.) from Finite Diff.: ',timeFinite:6:2);
  writeln(' % Diff. between Model-Exp. = ',diffA[n]:6:1,' %Diff. between
Finite Diff.-Exp. = ',diffB[n]:6:1);

  writeln(Result);
  writeln(Result,'n : ',n:1,' Yc['',n:1,'] = ',Ycx[n]:5:2);
  writeln(Result,'Time (min.) from Simple Model : ',timeModel:6:2,' Experimental
Time (min): ',timeExp:6:2,' Time (min.) from Finite Diff.: ',timeFinite:6:2);
  writeln(Result,' % Diff. between Model-Exp. = ',diffA[n]:6:1,' %Diff. between
Finite Diff.-Exp. = ',diffB[n]:6:1);

end;

END;
{*****}

                (START MAIN PROGRAM FOR NUMERICAL METHOD)

BEGIN
askprop;
R:=DD/2;
Writeshape(shape,Eo,Einf);
writeln('Eo = ',Eo:4:2,' Einf = ',Einf:4:2,' E = ',E:5:3);
Rt:=root(Shape,Bi);

Cp:=CCp*den*1E3;                                                    {Jm-3K-1}
Hc:=Bi*k/R;
Kg:=Hc*18/(Ca*29*Pt);                                             {Lewis Relationships, Surface Mass Transfer Coef., sm-1}

writeprop;

                (NUMERICAL PARTS)

Tequi(Ca,aw,rH,Ta,Tequ);
{Step to Use}

Dr:=R/J;
Dt:=Dtt(shape,Bi);
writeln('dt (s) ',dt:4:2);

For L:=0 to J Do                                                    {Establish Initial Condition}
  BEGIN
    Tnow[L]:=Ti;
    Tnew[L]:=Ti;
    Cnow[L]:=Ci;
    Cnew[L]:=Ci;
  END;

```

```

Tc:=Ti;
Ts:=Ti;
Tav:=Ti;
Cc:=Ci;
Cav:=Ci;
Cs:=Ci;
sum1:=0;
sum2:=0;

coef2(shape,R,Dr,J,PP,BB,C1,CO1,CO2,CO3,CO4,CO6,CO7);
Hini:=Cp*Ti*PP;
Mini:=Ci*PP;

                                                                    (Start Conditions)
Hflow:=0;
Mflow:=0;
time:=0;
telaps:=0;
Yc:=1;Yav:=1;Ys:=1;
count:=0;
nn:=0;
Fo:=K*time/Cp/R/R;

                                                                    (Start Calculation)
While Yc > 0.045 Do
  BEGIN
  if time =0 then
    begin
      Fo:=K*time/Cp/R/R;
      Tequi (Ca,aw,rH,Ta,Tequ);
      printout;
    end;

  time:=time+Dt;
  telaps:=telaps+Dt;

  Fo:=K*time/Cp/R/R;
  Pwj:=exp(23.4795-3990.56/(Tnow[J]+233.833));
  Pwa:=exp(23.4795-3990.56/(Ta+233.833));
  PJ:=aw*Pwj;                                {Partial Pressure of Water at Product Surface, pa}
  Pa:=rH*Pwa;                                {Partial Pressure of Air at Product Surface, pa}
  Hfg:=2.50E6-2.5E3*Tnow[J];                {Latent Heat of Evaporation, Jkg-1}

  check(J,Tnow,Ta,Hc,Dt,Hfg,Kg,PJ,Pa,Hflux,Hflow,Mflux,Mflow);
  coef1(K,Dt,Dr,Cp,Hc,Kg,Hfg,d,M,Q,W,MM,WW);

  For L:=1 to J-1 Do                                                                    (Internal node)
  begin
    coef3(shape,L,AA1,AA2);
    Tnew[L]:=Tnow[L]+M*(AA1*Tnow[L+1]-2*Tnow[L]+AA2*Tnow[L-1]);
    Cnew[L]:=Cnow[L]+MM*(AA1*Cnow[L+1]-2*Cnow[L]+AA2*Cnow[L-1]);
  end;

                                                                    (Node 0)
  Tnew[0]:=Tnow[0]+M*BB*(Tnow[1]-Tnow[0]);
  Cnew[0]:=Cnow[0]+MM*BB*(Cnow[1]-Cnow[0]);
  Tc:=Tnew[0];
  Cc:=Cnew[0];

                                                                    (Node J)
  Tnew[J]:=Tnow[J]+C1*M*CO1*(Tnow[J-1]-Tnow[J])
    -C1*Q*CO2*(Tnow[J]-Ta)-C1*W*CO2*(PJ-Pa);
  Cnew[J]:=Cnow[J]+C1*MM*CO1*(Cnow[J-1]-Cnow[J])-C1*WW*CO2*(PJ-Pa);
  Ts:=Tnew[J];
  Cs:=Cnew[J];

                                                                    (Mean Temp.& Mean Conc.)
  sum1:=CO3*Tnew[J]+CO4*Tnew[0];
  sum2:=CO3*Cnew[J]+CO4*Tnew[0];
  For L:=1 to J-1 Do
  begin
    CO5:=CO55(shape,L);
    sum1:=sum1+CO5*Tnew[L];
    sum2:=sum2+CO5*Cnew[L];
  end;

```

```

Tav:=sum1/CO6;
Cav:=sum2/CO6;

Y(Tc,Tav,Ts,Tequ,Yc,Yav,Ys);

                                                                    {Print out Partial Results}

if telaps>=tprint then
begin
  printout;
  If Yc <= 0.7 then
  begin
    if Yc >= 0.045 then
    begin
      count:=count+1;
      Foo[count]:=Fo;
      Ycc[count]:=Yc;
      telaps:=0;
    end;
  end;
end;

                                                                    {Update Temp. & Conc. Arrays}

For L:=0 to J Do
begin
  Tnow[L]:=Tnew[L];
  Cnow[L]:=Cnew[L];
end;

END;

                                                                    {Fitting Curves}

check_compare;
CompareTime (TeqExp, TeqCal, FcRef, JcRef, FcExp, JcExp, R, timeExp, timeModel, timeFinite);

Close(Result);
END.

```

APPENDIX B
SAMPLE OF CALCULATION

This sample calculation is for Run no. 12 of the peeled carrot data set shown in Table 9.1.

(A) Raw and Processed Measured Data

The raw data are shown in Table B.1. Using the method described in Section 8.4.4 to estimate T_c , and averaging the three T_a estimates the data in Table B.2 were derived.

(B) Summary of Measured Data

(1) Peeled Carrot:

$T_{in} = 22.8$ °C, $T_{eq,exp} = 9.2$ °C, $T_{eq,pred} = 9.1$ °C, $D = 0.02348$ mm, $a_w = 0.977$,
 $\rho = 1063.2$ kg m⁻³, $C = 3.8725$ kJ kg⁻¹ K⁻¹, $k = 0.5192$ W m⁻¹ K⁻¹ (Section 8.6).

(2) Air Tunnel:

$T_a = 10.6$ °C, $H_r = 0.808$, $v_a = 2.2$ m s⁻¹.

(C) Calculation of Bi and Convective Cooling Coefficients

Equation (8.4) can be rewritten as:

$$h_c = 0.267 \left(\frac{k_a}{D} \right) \left(\frac{D v_a}{v_a} \right)^{0.597} \quad (B.1)$$

At $T_a = 10.6$ °C: $k_a = 2.516 \times 10^{-2}$ W m⁻¹ K⁻¹, $v_a = 14.25 \times 10^{-6}$ m² s⁻¹ (Gupta Prakash, 1979). Hence:

$$h_c = 0.267 \left(\frac{2.516 \times 10^{-2}}{0.02348} \right) \left(\frac{(0.02348)(2.2)}{14.25 \times 10^{-6}} \right)^{0.597} = 38.1 \text{ Wm}^{-2}\text{K}^{-1}$$

$$Bi = \frac{h_c R}{k} = \frac{38.1 \times 0.01174}{0.5192} = 0.862$$

The analytical solution for β_1 of an infinite cylinder (equation 6.3) is:

$$\beta_1 J_1(\beta_1) - Bi J_0(\beta_1) = 0$$

and J_0 (equation 6.4) and J_1 (equation 6.5) are Zero- and first-order Bessel's functions, respectively:

$$J_0(\beta_1) = 1 - \frac{\beta_1^2}{2^2(1!)^2} + \frac{\beta_1^4}{2^4(2!)^2} - \frac{\beta_1^6}{2^6(3!)^2} \dots + \frac{(-1)^n \beta_1^{2n}}{2^{2n}(n!)^2}$$

$$J_1(\beta_1) = \frac{\beta_1}{2} - \frac{\beta_1^3}{2^3 1! 2!} + \frac{\beta_1^5}{2^5 2! 3!} - \frac{\beta_1^7}{2^7 3! 4!} \dots + \frac{(-1)^n \beta_1^{2n+1}}{2^{2n+1} n! (n+1)!}$$

Using an iterative method, at $Bi = 0.862$, $\beta_1 = 1.1825$.

C.1 convective cooling coefficients

(A) f_{cConv} :

Using equation (5.1), f_{cConv} , the slope of a plot of $\ln Y_c$ versus FO is:

$$f_{cConv} = -\beta_1^2 = -(1.1825)^2 = -1.398$$

(B) j_{cConv} :

Using equation (2.13), j_{cConv} , the intercept of a plot of $\ln Y_c$ versus FO (at $r = 0$) is:

$$j_{cConv} = \frac{2 Bi J_0(0)}{(\beta_1^2 + Bi^2) J_0(\beta_1)}$$

where

$$J_0(0) = 1$$

and at $\beta_1 = 1.1825$, using equation (6.4):

$$J_0(1.1825) = 1 - \frac{1.1825^2}{2^2(1!)^2} + \frac{1.1825^4}{2^4(2!)^2} - \frac{1.1825^6}{2^6(3!)^2} \dots = 0.681$$

Therefore:

$$j_{cConv} = \frac{2 Bi J_0(0)}{(\beta_1^2 + Bi^2) J_0(\beta_1)} = \frac{2 \times 0.86 \times 1}{(1.1825^2 + 0.86^2) 0.681} = 1.181$$

(D) Calculation of f_{cEvap}/f_{cConv} and j_{cEvap}/j_{cConv} from Experimental Data

Experimental temperature-time data in Table B.1 and Figure 9.8 were transformed into values of FO and $Y_{c,exp}$ using equation (7.7) and $T_{eq,exp} = 9.2$ °C. For example at time

= 900 sec., $T_{c,exp} = 11.2$ °C then:

$$Y_{c,exp} = \frac{(T_{c,exp} - T_{eq,exp})}{(T_{in} - T_{eq,exp})}$$

$$= \frac{(11.2 - 9.2)}{(22.8 - 9.2)} = 0.147$$

and

$$Fo = \frac{t_{exp} k}{\rho C R^2}$$

$$= \frac{(900)(0.5192)}{(1063.2)(3.8725 \times 10^3)(0.01174)^2} = 0.823$$

Figure 9.9 is a semi-log plot of the data in Figure 9.8. After application of linear regression to the data between $Y_{c,exp} = 0.7$ and $Y_{c,exp} = 0.1$ estimates of the slope ($f_{cEvap,exp}$) = -2.428, and intercept ($j_{cEvap,exp}$) = 1.199 were made.

Therefore:

$$\frac{f_{cEvap,exp}}{f_{cConv}} = \frac{-2.428}{-1.398} = 1.737$$

$$\frac{j_{cEvap,exp}}{j_{cConv}} = \frac{-1.199}{-1.181} = 1.015$$

(E) Calculation of f_{cEvap}/f_{cConv} and j_{cEvap}/j_{cConv} by Proposed Method

Using equation (5.21) where $E_o = 2$ and $E_\infty = 1.76$ (for an infinite cylinder):

$$E = \frac{Bi^{\frac{4}{3}} + 1.85}{\frac{Bi^{\frac{4}{3}}}{E_{\infty}} + \frac{1.85}{E_0}}$$

$$= \frac{0.86^{\frac{4}{3}} + 1.85}{\frac{0.86^{\frac{4}{3}}}{1.76} + \frac{1.85}{2}} = 1.92$$

Thus from equation (5.19):

$$\frac{j_{cEvap,pred(model)}}{j_{cConv}} = 1 + \frac{Bi}{15 (Bi^{1.5} + 1.5)} +$$

$$\frac{T_a(H_r + 0.34) + (5H_r + 0.12T_{in} + 9.87)a_w^{0.8}}{19(Bi^{1.2} + 1.2)}$$

$$= \frac{0.86}{1.5 (0.86^{1.5} + 1.5)} +$$

$$\frac{10.8(0.808 + 0.34) + (5 \times 0.808 + 0.12 \times 22.8 + 9.87)0.977^{0.8}}{19(0.86^{1.2} + 1.2)}$$

$$= 1.768$$

Therefore

$$j_{cEvap,pred(model)} = 1.768 \times -1.398 = -2.472$$

And from equation (5.20):

$$\frac{j_{cEvap,pred(model)}}{j_{cConv}} = 1 - \frac{0.0153 a_w^{2.4}}{Bi^{0.4}} + 0.0335 E e^{-(Bi-2.5)^2} +$$

$$0.0725 H_r e^{-(Bi-0.7)^2} + T_a (0.00338 H_r + 0.00413 e^{-(Bi-0.9)^2}) -$$

$$T_{in} (0.00447 e^{-1.33 Bi} + 0.000599)$$

$$\begin{aligned} \frac{j_{cEvap,pred(model)}}{j_{cConv}} &= 1 - \frac{0.0153 \times 0.977^{2.4}}{0.86^{0.4}} + 0.0335 \times 1.92 \times e^{-(0.86-2.5)^2} + \\ & 0.0725 \times 0.808 \times e^{-(0.86-0.7)^2} + \\ & 10.8(0.00338 \times 0.808 + 0.00413 \times e^{-(0.86-0.9)^2}) - \\ & 22.8(0.00447 \times e^{-1.33 \times 0.86} + 0.000599) \\ &= 1.072 \end{aligned}$$

Therefore:

$$j_{cEvap,pred(model)} = 1.072 \times 1.181 = 1.266$$

(F) Predictions by the Finite Difference Model

The results shown in Table B.3 were generated using the computer program of Appendix A. Input data were as listed in section (B) of this appendix. And the results of mathematical simulation are:

$$\frac{f_{cEvap,pred(finite\ diff.)}}{f_{cConv}} = 1.760$$

$$f_{cEvap,pred(finite\ diff.)} = 1.760 \times -1.398 = -2.460$$

and

$$\frac{j_{cEvap,pred(finite\ diff.)}}{j_{cConv}} = 1.070$$

$$f_{cEvap,pred(finite\ diff.)} = 1.070 \times -1.181 = -1.264$$

(G) Calculation of Time to Reach $Y_{c,exp} = 0.1$ (See Table 9.2)

$T_{c,exp}$ that correspondes to $Y_{c,exp}$ (equation 7.7) = 0.1 is:

$$\begin{aligned}
T_{c,exp} &= Y_{c,exp} (T_{in} - T_{eq,exp}) + T_{eq,exp} \\
&= 0.1 (22.8 - 9.2) + 9.2 \\
&= 10.56 \text{ } ^\circ\text{C}
\end{aligned}$$

The $Y_{c,pred}$ (equations 7.8) to make prediction at $T_{c,exp}$, is:

$$\begin{aligned}
Y_{c,pred} &= \frac{T_{c,exp} - T_{eq,pred}}{T_{in} - T_{eq,pred}} \\
&= \frac{10.56 - 9.10}{22.80 - 9.10} \\
&= 0.107
\end{aligned}$$

Substituting other data from section (B), the times to reach $T_{c,exp}$ corresponding to $Y_{c,exp} = 0.1$ are:

(1) Experimental Results

At $f_{cEvap,exp} = -2.428$, $j_{cEvap,exp} = 1.199$, the measured time, t_{exp} (equation 7.7) is:

$$\begin{aligned}
t_{exp} &= \left(\frac{\ln Y_{c,exp} - \ln j_{cEvap,exp}}{f_{cEvap,exp} k} \right) \rho C R^2 \\
&= \left(\frac{\ln 0.100 - \ln 1.199}{-2.428 \times 0.5192} \right) \times 1063.2 \times 3.8725 \times 10^3 \times 0.01174^2 \\
&= 1118 \text{ s} \quad (18.6 \text{ min})
\end{aligned}$$

(2) Simple Model

At $f_{cEvap,pred(model)} = -2.472$, $j_{cEvap,pred(model)} = 1.266$, the predicted time, $t_{pred(model)}$ (equation 7.9) is:

$$\begin{aligned}
t_{pred(model)} &= \left(\frac{\ln Y_{c,pred} - \ln j_{cEvap,pred(model)}}{f_{cEvap,pred(model)} k} \right) \rho C R^2 \\
&= \left(\frac{\ln 0.107 - \ln 1.266}{-2.472 \times 0.5192} \right) \times 1063.2 \times 3.8725 \times 10^3 \times 0.01174^2 \\
&= 1093 \text{ s} \quad (18.2 \text{ min})
\end{aligned}$$

(3) Finite Difference Model

At $f_{cEvap,pred(finite\ diff.)} = -2.460$, $j_{cEvap,pred(finite\ diff.)} = 1.264$, the predicted time, $t_{pred(finite\ diff.)}$ (equation 7.9) is:

$$\begin{aligned} t_{pred(finite\ diff.)} &= \left(\frac{\ln Y_{c,pred} - \ln j_{cEvap,pred(finite\ diff.)}}{f_{cEvap,pred(finite\ diff.)}^k} \right) \rho C R^2 \\ &= \left(\frac{\ln 0.107 - \ln 1.264}{-2.460 \times 0.5192} \right) \times 1063.2 \times 3.8725 \times 10^3 \times 0.01174^2 \\ &= 1097 \text{ s} \quad (18.3 \text{ min}) \end{aligned}$$

(H) Comparison Between f_{cEvap}/f_{cConv} and j_{cEvap}/j_{cConv} Values

$$\% \text{ difference} = \left(\frac{\text{finite difference model or simple model} - \text{experimental result}}{\text{experimental result}} \right) \times 100 \quad (\text{B.2})$$

(1) f_{cEvap}/f_{cConv} :

(1.1) Simple Model versus Experimental Results

Using equation (B.2):

$$\% \text{ difference} = \frac{1.77 - 1.74}{1.74} \times 100 = 1.7 \%$$

(1.2) Finite Difference Model versus Experimental Results

Using equation (B.2):

$$\% \text{ difference} = \frac{1.76 - 1.74}{1.74} \times 100 = 1.1 \%$$

(2) j_{cEvap}/j_{cConv} :

(2.1) Simple Model versus Experimental Results

Using equation (B.2):

$$\% \text{ difference} = \frac{1.07 - 1.02}{1.02} \times 100 = 4.9 \%$$

(2.2) Finite Difference Model versus Experimental Results

Using equation (B.2):

$$\% \text{ difference} = \frac{1.07 - 1.02}{1.02} \times 100 = 4.9 \%$$

(I) Difference in time to reach $Y_{c,exp} = 0.1$. (See Table 9.2)

(1) Simple Model versus Experimental Results

Using equation (B.2):

$$\% \text{ difference} = \frac{18.2 - 18.6}{18.6} \times 100 = -2.2 \%$$

(2) Finite Difference Model versus Experimental Results

Using equation (B.2):

$$\% \text{ difference} = \frac{18.3 - 18.6}{18.6} \times 100 = -1.6 \%$$

Table B.1 Experimental Data Collected During Run 12 for Peeled Carrots. The three estimates of $T_{c,exp}$ are at 3 heights in the carrot. The 3 T_a measurement positions were around the test sample. The first H_r estimate was made using Lee Integer Probe and the second using Vaisala Probe. (unit: time in sec., temperature in °C, and relative humidity in %)

Time	T_{c1} Top Position	T_{c2} Bottom Position	T_{c3} Centre Position	T_{a1}	T_{a2}	T_{a3}	H_{r1}	H_{r2}
0	22.78	22.62	22.40	10.61	10.42	10.55	80.6	80.2
60	22.43	22.26	19.17	10.86	10.67	10.79		
120	21.65	21.65	17.65	10.86	10.61	10.67	80.0	80.2
180	20.14	20.02	16.43	10.73	10.42	10.55		
240	18.81	18.75	15.46	10.86	10.61	10.67	79.8	80.2
300	17.47	17.29	14.42	10.67	10.36	10.48		
360	16.43	16.25	13.81	10.79	10.42	10.61	79.8	80.2
420	15.52	15.21	13.07	10.67	10.42	10.42		
480	14.54	14.36	12.52	10.79	10.67	13.25	80.2	80.2
540	13.87	13.56	12.03	10.73	10.42	10.61		
600	13.25	12.95	11.59	10.67	10.30	10.42	79.8	80.1
660	12.83	12.45	11.35	10.73	10.42	10.42		
720	12.39	12.09	11.04	10.73	10.36	10.48	79.8	80.1
780	11.97	11.59	10.79	10.67	10.30	10.42		
840	11.53	11.17	10.55	10.55	10.30	10.36	79.8	80.1
900	11.23	10.92	10.30	10.61	10.24	10.36		
960	11.10	10.67	10.30	10.67	10.36	10.42	79.9	80.1
1020	10.86	10.48	10.18	10.67	10.36	10.42		
1080	10.55	10.24	9.93	10.67	10.24	10.42	80.0	80.1
1140	10.42	10.12	9.87	10.67	10.36	10.42		
1200	10.30	9.93	9.74	10.61	10.24	10.42	80.1	80.2
1260	10.12	9.74	9.62	10.67	10.36	10.42		
1320	10.06	9.68	9.81	10.73	10.42	10.55	80.1	80.3
1380	9.81	9.56	9.62	10.67	10.30	10.42		
1440	9.81	9.56	9.56	10.73	10.42	10.55	80.2	80.4
1500	9.81	9.43	9.62	10.79	10.42	10.55		
1560	9.68	9.43	9.56	10.79	10.48	10.55	80.2	80.4
1620	9.74	9.43	9.62	10.79	10.55	10.73		
1680	9.62	9.37	9.49	10.73	10.36	10.55	80.3	80.4
1740	9.62	9.31	9.49	10.79	10.42	10.61		
1800	9.56	9.31	9.49	10.79	10.42	10.61	80.1	80.4
1860	9.49	9.37	9.56	10.79	10.42	10.61		
1920	9.37	9.19	9.43	10.67	10.30	10.48	80.1	80.3
1980	9.49	9.25	9.43	10.79	10.48	10.61		
2040	9.37	9.25	9.49	10.73	10.48	10.55	80.1	80.3
2100	9.43	9.25	9.56	10.79	10.55	10.67		
2160	9.37	9.13	9.31	10.67	10.36	10.48	80.0	80.1
2220	9.31	9.13	9.37	10.73	10.42	10.55		
2280	9.37	9.19	9.43	10.79	10.42	10.61	80.0	80.2
2340	9.43	9.19	9.49	10.73	10.42	10.61		
2400	9.37	9.19	9.43	10.73	10.42	10.61	80.0	80.3
2460	9.25	9.06	9.43	10.73	10.42	10.55		
2520	9.37	9.13	9.49	10.61	10.36	10.48	80.1	80.3
2580	9.31	9.19	9.49	10.73	10.42	10.55		
2640	9.31	9.19	9.43	10.73	10.42	10.55	80.0	80.2
2700	9.25	9.13	9.37	10.61	10.36	10.55		
2760	9.25	9.06	9.43	10.67	10.36	10.42	80.1	80.3
2820	9.31	9.19	9.43	10.67	10.42	10.48		
2880	9.19	9.13	9.37	10.67	10.36	10.55	80.0	80.3
2940	9.25	9.06	9.37	10.67	10.42	10.55		
3000	9.25	9.06	9.37	10.61	10.36	10.42	80.2	80.2
3060	9.25	9.13	9.37	10.67	10.42	10.61		
3120	9.25	9.00	9.37	10.67	10.36	10.55	80.1	80.3
3180	9.19	9.06	9.37	10.67	10.30	10.55		
3240	9.25	9.13	9.37	10.67	10.30	10.55	80.2	80.4
3300	9.25	9.13	9.43	10.67	10.36	10.55		
3360	9.19	9.06	9.37	10.61	10.30	10.48	80.1	80.4
3420	9.19	9.06	9.43	10.61	10.30	10.55		
3480	9.19	9.06	9.37	10.61	10.30	10.48	80.2	80.4

3540	9.31	9.13	9.56	10.73	10.42	10.61		
3600	9.19	9.13	9.49	10.73	10.36	10.61	80.1	80.4
3660	9.25	9.06	9.43	10.67	10.42	10.48		
3720	9.19	9.06	9.43	10.67	10.36	10.48	80.3	80.3
3780	9.19	9.06	9.43	10.73	10.42	10.55		
3840	9.25	9.13	9.43	10.67	10.36	10.55	80.2	80.4
3900	9.31	9.19	9.43	10.79	10.48	10.67		
3960	9.25	9.13	9.43	10.79	10.42	10.61	80.2	80.5
4020	9.31	9.06	9.43	10.73	10.42	10.55		
4080	9.19	9.06	9.43	10.67	10.42	10.55	80.2	80.5
4140	9.25	9.13	9.49	10.73	10.42	10.55		
4200	9.25	9.06	9.37	10.73	10.36	10.48	80.3	80.4
4260	9.31	9.13	9.49	10.86	10.55	10.67		
4320	9.25	9.13	9.49	10.67	10.36	10.48	80.3	80.5
4380	9.25	9.06	9.43	10.73	10.42	10.48		
4440	9.25	9.13	9.43	10.73	10.36	10.55	80.2	80.5
4500	9.25	9.06	9.43	10.67	10.42	10.61		
4560	9.25	9.06	9.43	10.73	10.42	10.55	80.5	80.6
4620	9.19	9.00	9.43	10.67	10.36	10.55		
4680	9.25	9.06	9.37	10.73	10.42	10.55	80.5	80.5
4740	9.31	9.13	9.56	10.92	10.48	10.73		
4800	9.31	9.19	9.49	10.79	10.42	10.61	80.6	80.6
4860	9.31	9.13	9.43	10.73	10.42	10.61		
4920	9.31	9.19	9.49	10.73	10.55	10.73	80.5	80.7
4980	9.25	9.06	9.43	10.67	10.36	10.55		
5040	9.19	9.06	9.49	10.73	10.42	10.61	80.6	80.7
5100	9.25	9.06	9.49	10.67	10.36	10.61		
5160	9.25	9.06	9.49	10.67	10.36	10.61	80.6	80.6
5220	9.25	9.13	9.43	10.67	10.36	10.55		
5280	9.31	9.19	9.49	10.73	10.48	10.55	80.5	80.7
5340	9.31	9.19	9.49	10.73	10.42	10.55		
5400	9.31	9.13	9.56	10.79	10.42	10.67	80.5	80.7
5460	9.19	9.13	9.49	10.61	10.36	10.55		
5520	9.31	9.13	9.49	10.67	10.42	10.61	80.6	80.7
5580	9.25	9.13	9.49	10.73	10.42	10.55		
5640	9.37	9.19	9.56	10.73	10.42	10.61	80.6	80.6
5700	9.25	9.13	9.49	10.67	10.36	10.55		
5760	9.31	9.13	9.56	10.67	10.30	10.48	80.6	80.7
5820	9.37	9.19	9.62	10.73	10.42	10.61		
5880	9.31	9.19	9.56	10.67	10.42	10.67	80.6	80.9
5940	9.37	9.19	9.56	10.67	10.36	10.55		
6000	9.31	9.13	9.56	10.67	10.36	10.55	80.6	80.9
6060	9.31	9.19	9.49	10.73	10.36	10.61		
6120	9.19	9.13	9.49	10.67	10.36	10.55	80.6	80.7
6180	9.25	9.06	9.49	10.61	10.36	10.48		
6240	9.31	9.19	9.56	10.67	10.36	10.55	80.7	80.9
6300	9.25	9.13	9.49	10.67	10.36	10.55		
6360	9.31	9.19	9.62	10.79	10.48	10.67	80.6	81.0
6420	9.25	9.06	9.56	10.61	10.30	10.48		
6480	9.25	9.19	9.56	10.67	10.36	10.55	80.8	81.0
6540	9.37	9.25	9.56	10.73	10.42	10.67		
6600	9.31	9.13	9.56	10.67	10.36	10.61	80.8	81.0
6660	9.31	9.19	9.56	10.73	10.48	10.67		
6720	9.37	9.19	9.68	10.73	10.42	10.61	80.8	81.0
6780	9.43	9.31	9.62	10.79	10.42	10.67		
6840	9.31	9.19	9.56	10.73	10.42	10.61	80.8	81.1
6900	9.43	9.25	9.62	10.73	10.36	10.61		
6960	9.25	9.19	9.56	10.67	10.36	10.55	80.8	81.1
7020	9.37	9.25	9.62	10.79	10.55	10.67		
7080	9.37	9.25	9.62	10.73	10.42	10.61	80.8	81.2
7140	9.37	9.25	9.62	10.79	10.48	10.61		
7200	9.31	9.25	9.62	10.79	10.42	10.67	80.8	81.2
7260	9.37	9.19	9.56	10.67	10.36	10.55		
7320	9.37	9.19	9.56	10.73	10.42	10.67	81.0	81.2
7380	9.43	9.31	9.68	10.86	10.55	10.79		
7440	9.31	9.25	9.68	10.67	10.36	10.61	80.8	81.1
7500	9.37	9.19	9.68	10.73	10.42	10.67		
7560	9.31	9.25	9.62	10.67	10.36	10.67	80.9	81.2
7620	9.37	9.19	9.68	10.79	10.36	10.61		
7680	9.37	9.31	9.68	10.86	10.55	10.79	80.9	81.3
7740	9.43	9.31	9.74	10.73	10.48	10.73		
7800	9.43	9.25	9.68	10.73	10.48	10.67	81.0	81.2
7860	9.43	9.31	9.68	10.86	10.55	10.79		
7920	9.37	9.25	9.68	10.79	10.48	10.67	80.9	81.2

7980	9.56	9.43	9.74	10.86	10.55	10.79		
8040	9.49	9.25	9.68	10.79	10.48	10.73	80.9	81.3
8100	9.43	9.25	9.68	10.73	10.48	10.67		
8160	9.43	9.25	9.68	10.73	10.42	10.67	81.0	81.4
8220	9.43	9.19	9.68	10.67	10.36	10.55		
8280	9.31	9.31	9.68	10.73	10.48	10.61	81.0	81.2
8340	9.37	9.25	9.81	10.79	10.55	10.67		
8400	9.31	9.25	9.62	10.67	10.36	10.61	81.0	81.3
8460	9.31	9.13	9.62	10.67	10.36	10.55		
8520	9.43	9.25	9.62	10.86	10.48	10.73	81.0	81.3
8580	9.31	9.19	9.62	10.67	10.42	10.55		
8640	9.37	9.19	9.62	10.73	10.42	10.67	81.2	81.4
8700	9.31	9.19	9.56	10.67	10.36	10.55		
8760	9.25	9.19	9.62	10.67	10.36	10.61	81.0	81.3
8820	9.43	9.25	9.74	10.79	10.48	10.73		
8880	9.25	9.19	9.62	10.67	10.36	10.61	81.0	81.3
8940	9.37	9.13	9.62	10.79	10.42	10.67		
9000	9.43	9.25	9.62	10.79	10.42	10.67	81.0	81.4
9060	9.43	9.37	9.68	10.79	10.48	10.67		
9120	9.49	9.31	9.74	10.92	10.55	10.73	81.2	81.4
9180	9.43	9.25	9.68	10.79	10.48	10.67		
9240	9.37	9.25	9.56	10.73	10.42	10.61	81.0	81.3
9300	9.31	9.25	9.62	10.73	10.48	10.61		
9360	9.43	9.31	9.68	10.79	10.55	10.73	81.0	81.4
9420	9.31	9.19	9.68	10.73	10.42	10.61		
9480	9.43	9.25	9.68	10.86	10.55	10.79	81.0	81.5
9540	9.37	9.25	9.68	10.73	10.42	10.67		
9600	9.37	9.25	9.56	10.73	10.42	10.67	81.3	81.4
9660	9.31	9.25	9.68	10.73	10.42	10.61		
9720	9.37	9.25	9.74	10.73	10.42	10.67	81.0	81.4
9780	9.43	9.31	9.74	10.86	10.55	10.73		
9840	9.37	9.19	9.68	10.67	10.36	10.61	81.0	81.4
9900	9.43	9.25	9.68	10.79	10.42	10.55		
9960	9.37	9.25	9.68	10.79	10.42	10.67	81.0	81.5
10020	9.31	9.19	9.62	10.73	10.30	10.55		
10080	9.37	9.19	9.62	10.73	10.48	10.67	81.3	81.3
10140	9.37	9.25	9.68	10.79	10.42	10.79		
10200	9.37	9.19	9.68	10.67	10.36	10.67	81.2	81.4
10260	9.37	9.19	9.68	10.73	10.36	10.61		
10320	9.43	9.25	9.62	10.79	10.42	10.67	81.2	81.4
10380	9.37	9.25	9.62	10.86	10.48	10.61		
10440	9.31	9.25	9.74	10.73	10.42	10.61	81.3	81.6
10500	9.37	9.25	9.62	10.73	10.36	10.61		
10560	9.31	9.25	9.68	10.73	10.36	10.55	81.3	81.4
10620	9.31	9.19	9.56	10.73	10.36	10.55		
10680	9.43	9.31	9.68	10.79	10.48	10.67	81.2	81.5
10740	9.37	9.19	9.68	10.73	10.36	10.61		
10800	9.37	9.19	9.62	10.67	10.42	10.55	81.2	81.5
10860	9.43	9.31	9.74	10.79	10.48	10.73		
10920	9.31	9.25	9.62	10.79	10.42	10.61	81.4	81.6
10980	9.43	9.25	9.68	10.79	10.48	10.67		
11040	9.37	9.19	9.74	10.79	10.42	10.61	81.3	81.5
11100	9.43	9.25	9.74	10.79	10.55	10.67		
11160	9.37	9.19	9.74	10.73	10.36	10.61	81.3	81.5
11220	9.31	9.25	9.62	10.73	10.42	10.61		
11280	9.37	9.31	9.74	10.86	10.48	10.73	81.3	81.6
11340	9.37	9.31	9.74	10.86	10.48	10.67		
11400	9.43	9.25	9.68	10.79	10.48	10.67	81.4	81.5
11460	9.43	9.25	9.81	10.86	10.48	10.61		
11520	9.31	9.25	9.74	10.79	10.42	10.61	81.3	81.5
11580	9.31	9.19	9.56	10.73	10.36	10.55		
11640	9.31	9.25	9.68	10.79	10.36	10.61	81.3	81.6
11700	9.37	9.19	9.62	10.67	10.42	10.61		
11760	9.37	9.25	9.68	10.79	10.42	10.67	81.3	81.6
11820	9.37	9.25	9.74	10.79	10.42	10.67		
11880	9.43	9.25	9.62	10.79	10.48	10.67	81.3	81.6
11940	9.37	9.25	9.68	10.79	10.42	10.67		
12000	9.31	9.19	9.56	10.67	10.36	10.61	81.3	81.5
12060	9.37	9.25	9.62	10.79	10.48	10.67		
12120	9.37	9.19	9.62	10.73	10.42	10.61	81.3	81.5
12180	9.37	9.25	9.74	10.79	10.48	10.67		
12240	9.37	9.19	9.62	10.92	10.48	10.67	81.2	81.6
12300	9.37	9.25	9.68	10.73	10.42	10.61		
12360	9.43	9.31	9.81	10.79	10.42	10.67	81.4	81.5

12420	9.37	9.37	9.68	10.86	10.48	10.73		
12480	9.25	9.19	9.56	10.61	10.36	10.55	81.3	81.4
12540	9.31	9.19	9.68	10.79	10.48	10.73		
12600	9.43	9.37	9.74	10.79	10.48	10.73	81.3	81.6
12660	9.37	9.25	9.62	10.79	10.48	10.67		
12720	9.37	9.25	9.68	10.86	10.55	10.73	81.3	81.5
12780	9.31	9.25	9.62	10.73	10.42	10.55		
12840	9.37	9.19	9.62	10.73	10.42	10.61	81.3	81.5
12900	9.37	9.25	9.68	10.86	10.48	10.73		
12960	9.31	9.25	9.62	10.79	10.36	10.61	81.9	82.2
13020	9.19	9.19	9.62	10.86	10.36	10.61		
13080	9.19	9.25	9.62	10.73	10.48	10.71	81.5	82.1

Table B.2 Processed experimental data for Run 12 with peeled carrots. Data for $Y_c < 0.1$ not included. (unit: time in sec. and temperature in ° C)

Time	F_0	$T_{a, avg}$	$T_{c, exp}$	$Y_{c, exp}$	$\ln Y_{c, exp}$
0	0.000	10.5	22.8	1.000	0.000
60	0.056	10.8	22.4	0.974	-0.026
120	0.113	10.7	21.7	0.917	-0.087
180	0.169	10.6	20.1	0.806	-0.216
240	0.225	10.7	18.8	0.708	-0.345
300	0.281	10.5	17.5	0.609	-0.495
360	0.338	10.6	16.4	0.533	-0.630
420	0.394	10.5	15.5	0.466	-0.764
480	0.450	11.6	14.5	0.394	-0.932
540	0.506	10.6	13.9	0.344	-1.066
600	0.563	10.5	13.3	0.299	-1.208
660	0.619	10.5	12.8	0.268	-1.317
720	0.675	10.5	12.4	0.235	-1.446
780	0.731	10.5	12.0	0.205	-1.587
840	0.788	10.4	11.5	0.172	-1.759
900	0.823	10.4	11.2	0.150	-1.896
960	0.900	10.5	11.1	0.141	-1.962
1020	0.956	10.5	10.9	0.123	-2.097
1080	1.013	10.4	10.6	0.100	-2.302

Table B.3 Predictions for Run 12 for peeled carrots by the finite difference method. Calculations performed using the program of Appendix A. (unit: time in sec. and temperature in °C)

time	F_0	$Y_{c,pred}$	$Y_{av,pred}$	$Y_{f,pred}$	$T_{c,pred}$	$T_{av,pred}$	$T_{f,pred}$	$T_{eq,pred}$
0.0	0.000	1.000	1.000	1.000	22.80	22.80	22.80	9.11
60.0	0.057	0.995	0.827	0.574	22.73	20.43	16.97	9.11
120.0	0.114	0.935	0.705	0.464	21.91	18.77	15.46	9.11
180.0	0.172	0.835	0.606	0.392	20.54	17.41	14.48	9.11
240.0	0.229	0.730	0.523	0.337	19.10	16.27	13.72	9.11
300.0	0.286	0.633	0.452	0.292	17.77	15.30	13.10	9.11
360.0	0.343	0.548	0.392	0.253	16.61	14.47	12.57	9.11
420.0	0.401	0.474	0.339	0.220	15.60	13.76	12.12	9.11
480.0	0.458	0.411	0.294	0.191	14.73	13.14	11.73	9.11
540.0	0.515	0.356	0.255	0.166	13.98	12.60	11.38	9.11
600.0	0.572	0.308	0.222	0.145	13.33	12.14	11.09	9.11
660.0	0.629	0.267	0.192	0.126	12.77	11.74	10.83	9.11
720.0	0.687	0.232	0.167	0.109	12.29	11.40	10.61	9.11
780.0	0.744	0.201	0.145	0.095	11.87	11.10	10.41	9.11
840.0	0.801	0.175	0.126	0.083	11.50	10.84	10.25	9.11
900.0	0.851	0.152	0.110	0.072	11.19	10.61	10.10	9.11
960.0	0.916	0.132	0.096	0.063	10.92	10.42	9.97	9.11
1020.0	0.973	0.115	0.083	0.055	10.68	10.25	9.86	9.11
1080.0	1.030	0.100	0.072	0.048	10.48	10.10	9.77	9.11
1140.0	1.087	0.087	0.063	0.042	10.30	9.97	9.68	9.11
1200.0	1.144	0.076	0.055	0.036	10.15	9.86	9.61	9.11
1260.0	1.202	0.066	0.048	0.032	10.01	9.77	9.55	9.11
1320.0	1.259	0.057	0.042	0.028	9.90	9.68	9.49	9.11
1380.0	1.316	0.050	0.036	0.024	9.80	9.61	9.44	9.11
1440.0	1.373	0.044	0.032	0.021	9.71	9.55	9.40	9.11
1500.0	1.431	0.038	0.028	0.019	9.63	9.49	9.37	9.11
1560.0	1.488	0.033	0.024	0.016	9.57	9.44	9.33	9.11
1620.0	1.545	0.029	0.021	0.014	9.51	9.40	9.31	9.11
1680.0	1.602	0.025	0.019	0.013	9.46	9.37	9.28	9.11
1740.0	1.659	0.022	0.016	0.011	9.41	9.33	9.26	9.11